Imperial College London

Investigation of the cyclophilin A:CD147 axis as a novel mediator of ventilator-induced lung injury

---

PhD Thesis

Marissa Wen Koh

Supervisors:

Dr Michael Wilson
Professor Masao Takata

Faculty of Medicine
Department of Surgery & Cancer

Section of Anaesthetics, Pain Medicine and Intensive Care
Chelsea & Westminster Hospital

Imperial College London

Abstract

Acute respiratory distress syndrome (ARDS) remains a significant cause of mortality and morbidity within the Intensive Care Unit. Despite increasing understanding of its pathogenesis in the past 50 years, management remains purely supportive with mechanical ventilation (MV) forming the mainstay of treatment. However, MV itself can worsen pre-existing ARDS, a phenomenon known as ventilator-induced lung injury (VILI). Since exposure to MV remains largely unavoidable, it is important that clinicians are able to limit the damage that occurs when patients are ventilated. While pharmacotherapies aimed at mitigating the inflammatory component of VILI have always been an attractive approach, to date, none have been shown to be successful in clinical trials. This suggests that there are still gaps in our current understanding of the disease and highlights the importance of studies investigating mechanistic pathways of ARDS.

In this thesis, we explore the role of the cyclophilin A (CypA):CD147 signalling axis in VILI. CypA is a ubiquitously distributed protein. Although previous research has focussed on its intracellular roles, recent studies suggest the involvement of extracellular CypA and its primary receptor CD147 in inflammatory diseases. We hypothesise that CypA is secreted into the alveolar space following epithelial insult where it can then interact with CD147 to promote inflammation and injury.

We have shown, for the first time, the involvement of CypA in VILI in animal models as well as in human ARDS patients. CypA is produced locally within the lungs at an early time point, most likely by alveolar epithelial cells. *In vitro*, recombinant CypA induces activation of macrophages, suggesting it is more than a mere biomarker of injury. Lastly, inhibition of extracellular CypA *in vivo* leads to improved survival and impressive attenuation physiological dysfunction, providing further evidence that CypA does play a role in the pathogenesis of VILI.

Table of Contents

Abstract **2**
Table of Contents **4**
Acknowledgements **8**
Statement of Originality **9**
Statement of Copyright **9**
Index of Figures **10**
Index of Tables **14**
Abbreviations **16**
1 Introduction **18**
1.1 Acute Respiratory Distress Syndrome (ARDS) **19**
1.1.1 Epidemiology 21
1.1.2 Aetiology 22
1.1.3 Risk factors 23
1.1.4 Pathogenesis 24
1.1.5 Management 26
1.1.6 Prevention 27
1.2 Ventilator induced lung injury **28**
1.2.1 Mechanisms of VILI 28
1.2.2 Management of VILI: Ventilatory strategies 37
1.2.3 Management of VILI: Adjunctive therapies 41
1.2.4 Management of VILI: pharmacological interventions 45
1.2.5 Identifying alternative therapeutic targets for VILI 47
1.3 CD147 ..... **49**
1.3.1 The CD147 gene 49
1.3.2 The structure of CD147 50
1.3.3 Expression and regulation of CD147 53
1.3.4 Functions of CD147 in physiologic and pathologic contexts 54
1.3.5 CD147 in disease 57
1.4 The cyclophilins **59**
1.4.1 Cyclophilin A 59
1.4.2 Molecular structure of CypA 60
1.4.3 Functions of CypA 60
1.4.4 Extracellular CypA as a novel mediator of intercellular communication 61
1.4.5 CypA:CD147 interactions 64
1.4.6 CypA:CD147 axis in inflammatory diseases 66
1.5 Hypothesis **72**
1.6 Aims **72**
2 Materials & Methods **73**
2.1 Materials **74**
2.1.1 Reagents 74
2.1.2 Commercial detection assays 78
2.1.3 Instruments, equipment, and software 79
2.2 Animals **80**
2.3 In vivo animal models of ventilator-induced lung injury **80**
2.3.1 Ventilator-Induced Lung Injury 80

2.4 Interventional studies 84
2.4.1 Alveolar macrophage depletion experiments 84
2.4.2 Extracellular Cyclophilin A inhibition with MM-284 85
2.5 Physiological data 87
2.5.1 Respiratory mechanics 87
2.5.2 Arterial blood gas sampling 87
2.6 Experimental samples and physiological measurements 88
2.6.1 Harvesting plasma samples 88
2.6.2 Lung wet/dry weight ratio 88
2.6.3 Bronchoalveolar lavage 88
2.6.4 BAL protein assay 89
2.6.5 Lungs 89
2.6.6 ELISA 89
2.7 Western Blot 90
2.7.1 Preparation of lung samples for western blot analyses 90
2.7.2 Bradford protein assay 90
2.7.3 Western blotting protocol 91
2.8 Gelatin zymography 93
2.9 Flow cytometric analyses 95
2.9.1 Cell surface staining *in vitro* 97
2.9.2 Intracellular staining *in vitro* 98
2.9.3 Antibodies 98
2.10 Cell culture techniques 102
2.10.1 Primary cells 103
2.11 In vitro cell stretching 106
2.12 Lactate dehydrogenase (LDH) assay 108
2.13 NO assay 109
2.14 Statistical analyses 109
3 Cyclophilin A and CD147 in ventilator-induced lung injury 111
3.1 Abstract 112
3.2 Introduction 114
3.3 Aim 116
3.4 Protocols 117
3.4.1 In vivo ventilator-induced lung injury model 117
3.4.2 Sample processing and analyses 117
3.4.3 Plasma and BAL analyses 118
3.4.4 Analysis of human ARDS samples 118
3.4.5 Statistics 120
3.5 Results 121
3.5.1 Cyclophilin A is dramatically upregulated during VILI 121
3.5.2 CypA kinetics during VILI 121
3.5.3 Markers of lung injury 124
3.5.4 Correlation between CypA and markers of lung injury 126
3.5.5 Pulmonary cell identification using flow cytometry 128
3.5.6 CD147 during ventilator-induced lung injury 133
3.5.7 Extracellular CypA is significantly increased in ARDS patients 134
3.6 Discussion 135
3.6.1 BAL levels of CypA are dramatically increased during VILI 135
3.6.2 CypA is produced locally in the alveolus 135

3.6.3 CypA in VILI, cause or consequence of injury? ... 136
3.6.4 CD147 upregulation during VILI ... 138
3.7 Concluding remarks ... 142
4 Source of Cyclophilin A ... 143
4.1 Abstract ... 144
4.2 Introduction ... 145
4.3 Aim ... 146
4.4 Protocols ... 147
4.4.1 LPS-induced lung injury model ... 147
4.4.2 Acid-induced lung injury model ... 147
4.4.3 *In vivo* alveolar macrophage depletion ... 148
4.4.4 *In vivo* intracellular CypA staining ... 148
4.4.5 Cell stretching *in vitro* ... 148
4.4.6 ELISA ... 153
4.4.7 Bradford assay ... 153
4.4.8 Western blotting ... 153
4.5 Results ... 155
4.5.1 Cyclophilin A levels are markedly increased in acid-induced lung injury – an epithelial insult dominant model ... 155
4.5.2 Optimisation of *in vivo* depletion of alveolar macrophages ... 157
4.5.3 Optimisation of alveolar macrophage depletion experiments ... 161
4.5.4 Alveolar macrophage depletion attenuates VILI ... 162
4.5.5 Intracellular levels of CypA decrease in only epithelial cells during VILI ... 165
4.5.6 *In vitro* cell stretching – alveolar epithelial cells ... 166
4.5.7 In vitro cell stretching – alveolar macrophages ... 177
4.6 Discussion ... 181
4.7 Concluding remarks ... 187
5 Inhibition of CypA in ventilator-induced lung injury ... 188
5.1 Abstract ... 189
5.2 Introduction ... 190
5.3 Aims ... 192
5.4 Protocols ... 193
5.4.1 Cyclophilin A inhibition experiments ... 193
5.4.2 MM-284 – mechanism of action and dose ... 194
5.4.3 Post-experiment sample processing and analyses ... 195
5.4.4 Homogenisation of lung samples ... 196
5.4.5 Gelatin Zymography ... 196
5.4.6 Western blotting ... 197
5.4.7 Statistics ... 198
5.5 Results ... 199
5.5.1 Optimisation of inhibitor administration ... 199
5.5.2 Treatment with MM-284 prior to high V_T ventilation attenuates VILI ... 202
5.5.3 Improved physiological markers of injury following MM-284 ... 204
5.5.4 Mechanistic investigation of cyclophilin A inhibition ... 208
5.6 Discussion ... 219
5.7 Concluding remarks ... 227
6 Exploration of CypA stimulation *in vitro* ... 228
6.1 Abstract ... 229

6.2 Introduction 230
6.3 Aims 232
6.4 Protocols 233
6.4.1 Isolation of murine bone-marrow-derived macrophage 233
6.4.2 Human monocyte-derived macrophage isolation 234
6.4.3 Stimulating cells with recombinant cyclophilin A 240
6.4.4 Cell viability: 7-AAD 242
6.4.5 Nitric oxide assay 242
6.4.6 Gelatin zymography 243
6.5 Results 244
6.5.1 Bone marrow-derived macrophages express the CypA receptor CD147 244
6.5.2 Effects of recombinant CypA on mouse BMDMs 244
6.5.3 HMDMs also express the CypA receptor CD147 248
6.5.4 Effects of recombinant CypA on HMDMs 249
6.5.5 Stimulation of A549 with recombinant CypA 253
6.6 Discussion 255
6.7 Concluding remarks 259
7 Final discussion 260
7.1 Aims of this work 262
7.2 Summary of findings 262
7.3 Limitations of work in this thesis 270
7.3.1 VILI model 270
7.3.2 Utilisation of different techniques to determine the source of CypA during VILI 270
7.3.3 MM-284 target engagement data 271
7.4 Future work 272
8 References 278

Acknowledgements

I would like to acknowledge Dr Michael Wilson and Professor Masao Takata, for their supervision over the past three years. I am so grateful to Mike for his unwavering support since day one. I thank him especially for sharing his research expertise and for always being willing to sit down for a discussion. Needless to say, this thesis would not have been possible without his help. I thank Masao for his willingness to take on a naïve Haematology BSc student and for guidance in the transition from clinical medicine to a taste of academia as a PhD student. His enthusiasm for clinical academic research has been a great inspiration and will no doubt shape the way I approach clinical medicine in the coming years.

Additionally, I thank Dr Kieran O'Dea for always being willing to share ideas, offer advice, and come to the rescue when the flow cytometer inevitably fails. I am also incredibly grateful for the friendship and support from Ying, Virginia, and Hera throughout this PhD. I must also thank all the other members and staff from the Section of Anaesthetics, Pain Medicine and Intensive Care – Sanooj, Faruq, Rhianna, Eirini, Brij, Rhodri, Sunil, Ineke, Dennis, Steffi – not only for their help and research expertise but for also making my time in the group so enjoyable.

I thank Professor Louise Donnelly and her PhD student, Catherine Wrench, for kindly teaching me how to perform gelatin zymography. I thank Professor Danny McAuley for providing the human ARDS samples. I thank Dr Malesevic for kindly gifting us the CypA inhibitor MM-284.

I thank the Agency for Science, Technology and Research (A*STAR) and the British Journal of Anaesthesia/Royal College of Anaesthetists for their funding support.

Finally, I thank Brandon and my flatmates, Lydia and Nikkita, who have tolerated me, continuously encouraged me, and kept me sane during this PhD. It goes without saying that the biggest thanks must go to my sister, Melanie, and parents, Mark and Doreen, who have supported me in every way possible throughout my MBBS and PhD.

Statement of Originality

All work within this thesis is my own and those that have assisted me with this work have been duly recognised within the Acknowledgements.

Statement of Copyright

The copyright of this thesis rests with the author. Unless otherwise indicated, its contents are licensed under a Creative Commons Attribution-Non Commercial-No Derivatives 4.0 International Licence (CC BY-NC-ND). Under this licence, you may copy and redistribute the material in any medium or format on the condition that; you credit the author, do not use it for commercial purposes and do not distribute modified versions of the work. When reusing or sharing this work, ensure you make the licence terms clear to others by naming the licence and linking to the licence text. Please seek permission from the copyright holder for uses of this work that are not included in this licence or permitted under UK Copyright Law.

Index of Figures

Figure 1.1 - Protein isoforms of CD147/Basigin (Bsg) 50
Figure 1.2 - Schematic diagram of CD147. 51
Figure 2.1 - Schematic of in vivo ventilation system set-up 82
Figure 2.2 - Protocol of CypA inhibition in vivo VILI experiments 86
Figure 2.3 - Airway flow and pressure graphs showing measurement and calculation of respiratory mechanics 87
Figure 2.4 - Alveolar epithelial cell gating strategy. 101
Figure 2.5 - Lung leukocyte gating strategy. 102
Figure 2.6 - Leucosep tubes with separated layers post-centrifugation 104
Figure 2.7 - Identification of monocytes, lymphocytes and counting beads from isolated PBMCs using flow cytometry 105
Figure 2.8 - Lactate dehydrogenase converts pyruvate to L-Lactate 108
Figure 3.1 – Levels of CypA in BAL of untreated mice and mice subjected to 3 hours of high V_T (VILI) 121
Figure 3.2 - *In vivo* kinetic profile of the levels of CypA in BAL following 1, 2, and 3 hours of either low or high V_T ventilation. 123
Figure 3.3 - *In vivo* kinetic profile of plasma CypA following 1, 2, and 3 hours of either low or high V_T ventilation.. 123
Figure 3.4 - Assessment of BAL protein, arterial oxygenation, lung W/D weight ratio and BAL sRAGE following 1, 2, and 3 hours of either low or high V_T ventilation. 125
Figure 3.5 - Assessment of the correlation between BAL CypA and (A) BAL protein, (B) PaO_2, (C) W/D weight ratio, (D) BAL sRAGE. 127
Figure 3.6 - Lung leukocyte gating strategy using flow cytometry. 129
Figure 3.7 - Lung epithelial cell gating strategy using flow cytometry. 132
Figure 3.8 – CD147 expression is upregulated on the surface of pulmonary cells following 1 hour of high stretch ventilation. 133

Figure 3.9 – Extracellular CypA is substantially increased in ARDS patients compared with healthy controls. 134
Figure 4.1 – Identification of epithelial cells by flow cytometry. 150
Figure 4.2 - Representative absorbance curves generated over 1 hour following assay kit protocol. 152
Figure 4.3 - Levels of CypA and sRAGE in BAL of untreated mice and mice subjected to 3 hours LPS challenge, acid-induced lung injury, or VILI. 156
Figure 4.4 - Flow cytometric analysis of alveolar macrophages depletion following intratracheal clodronate treatment. 158
Figure 4.5 – Comparison of alveolar macrophage depletion by clodronate liposomes using different routes of administration. 160
Figure 4.6 – Physiological parameters show protective effects of alveolar macrophage depletion with clodronate treatment following 150 minutes of injurious high V_T ventilation. 162
Figure 4.7 – Markers of lung injury decreased at 150 minutes following clodronate depletion of alveolar macrophages. 163
Figure 4.8 – Markers of lung injury at 120 minutes suggest the beginnings of lung injury in saline treated animals. 164
Figure 4.9 – Intracellular expression of CypA decrease in epithelial cells but not alveolar macrophages following 3 hours of high V_T ventilation. 166
Figure 4.10 – No differences were observed in cell surface markers and viability of MLE-12 cells following 6 hours of low (4%) and high (20%) *in* vitro stretch. 168
Figure 4.11 - Comparison of IL-6 and levels of CypA in release from MLE-12 cells following 6 hours of low (4%) and high (20%) *in vitro* stretch. 169
Figure 4.12 - No differences observed between MLE-12 cells held static (control) or subjected to *in vitro* stretch for 6 hours. 170
Figure 4.13 – Levels of IL-8 in conditioned media of A549 cells that were kept static (control) or stretched (20% elongation) for various time periods. 173
Figure 4.14 – Comparison of expression of ICAM-1 and CD147, and IL-8 release in H-AECs that were held static (control) or subjected to 20% stretched cells for 6 hours. 174
Figure 4.15 – Comparison of protein concentration of supernatants and cell counts between H-AECs that were held static (control) or subjected to 20% stretched cells for 6 hours. 175

Figure 4.16 – CypA released is increased following 6 hours of 20% stretch. 176
Figure 4.17 - Assessment of viability in H-AEC cells that were held static (control) or subjected to 20% stretched cells for 6 hours. 177
Figure 4.18 – Assessment of cell activation markers, viability, and IL-6 release from RAW cells following 6 hours of *in vitro* stretch. 179
Figure 5.1 - In vivo VILI protocol for inhibition experiments 193
Figure 5.2 - Respiratory mechanics in vehicle and MM-284 treated groups at baseline to 30 minutes post instillation of drug. 201
Figure 5.3 – (A) Kaplan-Meier survival curve and (B) blood pressures of animals in both vehicle and MM-284 treated groups over the course of 3 hours of high V_T ventilation. 203
Figure 5.4 - Time course of respiratory mechanics over the course of 3 hours of high V_T ventilation in both treatment groups. 205
Figure 5.5 - Time course of (A) arterial oxygenation (PaO_2) and (B) arterial carbon dioxide ($PaCO_2$) during 3 hours of high V_T ventilation in both treatment groups. 206
Figure 5.6 - Assessment of alveolar-capillary membrane permeability in both vehicle and MM-284 treated groups at the end of 3 hours of high V_T ventilation. 207
Figure 5.7 – BAL cytokines/chemokines in vehicle- and MM-284-treated groups following 3 hours of high V_T ventilation. 208
Figure 5.8 - Protective effect of MM-284 treatment appears to be independent to lung leukocyte recruitment during VILI. 210
Figure 5.9 - Assessment of pulmonary cell activation during VILI *in vivo* using surface expression of activation marker, ICAM-1, on (A) AECs, (B) alveolar macrophages, and (C) endothelial cells (ECs). 211
Figure 5.10 – BAL sRAGE levels was significantly decreased in the MM-284 treatment during *in vivo* VILI. 212
Figure 5.11 - Assessment of matrix metalloproteinases in lung homogenates from both vehicle and MM-284 treated groups following *in vivo* VILI using gelatin zymography. 214
Figure 5.12 – Representative gelatin zymography gel for MMP-2 and MMP-9 activity in the BAL of vehicle and MM-284 treated animals following *in vivo* VILI. 215

Figure 5.13 - Assessment of matrix metalloproteinases in BAL fluid from both groups following 3 hours of high V_T ventilation using gelatin zymography. 216
Figure 5.14 – No differences in lung occludin expression was observed in MM-284 treated mice compared with vehicle treated controls following 3 hours of high V_T ventilation. 217
Figure 6.1 - Representative flow cytometry plot of PBMCs isolated from peripheral blood. 235
Figure 6.2 - Comparison of flow cytometry plots before and after MACS sorting. 237
Figure 6.3 - Characterisation of HMDMs after seven days in culture. 239
Figure 6.4 – Representative flow cytometry histogram showing BMDM expression of CD147 receptor 244
Figure 6.5 – Assessment of cell surface activation markers following an 8- and 24-hour incubation with recombinant CypA. 245
Figure 6.6 – 8-hour stimulation with recombinant CypA leads to increased cell death (A), nitric oxide production (B), and IL-6 release (C). 246
Figure 6.7 – Dose titration of recombinant CypA. 248
Figure 6.8- Representative flow cytometry histogram showing BMDM expression of CD147 receptor 249
Figure 6.9 – 8-hour incubation of HMDMs with recombinant CypA leads to cell activation. 250
Figure 6.10 – Assessment of MMP activity in conditioned media from HMDMs stimulated with CypA. 252
Figure 6.11 – Representative flow cytometry histogram showing BMDM expression of CD147 receptor. 253
Figure 6.12 – A549 cells did not demonstrate signs of cellular activation following 8-hour stimulation recombinant CypA (1 µg/mL). 254
Figure 7.1 - Propose schematic for the CypA:CD147 signalling pathway during VILI 269

Index of Tables

Table 1.1 - The American-European Consensus Conference (1994) definition of ALI and ARDS 19
Table 1.2 - The Berlin Definition of ARDS 20
Table 1.3 - Non-exhaustive list of direct (pulmonary) and indirect (extrapulmonary) causes of ARDS 23
Table 1.4 - Secretion of CypA from various cell types 62
Table 2.1 - In vivo reagents 74
Table 2.2 - Flow cytometry reagents 75
Table 2.3 - Enzyme-linked immunosorbent assay (ELISA) reagents 75
Table 2.4 - Western blotting reagents 76
Table 2.5 - Gelatin zymography reagents 77
Table 2.6 - Commercial detection and quantification kits 78
Table 2.7 - Equipment for in vivo ventilation protocols 79
Table 2.8 - ELISA equipment 79
Table 2.9 - Flow cytometry equipment 79
Table 2.10 - Software packages 79
Table 2.11 - Ventilation parameters for low and high V_T ventilation strategies 83
Table 2.12 - Antibodies used in western blotting 93
Table 2.13 - 7-Channel CyAn ADP flow cytometer fluorescence channels and fluorophores 96
Table 2.14 - Lung parenchyma antibody panel to identify alveolar epithelial cells (AECs), endothelial cells, and leukocytes. 99
Table 2.15 - Lung leukocyte antibody panel to identify macrophages, monocytes, neutrophils and dendritic cells 99
Table 2.16 - Antibodies used to measure markers of interest/activation expressed on various cell types 100
Table 2.17 - Antibodies used to measure intracellular markers of interest in various cell types 100
Table 2.18 - Cell lines, media and splitting solution used 103
Table 3.1 - Surface expression markers T1α, EpCAM, and MHC-II used to differentiate distal lung cells. 131

Table 6.1 - An estimation of the concentration of CypA in the alveolar space based on the mean concentration of BAL CypA found *in vivo* and estimated BAL dilution factors 240
Table 6.2 - Seeding densities and media of macrophages and epithelial cells for CypA stimulation experiments 241

Abbreviations

7-AAD	7-Amino-Actinomycin D
ABG	Arterial blood gas
AEC	Alveolar epithelial cell
ALI	Acute lung injury
ARDS	Acute respiratory distress syndrome
BAL	Bronchoalveolar lavage
BALF	Bronchoalveolar lavage fluid
BSG	Basigin
CD	Cluster of differentiation
CypA	Cyclophilin A
DAMP	Damage-associated molecular pattern
EMMPRIN	Extracellular matrix metalloproteinase inducer
EpCAM	Epithelial cell adhesion marker
FWB	FACS wash buffer
HCl	Hydrochloric acid
HS	High stretch
I.P.	Intraperitoneal
I.T.	Intratracheal
ICAM-1	Intercellular adhesion molecule 1
IL	Interleukin
LPS	Lipopolysaccharide
LS	Low stretch
MCP	Monocyte chemoattractant protein
MHC	Major histocompatibility complex
MMP	Matrix metalloproteinase
mRNA	Messenger ribonucleic acid
NFκB	Nuclear-factor kappa B
PAMPs	Pathogen-associated molecular patterns
PaO_2	Arterial partial pressure of oxygen
PBS	Phosphate-buffered saline
PEEP	Peak end-expiratory pressure
Pro-SP-C	Pro-surfactant protein C

PWB	Permeabilisation wash buffer
ROS	Reactive oxygen species
RR	Respiratory rate
sRAGE	Soluble receptor for advanced glycation end products
T1α	Type 1 cell alpha protein
TNF-α	Tumour necrosis factor alpha
VILI	Ventilator-induced lung injury
V_T	Tidal volume
W/D	Wet/dry

1 Introduction

1.1 Acute Respiratory Distress Syndrome (ARDS)

Acute respiratory distress syndrome (ARDS) was first described by Ashbaugh et al in 1967 following observations they had made of 12 patients with severe acute respiratory failure (1). These patients had an 'acute onset of tachypnoea, hypoxaemia, and loss of compliance after a variety of stimuli'. Over the next 25 years, several definitions of ARDS were proposed, each attempting to provide a uniform diagnostic and classification criteria for this heterogenous syndrome. It was only in 1994 that the first widely adopted definition of ARDS was published by the American-European Consensus Conference (AECC) (Table 1.1) (2). Under this definition, patients presenting with an acute onset of hypoxaemia ($PaO_2/FiO_2 \leq 200$ mmHg) with bilateral diffuse pulmonary infiltrates on chest radiograph in the absence of left atrial hypertension were classified as having ARDS. This definition also described a less severe form of ARDS termed acute lung injury (ALI), differentiated by less severe hypoxemia ($PaO_2/FiO_2 \leq 300$ mm Hg).

Table 1.1 - The American-European Consensus Conference (1994) definition of ALI and ARDS

	Timing	Chest radiograph	Oxygenation	PAWP
ALI	Acute onset	Diffuse bilateral pulmonary infiltrates	$PaO_2/FiO_2 \leq 300$ mmHg	≤ 18 mmHg No left atrial hypertension
ARDS	Acute onset	Diffuse bilateral pulmonary infiltrates	$PaO_2/FiO_2 \leq 200$ mmHg	≤ 18 mmHg No left atrial hypertension

ALI: acute lung injury; ARDS: acute respiratory distress syndrome; PaO_2/FiO_2: arterial oxygen tension/fraction of inspired oxygen ratio; PAWP: pulmonary artery wedge pressure.

In 2012, the 'Berlin Definition of ARDS' (Table 2) emerged to update the definition of ARDS and address the limitations of the AECC definition that emerged in its 18 years of use (3). Where the AECC definition had previously not provided an explicit timeframe for defining an 'acute onset', the Berlin definition specified that the onset must be within one week of a known

clinical insult or new or worsening respiratory symptoms. The term ALI was removed and instead, three mutually exclusive subgroups of ARDS classified by severity (mild, moderate, and severe) based on the degree of hypoxaemia (PaO_2/FiO_2) were created (Table 1.2). To account for the sensitivity of PaO_2/FiO_2 to different ventilator settings, in particular to positive end-expiratory pressure (PEEP), the Berlin definition specifies that these measurements must be taken with a minimum level of PEEP (5 cmH_2O). Other limitations addressed in the Berlin definition included: clarification of chest radiograph criteria with development of a reference set of chest radiographs to enhance inter-observer reliability; removal of the pulmonary artery wedge pressure criterion for hydrostatic oedema as patients with ARDS were often found to have an elevated pulmonary artery wedge pressure (PAWP) due to elevated pleural pressure and/or vigorous fluid resuscitation with focus placed instead on ensuring that respiratory failure was not primarily due to hydrostatic oedema (4, 5); and the inclusion of underlying risk factors for ARDS.

Table 1.2 - The Berlin Definition of ARDS

The 2012 Berlin Definition of ARDS	
Timing	Within 1 week of a known clinical insult or new or worsening respiratory symptoms
Chest imaging[§]	Bilateral opacities – not fully explained by effusions, lobar/lung collapse, or nodules on chest radiographs or chest CT[§]
Origin of oedema	Respiratory failure not fully explained by cardiac failure or fluid overload. Need objective assessment (e.g. echocardiography) to exclude hydrostatic oedema if no risk factors are present.
Oxygenation	
Mild	200 mm Hg < PaO_2/FiO_2 ≤ 300 mm Hg With PEEP/CPAP ≥ 5 cm H_2O
Moderate	100 mm Hg < PaO_2/FiO_2 ≤ 200 mm Hg With PEEP ≥ 5 cm H_2O
Severe	PaO_2/FiO_2 ≤ 100 mm Hg With PEEP ≥ 5 cm H_2O

PaO_2/FiO_2: arterial oxygen tension/fraction of inspired oxygen ratio; CPAP: continuous positive airway pressure; PEEP: positive end-expiratory pressure.

[§]*CT: computed tomography scan.*

When the Berlin definition criteria was applied to existing clinical data, mortality was found to corelate with the severity categories, increasing from 27% in patients with mild ARDS to 32% in patients with moderate ARDS and 45% in patients with severe ARDS **(3)**. At present, the Berlin definition remains the standard within clinical care and research.

1.1.1 Epidemiology

Epidemiological understanding of this disease has been challenging. Most difficulties are associated with the manner in which ARDS is diagnosed. At present, there is still no simple diagnostic test for ARDS. Thus, in addition to the at times ambiguous evolving diagnostic criteria, many other epidemiological problems such as geography variation in availability of critical care resources (blood gas machines and imaging equipment) and clinical practice also contribute to challenge of establishing reliable incidence and mortality rates.

Incidence estimates can vary considerably between countries, which likely reflects differences in reporting rates (low-income countries tend to lack resources needed to obtain diagnostic clinical data and therefore, under report), rigor of study methodology, population demographics, and prevalence of risk factors for ARDS (6-8).

LUNG-SAFE (Large Observational Study to Understand the Global Impact of Severe Acute Respiratory Failure) is the most recent international, multi-centre, prospective cohort study to provide epidemiological data on ARDS (9). Among the 29,144 patients enrolled in this study, the incidence of ARDS represented 10.4% of total intensive care unit (ICU) admissions and constituted 0.42 cases/ICU beds over a 4-week period. This incidence rate was found to vary geographically, with Asia having a much lower incidence of 0.27 compared to Europe with an incidence of 0.48 cases/ICU bed over 4 weeks. In this study, unadjusted hospital mortality was 34.9% for patients with mild ARDS, 40% for those with moderate ARDS, and 46.1% for those with severe ARDS. A UK prospective study conducted in 2016 reported similar findings

(10). Incidence of ARDS in the UK were found to constitute 12.5% of ICU admissions over a 6-month period with an ICU and hospital mortality rate of 41.9% and 53.5%, respectively.

Importantly, results from both studies suggest that ARDS continues to be under recognised and consequently under treated. In the LUNG-SAFE study, clinical recognition rates of ARDS was found to be as low as 51% in mild ARDS and only 79% in severe ARDS (9). In the UK based study, only 2 of the 43 patients with ARDS were coded as such by the hospital coding department (10). This under-recognition may have implications on both the scale of the individual patient (e.g. ensuring they receive the optimal, recommended lung protective ventilation and other adjunctive treatment) and on a much larger scale with regard to resource planning to ensure that critical care facilities are able to meet the health burden of this disease.

1.1.2 Aetiology

ARDS may be precipitated by a variety of insults which culminate in a syndrome presenting with severe non-cardiogenic pulmonary oedema leading to life-threatening hypoxemia that often requires mechanical ventilatory support. These precipitants may be broadly divided into direct (pulmonary) and indirect (extrapulmonary) causes. ARDS develops most commonly in the setting of pneumonia (commonly bacterial and viral), non-pulmonary sepsis (sources including the peritoneum, urinary tract, soft tissue and skin), aspiration of gastric and/or oral and oesophageal contents, and severe trauma (such as blunt or penetrating injuries or burns) (11).

DIRECT (PULMONARY) CAUSES
Pneumonia (bacterial and viral more common, fungal less common)*
Gastric aspiration*
Near drowning
INDIRECT (EXTRAPULMONARY) CAUSES
Sepsis*
Severe trauma, e.g. lung contusions, fat embolism secondary to long bone fraction, severe burns
Massive transfusion (>15 units of RBCs)
Transfusion of blood products (FFP, platelet, RBC)
Lung transplant
Haematopoietic stem cell transplant
Acute pancreatitis
Cardiopulmonary bypass
Drugs – aspirin, cocaine, opioids, phenothiazines
Alcohol abuse

RBC: red blood cells; FFP: fresh frozen plasma

*Together, these three (pneumonia, gastric aspiration, and sepsis) causes account for more than 85% of cases of ARDS[8].

Table 1.3 - Non-exhaustive list of direct (pulmonary) and indirect (extrapulmonary) causes of ARDS

1.1.3 Risk factors

Even though pneumonia, sepsis, and gastric aspiration account for a large proportion of ARDS, most patients with these clinical risk factors do not actually go on to develop ARDS. This suggest that other factors, such as genetic or environmental factors, may contribute to the susceptibility for developing ARDS. While no specific loci with genome-wide significance for association with ARDS have been identified, a number of genetic variations have been associated with risk of development ARDS, and in some associations, with higher mortality. Some examples include, *ANGPT2* which encodes plasma angiopoietin-2, a biomarker of endothelial activation and mediator of increased lung vascular permeability (12); *IL1RN* gene which encodes the IL-1 receptor antagonist (IL1RA) protein and is associated with decreased risk of ARDS due to an increased plasma ILR1RA response (13); and the *PPFIA1* gene that encodes liprin alpha, a protein involved in cell adhesion, integrin expression, and cell-matrix

interaction which may contribute to the pathogenesis of ALI, particularly after major trauma, through altering cell adhesion and lung vascular permeability (14-16).

Environmental risk factors that have been shown to be associated with an increased susceptibility to ARDS include chronic alcohol abuse (17), cigarette smoking (18), air pollution (19), and vitamin D deficiency (20). The majority of studies investigating the association between ethnicity and ARDS outcomes have reported higher mortality for Blacks and Hispanics patients with ARDS than for Whites (21, 22). In a candidate gene study, the presence of a functional T-46C polymorphism (rs2814778) in the promoter region of the *DARC* gene (Duffy antigen/receptor for chemokines), which was found almost exclusively in only patients of African descent, was associated with a 17% increase in 60-day mortality. One of the mechanisms contributing to a worse clinical outcome in this group of patients might be the increase in circulating plasma IL-8 levels. Generally, the consequences of these disparities remains unclear.

1.1.4 Pathogenesis

The pathogenesis of ARDS has classically been divided into three phases: an exudative phase, a proliferative phase, and a fibrotic phase (8, 23, 24). The first phase, known as the exudative phase, typically spans the first 7 days of ARDS, featuring the innate immune system's response to the inciting cause of lung injury. In this phase, the insult leads to an increase in alveolar-capillary barrier permeability. Injury to the normally tight alveolar-capillary barrier allows translocation of oedematous fluid across the lung endothelium, into the lung interstitium, and eventually into the alveolar space. At the same, there is also an influx of inflammatory cells, including neutrophils and monocytes, which begin to release a barrage of injurious mediators (e.g. proteinases, reactive oxygen species, and inflammatory cytokines), further amplifying the ongoing inflammatory response. As a consequence, the alveolus is flooded by fluid, proteins, inflammatory leukocytes, red blood cells, platelets, and cellular

debris – this ‘diffuse alveolar damage (DAD)’ is the histopathological hallmark of ARDS (25). This pulmonary oedema leads to a reduction in lung compliance and an increased work of breathing. Furthermore, pulmonary oedema often contributes to ventilation-perfusion mismatch with right-to-left intrapulmonary shunting. This eventually leads to arterial hypoxaemia and respiratory failure, often necessitating mechanical ventilatory support.

The initial exudative phase is followed by the proliferative phase, which can last >3 weeks in survivors. This phase marks the initiation of repair mechanisms and is crucial for host survival. Alveolar fluid is reabsorbed, restoring lung fluid balance. Type II alveolar epithelial cells proliferate and differentiate into type I alveolar epithelial cells, mediating the repair of the damaged alveolar epithelium; Epithelial-mesenchymal transformation occurs, a process where interstitial fibroblasts and myofibroblasts infiltrate and mediate repair through deposition of extracellular matrix components such as collagen to restore alveolar architecture.

The last phase – the fibrotic phase, is characterised by significant upregulation of collagen and the development of fibrotic changes. In contrast to the previous phase, which is linked to host survival, the progression to the fibrotic phase occurs variably and appears to represent a pathological response in patients with ARDS. The interstitial and lung fibrosis that may occur as part of the reparative process can actually lead to a further reduction in lung compliance and decreased respiratory function. Multiple clinical studies have suggested that patients with evidence of pulmonary fibrosis often have worse clinical outcomes, including increased mortality rates and a greater severity of organ failure (26-28).

1.1.5 Management

Respiratory support

Currently, there are relatively few treatments available for ARDS. Management of ARDS focuses on the diagnosis and treatment of the underlying cause (e.g. antimicrobial therapy for pulmonary infections) and supportive therapy, with the mainstay of treatment being lung protective mechanical ventilation aimed at addressing life-threatening refractory hypoxemia whilst reducing the incidence of ventilator-induced lung injury (VILI; discussed further below).

Fluid management

Other supportive measures include conservative fluid management after shock has been resolved. This fluid-conservative approach was instituted after a randomised clinical trial in 2006 demonstrated a significant increase in ventilator-free days and improved oxygen index in patients assigned to a fluid-conservative treatment strategy compared with a liberal fluid strategy (29). Due to the lack of evidence of harm, the current recommendations include the use of conservative fluid management consisting of fluid restriction, diuretics, and in some cases hyperoncotic albumin to achieve a negative fluid balance (30).

Pharmacological or adjunct therapies

To date, no pharmacological therapy has been shown to reduce either short- or long-term mortality despite considerable efforts. Multiple strategies targeting different aspects of the disease process are currently being investigated. Anti-inflammatory therapies (e.g. glucocorticoids (31, 32), aspirin (33), macrolide antibiotics (34, 35)) aimed at modulating the inflammatory response have either proven disappointing or require further studies before becoming routine recommendations. Similarly, evidence surrounding the use of agents that enhance lung repair, such as keratinocyte growth factor (36) granulocyte-monocyte colony stimulating factor (GM-CSF) (37) and mesenchymal stem cells (MSCs) (38, 39) remains

inconclusive; while preclinical studies suggest attenuation of lung injury and association with increased survival, subsequent randomised trials have failed to detect any effects on mortality. A range of other promising pharmacotherapies such as antioxidants (40), neutrophil elastase inhibitors (41), statins (42), β-adrenergic agonists (43, 44), and surfactant replacement (45) have also failed to improve clinical outcomes in patients with ARDS.

1.1.6 Prevention

Given the rapid development of ARDS – median time to the onset of ARDS is 2 days after hospital admission (46) – drug-based preventive strategies remain a challenge, both to deliver within the small window of time and to assess in clinical trials. The two main approaches that have been evaluated for their efficacy to prevent ARDS are statins and aspirin. Data from a meta-analysis conducted by Xiong et al in 2016 evaluating the use of statins (most commonly simvastatin) in 13 studies, including four randomised control trials and nine cohort studies published between 2007-2015, showed that statin therapy had no impact on morbidity of ARDS in high-risk patients (47). Evaluation of clinical outcomes, including mortality, ventilator-free days, oxygen index, length of stay in intensive care unit and length of stay in hospital were neither improved nor worsened by statins. Following observational data suggesting that anti-platelet therapy with aspirin may prevent the development of ARDS (48), the efficacy of aspirin was assessed in a multi-centre randomised control trial (33). However, no significant differences between the aspirin or placebo treated group in the primary outcome of ARDS incidence or secondary outcomes (ventilator-free days, length of stay, 28-day survival and 1-year survival) were observed, opposing the use of aspirin in at-risk patients. As such, no treatment is currently available for the prevention of ARDS.

1.2 Ventilator induced lung injury

The concept that artificial mechanical ventilation has the potential for harm is not new. In 1744, John Fothergill published an essay in which he came to the insightful conclusion that artificial ventilation [using bellows] has the possibility to injure, stating “the lungs of one man may bear, without injury, as great a force as those of another man can exert; which by the bellows cannot always be determined” (49). While the advent of artificial mechanical ventilation has been a crucial development in critical care medicine, and it is currently the mainstay of treatment for patients with ARDS, it is also very clear that mechanical ventilation itself produces a form of lung injury known as ventilator-induced lung injury (VILI). Over the past few decades of its use, our understanding of the mechanisms by which it exacerbates lung injury has improved. The major factors that are thought to be involved in producing VILI can be broadly broken down into physical forces – which includes barotrauma, volutrauma, and atelectrauma – and biological forces – biotrauma.

1.2.1 Mechanisms of VILI

Barotrauma

The manifestation of lung injury, including alveolar rupture, air leaks, and gross barotrauma (e.g. pneumothorax, subcutaneous emphysema, pneumomediastinum), as a consequence of high airway pressures during positive pressure ventilation has been well-documented for many decades and has been collectively termed “barotrauma”. In 1944, Macklin and Macklin were the first to describe the mechanisms leading to barotrauma (or as they referred to ‘pneumomediastinum’) (50). They noted that the close apposition of the alveoli to the bronchovascular sheath made the membrane susceptible to tears following transient increases in the pressure gradient between the alveoli and the vessel sheath as alveolar pressure increases at high lung volumes. Air was then able to leak out into the interstitial tissues, subcutaneous tissue and retroperitoneum, resulting in a pneumothorax.

While ventilation at high airway pressures can lead to VILI, manifesting as barotrauma (alveolar rupture, air leaks, pneumothorax, etc), we now know that it is not high absolute airway pressures that leads to injury. Instead, the critical variable is regional lung overdistention, and this is determined by the transpulmonary pressure (alveolar pressure – pleural pressure).

Volutrauma

In a classic experiment, Webb and Tierney were the first to demonstrate that ventilation of rats with very high peak pressures (leading therefore to lung overdistension) and no positive end-expiratory pressure (PEEP) could lead to pulmonary oedema, a more subtle form of lung injury than gross barotrauma, alongside a clinical presentation of severe hypoxemia, decreased lung compliance, and, in the most severe cases, death (51). These findings were subsequently replicated by many investigators (52-55), who have also further clarified that the pulmonary oedema induced by mechanical ventilation is a result of increased alveolar-capillary permeability associated with diffuse alveolar damage as opposed to a hydrostatic mechanism initially postulated by Webb and Tierney.

In 1988, Dreyfuss et al elegantly demonstrated that lung volume (i.e. lung stretching) and not airway pressure was the variable responsible for the development of pulmonary oedema (56). Through ventilating rats with three strategies: (1) high pressure and high volume; (2) low pressure and high volume – delivered by a negative pressure ventilator; and (3) high pressure and low volume – achieved by binding the thorax and abdomen, they demonstrated that lung water was increased only where high volumes were delivered. Ventilation of animals with high end-inspiratory airway pressures but low tidal volumes achieved by limiting lung expansion through thoraco-abdominal strapping did not induce any detectable pulmonary oedema. These experiments demonstrated that alveolar distension rather than pressure itself was the key determinant of lung injury. To underscore the importance of volume instead of pressure

when assessing the risk of VILI, they coined the term ‘volutrauma’ to replace barotrauma. They reiterated the need to consider the degree of regional alveolar distension instead of absolute pressures or volume as the heterogenous states of lungs (healthy, recruitable, and diseased unresponsive) in ARDS makes it especially vulnerable to overdistension injury (57).

The heterogenous states of pre-injured ARDS lungs was first appreciated by Gattinoni and Pesenti following quantitative assessment of thoracic computed tomography (CT) images of 68 patients with ARDS (58). What was previously considered to be a “homogenous lung” on anteroposterior radiography was shown to be non-homogenous on CT, with the densities (non-aerated, collapsed or consolidated lung) primarily in the dependent regions. In patients with severe ARDS, only 300-500 g of tissue was found to be normally aerated. This reduced volume of lung available for gas exchange was roughly the equivalent of the size of a 5 year old child’s lung, leading to the concept of the “baby lung”. From this perspective, it was easy to understand why ARDS patients are at risk of VILI: the ventilator delivers a set tidal volume calculated according to the patient’s weight and height to a disproportionately small lung volume, resulting in significant deformation even when what would typically be considered moderate or low tidal volumes are applied. Ironically, it is the aeratable areas of healthy lungs that are damaged by the ventilator.

Atelectrauma

At the other end of the spectrum, lung injury can also occur when ventilating with low tidal volumes due to “atelectrauma”. This form of injury is characterised by epithelial disruption, hyaline membrane formation, pulmonary oedema and hypoxia (59). It occurs due to repetitive opening and closing of airways and alveoli units (59), inhibition of surfactant production and/or depletion of surfactant from alveoli (60), and the incidence of large cyclic stretching forces in regions interfacing between over-distended lung units and collapsed and consolidated lung (61). The shear forces generated by repeated recruitment and decruitment of lung units

causes structural damage to the epithelial and endothelial barriers, leading to leakage of fluid into the alveolar space.

Biotrauma

Not until more recently have we begun to appreciate that the deleterious effects caused by mechanical ventilation could extend beyond physical disruption of the lungs. In the absence of macro- and microscopic lung damage, Slutsky et al have proposed that mechanical ventilation can still induce molecular and cell-mediated events and coined the term “biotrauma” to encapsulate this hypothesis (62). This hypothesis consists of two independent components: firstly, that ventilation leads to the release of various mediators; secondly, that these mediators have physiological and clinical significance during VILI. The hypothesis postulates that the release of these mediators can cause local lung injury (promoting leukocyte recruitment in the lungs and initiating local inflammatory processes), and if they translocate into the systemic circulation, can affect systemic inflammation leading to distal organ dysfunction (63).

One of the earliest studies supporting the first component of this hypothesis was conducted by Kawano et al (64). Using a rabbit model of surfactant deficiency (achieved through repetitive saline lung lavage), they noticed that in response to mechanical ventilation, animals soon became hypoxemic. Post-mortem examination of lungs showed extensive hyaline formation and infiltration of lungs with granulocytes. To investigate the potential contribution of these marginated cells, neutrophils were depleted from some animals with nitrogen mustard prior to lung lavage. In striking contrast to their counterparts, these neutrophil depleted animals maintained good gas exchange, demonstrated only a small amount of protein leak into the lungs, and did not show pathological hyaline membrane formation. Repletion of granulocytes from donor rabbits quickly caused deterioration in these animals. From these findings, it was concluded that granulocytes released mediators including oxygen free radicals, proteases and products of arachidonic acid metabolism (mediators that we now recognise as endogenous

danger molecules, otherwise termed alarmins or damage-associated molecular patterns (DAMPs)), propagating lung injury (65, 66).

Tremblay and Slutsky were of the first to provide evidence suggesting that inflammatory injury may also occur in previously healthy lungs, and that the degree of inflammation can be modulated with different modes of ventilation (67). Using an *ex vivo* isolated lung model, they ventilated lungs for two hours using four different ventilator strategies (1: PEEP 3 cm H_2O + V_T 7 mL/kg; 2: PEEP 10 cm H_2O + V_T 15 mL/kg; 3: PEEP 0 cm H_2O + V_T 15 mL/kg; 4: PEEP 0 cm H_2O + V_T 40 mL/kg). In the group subjected to high V_T with no PEEP, they noticed a large increase in lung lavage cytokines including TNF-α, IL-1β, MIP-2, IL-6, IFN-γ and IL-10. By performing *in situ* hybridisation, they were able to localise the production of TNF-α and IL-6 to the airways and alveolar epithelium. In conjunction, they also detected an increase in *c-fos* messenger RNA (an early response genes), suggesting that mechanical forces applied to cells were transduced to a biochemical response, causing the activation of downstream inflammatory pathways.

Since these two studies, multiple experimental studies using *in vivo* and *ex vivo* models have reported upregulation of several cytokines in serum and bronchoalveolar lavage fluid in response to mechanical ventilation in both healthy and injured lungs (68-74). The most frequently implicated cytokines include IL-8 or its rodent equivalent MIP-2, TNF-α, IL-6, and IL-1β. Generally, the increase in cytokine levels is most pronounced when animals are subjected to more injurious ventilation strategies (larger tidal volumes or zero PEEP) or when a two-hit model is used (e.g. mechanical ventilation on top of another injurious stimuli such as hyperoxia (70)).

Data from clinical studies also supports the hypothesis that mechanical ventilation does influence pulmonary and systemic cytokine levels. An early randomised control trial conducted

by Ranieri et al tested this hypothesis by randomly allocating 44 patients to either 'protective' or 'standard' ventilation strategies, and found that the protective group which had received lower tidal volumes and higher PEEP had significantly lower concentrations of several inflammatory cytokines in plasma and BAL (75). This was accompanied by reduced neutrophil infiltration into the alveolar space, as assessed by BAL neutrophil counts, and a significant lower incidence of organ failure, with renal failure being the most prevalent organ dysfunction (76). Results from the ARDS Network trial (discussed further below) also showed than plasma levels of IL-6 were lower in patients who were ventilated with lower tidal volumes compared with traditional tidal volumes (77). The number of days without non-pulmonary organ or system failure (circulatory, coagulation and renal failure) was significantly higher in the group treated with lower tidal volume. In longitudinal studies, patients that present with persistent elevated levels of pro-inflammatory cytokines suggestive of ongoing inflammation tend to have more severe lung injury and are less likely to survive (78).

Perhaps somewhat surprisingly, several *in vivo* mouse studies have also detected cytokine release even in response to low tidal volume ventilation (5-8 mL/kg with PEEP 2-4 cmH_2O), suggesting that ventilation with clinically relevant "protective" strategies still induce an inflammatory response in absence of pre-existing lung injury (79-81). However, in these studies, the controls used were non-ventilated or spontaneously breathing animals. This makes results somewhat difficult to interpret as the experiments failed to control for other potential confounding factors that could have also caused an inflammatory response, including the invasive surgical procedures, anaesthesia, ventilation in a supine position, and atelectasis and inadequate oxygenation associated with low tidal volumes.

Nevertheless, there are results from pilot clinical studies which suggest that ventilation at low tidal volumes still induces an inflammatory response. The introduction of extracorporeal CO_2 removal has enabled the use of even lower tidal volumes than in a 'normal' lung protective

ventilation strategy. In two studies where patients were ventilated with an ultra-low tidal volume (~3 mL/kg instead of 6 mL/kg), they were found to have significantly reduced concentrations of pulmonary inflammatory cytokines, including IL-6, IL-8, and IL-1β (82, 83). These findings therefore suggest that whilst implementation of protective ventilation strategies (i.e. reducing tidal volume, applying PEEP) is crucial to reducing the risk of VILI, it does not fully address the inflammatory responses inherently associated with mechanical ventilation.

While the "biotrauma" hypothesis has been gaining traction since its proposal with an accumulating amount of evidence supporting the notion that ventilation or mechanical stretch leads to cellular activation and mediator release, some remain sceptical regarding the involvement and biological relevance of cytokines during VILI (84). These investigators highlight the inconsistencies within and between studies and cite evidence that demonstrates their production even with non-injurious ventilation to suggest that cytokine changes are merely a by-product of lung overdistension (72, 84, 85).

In response to these contentions, a number of explanations for these conflicting results have been proposed including: (1) differences between models – *in vivo*, *ex vivo*; (2) different ventilator strategies; (3) different species/strains; (4) different time points; (5) variation in severity of resulting lung injury; (6) endotoxin contamination of experimental subjects; (7) different assay reagents with different sensitivities, endogenous proteases, presence of inhibitors, etc (86).

For instance, to address the variability in what has previously been shown with TNF-α, Wilson et al performed an *in vivo* study in which they demonstrated that upregulation of intrapulmonary cytokines TNF-α and MIP-2 preceded signs of apparent lung injury, therefore implicating these cytokines as a mediator of injury rather than a consequence (87). Crucially, this study was the first to appreciate the transient nature of TNF-α upregulation during the

course of VILI; intra-pulmonary TNF-α peaked early in the course of injury for a relatively short period of time before rapidly declining to baseline levels. In contrast, the increase in MIP-2 was sustained for the entire duration of injury. These findings may therefore help to reconcile the controversial findings surrounding TNF-α in previous studies and provides further insight into why MIP-2 has more consistently been found to be increased in VILI models.

Furthermore, cytokine inhibition studies also add further support to the assertion that cytokines play a critical role during the pathogenesis of VILI. In a study conducted by our research group in 2005, we reported that both acute (administration of anti-TNF antibodies) and chronic inhibition (TNF receptor double knockout animals) of TNF signalling, led to a significant reduction (40% and 70% respectively) in the degree of intra-alveolar neutrophil infiltration following injurious high tidal volume ventilation (88). At that time, these findings were the first to provide direct evidence that TNF signalling plays a critical role in pulmonary inflammatory responses induced by high-stretch ventilation even in the absence of underlying lung injury. In another study, Belperio et al similarly found that inhibition of KC/CXCL1 and MIP-2/CXCL2/3 (using specific antibodies) or their shared receptor CXCR2 (using anti-CXCR2 antibodies or $CXCR2^{-/-}$ mice) during high-stretch ventilation protocol also resulted in significant reductions in neutrophil sequestration as compared with vehicle controls (89). Furthermore, inhibition of CXCR2 was also associated with decreased vascular permeability, pulmonary oedema, and alveolar haemorrhage. These findings support the contention that chemokines/cytokines, specifically CXCR2 and CXCR2 ligands in this study, do mediate neutrophil recruitment to the lungs and contribute to the pathogenesis of VILI.

Multi-organ failure

In patients with ARDS, clinical outcomes are mostly related to non-pulmonary factors, with the most common cause of death being multiple organ dysfunction and sepsis. Surprisingly, respiratory failure is responsible for death in only a small minority of cases (90-92). The

biotrauma hypothesis offers an explanation for this observation. It proposes that ventilation-induced pulmonary production of inflammatory mediators can also translocate into the systemic circulation, evidenced by the increase in plasma cytokine levels following injurious ventilation, contributing to distal organ dysfunction (75-78).

Another mechanism that is thought to be important in the development of multiple organ dysfunction is the translocation of bacteria or bacterial products (e.g. endotoxin) from the alveolar space into the systemic circulation. Mechanical ventilation is known to cause increase alveolar-vascular permeability and is thought to contribute to this 'decompartmentalisation' – a dissemination of injury from the lung to distal organs, resulting ultimately in multi-organ failure (93-95). This theory has been demonstrated in two animal models (95, 96). Murphy et al intratracheally instilled endotoxin into the lungs of rabbits that were subsequently subjected to either protective or non-protective mechanical ventilation. They observed a translocation of endotoxin into the circulation following non-protective ventilation (V_T: 15 mL/kg with PEEP 0 cmH_2O) but not protective ventilation (95). This increase in plasma level of endotoxin was also found to be significantly higher in non-survivors compared with survivors, suggesting that this process is actually pathological and contributes to worse clinical outcomes. Similarly, Nahum et al also demonstrated that injurious mechanical ventilation strategies that promote alveoli overdistension facilitate bacterial translocation into the bloodstream in dogs (96). When PEEP was applied, theoretically ameliorating any repetitive opening and collapsing of alveoli, the degree of bacteraemia and histologic indices of lung injury were significantly decreased. These findings provide further evidence to suggest that disruption of lung structures does lead to its increased permeability, facilitating the dissemination of inflammatory products from the lungs into the systemic circulation.

1.2.2 Management of VILI: Ventilatory strategies

With the recognition of the potential of mechanical ventilation to cause harm, there has also been an increasing amount of focus directed towards minimisation of this iatrogenic injury. To date, all the methods that have been proven to reduce mortality in ARDS revolve around minimising the deleterious effects of ventilation. This has been achieved by the implementation of various lung protective ventilation strategies.

Tidal volume

In 2000, the landmark ARDS Network randomised controlled trial demonstrated that lowering tidal volumes from previously conventional tidal volumes of 12 mL/kg predicted body weight (PBW) and maximum plateau pressure of 50 cmH_2O to 6 mL/kg PBW with a maximum plateau pressure of 30 cmH_2O led to a significant reduction of mortality rates from 39.8% to 31.0% (77). Since this trial, the importance of lowering tidal volumes and airways pressures to prevent regional lung overdistension is now universally recognised and accepted.

Although the use of lower tidal volumes undoubtedly reduces mortality in ARDS patients, scaling tidal volume to PBW targets assumes patients have aerated lung volumes of a healthy adult. We know, however, that this is not true. From the baby lung principle, we know that the ARDS lung is non-uniformly aerated, with large areas consolidated with oedema and inflammation. Thus, it is of significantly smaller volume than a normal, healthy lung. However, although it is known that lung volumes are reduced, the magnitude of reduction can differ widely from one patient to another, resulting in heterogeneity in volumes available for ventilation. A study conducted by Terragni et al demonstrated that the protective ventilatory strategy proposed by the ARDS Network trial may not be protective in all patients due to this issue – the heterogeneity in the size of the aerated lung (97). In a study of 30 patients, over one-third still experienced substantial tidal hyperinflation when ventilated with tidal volumes of 6 mL/kg PWB and a maximum plateau pressure lower than 30 cmH_2O. Tidal hyperinflation

was also independently associated with higher concentration of inflammatory mediators (IL-6, IL-1β, IL-8, TNF-α) and lower numbers of ventilator-free days, suggesting that even with lung protective ventilation strategies, lung injury still occurs. The authors noticed that plateau pressures in these patients were between 28-30 cmH_2O compared to 25-26 cmH_2O in patients that did not experience over-inflation and proposed that further limited plateau pressures might be important.

A number of strategies to optimise the delivery of tidal volumes have been proposed and explored. One that has been garnering attention over the last few years is driving pressure. Driving pressure is the ratio of tidal volume to static respiratory system compliance (98). It can be calculated at the bedside as plateau pressure minus PEEP, allowing tailoring of ventilation according to patient-specific mechanics (98). This strategy was first proposed by Amato et al who conducted a retrospective analysis of 9 randomised control trials and found that among ventilation strategies, driving pressure was the strongest predictor of mortality whereas individual changes in tidal volumes or PEEP were not independent associated with survival (98). However, the use of driving pressure has not been formally evaluated in a randomised control trial; there are currently a number of ongoing trials that should provide further insight into the potential benefits of it.

PEEP

PEEP is routinely used in combination with low tidal volumes (a ventilatory strategy termed the ‘open lung approach’ to ventilation) to prevent collapse of distal alveoli and to maintain alveolar recruitment. Ideally the optimal level of PEEP would high enough to maintain the appropriate level of pressure at the end of expiration such that cyclic recruitment and collapse of distal airspaces is prevented but not too high that tidal overdistension occurs (99, 100).

However, the optimal level of PEEP is difficult to determine as it depends on the recruitability (i.e. amount of lung tissue that can be inflated with higher levels of PEEP, restoring aeration) of an individual patient's lung and this has been shown to be extremely variable (101-103). Patients with highly recruitable lungs are more likely to be "PEEP responsive" and are likely to show improved oxygenation when ventilated with higher levels of PEEP. This is because an increase in PEEP effectively increases the amount of tissue available for gas exchange and promotes alveolar stability. However, in patients with less recruitable lungs, a high PEEP is likely to contribute to VILI. Any applied PEEP that fails to open collapsed or oedematous lung will inevitably injuriously over-distend already aerated lung units, effectively replicating the effects of excess tidal volume ventilation.

To date, no multi-centre clinical trial has shown any one PEEP titration strategy achieves better clinical outcomes (104-106). A systematic review and meta-analysis of the data acquired from these three clinical trials suggests that higher levels of PEEP were associated with improved survival in moderate or severe ARDS but not in patients with mild ARDS (107). As of 2017, the ATS/ESICM/SCCM guidelines conditionally recommend the use of higher rather than lower PEEP in adults with moderate or severe ARDS. However, it also encourages clinical judgement based on the individual patient, e.g. higher PEEP in patients with obesity, lower PEEP in patients with obstructive airway disease (108).

Unfortunately, there is no consensus on the ideal method of determining optimal PEEP level. An oesophageal pressure-guided PEEP titration strategy was initially found to be promising in a single-centre study but the follow up phase 2 randomised clinical trial (Esophageal Pressure-Guided Ventilation 2 [EPVent2]) failed to detect any significant differences in death and days free from mechanical ventilation between an empirical high PEEP and oesophageal pressure-guided PEEP strategy (109, 110). Other methods based on lung mechanics or imaging have been proposed and will need to be evaluated in future studies (111). Developing and validating

tests to assess lung recruitability may also be helpful for identifying patients who are likely to be “PEEP responders” and are most likely to benefit from higher PEEP (112, 113).

Recruitment manoeuvres

Recruitment manoeuvres (RMs) are procedures that transiently increase transpulmonary pressure and are designed to re-inflate collapsed alveoli. This can reduce atelectasis and increase the volume of lung available for tidal ventilation (114). However, studies investigating the use of RMs have yielded mixed results and the role of RMs in routine practice therefore remains controversial (107, 115, 116). A systematic review of 6 randomised control trials investigating the use of RMs in patients with moderate-severe ARDS found that lung RMs in combination with a higher PEEP ventilation strategy was associated with a reduction in mortality. However, their confidence in this finding was limited. Not only was the characteristics of the lung RMs widely variable across trials, 5 of the 6 trials included a higher PEEP ventilation strategy as a co-intervention making it impossible to evaluate the effect of RMs in isolation (117).

High-Frequency Oscillatory Ventilation

High-frequency oscillatory ventilation (HFOV) has also been investigated as a novel mechanism of alveolar ventilation as it permits very small tidal volumes to be delivered, theoretically limiting the risk of over distension. Unfortunately, two large multi-centre trials have demonstrated that it has no impact on patient outcomes (51,52). One multi-centre randomised control trial has even reported that use of HFOV may be associated with increased in-hospital mortality (118). Thus, due to the lack of benefit and even potential for harm, HFOV is currently not recommended for routine use in patients with moderate or severe ARDS.

1.2.3 Management of VILI: Adjunctive therapies

Prone positioning

Prone positioning is another strategy that has been used to improve oxygenation and lung recruitment in ARDS. Proning changes the regional distribution of transpulmonary pressure, which decreases regional heterogeneity of lung aeration, thus improving ventilation-perfusion matching (by increasing blood flow to the dependent lung), reducing atelectasis, and increasing end-expiratory lung volume (119).

Gattinoni et al were the first to suggest the prone positioning improves oxygenation and reduces mortality in the subgroup of severely hypoxemic patients (120). Since then, there have been multiple conflicting randomised control trials. However, a patient-level meta-analysis of four major clinical trials conducted in 2010 demonstrated that prone positioning clearly leads to a reduction in absolute mortality of patients with severe ARDS (120). This has been subsequently confirmed by the Proning Severe ARDS Patients (PROSEVA) trial which demonstrated that patients that were proned early in the course of their disease and for at least 16 hours a day showed significantly lower rates of mortality compared with the supine group (28-day mortality 16% vs 32.8%) (121). Long sessions (>12 hours) of prone positioning are now recommended in most adult patients with severe ARDS (108).

Neuromuscular blockade

Even while sedated, ventilated patients with ARDS often show strong respiratory effort due to the high respiratory drive (11). This results in patient self-inflicted lung injury (P-SILI), an emerging concept whereby intense inspiratory efforts by spontaneously breathing patients can lead to exacerbation of lung injury (122, 123). This can occur in both ventilated and unventilated patients. In patients that are receiving ventilatory support, patient-ventilator dyssynchronies generates excessive transpulmonary pressures by inspiratory efforts and de-recruitment by expiratory efforts, causing increased mechanical lung injury from

overdistension and atelectasis (124, 125). Muscle paralysis with neuromuscular blocking agents may help prevent these effects. In a multi-centre trial, 340 patients with severe ARDS were randomly assigned to received either cisatracurium or placebo within 48 hours of symptom onset. Patients in the cisatracurium group had improved 90-day survival rates and increased ventilator-free days without increasing muscle weakness compared with the placebo group (126). However, a recently published follow-up multi-centre trial (Re-evaluation Of Systemic Early Neuromuscular Blockade [ROSE]) designed to re-evaluate the findings of the initial trial compared cisatracurium with deep sedation to usual-care management without neuromuscular blockade and with light sedation found no significant difference in the primary endpoint of mortality at 90 days between the groups (127). Authors of the second study have proposed that the use of a higher PEEP strategy than the previous trial in both intervention and control groups might have reduced mortality, blunting the potential treatment effect of neuromuscular blockade. Overall, the benefits of early continuous neuromuscular blockade in ARDS patients remain unclear and will require further investigation.

Surfactant administration

Pulmonary surfactant dysfunction may contribute to the pathophysiology of VILI. An early study conducted by Gunther et al analysed BAL fluid of patients with ARDS for surfactant abnormalities (128). They found that in comparison with healthy controls, surfactant from ARDS patients had marked disturbances of biophysical (increased minimal surface tension) and biochemical (decrease alveolar phospholipid content, surfactant protein-A concentration) properties, which is thought to promote alveolar collapse, and subsequently exacerbate shunting and hypoxemia, and induce oedema formation.

It was therefore hypothesised that administration of exogenous surfactant might confer protection against VILI. Evaluation of its efficacy has been performed in a number of experimental models. In some studies, administration of surfactant was found to reduce

deterioration of lung mechanics, improve oxygenation, reduce alveolar permeability, and even prevent systemic spill over of inflammatory cytokines (129, 130). However, others have failed to replicate these findings (131), with some even suggesting that surfactant treatment may exacerbate the inflammatory response in an injured lung (132). While surfactant therapy in paediatric patients has been consistently associated with increased survival and improved oxygen index (133, 134), trials evaluating the use of aerosolised surfactant in adults with ARDS have been disappointing in comparison. Most fail to show any improvements in survival or clinical outcomes (135-138).

Extracorporeal membrane oxygenation

In patients with severe ARDS, veno-venous extracorporeal membrane oxygenation (VV-ECMO) has been proposed as a rescue therapy. VV-ECMO is a treatment in which blood is circulated outside of the body for oxygenation on a gas-permeable membrane (11). Its use gained momentum following promising results in the 2009 publication of the UK CESAR prospective randomized trial (139). Patients assigned to ECMO had a significantly lower 6-month mortality or severe disability compared with those receiving conventional treatment (37 vs 53%). Despite significant limitations of the trial – not all patients in the ECMO group received ECMO and heterogenous ventilation strategies in the control group – this trial led to renewed interest in ECMO worldwide.

This interest in ECMO as a rescue therapy was boosted during the 2009 influenza A H1N1 virus epidemic. Case series reports from Australia, New Zealand and Italy suggested that patients receiving ECMO had a 70-80% survival rate (140, 141). In a UK cohort study, hospital mortality of ECMO-referred H1N1-related ARDS patients with matched patients who were not referred for ECMO was significantly reduced (23.7% vs 52.5%), providing further evidence to support the assertion that ECMO was advantageous to conventional mechanical ventilation (142).

However, the efficacy of routine use of ECMO was later called into question by Combes et al in 2018 who conducted an international, randomised trial specifically designed to address weaknesses of previous ECMO trials (143). In contrast to previous findings, Combes et al reported that the primary end point of 60-day mortality in patients receiving ECMO was not significantly lower than patients receiving conventional mechanical ventilation. However, the interpretation of these negative results was complicated by its own limitations. Firstly, there was a 28% cross over rate from control to ECMO group due to refractory respiratory failure and deteriorating haemodynamics which may have diluted the potential effect of ECMO. Secondly, the trial was halted after 75% of full enrolment and thus may have been underpowered to detect lower mortality rate in ECMO group.

At present, it appears that routine use of ECMO in patients with severe ARDS does not appear to confer any benefit. Thus, ECMO should be reserved as a rescue therapy for patients who continue to deteriorate despite use of all other evidence-based interventions (144).

Extracorporeal CO_2 removal

Extracorporeal CO_2 removal ($ECCO_2R$) is another rapidly evolving rescue therapy that has been proposed for use in conjunction with very low tidal volume (V_T; 3-4 mL/kg predicted body weight) mechanical ventilation (145). While reducing V_T (conventionally to 6 mL/kg predicted body weight) in ARDS to prevent regional overdistension is known to lead to better patient outcomes, the extent to which tidal volume can be reduced is limited by the resultant hypercapnia and severe respiratory acidosis (145). By facilitating CO_2 removal from venous blood using an extracorporeal gas exchanger, $ECCO_2R$ reduces the intensity of ventilatory support required, enabling the use of these so-called ultra-protective ventilation strategies. Use of this strategy was associated with a significant decrease in pulmonary inflammatory biomarkers in bronchoalveolar lavage and plasma in pilot trials in humans, suggesting a

further reduction in inflammation beyond that achieved with conventional protective ventilation strategies (82, 83). Findings from the recently published Strategy of Ultraprotective Lung Ventilation with Extracorporeal CO_2 Removal for New-Onset Moderate to Severe ARDS (SUPERNOVA) trial suggest that the use of $ECCO_2R$ to facilitate ultra-protective ventilation (V_T: 4 mL/kg) in patients with moderate ARDS is both feasible and safe (146). However, because $ECCO_2R$ is relatively invasive with its own risks, it is important that the benefits outweigh these risks. At present there is a paucity of high-quality evidence to show the use of $ECCO_2R$ leads to a reduction in mortality or other important clinical outcomes (147). Results from the ongoing Protective Ventilation with Veno-Venous Lung Assist in Respiratory Failure (REST) trial (ClinicalTrials.gov Identifier no: NCT02654327) will hopefully provide further insight.

1.2.4 Management of VILI: pharmacological interventions

While lung-protective ventilation strategies may mitigate lung injury, they do not completely prevent it; mechanical ventilation can still promote inflammation, resulting in biotrauma. As such, there is a need to develop alternative measures that will allow clinicians to limit the deleterious effects while patients are unavoidably exposed to the stimulus of ventilation. Pharmacotherapies aimed at mitigating the inflammatory component of VILI have always been an attractive approach. With VILI, clinicians have the unique opportunity to administer a pharmacological intervention before the inciting cause of injury (mechanical ventilation) is commenced and potentially completely prevent any downstream consequences. Incidentally, this approach is particularly promising as the aeratable regions, which are the most susceptible to VILI, are also the most accessible for drug delivery.

To this end, many different pharmacological interventions targeting different aspects and pathways involved in VILI have been assessed in experimental models. Some specific areas that have been targeted include: alveolar-capillary barrier permeability through blockade of

stretch-activated cation channels (148) and β-adrenergic agonists (149, 150); inhibition of inflammatory signalling pathways with anti-TNF-α antibodies (151) and mediators involved in the NF-κB pathway (152); mitogen-activate protein kinase (MAPK) pathway (153, 154); mesenchymal stem cell therapy (155, 156); manipulation of hormonal and metabolic pathways such as inhibition of 3-hydroxy-3-methylglutaryl coenzyme A reductase (statins) to reduce inflammation (157, 158), and inhibition of the renin-angiotension system with angiotensin-converting enzyme inhibitor or angiotensin receptor antagonist (159, 160).

However, despite many of these pharmacological interventions showing promising results in experimental models, none of them have shown efficacy in subsequent phase II and phase III clinical trials (161). Understandable, this overwhelming failure rate has been disappointing and frustrating for many involved in this area of research; a lot of effort has been made to identify explanations for this repeated failure to translate therapeutics. It is believed that one of the main reasons for this stark failure rate is the clinical and biological heterogeneity among ARDS patients. Multiple different aetiologies (including aspiration, sepsis, trauma) lead to the same set of symptoms which is collectively recognised and diagnosed as ARDS. It is likely that each aetiology is likely to have different pathologies despite a shared endpoint.

Following the lead of other areas of medicine where diseases also display the same heterogeneity (e.g. cancer) and patients are routinely offered targeted therapy based on identification of biological distinct subtypes of diseases, further investigation into a more precise approach has been conducted.

In 2014, Calfee et al acquired clinical and biological data from 1,022 patients previously enrolled in two large randomised control trials – ARMA and ALVEOLI – and applied latent class modelling to identify subphenotypes (162). In both patient cohorts, they identified two different subphenotypes: a hyperinflammatory and a hypoinflammatory subphenotype. The

hyperinflammatory subphenotype was characterised by higher plasma concentration of inflammatory biomarkers (including IL-6, IL-8, soluble TNF receptor-1, plasminogen activator inhibitor-1), lower systolic blood pressure, lower serum bicarbonate concentration, and a higher prevalence of sepsis than the hypoinflammatory subphenotype. Patients that fell under the hyperinflammatory category also had worse clinical outcomes – higher mortality, fewer ventilator-free days, and organ failure free-days. Interestingly, when the response to treatment in the ALVEOLI cohort (low PEEP vs high PEEP) was assessed for each phenotype, the authors found differences in the response to treatment, suggesting that identification of subphenotypes might be an important consideration for future trial design.

Indeed, further support for use of a predictive enrichment strategy was garnered by the study recently published by the same authors who performed a secondary analysis of data from the HARP-2 trial which investigated the effects of simvastatin in ARDS patients (163). While the initial study failed to demonstrate any difference in 28-day survival between placebo and simvastatin (42), latent class analysis found that patient with a hyperinflammatory sub-phenotype who received simvastatin actually had significantly improved survival at both 28-days and 90-days compared with those given placebo (163).

1.2.5 Identifying alternative therapeutic targets for VILI

In an attempt to identify alternative therapeutic targets for VILI, our group recently conducted a study in which we first identified sub-populations which appeared to possess ‘natural resistance’ to VILI and then tried to pin-point specific mechanisms which afforded them these advantageous characteristics (164). The protective phenotype we chose to focus on was obesity. Although obesity is implicated with increased susceptibility to development of ARDS, subsequent mortality has been shown to be decreased (165, 166). In 2015, a study conducted by Sasabuchi et al reported that an increased body mass index is associated with low mortality in patients who were mechanically ventilated (167).

Using an obese (high fat feeding) mouse model, we demonstrated that obesity did confer protection against development of VILI; when subjected to high tidal volume ventilation, obese mice displayed lower peak inspiratory pressure, improved respiratory mechanics and gas exchange, and less alveolar-epithelial permeability compared with lean control mice (164). Interestingly however, this protection was not due to alterations in classical inflammatory cytokines/chemokines, including TNF, IL-6, CXCL1, or in lung leukocyte (neutrophils and monocytes) recruitment. Instead, a novel mechanism whereby fat-feeding blunted stretch-induced upregulation of CD147 was identified. Alongside this decrease in CD147 expression on the surface of alveolar epithelial cells, obese mice displayed significantly lower levels of matrix metalloproteinases (MMPs) activity. Although a direct link between CD147 and subsequent MMP activity was not demonstrated in this study, CD147 on epithelial and endothelial cells has been directly linked to ventilator induced MMP activation (168, 169). Thus, it is highly plausible that the same stretch-CD147-MMP pathway was involved.

1.3 CD147

The cluster of differentiation 147 (CD147), also known as Extracellular Matrix Metalloproteinase Inducer (EMMPRIN) or basigin (bsg), is a widely expressed type 1 transmembrane glycoprotein that is a member of the immunoglobulin (Ig) superfamily (170). It was first described in 1982 by Biswas as a 'tumour cell-derived collagenase stimulatory factor' expressed on the surface of lung carcinoma cells, which upon interaction with fibroblasts, stimulated the expression and production of matrix metalloproteinases (MMPs) (171). In the next decade, CD147 was identified and independently characterised by a number of different research groups across different species and tissue, accumulating a number of different names, including: antigens RET-PE2, gp42, 5A11, human leukocyte activation-associated antigen M6, and blood group Ok^a antigen; CE9, OX-47, bsg, tumour cell collagenase-stimulatory factor, HT7, neurothelin, and EMMPRIN (172-183). In 1995, analysis of the amino acid sequence of CD147 revealed that it identical to that reported for all these supposedly unique molecules, confirming that all these proteins were in fact the same (184). They are now commonly termed CD147 or extracellular matrix metalloproteinase inducer (EMMPRIN).

1.3.1 The CD147 gene

In humans, CD147 is encoded by the *BSG* gene located on chromosome 19p3.3 (185). The CD147 gene consists of 10 exons spanning roughly 15,000 nucleotides. It is transcribed into four different mRNA variants through alternative promoters and splicing (186-188), resulting in four protein isoforms: CD147/Bsg-1, -2, -3, and -4 (Figure 1.1) (189). CD147/Bsg-1 is a retina-specific variant with three Ig domains; CD147/Bsg-2 contains two Ig-like domains; and CD147/Bsg-3 and -4 both contain a single Ig-like domain. CD147/Bsg-2 is the most abundantly expressed splice variant of CD147 and will be referred to as CD147 hereafter.

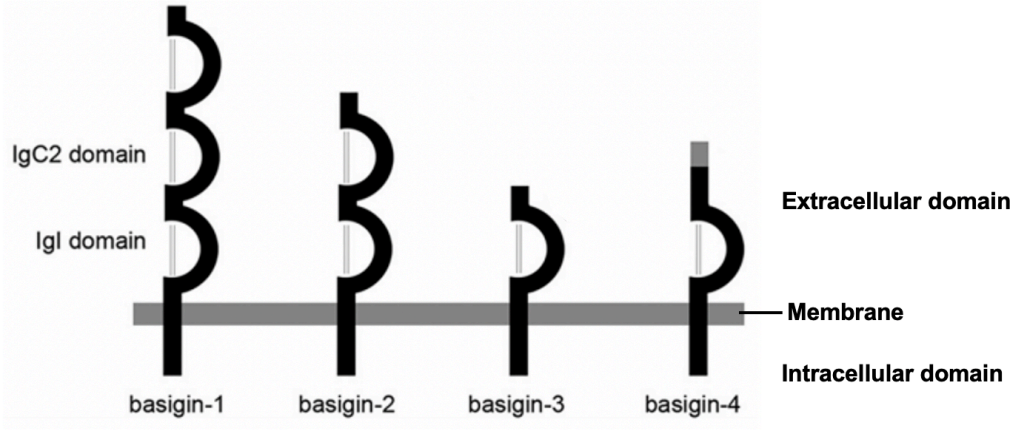


Figure 1.1 - Protein isoforms of CD147/Basigin (Bsg)

Schematic presenting of the four isoforms of CD147 generated by differential splicing and transcription initiation sites. Figure adapted from Liao et al (189).

1.3.2 The structure of CD147

The human CD147 mRNA transcript encodes a 269 amino acid (AA)-long protein that consists of a 21-residue signal sequence, a 186-residue extracellular region that consists two immunoglobulin (Ig)-like domains at the N-terminus; a 21-residue transmembrane hydrophobic domain; and a 41-residue C-terminus intracellular domain (Figure 1.2) (190). CD147 has a predicted molecular mass of 27-29 kDa. However, it can exist at a range of molecular weights ranging from 31 to 65 kDa (171). This variance in size is due to heterogenous N-glycosylation (191).

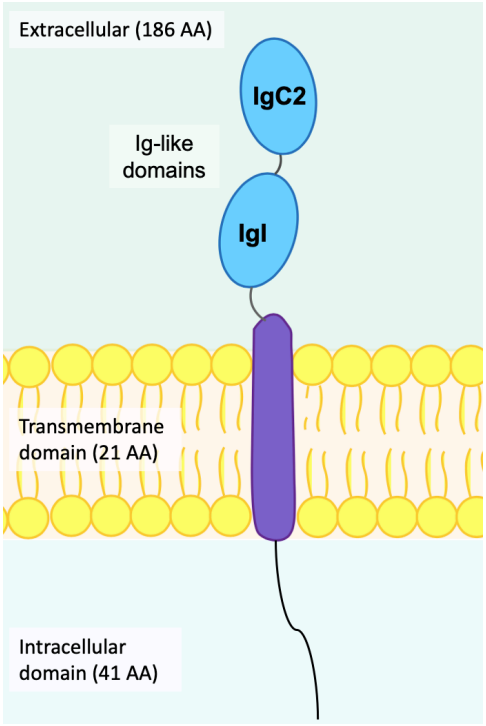


Figure 1.2 - Schematic diagram of CD147.

The CD147 molecule can be broadly divided into three regions: extracellular region spanning 186 amino acids (AA) made up of immunoglobulin (Ig)-like domains IgC2 and IgI; transmembrane domain spanning 21 AA; and a cytoplasmic domain spanning 41 AA. Ig-like domain I is involved in MMP induction.

CD147 can undergo glycosylation at three asparagine *(N)*-glycosylation sites: Asn44 (located within the IgC2 domain) or Asn152 and Asn186 (located within the IgI domain) (179). Broadly, three different glycoforms have been identified: an unglycosylated form with a corresponding molecular weight (MW) of 27 kDa; a low-glycosylated (LG-CD147) form (MW ~32 kDa); and a high-glycosylated (HG-CD147) form (MW ~40-60 kDa) (171). It is believed that the unglycosylated protein is localised to the cytoplasm and represents the pre-cursor form. It then undergoes modification within the endoplasmic reticulum to form the immature high mannose LG-CD147 before further glycosylation to yield the mature, fully glycosylated HG-CD147 that is translocated to the plasma membrane for surface expression. However, whether full

glycosylation is a prerequisite for surface expression remains to be determined; studies conducted on different cell types appear to yield contradictory results with some claiming that both HG- and LG-CD147 can be detected on the plasma membrane (191), while others maintain that only HG-CD147 is present (190, 192).

One of its earliest ascribed roles, and perhaps most widely investigated, is MMP induction. This has been attributed largely to the N-terminus Ig-like C2 domain, which allows CD147 to self-associate with CD147 expressed on the same cell's surface (*cis*-interactions) and CD147 expressed on other cells (*trans*-interactions) (192, 193). Subsequent dimerisation and/or multimerisation of CD147 promotes MMP induction (194).

Moving towards the C' terminus, the next domain is the Ig-like I domain. This domain mediates heterophilic protein-protein interactions with binding partners including: caveolin-1, integrins, annexin A2, and cyclophilin A (CypA) and B (190, 192). Interactions with the aforementioned proteins have been largely reported in the context of cancer studies where they regulate MMP activity to influence cancer cell migration and invasion (170, 195-197). Of particular interest, CypA:CD147 interactions are believed to play a key role in orchestrating inflammatory processes and promote disease pathogenesis (discussed in further detail below).

The transmembrane domain of CD147 is notable for its unique amino acid sequencing, which contains an acidic glutamate residue within a hydrophobic stretch of amino acid (190). The presence of a charged residue embedded within the lipid bilayer is energetically unfavourable. As such, this structural feature is commonly found in proteins with a proclivity for assembling into complexes which shield the charge in an energetically stable conformation. This is likely responsible for the diverse interactions between CD147 and other proteins.

As yet, no function has been assigned to the cytoplasmic tail. Of note, its presence does not appear to be involved in the transduction of signalling events triggered by CypA:CD147 interactions (198).

1.3.3 Expression and regulation of CD147

CD147 is widely expressed in its various glycoforms on many cell types, including epithelial, neuronal, lymphoid and myeloid cells (190, 199, 200). On a cellular level, CD147 is expressed on the plasma membrane (179, 201), with a tendency to localise at the interface between cells, in sub-cellular vesicular compartments (202, 203), and also in microvesicles or exosomes released from cells (204, 205).

Regulation of CD147 occurs at the level of transcription, translation and cell surface presentation. The mechanisms governing these processes are complex and likely to be dependent on the tissue type. Multiple transcription factors involved in the regulation CD147 expression has been identified, including epithelial-mesenchymal transition (EMT)-associated factors (Snail and Slug), hypoxia-inducible factor-1α (HIF-1α), and specificity protein 1 (Sp1) (170, 206). There is evidence that transcription can also be influenced by methylation of motifs within *CD147* promoter region. In cancer tissue, hypomethylation of the *CD147* promoter Sp1 binding results in increased CD147 expression (193). Following transcription, CD147 may be further regulated by several microRNAs (miRNA), including let-7 (207), *miR-146a (208)*, and *miR-22 (209)*. Additionally, various soluble mediators from growth factors to cytokines and hormones have been shown to be involved in the regulation of CD147 transcription and translation. The growth factors which induce increased CD147 expression include epidermal growth factor (EFG) (210), and transforming growth factor β (TGF-β) (211); Inflammatory mediators include TNF-α, interleukins and prostaglandins (212-214); and sex hormones include progesterone and oestrogen (215-217).

As well as regulation at the level of transcription and translation, CD147 can be controlled at the level of surface expression by various proteins. Monocarboxylate transporters (MCTs) have been identified as an important binding partner of CD147 and interaction between these two proteins appears to be important in their proper expression at the cell surface (218, 219). Another family of proteins that influences CD147 expression is the cyclophilin (Cyp) protein family. Due to their proteins which share peptidyl-prolyl *cis-trans* isomerase (PPIase) activity, the Cyp protein family are known to play an important role in protein folding and protein trafficking in cells. Intracellular interaction between Cyp60 and proline 211 residue of CD147 have been demonstrated to be crucial in the translocation of CD147 to the cell surface (198). Both mutation of this proline residue on CD147 and suppression of Cyp60 using RNA interference led to a downregulation in surface expression of CD147 (198). Cell treated with cyclosporin A, an immunosuppressive drug that binds specifically to cyclophilins and inhibits its activity, have significantly reduced surface expression of CD147 (220).

1.3.4 Functions of CD147 in physiologic and pathologic contexts

The functions of CD147 are diverse and wide ranging. Most of our understanding of the role of CD147 in normal cell physiology comes from studying $CD147^{-/-}$ mice. Knock-out of the CD147 gene has high embryonic lethality rates (221, 222). While embryos show normal development during pre-implantation stages, most die around the time of blastocyst implantation, suggesting that CD147 is crucial in intercellular recognition during the implantation phase (221, 222). Those that do manage to survive till birth tend to die soon after due to interstitial pneumonia (221, 222). The small minority that survives till adulthood remain small and sterile due to arrested spermatogenesis in males, and implantation and fertilisation defects in females (221, 223). Other processes such as lymphocyte response, retinal function, wound healing, and neurological functions also appear to be detrimentally affected (224-227).

One of the most well characterised functions of CD147 is its role as an upstream inducer of MMP. MMPs are enzymes that play a crucial role in maintaining the integrity of the extracellular matrix. The initial characterisation in the 1980s by Biswas described it as a factor shed from the surface of tumour cells that was capable of stimulating MMP-1 production by fibroblasts (228, 229). Since then, CD147 has been shown to be capable of mediating expression and activity of several soluble and membrane-type MMPs (MT-MMP), including MMP-1, MMP-2, MMP-3, MMP-9, MMP-14, MMP-15, MT1-MMP, MT2-MMP (170, 193, 230, 231). It has also been demonstrated that CD147 is not exclusively produced by malignant tumour cells but also by non-malignant cells, including fibroblasts, endothelial cells, macrophages, and epithelial cells (232-234). To date, multiple mechanisms underlying CD147-mediated MMP activity have been described. It appears many factors, including glycosylation status, homophilic or heterophilic protein-protein interactions, all contribute to a facet of MMP regulation (170, 196).

As discussed above, CD147 can exists as three different glycoforms, each differing in the degree of glycosylation. It is believed that the glycosylation status of CD147 regulates its ability to induce MMP. Multiple studies have demonstrated that the non-glycosylated form (27 kDa) has no MMP-inducing activity (194, 235). In contrast, HG-CD147 is consistently able to induce MMP production (194, 236). Whether LG-CD147 does contribute to MMP activity is less certain – some studies suggest it does not, while others do (235-237). Taken together, these data do suggest that the efficiency of MMP induction appears to be more pronounced in higher glycosylated forms.

Interaction of CD147 either with itself (homophilic) or other proteins (heterophilic) has also been shown to determine its ability to induce MMPs. CD147 can homo-dimerise/oligomerise (i.e. interact with another CD147 on the surface of a neighbouring cell) in both *cis* and *trans* fashion dependent on the IgC2 domain (192, 238). This interaction then propagates signals

that facilitates MMP-induction. Inhibition of CD147 dimerisation/oligomerisation using either antibodies which specifically bind to multimerised CD147 or mutant CD147 that can no longer self-associate also led to inhibition of MMP induction (192, 238).

Additionally, CD147 can also associated with a host of other binding partners, including caveolin-1, annexin A2, α3β1 and α6β1 integrins, mostly via its IgI domain, with each interaction regulating CD147-induced MMP activity (203, 239-241). For instance, the formation of caveolin-1–CD147 complexes appear to inhibit CD147 self-aggregating, subsequently inhibiting downstream MMP induction (191, 203).

In addition to regulating MMP activity, CD147 has also been identified as being essential for Cyp-mediated signalling, contributing to inflammatory processes such as chemotaxis of cells (discussed in further detail below). Interaction between CD147 and CypA has also been shown to enhance viral infections by facilitating entry of several viruses into their target cells, including human immunodeficiency virus 1 (HIV-1), human cytomegalovirus (CMV), hepatitis B, and severe acute respiratory syndrome coronavirus (SARS-CoV) (242-245).

It has also been proposed that CD147 plays a role in cell adhesion. Recent data show that expression of CD147 on the surface of erythrocytes acts as an adhesion molecule and plays a crucial role in facilitating the trafficking of mature erythrocytes from the spleen into the general circulation (246). Blockade of CD147 using an anti-CD147 antibody led to trapping of red blood cells within the spleen, resulting in anaemia and *de novo* erythropoiesis in the spleen (246). Expression of CD147 on the surface of brain endothelial cells which form the blood-brain barrier (BBB) is thought to be important in cell surface recognition and may also be involved in regulation of BBB permeability (182, 247). In a model of ischaemic stroke, inhibition of CD147 led to substantially reduced BBB damage, inflammation, thrombosis, and

microvascular damage (248). Possible mechanisms underlying this protection include inhibition of CD147-mediated NF-κB activation and induction MMP-9 activity.

1.3.5 CD147 in disease

CD147 has also been implicated in the progression of many diseases, including atherosclerosis (249), arthritis (250, 251), and cancer (230, 252). CD147 is commonly found to be upregulated in human atherosclerotic carotid lesions, predominantly in areas rich in macrophage infiltrates, vascular smooth muscle cells, and MMP-9 positive cells (228, 229). Patients with coronary artery disease also show elevated levels of CD147 on circulating leukocytes, platelets and soluble CD147, with strong associations between CD147 expression and disease severity (253). In arthritis, *in vitro* studies have demonstrated that overexpression of CD147 on macrophage-like and fibroblast-like synoviocytes (the principal cells driving disease progression) has been implicated in enhancing MMP secretion and activation, thus promoting invasion of the articular cartilage (251). The role of CD147 in cancer remains the most well studied. CD147 is highly enriched on the surfaces of most malignant cancer cell types, whereas expression in normal tissue is usually low and compartmentalized (Li et al 2009, Riethdorf et al 2006). Overexpression of CD147 on cancer cells has been implicated in increased tumour invasion, proliferation and metastasis due to corresponding upregulation of MMPs and downstream extracellular matrix degradation (195).

In health, CD147 expression in the lung is low (254, 255). However, it is upregulated in the context of several diseases, including chronic inflammatory disease such as chronic obstructive pulmonary disease and asthma, but most notably during non-small cell lung cancer (256-259). Of particular interest, CD147 has also been implicated in the pathophysiology of VILI. In a study conducted by Foda et al, rats were ventilated for four hours at either a high volume (V_T: 20 mL/kg, PEEP: 0 cmH_2O) or low volumes (V_T: 7 mL/kg, PEEP: 2 cmH_2O) (169). Using *in situ* hybridisation, they detected an increase in CD147 in alveolar macrophages,

alveolar epithelial cells, and endothelial cells in the lungs of rats subjected to high-volume ventilation compared with rats subjected to low-volume ventilation. The increase was seen after 1 hour of high-volume ventilation and increased over time. Additionally, they also observed an increase in the amount of MMP-2, MMP-9 and MT1-MMP mRNA synthesis in epithelial and endothelial cells in the lungs of rats subjected to high-volume ventilation compared with rats subjected to low-volume ventilation. This upregulation in CD147 appeared to precede an increase in levels of both pro and active forms of MMP-2 and MMP-9 in BAL, suggesting stretch-induced CD147 upregulation played a role in subsequent MMP activity. Treatment with an MMP inhibitor, Prinomastat, significantly attenuated lung injury and prevented the release and activation of MMP-2 and MMP-9, providing evidence that CD147-induced increases in MMP does play a role in the development of acute lung injury. However, there was no further exploration of the mechanisms underlying CD147 activation and its downstream signalling.

1.4 The cyclophilins

Among the many binding partners of CD147, cyclophilins are of particular interest in the context of inflammatory diseases. Cyclophilins are a family of ubiquitously distributed, evolutionarily conserved proteins present in all prokaryotes and eukaryotes (260). Cyclophilins play a crucial role in the isomerisation of peptidyl-prolyl bonds from the sterically favoured *trans* form to the *cis* form required for protein folding (260). In the absence of cyclophilins, spontaneous *cis-trans* isomerisation of such bonds is a slow process requiring free energy and represents the rate-limiting step. Cyclophilins possess peptidyl-prolyl isomerase (PPIase) enzymatic activity which catalyse the isomerisation, thus facilitating both *de novo* protein folding and the assembly of multi-domain proteins (260, 261).

In humans, there are a total of 16 unique members of the cyclophilin protein family, each differing in their molecular mass which ranges from 18 to 150 kDa. These 16 proteins are further divided into 7 major cyclophilins, including human CypA (hCypA or hCyp-18a, i.e. cyclophilin with a molecular mass of 18 kDa), hCypB (22 kDa), hCypC, hCypD, hCypE, hCyp40 (40 kDa), and hCypNK (this cyclophilin was first identified on the surface of natural killer cells) (262, 263). All of them share a common cyclophilin-like domain (CLD) made up of 109 amino acids. Surrounding the CLD domain are domains that are unique to each member of the family, which dictate subcellular compartmentalisation and their specialised functions (264, 265).

1.4.1 Cyclophilin A

Of the cyclophilin family, cyclophilin A (CypA) is the most abundant member. It is expressed in all tissues and accounts for ~0.1-0.6% of total cytosolic proteins. Within the cytoplasm, it is partially associated with the cytoplasmic vesicles and the Golgi apparatus (266, 267). The level of its expression appears to depend on the state of the cell. States that have been associated with an increased CypA expression include proliferating cells, neoplastic tissue,

and following CsA treatment. On the other hand, CypA has been observed to be decreased following viral infections (268). However, how CypA expression levels are regulated have not been explored.

1.4.2 Molecular structure of CypA

CypA is encoded by the *PPIA* gene, which encodes an 18-kDa protein. This cytosolic protein has an anti-parallel β-barrel structure with two α helices (269, 270). Enclosed with the barrel is a compact hydrophobic core made up of seven aromatic and hydrophobic residues, which is the binding site for proline-containing peptides (including cyclosporin A) as well as the enzymatic active site (269-271).

1.4.3 Functions of CypA

For many years, the majority of research has been focused on its role as an intracellular protein, where it is most widely known for being the main cytosolic binding protein responsible for binding cyclosporin A (CsA) – a potent immunosuppressant (272). CsA binds to CypA which in turn binds to calcineurin at the interface between its catalytic and regulatory subunits, forming a ternary complex. As a result, calcineurin is unable to exert its phosphatase activity which is crucial to downstream T cell signalling (273). Owing to its PPIase activity, CypA also plays an important role in the regulation of protein folding and as a molecular chaperone in protein trafficking (260). It has also been identified as a modulator of CD4+ T-cell signal transduction and regulates the production of T helper type II cytokines (274). Additionally, CypA has been reported to bind the CA domain of human HIV-1 Gag protein and is thought to be required for the infectious activity of HIV-1 virions by acting as a molecular chaperon during the coating/uncoating process (275).

1.4.4 Extracellular CypA as a novel mediator of intercellular communication

More recent studies have provided an accumulating amount of evidence to suggest a novel role of extracellular CypA in both autocrine and paracrine intercellular communication (276). In response to inflammatory stimuli, hypoxia, and oxidative stress, CypA can be secreted from cells into the extracellular space (277-285) (**Error! Reference source not found.**). The first report of CypA secretion was from RAW 264.7 murine macrophages in response to LPS stimulation (279). More specialised macrophages - human primary microglia and BV2 murine microglial cells (resident macrophages of the brain and spinal cord), have also been shown to secrete CypA in response to pro-inflammatory (LPS) and oxidative stimuli (oxidative stress inducer, LY8353) (283). In this study, the authors also proposed that the absence of intracellular cytoskeletal protein β-tubulin in culture supernatant was indicative that CypA was actively secreted and not the result of cell lysis. Human umbilical vein endothelial cells (HUVECs) have also been shown to secrete CypA in response to LPS treatment in a time- and dose-dependent manner, with highest levels detected at 12-hours (281). On the other end of the spectrum, platelets have been reported to rapidly (within 3 minutes) release CypA upon activation with adenosine diphosphate (ADP) and following thrombin stimulation (280, 284). However, the pathway or mechanism of CypA secretion was not explored in all the above studies.

Perhaps the most well studied cell type in terms of its CypA release is the vascular smooth muscle cell (VSMC). A number of studies have shown that CypA is released from VSMCs in response to reactive oxygen species (ROS) generated by the oxidative stress inducer, LY8353, angiotensin II, or hydrogen peroxide (H_2O_2) (277, 278, 282). Suzuki et al also demonstrated that in VSMCs, CypA is released via a vesicular secretory pathway that involves vesicle formation, vesicle transport to the plasma membrane (requiring myosin II), docking, and fusion (requiring actin cytoskeleton remodelling) (277).

Table 1.4 - Secretion of CypA from various cell types

Cell type	Stimuli	Mechanism of secretion	
Macrophages			
RAW 264.7 (murine)	16-hour incubation with LPS (1 µg/mL)	–	(279)
Primary microglial (human) **BV2 microglial cell line (murine)**	Constitutive secretion; 2- and 4-hour LPS exposure; 4-hour LY83583 treatment	Active secretion but pathway not elucidated	(283)
Endothelial cells			
HUVEC (human)	12-hour LPS (1 µg/mL)	–	(281)
Platelets			
Primary platelets (human)	3-minute stimulation with ADP (10 µmol/l)	–	(280)
	3-minute stimulation with thrombin (0.5 U/mL)	–	(284)
VSMCs			
VSMC (rat)	2-hour stimulation with LY83583 (1µmol/l) or H_2O_2 (200 µmol/l)	Regulated pathway involving vesicle pathway	(277, 282)
RASMC (rat)	24-hour stimulation with angiotensin II (300 nM)	Dependent on acetylation of CypA at K82 and K125 residues	(278)
Fibroblasts			
L929 (murine)	4- and 8-hour stimulation with 100 µM zVAD.fmk	Passive following necroptosis but not apoptosis	(285)

LPS = lipopolysaccharide, HUVEC = human umbilical vein endothelial cell, ADP = adenosine diphosphate, VSMC = vascular smooth muscle cell, RASMC = Rat aortic smooth muscle cell,

CypA = cyclophilin A, H_2O_2 = hydrogen peroxide, zVAD.fmk = carbobenzoxy-valyl-alanyl-aspartyl-[O-methyl]- fluoromethylketone

In contrast to the active process of secretion proposed above, Christofferson and Yuan have suggested that CypA is passively released during the early stages of necroptosis, a form of programmed necrotic cell death, as a consequence of cell membrane permeabilisation (285). They demonstrated that treatment of L929 (fibroblast cell line) cells with zVAD.fmk, a pan-caspase inhibitor that induces necroptosis, results in release of CypA detected at 4- and 8-hours. This release of CypA was inhibited in the presence of necrostatin-1, a specific inhibitor of necroptosis. Further, they showed that CypA release was specific to necroptosis as no CypA was detected in the supernatant of FADD-deficient Jurkat cells treated with TNF-α and cyclohexamide to induce apoptosis (285).

Although it is now established that CypA can be secreted, the mechanism of its secretion remains uncertain. Unlike other members within the cyclophilin family (e.g. cyclophilin B), CypA is not synthesised with the prototypic signal peptides at the N-terminus which is found on most proteins destined for secretion via the classical pathway (276). Instead, it has been suggested that CypA secretion follows a vesicular pathway. In these studies, secretion of CypA from reactive oxygen species (ROS) stimulated vascular smooth muscle cells was shown to proceed in a manner dependent on Rho signalling, myosin activation, and actin remodelling (286). However, another study has suggested that intracellular CypA is not actively secreted but simply gains access into the extracellular space when cells are dead or dying due to the increase in cell membrane permeability and proposed it as a biomarker of necrotic cell death (285).

Regardless of the mechanism of release/secretion, once in the extracellular space CypA, has been shown to be involved in a wide range of cell signalling events across numerous cell types. Initial studies demonstrated that extracellular CypA was capable of initiating signalling

response (e.g. activation of the extracellular signal-regulated kinases [ERK1/2] and NF-κB pathway (287)), and acting as a chemotactic agent to leukocytes, including neutrophils, eosinophils, monocytes, and T cells in both *in vitro* and *in vivo* systems (279, 288-290). Since then, the functions of extracellular CypA has been extended to include stimulation of ROS production, cell proliferation, and apoptosis (287, 288, 291-302).

1.4.5 CypA:CD147 interactions

Following the recognition that extracellular CypA was capable of mediating intercellular effector activities, studies were conducted to identify the cell surface receptor responsible for binding and transducing the extracellular activities of extracellular CypA. In 2002, Yurchenko et al identified CD147 as a cell surface receptor for CypA. Subsequent analysis demonstrated that signalling and chemotactic activities of CypA required CD147 to be present (290).

Currently, the signal transduction mechanisms downstream of CypA-CD147 interactions remain unclear. Extracellular CypA stimulation of CD147-expressing cells leads to signalling activity characterised by a flux in intracellular Ca^{2+} and an increase in the level of ERK phosphorylation (290). Interestingly, a study conducted by Pushkarsky et al demonstrated that the cytoplasmic domain of CD147 is not required for ERK activation (303). Instead, they proposed that CD147-mediated signal transduction likely occurs following association of the transmembrane domain of CD147 with other membrane proteins. In support of this hypothesis, they highlight the propensity of CD147 to form complexes with other membrane proteins due to its unusual molecular structure which features a charged residue (glutamic acid) within its 24 residue long transmembrane region. The presence of a charged residue in the middle of the lipid bilayer is a feature that is not usually found in proteins spanning the membrane only once as it is highly energetically unfavourable. Proteins with such molecular features often complex with other membrane proteins to shield the charge in an energetically stable state

(196). Indeed CD147 has been shown to interact with several other transmembrane proteins including β1 integrins, CD43 and syndecan (241, 304, 305).

Genetic analysis demonstrated that amino acids proline 280 and glycine 281 located near the end of the transmembrane domain facing the outside of the cell are critical for CypA-CD147 signalling (290). Nuclear magnetic resonance studies have revealed that binding of CypA to CD147 isomerises the *cis*-conformer of the tryptophan 210-proline 211 peptidyl-prolyl bond within it (306). This might suggest a novel mechanism of ligand-receptor interaction in which isomerisation of a peptidyl-prolyl bond on the outside of the cell results in intracellular signalling on the inside of the cell – a 'proline switch' of sorts (306). In addition, the proline 180 and glycine 181 residues located in the extracellular domain of CD147 were found to be critical for CypA-mediated CD147 signalling. Mutant CD147 constructs (which had alternative proline 180 and glycine 181 residues) failed to respond to CypA stimulation (290). Preservation of the active site residues of CypA and thus its PPIase activity was also shown to be crucial for its signalling activity. Similarly, mutants that were PPIase defective failed to initiate downstream signalling events (290). Taken together, these data suggest that CD147 mediated CypA signalling occurs through a unique PPIase-dependent mechanism.

In addition to CD147, it has also been shown that both signalling and chemotactic activities of CypA are dependent on the presence of cell surface heparan sulphate proteoglycans (HSPGs) (196, 197, 290). It is thought that these HSPGs serve as a primary binding site for cyclophilins on target cells, which bring CypA into close proximity with the CD147 receptor, facilitating what is known to be a low-affinity interaction between CypA and CD147 (196, 197, 290). Pre-treatment of neutrophils with a heparitinase to remove HSPGs also eliminated CypA-induced chemotaxis (290). However, interestingly, it appears that HSPGs are especially important when cells are in their non-activated states with low CD147 expression. Constant and Bukrinsky reported that in activated T cells where CD147 expression was upregulated, the

binding of CypA to CD147 was enhanced independently of heparans, suggesting a redundancy of HSPGs once a certain threshold of CD147 expression is crossed (197).

It is now widely accepted that CD147 is the principal signalling receptor for extracellular CypA. However, whether all CypA activities are mediated through CD147 is not known. In a study investigating the effects of CypA in human vascular smooth muscle cells and endothelial cells, Yang et al demonstrated that CypA mediated cell proliferation was not blocked by an anti-CD147 antibody, suggesting that CD147 may not be involved in the mitogenic effects of CypA (307). In a study conducted by Xue et al, it was also reported that multiple signals activated by extracellular CypA in VSMC and EC were unaffected by knockdown of CD147 (308). Hence, it is possible that other unknown receptor(s) for CypA exist and further investigations are required.

1.4.6 CypA:CD147 axis in inflammatory diseases

Both CD147 and extracellular CypA has been shown to be upregulated in the pathogenesis of a host of human disease, in particular diseases with an inflammatory component such as sepsis, atherosclerosis, cancer, and rheumatoid arthritis. While not all studies explicitly demonstrate the interaction between CD147 and CypA, the overlap between diseases implicating CD147 and CypA is highly suggestive that interactions between these two players contribute to the inflammatory responses observed. Further, there is a growing body of evidence to suggest that CypA-CD147 interactions are involved in key processes underlying the pathogenesis of inflammatory diseases. To date, most studies have focused on two downstream consequences of CypA:CD147 interactions: (1) MMP induction; and (2) chemotaxis of leukocytes. The following sections will discuss a few examples of where the CypA:CD147 axis has been implicated, although it is by no means exhaustive.

Rheumatoid arthritis

In rheumatoid arthritis, CypA has been found to be elevated in both serum and synovial fluid of patients (309, 310). This increase in CypA has been found to be positively correlated with not only the number of neutrophils present in the synovial fluid but also with the disease severity (311). Using an *in vitro* model, Kim et al investigate the functions of CypA in the setting of rheumatoid arthritis. Human and mice monocyte/macrophage cell lines were stimulated with CypA and the results presented from this study further implicates CypA in the pathogenesis of rheumatoid arthritis (294). CypA induced secretion of pro-inflammatory cytokines, including IL-8, TNF-α, MCP-1 and IL-1β, which are known to contribute to further activation of inflammatory cells within the synovium. Additionally, CypA stimulation also led to the expression and activation of both MMP-2 and MMP-9 via a NF-κB dependent mechanism.

Concurrently, CD147 has also been reported to be increased on reactive leucocytes (including macrophage-like synoviocytes, fibroblasts-like synovial cells, and granulocytes) in the synovial fluid and in the invasive synovium at sites of joint destruction (311-314). This upregulation in CD147 is almost always associated with a significantly elevation in secretion and activation of MMP-2 and MMP-9 (312-314), and is believed to be responsible for the promotion of cartilage invasion, progression of joint destruction, and recruitment of inflammatory neutrophils into the joint space via CypA-dependent signalling. Many have demonstrated benefits conferred by inhibition of CD147, either with an anti-CD147 antibody or a CD147 antagonistic peptide. In a model of collagen-induced arthritis, Constant and Burkinsky observed up to 75% reduction in joint inflammation (197). This finding is consistent with a study by Zhu et al where administration of an anti-CD147 antibody resulted in a significant reduction in chemotaxis of monocytes to synovial fluid from RA patients (312).

A pathway between CypA and CD147 was suggested by Yang et al who demonstrated that CypA-induced MMP-9 production in monocytes/macrophages was inhibited when cells were pre-treated with a small interfering RNA (siRNA) against CD147 (301). Unsurprisingly, both

CD147 and CypA are attractive new targets for intervention in the treatment of rheumatoid arthritis.

Coronary artery disease

There has also been an increasing amount of evidence to highlight the role of CypA and CD147 in the pathogenesis of coronary artery disease (CAD), including abdominal aortic aneurysms, atherosclerosis, cardiac hypertrophy, and pulmonary hypertension (315).

ROS formation and production plays a crucial role in the pathogenesis of cardiovascular diseases. Risk factors for CAD, including hyperlipidaemia, high blood pressure, smoking, and diabetes all contribute to increase ROS, creating an environment of oxidative stress. In response to oxidative stress, CypA is released from vascular smooth muscle cells, platelets and macrophages (277, 278, 281, 282). Once in the extracellular space, CypA induces further ROS production in smooth muscle cell (315). This augments further CypA secretion and also promotes damage to the intima by causing a decrease in nitric oxide release, an important mediator of vasodilation, thus facilitating platelet aggregation and upregulation of adhesion molecules (316, 317).

CypA has also been shown to activate endothelial cells, leading to the upregulation of adhesion molecules such as vascular cell adhesion molecule (VCAM)-1 and E-selectin, contributing to the initial process of leukocyte recruitment (281, 317). Moreover, CypA itself can function as a direct chemoattractant for leukocytes, promoting the recruitment of key effector cells including neutrophils, eosinophils, monocytes, and T lymphocytes into the atheroma lesion in a CD147-dependent manner (318). In support of this, immunohistochemistry staining of cardiac sections from human autopsies of patients who died from acute myocardial infarction revealed high expression levels of both CypA and CD147 in myocardium (319). CD147 was predominantly localised to the cardiomyocytes and CypA to

the infiltrating leukocytes consisting mainly of neutrophils and macrophages. Areas of infiltrating leukocytes also stained positively for MMP-9, providing support for CD147-induced MMP activity in cardiovascular pathologies (320, 321).

Both CypA and CD147 are thought to play functional roles in the process of foam cell formation. In an *in vitro* study, CD34+ progenitor cells were observed to upregulate CD147 as they differentiated into foam cells (320). During this differentiation process, there was also a significant increase in CypA secretion. This upregulation of CD147 was associated with an increase in MMP-9 secretion, which was further enhanced by the addition of recombinant CypA. Both gene silencing of CD147 using siRNA and treatment of cells with a CypA inhibitor (NIM811) led to a significant decrease in MMP-9 secretion from mature foam cells. In a study published late last year (2019), Pahk et al investigated the anti-atherosclerotic effects of a novel drug, SP-8356, that inhibits CypA-CD147 interactions (322). In a mice model of atherosclerosis, advanced plaques were induced in apolipoprotein E-deficient (ApoE KO) mice via partial ligation of the right carotid artery. Following this injury, mice received SP-8356 once daily orally for three weeks. The authors demonstrated that mice treated with SP-8356 had significantly reduced plaque size and attenuated plaque vulnerability (thicker fibrous cap with decreased lipid and necrotic core areas) compared with vehicle-treated mice. Furthermore, *in situ* zymography also revealed significantly decreased MMP-9 activity within plaque lesions. These results provide further evidence for the pathogenic role of CypA:CD147 interactions in atherosclerosis and highlights this pathway as a promising target for future translational efforts.

Importantly, clinical studies have also highlighted the involvement of CypA in patients with CAD. Several studies have demonstrated the role of CypA as a biomarker of CADs (323-326). CypA can be used to predict important clinical outcomes, including all-cause mortality, re-hospitalisation, and coronary revascularisation in patients (327). In 2012, a prospective

observation study proposed that CypA may also provide superior prognostic value. 320 patients with symptoms of CAD were screened and it was demonstrated that plasma levels of CypA were significantly increased in patients with angiographically proven CAD (328). Furthermore, CypA was also found to be upregulated in patients with atherosclerotic risk factors, including hypertension, diabetes, smoking, and dyslipidaemia (328).

Asthma

Currently, very little is known about the role of CypA:CD147 interactions within the lungs. A study conducted by Gwinn et al sought to investigate the role that extracellular CypA:CD147 interactions might have in asthmatic lung injury (329). Using a mouse model of asthmatic inflammation characterised by an influx of effector cells (eosinophils and Th2 lymphocytes), they detected elevated levels of CypA in the BAL fluid from airways of diseased mice. CD147 was found on the surface of circulating eosinophils and $CD4^+$ T cells and the authors believed that CD147 expression was critical for the recruitment of these cells into the areas of inflammation. This was supported by the dramatic reduction (up to 50%) in numbers of eosinophils and T-cells accumulating in lung tissues of asthmatic mice following an intraperitoneal administration of an anti-CD147 antibody. Further, following methacholine challenge, these anti-CD147-treated mice also showed significantly less airway epithelial mucin production and bronchial hypersensitivity.

Acute lung injury

There is currently only one other study which has investigated the role of CypA in acute lung injury. The same research group demonstrated using western blotting an increase in CypA in the bronchoalveolar lavage fluid 18 hours after mice were treated with intranasal lipopolysaccharide (LPS; 2 μg) (291). This increase in CypA was associated with an increase in several proinflammatory cytokines and chemokines as well as a neutrophilia in lung tissues and airways, with the latter correlated closely with the level of CypA. The group then went on

to test both arms of the CypA:CD147 axis. Blockade of CD147 with an intraperitoneal injection of an anti-CD147 monoclonal antibody prior to the intranasal LPS challenge led to a significant reduction in neutrophil infiltration in lung tissues and airways. Inhibition of CypA with a non-immunosuppressive cyclosporine analogue (SDZNIM811) resulted in a similar reduction in neutrophil infiltration. When both treatments were used in conjunction, only a minor further reduction in neutrophil numbers was observed, suggesting that both interventions were acting on the same CypA:CD147 interactions.

While these two studies exploring the role of CypA and CD147 in the lungs are interesting and do provide evidence for the relevance of the CypA:CD147 axis in inflammatory lung diseases, the mechanisms underlying the protective effects observed following blockade of CypA and/or CD147 were not elucidated. Therefore, despite the growing body of evidence suggesting that the CypA:CD147 axis plays a key role in multiple inflammatory diseases, there is still very little known about its role in the lungs and how exactly it contributes to the inflammatory response.

The data presented in this thesis are my effort to provide further information on how this novel CypA:CD147 axis may contribute to acute lung injury, with a specific focus on its role during the pathogenesis of ventilator-induced lung injury.

1.5 Hypothesis

We hypothesise that the CypA:CD147 axis plays a pathogenic role in the lungs following mechanical ventilation, contributing to VILI.

1.6 Aims

1) To explore the involvement of CypA and CD147 in the lungs using a mouse model of VILI.
2) To investigate CypA release in response to stretch using *in vivo* mechanical ventilation and *in vitro* stretch models.
3) To assess whether CypA inhibition during *in vivo* ventilation attenuates VILI and investigate possible mechanisms behind any observed protective effects.
4) To investigate the mechanisms through which extracellular CypA contributes to the pathogenesis of VILI using *in vitro* methods.

2 Materials & Methods

This chapter describes the materials (reagents and equipment), and various methodologies utilised within this thesis. Additional details of materials and methods pertaining to specific chapters can be found in the methods section of its respective chapter.

2.1 Materials

2.1.1 Reagents

Table 2.1 - In vivo reagents

Reagent	Constituents	Application	Source
Ketamine	-	In vivo ventilation	Imperial CBS
Xylazine	-	In vivo ventilation	Imperial CBS
Iodine	-	In vivo ventilation	Imperial CBS
Oxygen gas	-	In vivo ventilation	BOC
4% carbon dioxide gas	-	In vivo ventilation	BOC
Saline	-	In vivo ventilation	NHS supplies
Heparin	-	In vivo ventilation	Imperial CBS
Hydrochloric acid (1M)	-	In vivo ventilation	VWR International
Lipopolysaccharide, Ultrapure (from *E.coli* O111:B4)	-	In vivo ventilation	InvivoGen

Table 2.2 - Flow cytometry reagents

Reagent	Constituents	Application	Source
Intracellular fixation buffer	Paraformaldehyde	Cell fixation for flow cytometric analyses	eBioscience
BD Cytofix/Cytoperm	-	Cell permeabilisation for intracellular staining	BD Bioscience
Flow cytometry wash buffer (FWB)	Phosphate buffered saline (PBS) with 2% foetal calf serum (FCS), 0.1% sodium azide, 5mM EDTA	Flow cytometry	Invitrogen Invitrogen Invitrogen Thermofisher Scientific
Flow cytometry permeabilisation wash buffer (PWB)	PBS with 0.2% saponin, 0.5% bovine serum albumin (BSA), 0.1% sodium azide	Flow cytometry	Invitrogen
AccuCheck counting beads	-	Cell quantification	Invitrogen
Collagenase	-	Enzymatic lung digestion	Sigma-Aldrich
DNase I	-	Enzymatic lung digestion	Roche Diagnostics

Table 2.3 - Enzyme-linked immunosorbent assay (ELISA) reagents

Reagent	Constituents	Source
ELISA wash buffer	1X PBS 0.05% Tween-20 (v/v)	Gibco Invitrogen
ELISA reagent diluent	1X PBS 1% BSA (w/v)	Gibco Sigma Aldrich
ELISA substrate solution	3,3’,5,5’ Tetramethylbenzidine liquid substrate system super sensitive form	Sigma Aldrich
ELISA stop solution	Sulphuric acid	Gibco

Table 2.4 - Western blotting reagents

Reagent	Constituents	Source
Cell lysis buffer	10X RIPA lysis buffer 100X Protease inhibitor 10X Phosphatase inhibitor (PhosSTOP) 5mM EDTA 1mM PMSF	Cell Signalling Technology Cell Signalling Technology Cell Signalling Technology ThermoFisher Scientific Sigma
NuPAGE™ Sample Reducing Agent (10X)	500 mM dithioreitol (DTT)	Invitrogen
NuPAGE™ LDS Sample buffer (4X)	-	Invitrogen
NuPAGE™ MOPS SDS Running Buffer	-	ThermoFisher Scientific
NuPAGE™ 4-12% Bis-Tris Protein Gels, 1.0 mm, 10-well	-	ThermoFisher Scientific
Color-coded Prestained Protein Marker, Broad Range (11-250 kDa)	-	Cell Signalling Technology
MagicMark™ XP Western Protein Standard	-	ThermoFisher Scientific
NuPAGE™ Transfer Buffer	-	Invitrogen
Nitrocellulose membranes, 0.2µm, 8 x 8 cm	-	ThermoFisher Scientific
Western Blotting Filter Paper, 7cm x 8.4 cm, 0.83mm thickness	-	ThermoFisher Scientific
iBlot 2 NC Regular Stacks	-	ThermoFisher Scientific
Tris-buffered saline-Tween 20 (TBS-T)	Tris-buffered saline 0.1% Tween-20 (v/v)	ThermoFisher Scientific Invitrogen
Blocking buffer	5% non-fat dry milk (w/v) TBS-T	Marvel
Luminol reagent	Luminol reagent Hydrogen peroxide	Santa Cruz Biotechnology
SuperSignal™ West Femto Maximum Sensitivity Substrate	-	ThermoFisher Scientific
Restore™ PLUS Western Blot Stripping Buffer	-	ThermoFisher Scientific

Table 2.5 - Gelatin zymography reagents

Reagent	Constituents	Source
Novex™ Tris-Glycine SDS Sample Buffer	-	Invitrogen
Tris-Glycine SDS Running Buffer	-	Invitrogen
Novex™ 10% Zymogram (Gelatin) Protein Gels	-	Invitrogen
Color-coded Prestained Protein Marker, Broad Range (11-250 kDa)	-	Cell Signalling Technology
Recombinant Mouse MMP-2 Western Blot Standard Protein	-	R&D Systems
Recombinant Mouse MMP-9 Western Blot Standard Protein	-	R&D Systems
Zymography Renaturing Buffer (10X)	-	Invitrogen
Zymography Developing Buffer (10X)	-	Invitrogen
Colloidal Blue Staining Kit	Stainer A Stainer B	Invitrogen
Methanol	-	VWR International

2.1.2 Commercial detection assays

Table 2.6 - Commercial detection and quantification kits

Kit	Constituents	Source
Mouse: RAGE Duoset IL-6 Duoset KC Duoset IL-1β Duoset	Capture antibody Biotinylated detection antibody Recombinant standard Streptavidin-HRP	R&D systems
Mouse cyclophilin A (CYPA) ELISA	Pre-coated micro ELISA plate Recombinant standards Biotinylated detection antibody Avidin-horseradish peroxidase (HRP) conjugate Wash buffer	Elabscience
Human: TNF Duoset IL-8 Duoset IL-6 Duoset	Capture antibody Biotinylated detection antibody Recombinant standard Streptavidin-HRP	R&D systems
Human peptidylprolyl isomerase A/CYPA (PPIA) ELISA	Pre-coated micro ELISA plate Recombinant standards Biotinylated detection antibody Avidin-horseradish peroxidase (HRP) conjugate Wash buffer	Abbexa
Bradford protein assay	Coomassie Brilliant Blue G-250 BSA standard	Bio-Rad ThermoFisher Scientific
Qubit™ protein assay	Qubit™ protein reagent (component A) Qubit™ protein buffer (component B) Qubit™ protein standard #1 Qubit™ protein standard #2 Qubit™ protein standard #3	ThermoFisher Scientific
Lactate Dehydrogenase Assay Kit	LDH assay buffer LDH positive control (lyophilised) LDH substrate mix NADH standard	Abcam
Nitrite/Nitrate Assay Kit, colorimetric	$NaNO_2$ Standard Solution (100 µM) $NaNO_3$ Standard Solution (100 µM) Buffer solution (20 mM, pH 7.6) Nitrate Reductase Enzyme co-factors Griess Reagent A Griess Reagent B	Sigma-Aldrich

2.1.3 Instruments, equipment, and software

Table 2.7 - Equipment for in vivo ventilation protocols

Equipment	Application	Source
Infusion pump	In vivo fluid administration	Harvard Apparatus
PowerLab data acquisition system	Record physiology data	AD Instruments
RapidLab 248 blood gas machine	In vivo blood gas analyser	Siemens healthcare

Table 2.8 - ELISA equipment

Equipment	Application	Source
MRW Microplate washer	ELISA automated plate washer	Dynex Technologies
BioTek ELx800	ELISA colorimetric plate reader	BioTek Instruments

Table 2.9 - Flow cytometry equipment

Equipment	Application	Source
GentleMACS tissue dissociator	Homogenisation of lung tissue	Miltenyi Biotec Ltd
40 µm Nylon strainer	Single cell suspension	BD Falcon
CyAn ADP flow cytometer	Flow cytometric analyses	Beckman Coulter

Table 2.10 - Software packages

Software	Application	Source
Prism v6	Statistical analysis	Graphpad
FlowJo	Flow cytometry analysis	Tree Star Inc.
LabChart reader	Physiology data	AD Instruments
GeneSnap	Acquisition of western blot image	Syngene
GeneTools	Image analysis for western blots	Syngene
ImageJ	Image analysis for western blots	National Institutes of Health

2.2 Animals

All protocols were approved by the Ethical Review Board of Imperial College London and carried out under the authority of the UK Home Office in accordance with the Animals (Scientific Procedures) Act 1986 UK (Personal License number I8A02F01D, Project License number P8E434E5B) and the ARRIVE guidelines for use and reporting of animals in research. Male C57BL/6 mice, purchased from Charles River, Margate, UK, were used in all *in vivo* experiments. All mice were aged between 7-14 weeks and weighed 21-30g. Animals were housed in individual ventilated cages, with a maximum of 5 mice per cage. Animals had free access to food and water and were exposed to 12-hour light and dark cycles. All experiments were initiated and completed during the light cycle and no adverse effects were observed in any of the treatment groups.

2.3 In vivo animal models of ventilator-induced lung injury

2.3.1 Ventilator-Induced Lung Injury

Surgical preparation

Mice were anaesthetised with an intraperitoneal injection of a combined dose of ketamine (80 mg/mL) and xylazine (8 mg/mL). Once animals lost consciousness (within 2-3 minutes), they were transferred onto a heat pad and covered with a blanket (large cotton wool pad) to ensure that a constant body temperature was maintained throughout the experiment. The surgical area was shaved and cleaned with iodine in preparation for the procedure. Once a suitable depth of anaesthesia was reached, as assessed by the loss of pedal reflex, the surgical procedure commenced.

Mice underwent a tracheostomy and a custom-made endotracheal tube (ET) was inserted and secured in situ with a 3-0 surgical suture. The left carotid artery was then cannulated to monitor blood pressure, withdraw arterial blood samples for blood gas analysis, and provide an

infusion (0.4 mL/hr) of maintenance saline. An intraperitoneal (IP) line was instrumented into the abdomen to provide reliable and convenient access for delivering maintenance anaesthesia. Physiology temperatures (36.5 – 37.5ºC) were maintained and monitored by a rectal temperature probe.

Ventilation system set-up

This custom-made mouse ventilator is a 'constant flow generator'. In this system (Figure 2.1), high pressure gas from a gas cylinder flows through a metering valve (Swagelok). The high resistance flow regulator (A) allows the system to deliver an inspiratory flow effectively at a controlled constant rate (adjusted by the valve), regardless of the inherent resistance/elastance of the mouse's respiratory system. The custom-made electric ventilator controller, controls opening and closing of the electrically-driven solenoid valves and provides an inspiratory:expiratory (I/E) ratio of 1:2.

During inspiration when the inspiratory solenoid (B) opens and the expiratory solenoid closes, a constant inspiratory flow is delivered through the miniature pneumotachograph (C) and into the mouse's lungs via a custom-made endotracheal tube (D). During expiration, the inspiratory solenoid closes, the expiratory solenoid (E) opens and the mouse exhales passively against either atmospheric pressure or a set positive end expiratory pressure (PEEP) regulated by the volume of water present in the corresponding water cylinder.

Airway pressure is monitored by a pressure transducer (F) (MLT0380, ADInstruments, Chalgrove, UK); Airway flow is determined by a differential pressure transducer (G) (PX137, Omega Engineering, Manchester, UK) connected to the pneumotachograph in the ventilator circuit. The miniature pneumotach is essentially a custom-made metal pipe with two side pressure ports, which are connected to a differential pressure transducer. At this diameter

(~1.35 mm), flow through this small pipe is effectively laminar, allowing estimation of flow by measuring the pressure difference between these two ports.

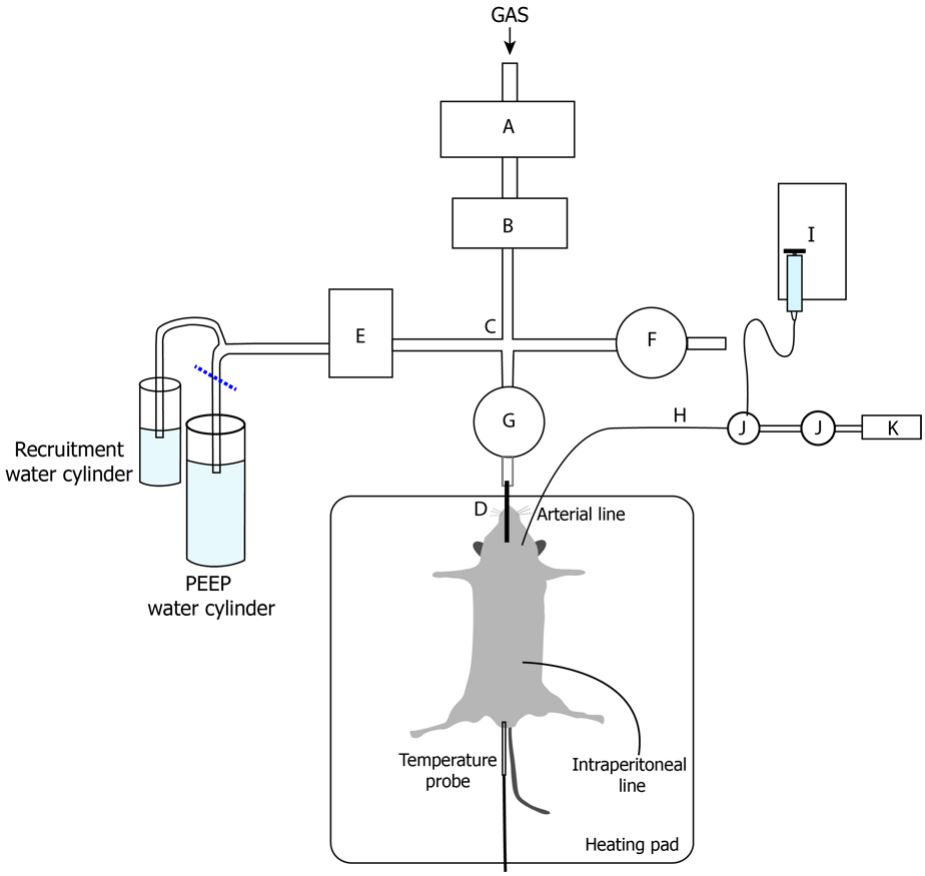


Figure 2.1 - Schematic of in vivo ventilation system set-up

The controller has three different ventilation modes – a constant flow mode, a positive pressure ventilation mode, and an end-inspiratory occlusion mode. The constant flow mode (CPAP) provides a constant flow, where both inspiratory and expiratory solenoids remain open. The positive pressure ventilation mode enables time-cycled ventilation, where the inspiratory and expiratory time is defined by the RR set by the operator. The ventilator controller enables changes in respiratory rate (RR) from 50 to 300, but the I/E ratio is fixed at 1:2. The end-inspiratory occlusion mode adds an inspiratory pause of ~20 msec to positive pressure ventilation; during this mode inspiratory and expiratory time remains unchanged from that in positive pressure ventilation mode as defined by the RR.

Recruitment manoeuvres are performed by setting the ventilator to constant flow mode and then occluding the tubing feeding into the PEEP water cylinder (Figure 2.1 – blue dotted line). This causes airway pressure to rise to a set airway pressure (30 cmH2O or as otherwise dictated by the volume of water in the recruitment water cylinder); usually the mouse's lungs are subjected to a sustained inflation at the set recruitment pressure for 5 seconds, terminated by releasing the PEEP tubing.

All data from the transducer is collected by a PowerLab data acquisition system (AD Instruments) and analysed by LabChart Reader software (AD Instruments, UK).

Ventilation protocol

The ventilator was initially set at low tidal volume (V_T) settings (Table 2.11) regardless of intended final experimental ventilator strategy. Three pulmonary recruitment manoeuvres, 30-seconds apart, were performed to reverse any temporary atelectasis and standardise the volume history of the lungs for the effects of surgery and anaesthesia. After the last recruitment, an inspiratory pause is performed to determine the respiratory mechanics at baseline. At this point, the settings of the ventilator were then either maintained to deliver low V_T ventilation or adjusted to a high V_T ventilation strategy.

Table 2.11 - Ventilation parameters for low and high V_T ventilation strategies

	Low V_T	**High V_T**
Tidal volume (V_T)	8 mL/kg	40 mL/kg
Respiratory rate (RR)	120 breaths/min	80 breaths/min
Peak end expiratory pressure (PEEP)	3.0 cmH_2O	3.0 cmH_2O
Gas	100% O_2	O_2 + 4% CO_2

Mice were ventilated for 1, 2, or 3 hours. At the end of the experiment, mice were exsanguinated under general anaesthesia by severing the left carotid artery. Samples were then collected and processed as detailed in following sections.

Rationale for use of very high V_T strategy

In these experiments, mice were ventilated with very high V_T strategies (i.e. 30-40 mL/kg). While the use of ventilatory strategies such as those used in our experiments have been criticised for being too extreme to be clinically relevant to humans, there are a number of reasons for using large magnitudes of stretch. Firstly, we have previously demonstrated that the use of "clinically relevant" tidal volumes (≤20 mL/kg) are unlikely to induce substantial lung overstretch in mice (330). These settings are necessary to induce stretch-induced inflammation and injury within the lungs of healthy mice which are much more compliant that human lungs. Furthermore, application of high V_T also reflects the degree of stretch that would be experienced by the heterogeneously injured "baby lung" of patients with ARDS (58).

2.4 Interventional studies

2.4.1 Alveolar macrophage depletion experiments

Mice were randomly allocated to receive either 50 µL of saline or clodronate-containing liposomes (7 mg/mL, 50 µL; FormuMax Scientific, Palo Alto, CA, USA); the investigator performing the ventilation was blinded to the group assignment.

Animals were anaesthetised with an intraperitoneal injection of a combined dose of ketamine (60 mg/mL) and xylazine (6 mg/mL). Once animals lost consciousness and a suitable depth of anaesthesia, as assessed by the loss of pedal reflex, was reached, animals were vertically suspended using a custom-made stand. The mouth was opened, tongue moved aside, and the vocal cords were visualised and identified using a microscope and an external light source.

A fine catheter was then passed between the vocal cords, about 1 cm down into the trachea and 50 µL of clodronate-containing liposomes or saline was instilled intratracheally (i.t.). The mice were suspended in an upright position for a further 30 seconds to allow equal bilateral distribution of the fluid. Once the fluid is fully inhaled, mice were then returned to a horizontal position and placed in a custom-made recovery box providing humification, warming, and oxygen supplementation until the effects of the anaesthetic had fully worn off.

48 hours after pre-treatment, mice were ventilated at high V_T as described above for up to 150 minutes or until mortality surrogates – blood pressure <50 mmHg or PIP increased >20% – were reached.

2.4.2 Extracellular Cyclophilin A inhibition with MM-284

To investigate the role of CypA during VILI, the impact of *in vivo* CypA inhibition was explored using the inhibitor MM-284 (kind gift from Dr Malesevic at Martin Luther University), a cyclosporin A-derivative selective for extracellular cyclophilins.

Mice were randomly allocated to receive either 50 µL of vehicle (10% DMSO; Sigma-Aldrich) or MM-284 (0.67 mM); the investigator performing the ventilation was blinded to the group assignment. Animals were anaesthetised and ventilated at low V_T as per the VILI model. An inspiratory pause (IP) was performed once V_T was established to measure the respiratory mechanics at baseline. This was of particular importance as the intratracheal instillation of fluid is known to affect both the elastic and resistive component of the respiratory system and therefore peak inspiratory pressure (PIP) readings.

Mice were then briefly detached from the ventilator and vertically suspended using a custom-made stand. 50 µL of the MM-284 inhibitor or 10% DMSO was intratracheally instilled via a thin tubing fed into the endotracheal tube. Mice were then returned to a horizontal plane,

reattached to the ventilator, and immediately received three recruitment manoeuvres at 30 cmH2O to ensure that the fluid was driven distally into the respiratory tract. Mice were then maintained at low V_T for 30 minutes to allow the fluid to distribute as equally as possible within the respiratory tract. During this time, recruitment manoeuvres and inspiratory pauses were performed every 15 minutes to recruit for any atelectasis component which inevitably occurs after fluid is introduced into the airway and to monitor changes to respiratory mechanics. After 30 minutes, PIP readings were usually not significantly different to that of baseline. V_T was then increased to 30-35 mL/kg until the PIP reached 40 cmH_2O and ventilated for up to 3 hours or until mortality surrogates – blood pressure <50 mmHg or PIP increased >20% – were reached.

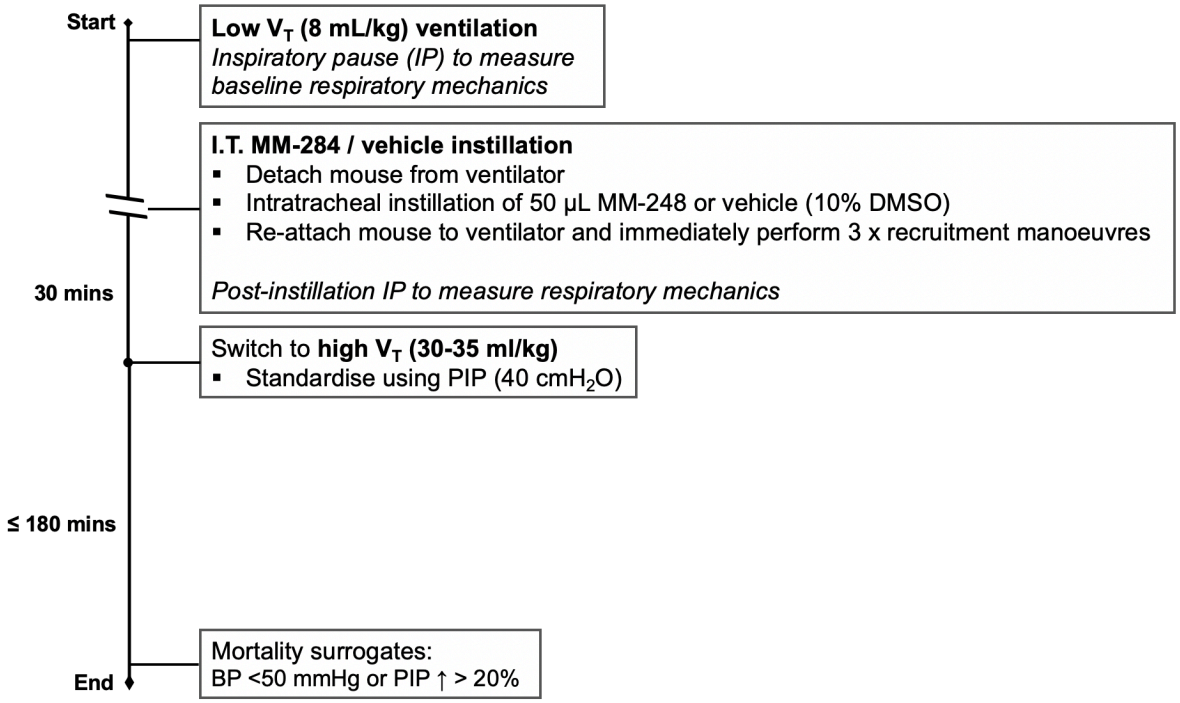
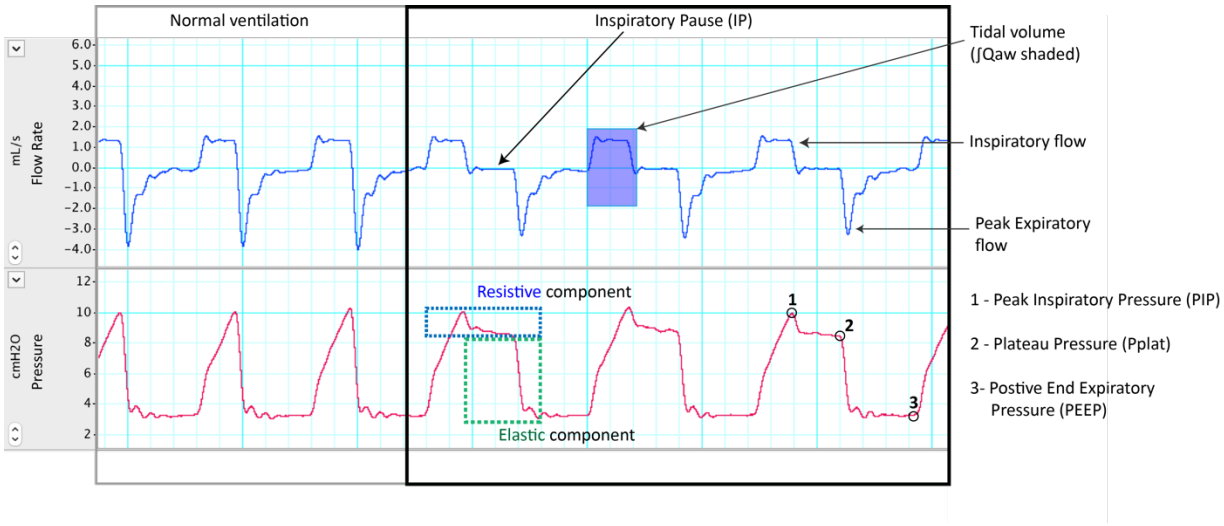


Figure 2.2 - Protocol of CypA inhibition in vivo VILI experiments

2.5 Physiological data

2.5.1 Respiratory mechanics

Respiratory mechanics were measured using the end-inspiratory occlusion technique, as described in detail by Ewart et al (331). During the inspiratory pause, both solenoid valves are closed and producing zero flow at the end of inspiration. By measuring airway pressures and gas flow, the elastance and resistance of the lungs can be calculated.



$$Compliance = \frac{Tidal\ volume}{P_{plat} - PEEP}$$

$$Elastance = \frac{1}{Compliance} = \frac{P_{plat} - PEEP}{Tidal\ volume}$$

$$Resistance = \frac{PIP - P_{plat}}{Flow}$$

Figure 2.3 - Airway flow and pressure graphs showing measurement and calculation of respiratory mechanics

2.5.2 Arterial blood gas sampling

As detailed above, the left internal carotid is cannulated and attached to a pressure transducer and a syringe pump. A continuous infusion of heparinised saline is administered for the entire

duration of the surgery at a rate of 0.4 mL/hour. At set intervals (initial reading at 15 minutes and then subsequently, hourly) blood (~100 µL) was sampled using a glass capillary tubes and analysed with a Rapid Lab 248 blood gas analyser. After each sample is withdrawn, 150µL bolus of heparin/saline infusion was administered through the carotid line.

2.6 Experimental samples and physiological measurements

2.6.1 Harvesting plasma samples

Blood samples were collected after the carotid artery was severed. Samples were centrifuged at 4,000 rpm, 5 minutes, 4°C to isolate the plasma fraction. Plasma was then pipetted off and aliquots were stored at -80°C.

2.6.2 Lung wet/dry weight ratio

Once death was confirmed, the chest cavity was opened. The right lower lung lobe was identified and securely tied off at the hilum. After BAL was performed (as detailed below), the right lower lobe was removed, briefly rinsed in saline and blotted to remove any excess liquid on the surface. The wet weight was immediately determined before lungs were placed in a 60°C oven for 24 hours (or until weight constant), after which they were re-weighed for dry weight.

2.6.3 Bronchoalveolar lavage

Bronchoalveolar lavage (BAL) was sampled by flushing and gently aspirating 650µL of saline in and out of the lungs via the endotracheal tubes three times. The recovered BAL fluid was centrifuged at 1,500 rpm for 5 mins at 4°C and the supernatant was pipetted off to store at -80°C for later analyses.

2.6.4 BAL protein assay

BAL fluid protein measurement was performed using the Qubit Protein Assay Kit. The QUBIT assay uses a dye-based system which emits a fluorescence signal when bound to proteins. Protocol was performed as per manufacturer's instructions. In brief, standards and BAL sample were diluted in the Qubit working solution, which was prepared by diluting the Qubit Protein Reagent 1:200 in Qubit Protein Buffer. Samples were then incubated at room temperature in the dark for 15 minutes to allow the sample to reach optimal fluorescence. The Qubit Fluorometer was then calibrated with the standards and the samples were analysed to determine the protein concentration of each sample.

2.6.5 Lungs

As described above, the right lower lobe was removed to determine the wet/dry weight ratio. The remaining right lung lobe were also briefly rinsed with saline and blotted dry before homogenisation using a GentleMACS tissue dissociator for flow cytometric analysis. The left lobe was removed, immediately snap frozen and subsequently stored at -80°C for later analysis with western blotting.

2.6.6 ELISA

Levels of soluble mediators in BAL and plasma were measured using appropriate sandwich ELISA kits. BAL and plasma levels of CypA was measured using a commercially available mouse cyclophilin A ELISA kit (Elabscience, China), which included pre-coated micro ELISA plate wells. The assays were conducted as per manufacturer's instructions. BAL levels of other mediators (RAGE, IL-6, KC) were measured using a Duoset ELISA (R&D). In brief, 96-well plates were coated overnight at room temperature with 50µL of the appropriate specific antibody diluted in filtered PBS. The following morning, plates were blocked with 1% BSA for one hour and then washed three times before the addition of 50µL of standards and samples. Plates left to incubate for two hours at room temperature. After washing, 50µL of the respective

biotinylated detection antibodies were added and incubated again for two hours. After washing, streptavidin conjugated horseradish peroxidase (HRP) was added and incubated for 20 minutes at room temperature in the dark. After the final wash cycle, a liquid substrate (3,3',5,5' Tetramethylbenzidine Liquid Substrate System Super Sensitive Form) was added for colour development over 15-20 minutes. Once standards were suitably developed, the reaction was stopped using sulphuric acid and plates were read at 450 nm in an absorbance microplate reader (Biotek ELx800).

2.7 Western Blot

2.7.1 Preparation of lung samples for western blot analyses

Frozen left lung lobes were mechanically homogenised in 200 µL of ice-cold PBS in Precelly's homogeniser tubes at 500 rpm, 1 minute. Homogenised samples were then incubated with 100 µL of cell lysate buffer (RIPA buffer, protease inhibitor, phosphatase inhibitor, EDTA, PMSF prepared in deionised water) for 30 minutes on ice. Samples were vortex intermittently to ensure thorough lysis of cells. Samples were then centrifuged at 14,000 g for 10 mins at 4ºC to pellet cell debris and supernatants were collected for downstream western blotting procedure. The protein content of supernatants was then quantified with the Bradford protein assay.

2.7.2 Bradford protein assay

The Bradford protein assay (BioRad) is based on the use of the dye Coomassie Brilliant Blue G-250 which binds to proteins in solution. When proteins are not present, the dye is red. Once bound to proteins, the dye is converted to its blue, unprotonated form which has an absorbance maximum of 595 nm. The amount of blue anionic form of the dye is proportional to the amount of the protein in the sample, therefore the protein content of a solution can be measured by measuring the absorption at 595 nm using a colorimetric plate reader.

BSA standards were prepared in PBS at the following concentrations: 2 mg/mL, 1.5 mg/mL, 1 mg/mL, 0.75 mg/mL, 0.5 mg/mL, 0.125 mg/mL, 0 mg/mL. 5 µL of standard and samples (appropriately diluted in saline where necessary) were added to a 96-well plate. Bradford dye (250 µL) was added to each well and wells were mixed with a microplate shaker for 30 seconds. The samples were then incubated at room temperature for 10 minutes before absorbances was measured at 595 nm. Samples and standards were ran in duplicates and the averages were used to determine the protein concentration of samples.

2.7.3 Western blotting protocol

Samples were prepared in 1X NuPAGE LDS Sample Buffer (Invitrogen) and 1X Sample Reducing agent, Dithiothreitol (DTT, Invitrogen), to a final volume of 25 µL in deionised water. The electrophoresis tank was prepared by filling a Mini Gel Tank (ThermoFisher) with 1X NuPAGE™ MOPS SDS Running Buffer made up in deionised water. Prepared samples were denatured by heating up to 95ºC for 10 minutes on a heating block and 25 µL of each sample was loaded into wells of a 10-well NuPAGE 4-12% or 15% Bis-Tris gel (Invitrogen).

On each gel, two different standards were used as protein molecular weight references. The first was a colour-coded pre-stained marker, broad range (11-250 kDa; Cell Signalling) which enabled visual monitoring of protein separation during electrophoresis and verification of transfer efficiency onto nitrocellulose membranes. The second was a MagicMark XP western protein standard (20-220 kDa; Invitrogen) which contained recombinant proteins with IgG binding sites that could bind the primary or secondary antibody used for detection and therefore allowed direct visualisation of the standards on the western blot. Volumes loaded onto the gels were 10 µL and 1 µL respectively.

The samples were then electrophoresed for 50 minutes (or until the protein front had ran sufficiently down the gel) at 200 V, 0.12 AMPs, 25 watts (Power ease 200W, ThermoFisher). Post-electrophoresis, gel cassettes were dismantled, and the gel was extracted from its casing. The proteins were then transferred from the gel to a nitrocellulose membrane.

Two different transfer systems were used. For the first system, 4 sheets of western blotting filter paper and one sheet of nitrocellulose membrane of the same size as the gel were soaked in NuPAGE Transfer Buffer to allow for equilibration. Using tweezers, the transfer stack/sandwich was then assembled directly on the anode plate of the transfer cassette (ThermoScientific) by layering the various components in the following order: 2 sheets of pre-wet filter paper, nitrocellulose membrane, extracted gel, and 2 sheets of pre-wet filter paper. The rolling blotter was used to roll over the stack after each layer was added to remove any bubbles. Once assembly was complete, the top of the cassette (cathode) was placed on top and locked into the place. The cassette was then placed in the Power Station, ready for transfer using a pre-programmed method appropriate for the molecular weight of the protein of interest (e.g. low molecular weight protein <25 kDa (such as cyclophilin A) was transferred at 25V, 1.3A, 5 minutes; mixed-ranged molecular weight proteins ranging from 25-150 kDa (such as CD147) was transferred at 25V, 1.3A, 7 minutes). The second system used was the iBlot™ 2 Dry Blotting System (ThermoFisher). Protocol was followed as per manufacturer's guidelines. Similarly, a transfer stack was assembled by placing the extracted gel in the appropriate position within a pre-assembled iBlot™ 2 Transfer Stack. The entire stack was placed in the iBlot™ 2 Gel Transfer Device and the transfer was performed using pre-programmed methods.

Upon transfer completion, the membrane was incubated in a blocking buffer (non-fat milk/Tris-Buffered Saline with 0.1% Tween-20) for one hour and then probed with the appropriate primary antibodies (Table 2.12) overnight at 4ºC. The following day, membranes were rinsed

in TBST before incubation with the appropriate HRP-conjugated secondary antibody (Table 2.12) for 1 hour. Blots were visualised with Luminol reagent (Santa Cruz Biotechnology) or Femto reagent (ThermoFisher) if enhanced chemiluminescence detection was necessary. Blots were captured with GeneSnap (Syngene) and analysed with GeneSnap (Syngene) or ImageJ (National Institutes of Health).

Table 2.12 - Antibodies used in western blotting

Antibody	Source	Final Concentration
Rabbit monoclonal to CD147, clone EPR4025	Abcam	1:1000
Rabbit polyclonal to Cyclophilin A	Abcam	1:500
Rabbit polyclonal to GAPDH (loading control)	Abcam	1:1000
Goat polyclonal to β-actin (loading control)	Abcam	1:1000
HRP-conjugated goat anti-rabbit IgG H&L	Abcam	1:2000
HRP-conjugated donkey anti-goat IgG H&L	Abcam	1:2000

2.8 Gelatin zymography

Gelatin zymography is a technique used to identify matrix metalloproteinase (MMP) activity, specifically MMP-2 and MMP-9 owing to their efficiency in hydrolysing denatured collagen I (i.e. gelatin), in condition media. This procedure is essentially an adaptation of the methodology for sodium dodecyl sulphate (SDS)-polyacrylamide gel electrophoresis (PAGE).

Samples were prepared in 1X Novex™ Tris-Glycine SDS Sample Buffer (Invitrogen) and diluted appropriately in deionised water to make a final volume of 25 µL. The electrophoresis tank was prepared by filling a Mini Gel Tank (ThermoFisher) with 1X Tris-Glycine SDS Running Buffer made up in deionised water. 25 µL of each sample was loaded into wells of a Novex™ 10% Zymogram (Gelatin) Protein Gels (Invitrogen).

On each gel, a protein molecular weight reference standard, a recombinant MMP-2 standard, and a recombinant MMP-9 standard was also used. The protein molecular weight standard was a colour-coded pre-stained marker, broad range (11-250 kDa; Cell Signalling) which enabled visual monitoring of protein separation during electrophoresis. Both MMP-2 (R&D Systems) and MMP-9 (R&D Systems) standards were recombinant mouse proteins.

The samples were then electrophoresed for 90 minutes at 125 V, 0.12 AMPs, 25 watts (Power ease 200W, ThermoFisher) under non-reducing conditions to ensure that the enzymatic activity of gelatinases are preserved. Post-electrophoresis, gel cassettes were dismantled, and the gel was extracted from its casing. Gels were then sequentially incubated in 1X Zymography Renaturing Buffer (Invitrogen) for 30 minutes at room temperature, 1X Zymogram Developing Buffer (Invitrogen) for 30 minutes at room temperature, and fresh 1X Zymogram Developing Buffer overnight (16-18 hours) at 37ºC. The renaturing buffers contains Triton X-100 which removes SDS from gels and the developing buffer is a calcium-containing solution which activates both latent and active forms of the gelatinases, allow them to digest gelatin embedded within the gels.

The following day, gels were rinsed three times by incubating gels in deionised water for five minutes per wash with gentle agitation at room temperature. Gels were stained then with 100 mL of Colloidal Blue Staining Kit (55 mL water, 20 mL methanol, 20 mL solution A and 5 mL solution B; Invitrogen) for three hours at room temperature on a rocker. Post-staining, gels were de-stained by washing gels with deionised water for 2-5 hours (until areas of degradation visible as clear bands on a blue-stained background were clearly visible), changing water at 30-minute intervals. Gels were then removed from water, placed in a plastic sheet protector and scanned with a resolution of 300 dpi or higher using a flat-bed scanner. Gels were analysed with ImageJ.

Although gelatin zymography is a very useful qualitative tool for the detection and analysis of the level and type of gelatinases in a given sample, there are a few caveats that should be noted. Firstly, the process of reactivating gelatinases post-electrophoresis also activates latent forms of the enzymes (pro-MMP-2 and -9) which still possess the inhibitory N-terminal domain. Under physiological conditions, these enzymes would not possess any enzymatic activity. Gelatin zymography, therefore, assesses the total potential MMP activity within a sample. In some cases, latent and active forms may be differentiated on the basis of their molecular weights (pro forms are usually ~10 kDa heavier due to the presence of the inhibitory domain). Secondly, exposure to SDS disrupts the non-covalent interactions between gelatinases and their endogenous inhibitors – tissue inhibitor of metalloproteinase (TIMPs). Again, this assay detects enzymatic activity that would otherwise be inhibited under physiological conditions. Thus, gelatin zymography cannot be relied on to provide information about the net MMP activity in a given sample.

2.9 Flow cytometric analyses

Our group has well established flow cytometric methods to determine identity, quantity and localisation of leukocytes within different lung compartments. Fluorophore-conjugated antibodies bind to specific cell antigens and are detected as cells are passed through a laser beam one cell at a time. Specific sub-population of cells can subsequently be distinguished through cell size (detected as forward scatter), granularity (detected as side scatter), and the expression of various combinations of cell surface markers.

All flow cytometric analyses were performed using a 7-channel CyAn ADP flow cytometer (Beckman Coulter, High Wycombe, UK) fitted with a blue (488nm) and red (638nm) laser and filters to detect fluorescence in 7 different wavelength ranges (Table 2.13).

	Channels	Fluorescence channels (bandpass)	Fluorophores
Blue laser excitation wavelength: 488nm	FL-1	525/40	FITC or Ax488
	FL-2	585/42	PE
	FL-3	610/20	PE-TexasRed (PETR)
	FL-4	690/50	PE-Cy5 or PerCP
	FL-5	780/60	PE-Cy7
Red laser excitation wavelength: 638nm	FL-8	660/20	APC or Ax647
	FL-9	712/25	APC-Cy7 or Ax780

Table 2.13 - 7-Channel CyAn ADP flow cytometer fluorescence channels and fluorophores

Processing tissue to yield single cell suspension

Right lung lobes were homogenised either with or without fixation. Initially, lungs were mechanically dissociated in suspension with fixation buffer as our lab has previously found that simultaneous fixation and homogenisation of tissues maximised cell recovery, providing accurate cell counts. However, fixation of tissues prior to antibody staining has been known to alter and/or denature antigen epitopes, creating the impression of the lack of cell surface receptors/markers (as was suspected to be the case with my receptor of interest, CD147). Therefore, an alternative method of processing without fixation was also performed.

Lung samples that were fixed were placed in an orange M gentleMACS tube (Miltenyi Biotec, Surrey, UK) containing 2 mL of room temperature IC Fixation buffer (eBioscience, Inc, San Diego, CA, USA). The sample was then mechanically dissociated for 1 minute using a GentleMACS dissociator (Miltenyi Biotec, Surrey, UK). Immediately after, the fixation process was stopped with the addition of 10 mL of ice-cold FACS wash buffer (FWB) containing phosphate buffered saline (PBS), 2% foetal calf serum (FCS), 0.1% sodium azide, and 5mM EDTA and placed on ice.

Lung samples that were not fixed were placed in a blue C gentleMACS tube containing 2 mL PBS, collagenase (1:10) and DNAse (1:100). Samples were mechanically dissociated as detailed previously and subsequently incubated at 37°C for 20 minutes with constant agitation. Following the 20-minute incubation period, 10 mL of ice-cold FWB was added and samples were kept on ice.

Both samples were processed as follows thereafter. Lung homogenates were sieved through a 40µm nylon strainer (BD Falcon, New Jersey, USA) to produce a single-cell suspension which was then centrifuged at 2,000 rpm for 5 minutes at 4°C. Supernatants were discarded and cell pellets were re-suspended in 4mL FWB before centrifugation with the same settings. Supernatants were discarded again and the final cell pellets were re-suspended in 500 µL of FWB and kept on ice.

2.9.1 Cell surface staining *in vitro*

Lung single cell suspensions were incubated with various panels of fluorochrome-conjugated antibodies (Table 2.14, Table 2.15, Table 2.16) in FACS tubes for 30 minutes at 4°C in the dark in order to stain extracellular antigen markers and facilitate identification of cell populations.

Antibody cocktails were prepared in FWB to achieve the final concentration stated. After the 30-minute incubation period, 4 mL of FWB was added to each FACS tube to stop further antibody binding and samples were centrifuged at 2,000 rpm at 4°C for 5 minutes. Supernatants were discarded and the cell pellets were re-suspended in 400µL of FWB for analyses on the flow cytometer. Immediately prior to flow cytometric analysis, AccuCheck counting beads (Invitrogen) were added to determine cell counts. Following analysis on the flow cytometer, alveolar epithelial cells (Figure 2.4) and lung leukocytes (Figure 2.5) were gated according to different gating strategies (see figures for details).

2.9.2 Intracellular staining *in vitro*

An adapted flow cytometry based staining protocol was used to measure intracellular CypA. Lungs were processed as described above. Once a single-cell suspension was achieved, cell pellets were incubated with 250 µL of BD Cytofix/Cytoperm solution for 20 minutes at 4ºC. Cells were then washed by re-suspended in 4 mL of permeabilisation wash buffer (PWB) and centrifuged at 2,000 rpm for 5 minutes at 4ºC. Supernatants were discarded and cell pellets were re-suspended in 4 mL PWB before centrifugation with the same settings. Supernatants were discarded again and the final cell pellets were re-suspended in 50 µL of PWB.

A three-step staining procedure was performed: (1) Permeabilised single cell suspension was incubated for an hour at 4ºC with primary anti-cyclophilin A antibody (1:50 concentration or 10 µg/mL; Table 2.17); (2) 30 minute incubation at 4ºC with rabbit IgG APC-conjugated antibody (1:300 concentration or 80 ng/mL; Table 2.17); (3) 30 minute incubation at 4ºC with surface antigen antibody panels (Table 2.14, Table 2.15). Samples were washed twice with PWB between each step.

2.9.3 Antibodies

Different antibody panels were used to identify lung parenchyma cell populations (Table 2.14) and leukocyte populations (Table 2.15). Further antibodies were also added to the antibody cocktail to measure expression of various molecules of interest (Table 2.16) as detailed.

Lung parenchymal antibody panel					
Fluorochrome	**Antigen**	**Clone**	**Final concentration**	**Source**	**Expression**
FITC	EpCAM	G8.8	1:200	Biolegend	AECs
PE-CF594	CD31	Mec 13.3	1:800	BD Bioscience	Endothelium
PERCP	MHC-II	M5/114.15.2	1:400	Biolegend	AECs
PE-CY7	T1α (Podoplanin)	8.1.1	1:1500	Biolegend	AECs
APC	CD45	30-f11	1:1500	Biolegend	Leukocytes

Table 2.14 - Lung parenchyma antibody panel to identify alveolar epithelial cells (AECs), endothelial cells, and leukocytes.

Lung leukocyte antibody panel					
Fluorochrome	**Antigen**	**Clone**	**Final concentration**	**Source**	**Expression**
FITC	F4/80	BM8	1:400	Biolegend	Macrophages ++, monocytes +
PE-DAZZLE^{594}	CD11b	M1/70	1:800	Biolegend	Neutrophils, monocytes
PERCP	CD45	30-F11	1:400	Biolegend	Leukocytes
PE-CY7	Ly-6C	HK1.4	1:1500	Biolegend	Ly-6C high (classical) monocytes
APC	Ly-6G	1A8	1:1000	Biolegend	Neutrophils
AX780	CD11c	BU15	1:1000	eBioscience	Macrophages, dendritic cells

Table 2.15 - Lung leukocyte antibody panel to identify macrophages, monocytes, neutrophils and dendritic cells

Markers of interest / activation					
Fluorochrome	**Antigen**	**Clone**	**Concentration**	**Source**	**Expression**
PE	CD147	RL73	1:100	eBioscience	AEC, leukocytes
PE	ICAM-1 (CD54)	YN1/1.7.4	1:100	BioLegend	AEC, leukocytes

Table 2.16 - Antibodies used to measure markers of interest/activation expressed on various cell types

Fluorochrome	**Antigen**	**Clone**	**Concentration**	**Source**	**Expression**
-	Cyclophilin A	Polyclonal	1:50	Abcam (41684)	AEC, leukocytes
APC	Rabbit IgG	Polyclonal	1:300	R&D	-

Table 2.17 - Antibodies used to measure intracellular markers of interest in various cell types

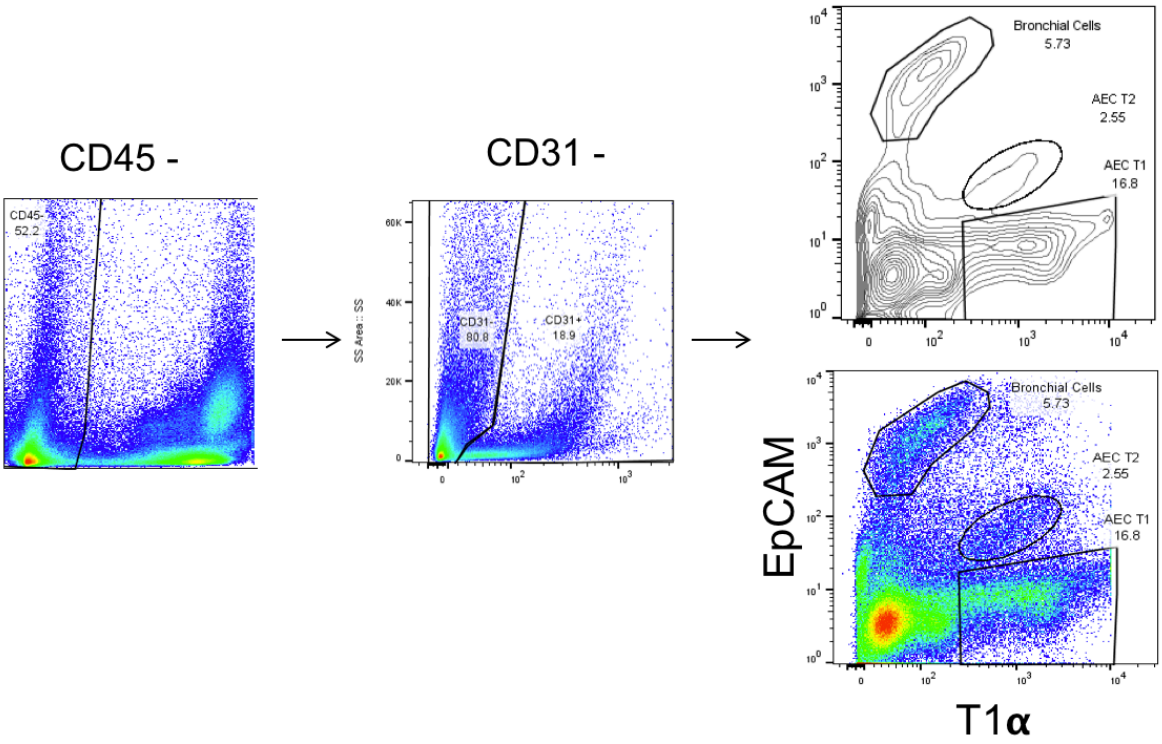


Figure 2.4 - Alveolar epithelial cell gating strategy.

(Left – right) CD45 negative (–ve) cells were gated; CD31 positive (+ve) cells were defined as pulmonary endothelium. CD31 –ve cells were gated; CD31 –ve cells separated based on their EpCAM and T1α expression.

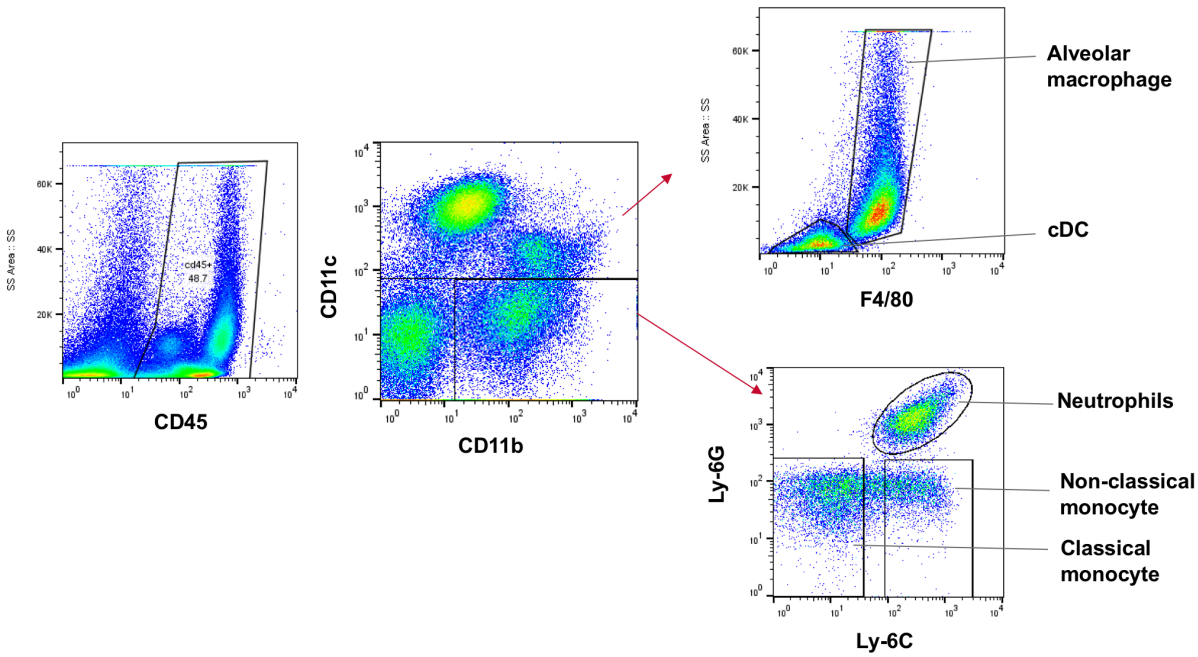


Figure 2.5 - Lung leukocyte gating strategy.

(*Left – right) CD45+ve were gated; Cells were separated based on CD11c and CD11b expression; (Top) CD11c +ve cells gated based on their F4/80 expression into alveolar macrophages (CD45 -ve, CD11c +ve, F4/80^{high}) and conventional dendritic cells (cDCs) (CD45 -ve, CD11c +ve, F4/80^{low}); (Bottom) CD11b +ve cells gated based on Ly-6G and Ly-6C expression into neutrophils (CD45 -ve, CD11b +ve, Ly-6G^{high}, Ly-6C^{high}), non-classical monocytes (CD45 -ve, CD11b +ve, Ly-6G -ve, Ly-6C^{low}), and classical monocytes (CD45 -ve, CD11b +ve, Ly-6G -ve, Ly-6C^{high}).*

2.10 Cell culture techniques

Both immortalised cell lines and primary cells were used. All cell cultures were grown and maintained in 175 cm^2 cell culture flasks with vented caps (BD Biosciences) in incubators maintained at 37ºC in a humidified 5% CO_2 atmosphere. Media was replaced every 2 to 3 days and cells were split when they reached confluence.

Table 2.18 - Cell lines, media and splitting solution used

Cell line	Media	Split with…
MLE-12 (ATCC, UK)	DMEM, 10% heat-inactivated foetal bovine serum (FBS), 1% penicillin-streptomycin-glutamine (PSG) (Sigma, Sigma, Life Technologies)	Accutase (ThermoFisher)
A549 (ATCC CCL-185, USA)	DMEM, 10% FBS, 1% PSG	Accutase (ThermoFisher)
Primary human alveolar epithelial cells (CellBiologics)	Complete human epithelial cell medium, 0.5 mL Insulin-Transferrin-Selenium, 0.5 mL EGF, 0.5 mL hydrocortisone, 5 mL L-Glutamine, 5 mL antibiotic-antimycotic solution, 25 mL FBS (CellBiologics)	1X Trypsin-EDTA solution (Sigma)
RAW264.7 (Sigma-Aldrich, UK)	RPMI-1640, 10% FBS, 1% PSG (Sigma)	Versene (ThermoFisher)
Murine bone marrow-derived macrophages (BMDM)	RPMI-1640, 10% FBS, 1% PSG (Sigma)	Versene (ThermoFisher)
Human monocyte-derived macrophages (HMDM)	RPMI-1640, 10% FBS, 1% PSG (Sigma)	1X Trypsin-EDTA solution (Sigma)

2.10.1 Primary cells

Murine bone marrow-derived macrophages (BMDM)

To isolate bone marrow derived macrophages, C57BL/6 mice were sacrificed, and trunks/legs of animals were sprayed with 70% ethanol solution. Both femurs were isolated and flushed with 1 mL of sterile RPMI to extract bone marrow cells. Media containing bone marrow cells was passed through 40 µm filters and resuspended to a final volume of 10 mL with fresh RPMI, 10% FCS, 1% PSG, supplemented with 50 ng/mL recombinant macrophage colony-stimulating factor (M-CSF) (PeproTech, New Jersey, USA). Cells were seeded into 55 cm^2 dishes and cultured for five days in incubators maintained at 37ºC in a humidified 5% CO_2 atmosphere. Media was replaced every other day.

Peripheral blood mononuclear cells (PBMC) isolation

50 mL Leucosep tubes containing 15 mL Histopaque-1077 (Sigma-Aldrich) were centrifuged at 28,000 rpm for 1 minute at RT. Blood was collected from healthy volunteers in EDTA containing BD Vacutainer tube. To each Leucosep tube, 20 mL of blood was added and centrifuged at 28,000 rpm for 1 minute at RT. Following separation, whole blood should be separated into layers: plasma, PBMCs, followed by red blood cells (RBCs) and granulocytes (Figure 2.6). The top plasma layer was removed and discarded using a pasteur pipette and the middle PBMC layer was gently aspirated and transferred to a new 50 mL Falcon tube.

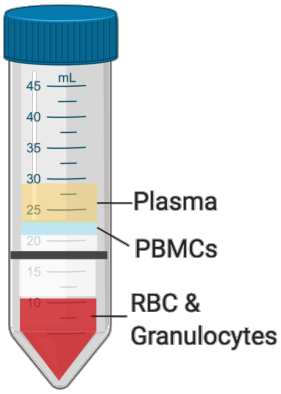


Figure 2.6 - Leucosep tubes with separated layers post-centrifugation

PBMCs were washed by addition of cold sterile PBS to a final volume of 50 mL and centrifuged at 300 x *g* for 10 minutes at 4ºC. After the first centrifugation, supernatant was removed, discarded, and wash step repeated. The final cell pellet was resuspended in 1 mL of cell sorting buffer (PBS, 1% FCS, 2 mM EDTA, 1% penicillin-streptomycin).

10 µL of cells were transferred to a FACS tube containing 10 µL AccuCheck counting beads (ThermoFisher Scientific) for a cell count using flow-cytometry. Different cell populations were identified based on their characteristic forward scatter (FCs) and side scatter (SSc) (Figure 2.7). Cell counts were determined.

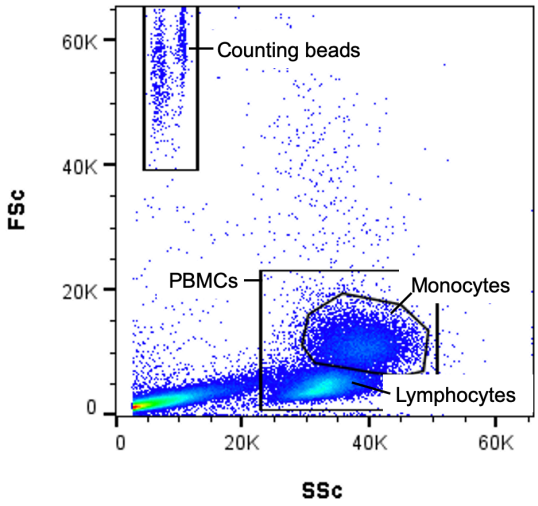


Figure 2.7 - Identification of monocytes, lymphocytes and counting beads from isolated PBMCs using flow cytometry

MACS® separation to isolate monocytes

A pan monocyte isolation kit (Miltenyi Biotec) was used to isolate monocytes from the PBMCs. Protocol was performed as manufacturer's instructions. In brief, the PBMC pellet was first resuspended in sorting buffer with addition of FcR Blocking Reagent and Pan Monocyte Biotin-Antibody Cocktail (containing a cocktail of biotin-conjugated monoclonal antibodies against antigens that are not expressed on human monocytes) for 5 minutes before a 10-minute secondary incubation with Anti-Biotin Microbeads. Magnetic cell separation was then performed using appropriately sized MACS Separator and MACS Columns determined based on the number of labelled and total cells. The cell suspension was applied onto the column and flow-through containing unlabelled, enriched monocyte cells were collected. Monocytes were centrifuged at 300 x *g* for 5 minutes at 4ºC and the cell pellet was resuspended in RPMI, 10% FCS, 1% PSG supplemented with 20 ng/mL recombinant granulocyte-macrophage colony-stimulating factor (GM-CSF) (PeproTech, New Jersey, USA).

Monocytes were then seeded into 55 cm^2 dishes and cultured for five days in incubators maintained at 37ºC in a humidified 5% CO_2 atmosphere. Media was first replaced on day 3, and then every other day subsequently. Cells were ready for use from day 7 onwards.

2.11 In vitro cell stretching

Flexcell FX-5000 Tension System

All stretch experiments were performed using the Flexcell® FX-5000™ Tension System made up of the following components: FlexSoft FX-5000™ software; FX5K™ Tension FlexLink®; BioFlex® baseplate and four gaskets; and BioFlex® Loading Stations™ with 25 mm Loading Posts.

The Flexcell Tension System uses regulated vacuum pressure and positive air pressure to deliver an equibiaxial tension to cells grown in a monolayer on flexible-bottomed silicone culture plates, better recapitulating the *in vivo* environment. The software allows for users to customise stretch parameters to design a regimen that best simulates the *in vivo* tissue strains and frequencies in an *in vitro* setting.

The parameters that were of interest to my experiments were:

i. Desired waveform shape
ii. Minimum and maximum % elongation for the plate membranes
iii. (N.B. The equibiaxial loading stations have maximum and minimum strain capabilities with respect to vacuum level. The 25 mm loading station that our system was equipped with was able to achieve a minimum % elongation of 0.8% and a maximum of 23.0%.)
iv. Frequency for the waveform (0.01 - 5 Hertz (Hz))
v. Duty cycle for the waveform, i.e. the percent of time that the waveform shape remains on at the high or rising part of the waveform.
vi. Duration of the regimen (day:hours:minutes:seconds), which will automatically be updated to the calculated regimen time accordingly.

For stretch experiments, cells were seeded in a specially designed flexible bottomed 6-well BioFlex® culture plates coated with type I collagen (Flexcell International) in the appropriate media. The cells were then left to reach 90-100% confluence, as assessed by light microscopy, for 24 hours at 37ºC in a humidified 5% CO2 atmosphere.

Once >90% confluence was achieved, cells were deemed ready for stretching. Immediately prior to stretching, cell culture media were removed, cells were gently washed twice with PBS, and media was replaced with fresh serum-free media. The BioFlex® culture plates were fitting into a rubber gasket and then inserted into the Flexcell baseplate within a cell culture incubator maintained at 37ºC and 5% CO_2. A plexiglass plate was placed on top of the culture plates to ensure an airtight seal between the culture plates and the baseplate was maintained for the full duration of the stretching experiment. Cells were then exposed to mechanical strain at the appropriate desired setting, e.g. maximum elongation of 20% at 0.25 Hz (or 15 cycles per minute) and a 33.3% duty cycle (the equivalent of a 1:2 inspiratory:expiratory ratio). Static control cells were also seeded and cultured on BioFlex culture plates and placed into the same incubator for the same stretch exposure time.

Sample processing post-stretching

At the end of stretch, conditioned culture media were collected and centrifuged at 300g for 5 minutes at 4ºC to yield cell-free supernatant which were aliquoted and frozen at -20ºC for future analyses. Cells were washed with PBS, harvested with cell dissociation solution (Sigma) diluted in FACS wash buffer (FWB), centrifuged at 2000 rpm for 5 minutes at 4ºC, and incubated for 30 minutes with the appropriate flurorophore-conjugated antibody panels against alveolar epithelial cell identification markers and cell surface activation markers and their corresponding isotope controls. After staining, cells were washed twice with FWB and then analysed by flow cytometry. Reported expression levels were expressed as mean

fluorescence intensity (MFI) of stained cells with corresponding isotype control values subtracted.

2.12 Lactate dehydrogenase (LDH) assay

Lactate dehydrogenase (LDH) is an oxidoreductase enzyme present in a wide variety of organisms. It catalyses the inter-conversion of pyruvate and lactate with concomitant interconversion of NADH and NAD+ (Figure 2.8). Upon damage to the plasma membrane of cells, LDH is rapidly released into the cell culture media. Since LDH is a fairly stable enzyme, the amount of LDH in the media can be evaluated to assess the level of plasma membrane damage.

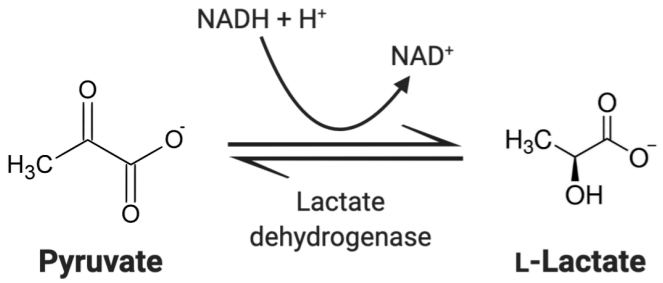


Figure 2.8 - Lactate dehydrogenase converts pyruvate to L-Lactate

In this assay, LDH reduces NAD to NADH, which then interacts with a specific probe to produce a detectable colour at 450 nm. Protocol was performed as per manufacturer's instructions. In brief, reaction wells were set up; 50 µL of standards (12.5, 10, 7.5, 5, 2.5, 0 nmol NADH), 50 µL sample (diluted 1 in 2 with LDH assay buffer), or 50 µL positive control sample were added to a 96-well plate. 50 µL of Reaction mix (2 µL of LDH Substrate Mix + 48 µL LDH Assay buffer) was added to every well and mixed well. Plate was then placed in a microplate reader set to kinetic mode reading at an OD of 450 nm every 2-3 minutes for at least 30-60 minutes at 37ºC protected from light. To calculate the amount of LDH present in samples, two time points in the linear range were used.

2.13 NO assay

Nitric oxide is a molecular mediator of many physiology processes, and therefore measuring its levels in cell culture media is often of interest. This kit utilises the Griess reaction to detect both nitrite, formed by the spontaneous oxidation of NO under physiological conditions, and nitrate that has been catalytically reduced to nitrite. The Griess reaction is summarised as the azo coupling between diazonium species, which are produced from sulphanilamide with NO_2, and naphthylethylenediamine, resulting in a colorimetric (540 or 570 nm) product proportional to the NO metabolite present.

Protocol was performed as per manufacturer's instructions. In brief, cell culture media was centrifuged at 1,000 x *g* for 15 minutes at 4ºC to remove any insoluble material. Supernatant was collected and used for assays. Standard curves for both NO_2 and NO_3 were generated by diluting appropriate amounts of provided standards with buffer solution. 50 µL of samples were added into four wells of a 96-well plate. Two wells were used for the NO_2^- detection and the other two were used for the [NO3- + NO_2^-] detection step. Buffer solution was added to wells to bring samples to a final volume of 100 µL for NO_2^- and 80 µL for [NO3- + NO_2^-] detection. In the wells for [NO3- + NO_2^-] detection, 10 µL of Nitrate Reductase solution and 10 µL of Enzyme Co-factors solution was added. The plate was then mixed using a horizontal plate shaker and incubated for two hours at 25ºC. After two hours, 50 µL of Griess Reagent A was added to all wells, mixed, and incubated for 5 minutes at 25ºC. Then 50 µL of Griess Reagent B was added to all wells, mixed, and incubated for 10 minutes at 25ºC. The plate was then read at 540 nm in a microplate reader.

2.14 Statistical analyses

All data are shown/expressed as means ± SD (if parametric), or box and whisker plots and scatter dot plots with means (if non-parametric). The model assumption of normality of residual was assessed by the Shapiro-Wilk test. Statistical analyses of data between groups were

performed using a two-tailed Student's t test or one-way ANOVA with Sidak's or Bonferroni tests for multiple comparisons (if parametric) and Mann-Whitney U-test and Kruskal-Wallis test with Dunn's multiple comparisons test (if non-parametric). All time course data were analysed using a two-way ANOVA or a t-test of end point values. Correlation data were assessed using non-parametric Spearman's correlation test. All data were analysed on GrapPad Prism software. A p-value of less than 0.05 was defined as the minimum threshold for statistical significance.

3 Cyclophilin A and CD147 in ventilator-induced lung injury

3.1 Abstract

Despite the increasing amount of evidence to suggest the involvement of extracellular cyclophilin A and its primary receptor, CD147, as a signalling axis in inflammatory diseases, very little is known about its role in the lung. The aim of this chapter was to investigate the involvement of CypA and CD147 in ventilator-induced lung injury.

Following high V_T ventilation, there is a substantial increase in the levels of extracellular CypA in bronchoalveolar lavage fluid compared with untreated animals. Assessment of the kinetics of CypA over the course of VILI revealed a significant early upregulation of CypA in BAL at two hours, preceding signs of physiological deteriorations. In contrast to BAL, plasma levels of CypA remained relatively low at all time points regardless of ventilation strategy, suggesting that CypA is produced locally within the lungs. Additionally, there was also an early upregulation of CD147 on the surfaces of pulmonary cells after 1 hour of high V_T ventilation. Assessment of the correlation between CypA and markers of lung injury revealed a close correlation between BAL CypA and the soluble receptor of advanced glycation end products (sRAGE), an established marker of epithelial injury, suggesting an association between the processes of CypA release and epithelial damage.

Together these findings demonstrate the presence of extracellular CypA and its primary receptor, CD147, in the lungs. The early upregulation of both CypA and CD147 supports the likelihood that the CypA:CD147 axis plays a novel pathogenic role in ALI. However, the close correlation between CypA and sRAGE might indicate that the increase in CypA in the alveolar space is a consequence of epithelial injury during VILI.

Lastly, we demonstrate for the first time the presence of extracellular CypA in the alveolar space of ARDS patients. BAL fluid samples from ARDS patients who had been previously recruited into randomised control trials (KARE and HARP) showed significantly higher levels

of extracellular CypA compared with BAL obtained from healthy volunteers. Importantly, this demonstrates the relevance of CypA in human disease and provides further support for its plausibility as a potential therapeutic target.

3.2 Introduction

Cyclophilin A (CypA) is a ubiquitously distributed intracellular protein present in all prokaryotes and eukaryotes (260). It makes up 0.1-0.6% of total cytosolic protein and its peptide-propyl-isomerase activity makes it important in facilitating processes such as protein folding and trafficking within cells (332). While most of the focus to date has been on its intracellular roles, more recent studies have begun to appreciate its role in the extracellular space. In response to stimuli such as hypoxia, infection, or oxidative stress, CypA can be released from cells (201, 293, 333). Once in the extracellular space, CypA is able to interact with its primary cell surface receptor, cluster of differentiation 147 (CD147), triggering downstream inflammatory responses (196, 197).

CD147, also known as Extracellular Matrix Metalloproteinase Inducer (EMMPRIN) or basigin (BSG), is a member of the immunoglobulin superfamily (170). This type 1 transmembrane glycoprotein is widely expressed in its various glycoforms on many cell types, including epithelial, neuronal, lymphoid and myeloid cells (200, 334). Through studies with CD147 knock-out mice, CD147 has been shown to play an important physiological role in early developmental processes such as spermatogenesis, lymphocyte response, retinal and neurological functions, as well as fertility and reproductive processes (196). CD147 also mediates pathogenic effects through its role as a matrix metalloproteinase (MMP) inducer and its capacity to mediate chemotactic activity in leukocytes.

While the mechanisms underlying CypA-CD147 activities are still not fully elucidated, the contribution of the CypA:CD147 axis to the pathogenesis of a host of inflammatory diseases, such as sepsis (295), atherosclerosis (249), arthritis (250, 251), and cancer (252) is increasingly evident.

Currently, very little is known about the role of CypA:CD147 interactions within the lungs. Inhibition of CD147 with an intraperitoneally (i.p.) delivered anti-CD147 antibody in a mouse model of asthmatic lung injury has been shown to significantly reduce the accumulation of eosinophils and T-cells in lung tissue of asthmatic mice (335). The same research group has also investigated the role of CypA in lipopolysaccharide (LPS)-induced pulmonary inflammation (291). Using a mouse model, they demonstrated that inhibition of CD147 using the same approach (i.p. injection of an anti-CD147 antibody) prior to an intranasal LPS challenge led to a significant reduction in neutrophil infiltration into lung tissues and airways. Additionally, they also explored the effects of CypA inhibition with a non-immunosuppressive cyclosporine analogue (SDZNIM811). Mice receiving the drug displayed a similar reduction in neutrophil numbers to those that received that anti-CD147 antibody. Use of both treatments simultaneously resulted in only a minor further reduction in neutrophil numbers, which the authors interpreted as suggestive of both mechanisms acting on the same CypA:CD147 pathway.

However, in both studies, the exact mechanisms underlying the reduction in asthmatic lung inflammation and leukocyte infiltration were not explored. Was CypA translocating from the alveolar space into the blood and binding to CD147 on the surface of leukocytes, causing them to migrate into the lungs? Was CypA somehow presented on the surface of the endothelium, e.g. in the glycocalyx layer? Or was CypA causing the upregulation of a secondary mediator/cytokine in the airways which is then exerting a chemotactic effect? Additionally, the inhibitors were delivered i.p. in all instances. Was the anti-CD147 antibody or CypA inhibitor exerting its effects in the blood or in the airways? If it was thought to be the latter, can we confidently say that the inhibitors were able to gain access into the alveolar space? Evidently, there is a lot that is still not understood about how CypA and CD147 contribute to the inflammatory response in the lungs.

One of our main area of interest as a research group is ventilator-induced lung injury (VILI). The experiments presented in this chapter are therefore focused specifically on the previously unexplored role of the CypA:CD147 axis during VILI.

As discussed in the introduction, we and others have observed an increase in MMPs following high tidal volume ventilation (164, 169). Correspondingly, CD147 expression on the surface of pulmonary cells was also upregulated (164, 169). Because CD147 is a major player in MMP activation, it is likely that the increase in CD147 is related to subsequent MMP induction. However, to date, no one has described a mechanism whereby mechanical ventilation leads to activation of MMPs via CD147. Given that CypA is seemingly the primary soluble ligand of CD147, we hypothesised that secreted CypA may play an important, hitherto unexplored role in VILI. In this chapter, we present our findings from our initial exploration of the involvement of CypA during VILI.

3.3 Aim

This chapter aims to evaluate the potential involvement of CypA and CD147 in the lungs during injurious using an *in vivo* model of VILI by:

a) Determining the levels of CypA in the alveolar space and circulating plasma.
b) Evaluating the expression of the receptor CD147.

3.4 Protocols

3.4.1 In vivo ventilator-induced lung injury model

The VILI model is described in detail in 'Materials and methods' chapter (see chapter 2.3.1). In brief, C57BL/6 mice were anaesthetised, tracheostomised for mechanical ventilation, and the left carotid artery was cannulated. The ventilator was initially set at low V_T settings (V_T: 8 mL/kg, RR: 120 bpm, PEEP 3.0 cmH_2O, 100% O_2) regardless of intended final experimental ventilator strategy. Three pulmonary recruitment manoeuvres, 30-seconds apart, were performed to reverse any temporary atelectasis and standardise the volume history of the lungs for the effects of surgery and anaesthesia. After the last recruitment, an inspiratory pause was performed to determine the respiratory mechanics at baseline. At this point, the settings of the ventilator were then either maintained to deliver low V_T ventilation (V_T: 8 mL/kg, RR: 120 bpm, PEEP 3.0 cmH_2O, 100% O_2) or adjusted to a high V_T ventilation strategy (V_T: 35-40 mL/kg, RR: 80 bpm, PEEP 3.0 cmH_2O, 4% CO_2 + O_2). Mice were ventilated for 1, 2, or 3 hours.

Throughout the ventilation period, respiratory mechanics were measured every 15 minutes. Arterial blood gas analysis was performed at set intervals, with an initial reading at 15 minutes and then subsequently, hourly (i.e. at 1, 2, and 3 hours). Blood pressure was continuously monitored throughout the experiment.

3.4.2 Sample processing and analyses

At the end of the protocol, mice were exsanguinated under general anaesthesia by severing the left carotid artery. Blood was collected and centrifuged at 4,000 rpm, 5 minutes, 4°C to isolate the plasma fraction. Bronchoalveolar lavage (BAL) was performed and BAL fluid was collected, and centrifuged at 300 *x g*, 5 minutes to yield cell-free supernatant which was then stored at -80ºC for subsequent analyses. The right lower lobe of lung, which was tied off before

BAL was performed, was removed to determine wet/dry (W/D) weight ratio. The remaining lobes of the lung were homogenised using a GentleMACS tissue dissociator to produce a single-cell suspension for antibody staining and subsequent flow cytometric analyses of surface CD147 expression and leukocyte counts.

3.4.3 Plasma and BAL analyses

Plasma and BAL samples were evaluated using ELISA to determine levels of CypA. The concentration of soluble receptor for advanced glycation end products (sRAGE) in BAL samples were also determined using ELISA. BAL fluid protein measurement was performed using the Qubit Protein Assay Kit as detailed in chapter 2.

3.4.4 Analysis of human ARDS samples

Human ARDS samples were kindly provided by Professor Danny McAuley. All samples were collected and stored in accordance with the protocol and ethics of the 'Keratinocyte growth factor for the treatment of the acute respiratory distress syndrome' (KARE) and 'A randomised clinical trial of hydroxymethylglutaryl-coenzyme A reductase inhibition for acute lung injury' (HARP) studies. These studies and their protocols have been published (36, 336, 337).

All 'ARDS' samples analysed in the chapter were from patients who fulfilled the following inclusion criteria of acute lung injury (ALI) defined by acute onset of and were thus deemed to be eligible to participate in the studies:

a) Hypoxic respiratory failure (PaO_2/FiO_2 ≤40 kPa);
b) Bilateral infiltrates on chest X-ray consistent with pulmonary oedema;
c) No clinical evidence of left atrial hypertension or, if measured, pulmonary arterial occlusion pressure ≤18 mmHg;
d) Requirement for positive pressure mechanical ventilation via an endotracheal tube or tracheostomy.

All four ALI criteria listed above must over within the same 24-hour period. The onset of ALI when the last ALI criteria is met. Patients from the HARP and KARE studies were enrolled within 48 hours and 72 hours, respectively, of ALI onset.

All the samples were from patients that had been randomised to the control group and thus would have received either a placebo administered once daily enterally for up to 28 days if they had been enrolled on the HARP trial or normal saline once daily as a bolus intravenous injection for up to 6 days if they were enrolled on the KARE trial. Control samples were from healthy volunteers enrolled in the HARP study (trial no: ISRCTN70127774) who underwent BAL as controls.

BAL sampling

The samples that were analysed were from BAL performed at baseline according to standard guidelines and are detailed in the publications (336, 337). In brief, three successive 50 mL aliquots of 0.9% saline were instilled into a sub-segment of the right middle lobe and each aspirated immediately with low suction. BAL fluid retrieved was then immediately placed on ice until transferred to the laboratory for processing. BAL fluid was centrifuged at 900 *x g* for 5 minutes at 4ºC. The supernatant was removed and stored at 80ºC for subsequent analyses. Samples were transferred to our laboratory at this stage where they were then thawed out immediately prior to analyses.

ELISA

BAL fluid levels of CypA were measured using a commercially available human cyclophilin A ELISA kit (Abbexa, UK), which included pre-coated micro ELISA plate wells. The assay was conducted as per manufacturer's instructions and detailed in chapter 2.

3.4.5 Statistics

Power calculations were performed for the *in vivo* studies in this chapter. The final peak inspiratory pressure was considered to be the most indicative endpoint of ventilation studies. From previous experience, if the final peak inspiratory pressure is different, most other physiological measures of injury will also be different. Therefore, this was to carry out power calculations to estimate group sizes. Given a standard deviation of 4.5 (cmH_2O) and 'relevant' mean difference of 7, with values of 0.05 and 0.8 for alpha and beta in a 2-sided test, we estimate group sizes of 5-7 for physiological experiments would be sufficient to achieve 80% power at 0.05 alpha.

3.5 Results

3.5.1 Cyclophilin A is dramatically upregulated during VILI

To determine if CypA is released in response to stretch during mechanical ventilation, levels of CypA in BAL from mice ventilated at high V_T for 3 hours were measured and compared with untreated controls (Figure 3.1). Following three hours of high V_T ventilation, an impressive increase in BAL CypA was observed, with levels roughly 120-fold greater than in the untreated group (untreated: 53.6 ± 25.3 pg/mL vs VILI: 5,918.5 ± 3,036.3 pg/mL).

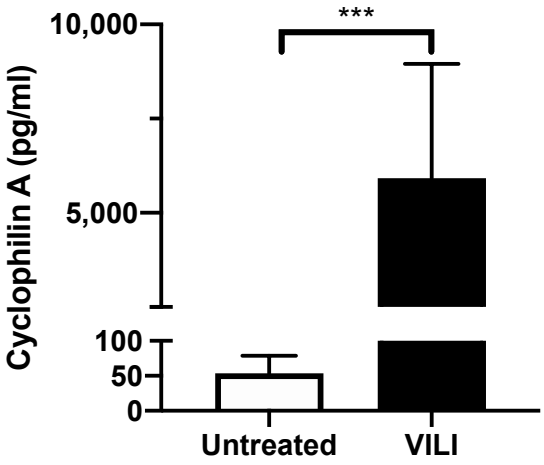


Figure 3.1 – Levels of CypA in BAL of untreated mice and mice subjected to 3 hours of high V_T (VILI)

*A substantial 120-fold increase in CypA was observed following VILI (untreated: 53.6 ± 25.3 pg/mL vs VILI: 5,918.5 ± 3,036.3 pg/mL). Data were normally distributed and shown as mean ± SD. N=6. ***p<0.001. Data were evaluated by an unpaired t-test.*

3.5.2 CypA kinetics during VILI

From the data above, it was clear that CypA is significantly upregulated following 3 hours of high V_T ventilation. However, it was unclear if this increase in CypA is a cause or a consequence of VILI. To address this, we explored the kinetics of CypA during the course of

injury. Animals were ventilated at either low V_T (8 mL/kg) or high V_T (35-40 mL/kg) for 1, 2, or 3 hour(s) and the level of CypA in the BAL and plasma were measured.

Compared to untreated animals, BAL CypA levels following only 1 hour of low V_T ventilation were significantly increased (untreated: 53.6 ± 25.3 pg/mL vs 1H LV_T: 651.6 ± 282.0 pg/mL, $p<0.0004$). Comparison of BAL CypA levels after 1, 2, and 3 hour(s) of low V_T ventilation revealed no further increases with increasing ventilation times (Figure 3.2). In contrast, there was a progressive increase in the level of CypA in animals ventilated at high V_T over the course of ventilation, with highest levels seen at 3 hours (3H LV_T: 765.9 ± 408.3 pg/mL vs. 3H HV_T: 5,918.5 ± 3,036.3 pg/mL).

At 1 hour, there were no differences between CypA in the low V_T and high V_T group (1H LV_T: 651.6 ± 282.0 pg/mL vs 1H HV_T 842.6 ± 117.4 pg/mL). At both 2 and 3 hours, CypA was significantly higher in the high V_T group compared with the low V_T group (2H LV_T: 662.5 ± 268.3 pg/mL vs. 2H HV_T: 2,586.6 ± 1,054.1 pg/mL).

In contrast, plasma levels of CypA remain consistent across all time points, regardless of ventilation protocol, with significant variability seen between animals in the same group (Figure 3.3).

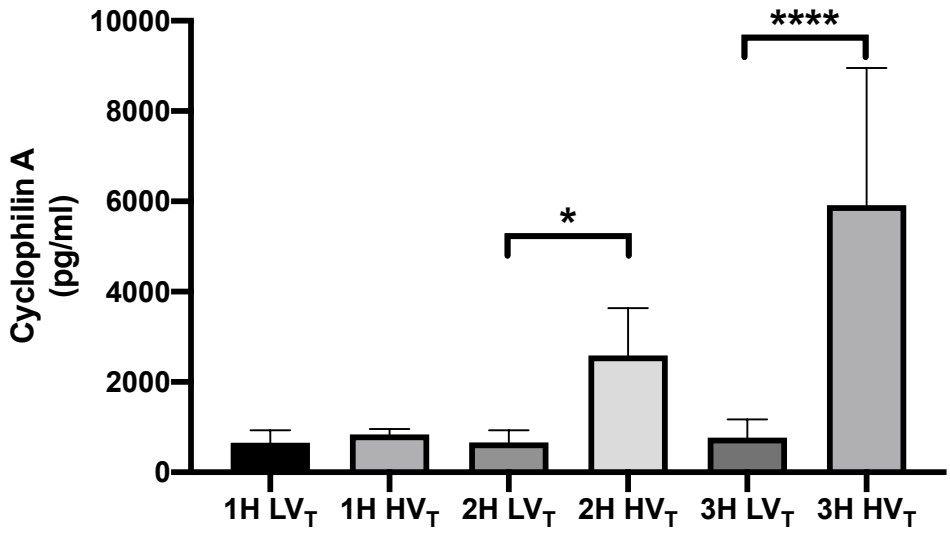


Figure 3.2 - *In vivo* kinetic profile of the levels of CypA in BAL following 1, 2, and 3 hours of either low or high V_T ventilation.

*The level of CypA was significantly greater in animals ventilated at high V_T compared with those ventilated at low V_T at 2 and 3 hours. Data shown as mean ± SD. N=5-6. *p<0.05, ****p<0.0001. One-way ANOVA with Bonferroni's multiple comparisons test was used to assess difference between low and high V_T at each time point.*

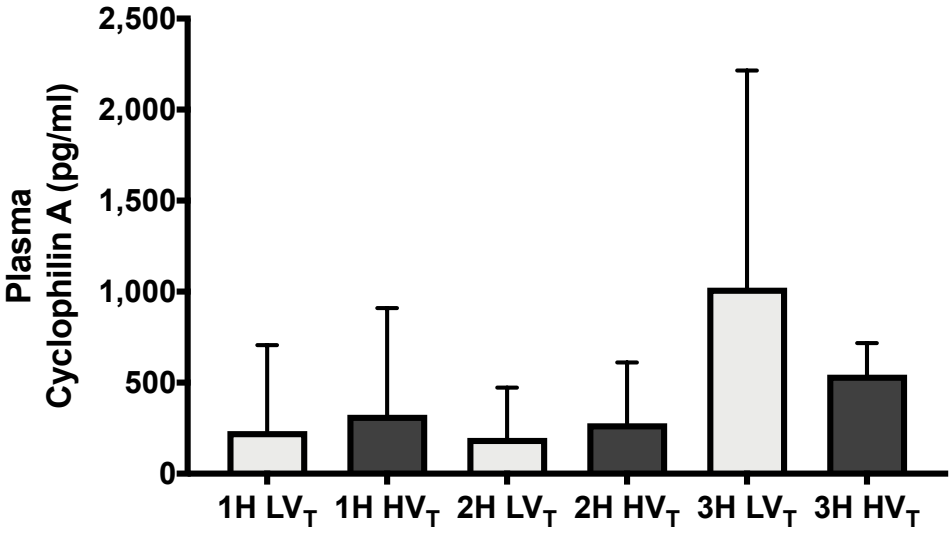


Figure 3.3 - *In vivo* kinetic profile of plasma CypA following 1, 2, and 3 hours of either low or high V_T ventilation..

No significant changes in the level of CypA in plasma at 1, 2, or 3-hour(s) in both low V_T and high V_T group. Data shown as mean ± SD. N=5-6. NS. One-way ANOVA with Bonferroni's multiple comparisons test.

3.5.3 Markers of lung injury

Given the early upregulation of CypA in the alveolar space, other established markers of lung injury were assessed to determine if physiological signs of VILI were also apparent at early time points.

There were no differences in BAL protein concentration (Figure 3.4A) and no deterioration in arterial oxygenation (PaO_2; Figure 3.4B) at both 1 and 2 hour(s) between the low V_T and high V_T group. At 3 hours, there was a significant increase in BAL protein and a significant decrease in PaO_2 in the high V_T group compared with the low V_T group. W/D weight ratio showed an increase at 2 hours in the high V_T group; this increase became more apparent at 3 hours (Figure 3.4C). BAL sRAGE was also significantly increased at 2 hours in the high V_T group and this increase was sustained at 3 hours (Figure 3.4D).

Leukocyte counts were also assessed but there were no significant changes in leukocyte numbers between the ventilation groups and time points (data not shown).

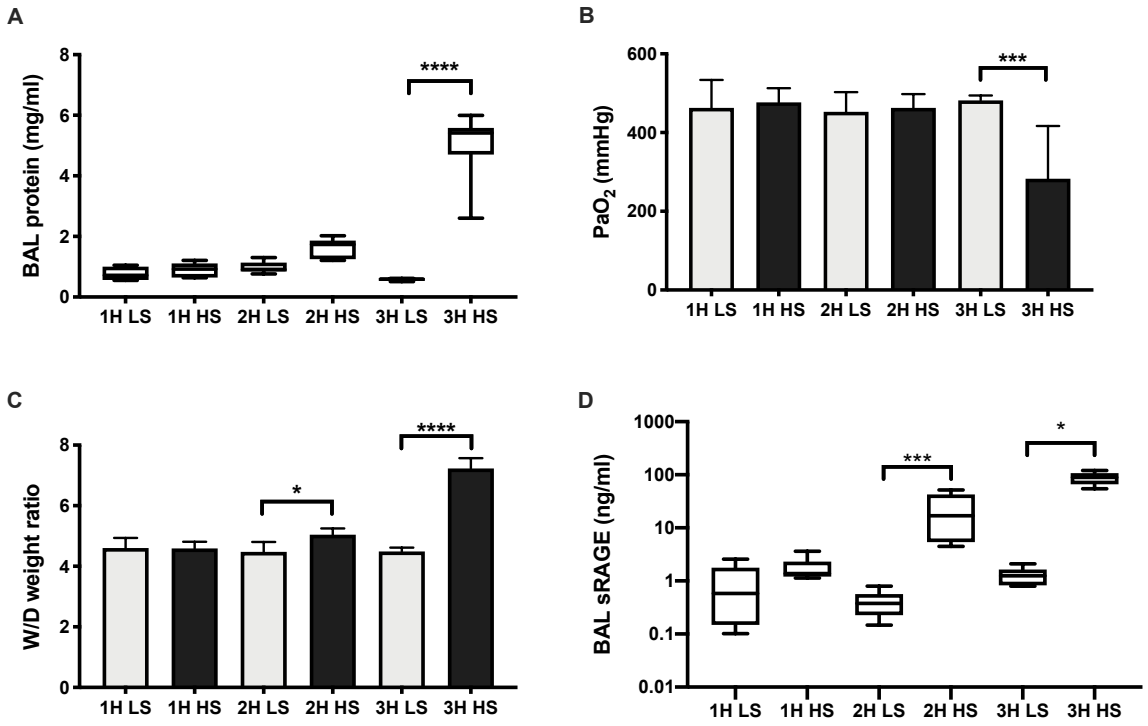


Figure 3.4 - Assessment of BAL protein, arterial oxygenation, lung W/D weight ratio and BAL sRAGE following 1, 2, and 3 hours of either low or high V_T ventilation.

*(A) BAL Protein, (B) Arterial oxygenation (PaO_2), (C) Weight/dry weight ratio, and (D) BAL sRAGE (y-axis displayed on a logarithmic scale). No significant differences in either BAL protein or PaO_2 were observed between the low and high V_T groups until 3 hours. An increase in W/D weight ratio and BAL sRAGE in the high V_T group compared with low V_T group was first observed at 2 hours and sustained at 3 hours. N=2-6. *p<0.05, ***p<0.001, ****p<0.0001. Data for PaO_2 and W/D weight ratio were normally distributed and thus displayed as mean ± SD and evaluated with a one-way ANOVA with Bonferroni's multiple comparisons test. Data for BAL protein and sRAGE were not normally distributed and thus displayed as box-whisker plot and evaluated with a Kruskal-Wallis test with Dunn's multiple comparisons test.*

3.5.4 Correlation between CypA and markers of lung injury

To determine if CypA is a potential biomarker of lung injury, specifically if it is a good predictor of the severity of injury, the correlations between BAL fluid levels of CypA and the markers of lung injury mentioned above were assessed. CypA levels showed positive correlation with BAL protein ($r=0.48$, $p<0.01$; Figure 3.5A), strong positive correlation with sRAGE ($r=0.71$; $p<0.0001$; Figure 3.5B), and negatively correlated with PaO2 ($r=-0.47$, $p<0.05$; Figure 3.5C). CypA did not show any overall correlations with W/D weight ratio (Figure 3.5D). However, this may be due to the lack of correlation between CypA and W/D weight ratio when CypA levels are <1,000 pg/mL. When concentrations of CypA increase beyond 1,000 pg/mL, W/D weight ratio begins to show corresponding increases. This might suggest that W/D weight ratio is not a very sensitive marker and also that CypA is not merely a marker of permeability.

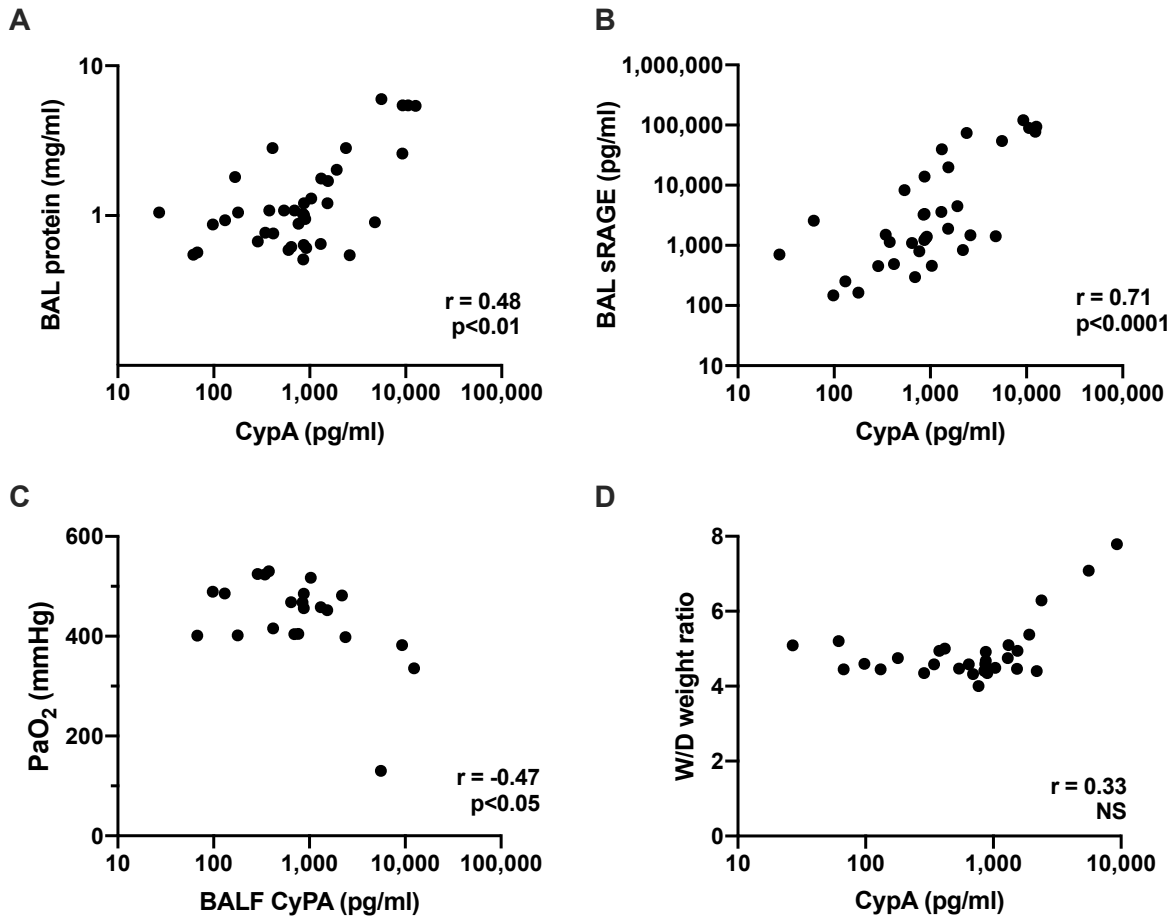


Figure 3.5 - Assessment of the correlation between BAL CypA and (A) BAL protein, (B) PaO_2, (C) W/D weight ratio, (D) BAL sRAGE.

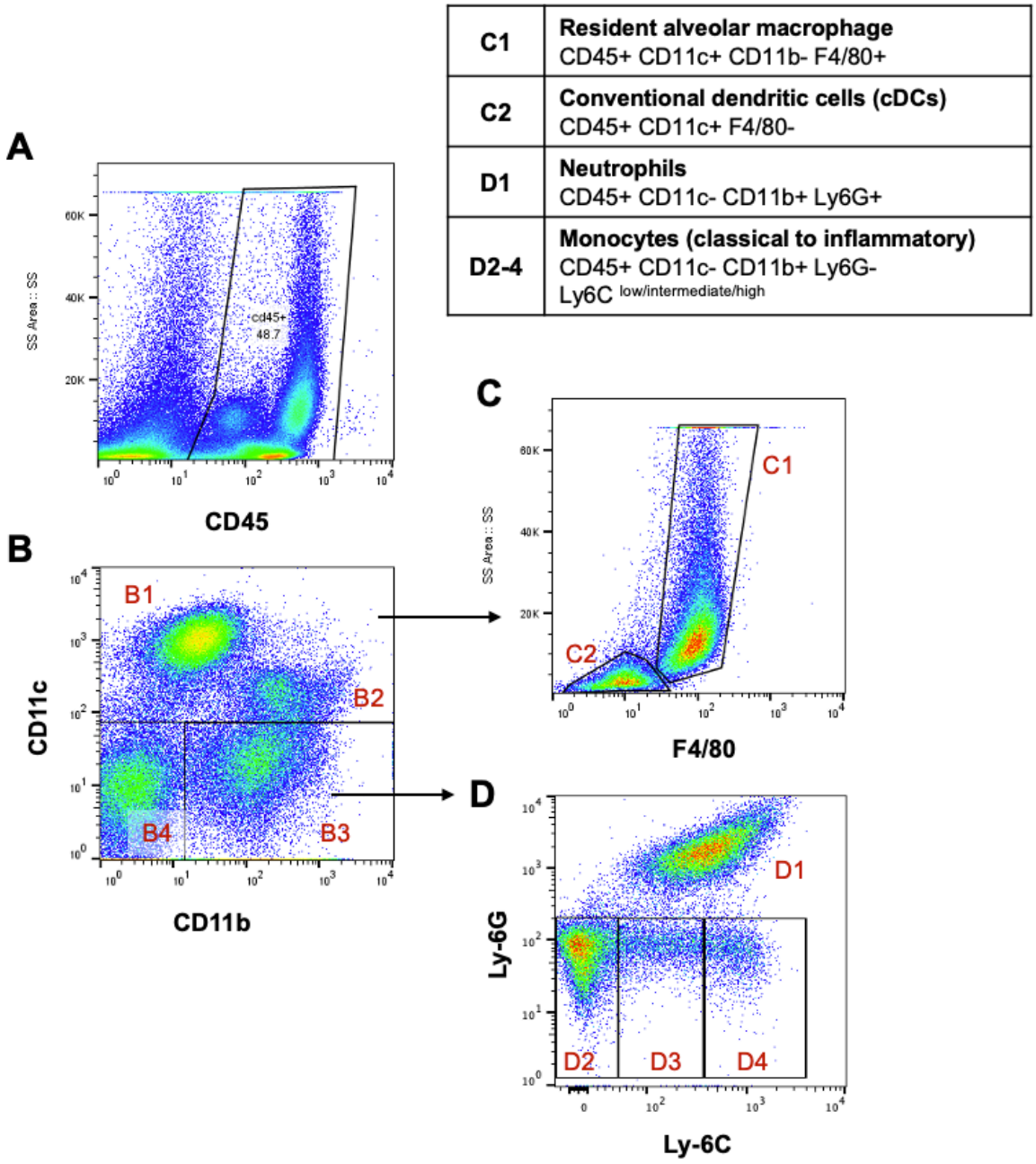
A positive correlation between CypA and BAL protein (A), and CypA and sRAGE (B) and a negative correlation between CypA and PaO_2 (C) were observed. CypA showed no correlation with W/D weight ratio. On graphs A to D, the x-axes showing BAL CypA levels were displayed on a logarithimic scale. On graphs A and B, the y-axes showing BAL protein and BAL sRAGE, respectively, were also displayed on a logarithimic scale. The data were not transformed to logarithimic for analyses. Data were analysed using non-parametric Spearman correlation test, where r = Spearman's rank correlation coefficient.

3.5.5 Pulmonary cell identification using flow cytometry

To assess the levels of surface CD147 expression on different pulmonary cells during VILI, cells were subdivided into pulmonary leukocytes and pulmonary epithelial cells.

The phenotype of resident leukocyte subtypes within the lung tissue has been well characterised and established within our research group (338). Leukocytes were identified as CD45 positive (+) events (Figure 3.6A) and then separated into four distinct populations on the basis of their CD11c and CD11b expression (Figure 3.6B, B1-4).

The CD11c+ populations (Figure 3.6B, B1 and B2) consisted of two different populations of cells which were then gated on the basis of their F4/80 expression (Figure 3.6C). One population (Figure 3.6C, C1) had a high F4/80 expression and was highly auto fluorescent – these were considered to be resident alveolar macrophages. The second population (Figure 3.6C, C2) was F4/80 negative (-) and were considered to be conventional dendritic cells (cDCs). The CD11c- populations (Figure 3.6B, B3 and B4) were made up of another two distinct cell populations – CD11b+ (B3) and CD11b- (B4). CD11b is an integrin expressed predominantly by neutrophils and mononuclear cells. CD11b+ (B3) population was therefore likely made up by monocyte and neutrophils. The CD11c-CD11b- (B4) population was likely made up by non-myeloid cells such as lymphocytes. The CD11b+ population was then further differentiated based on their Ly6G and Ly6C expression into four populations (Figure 3.6D, D1-4). The $Ly6G^{high}$ cells were identified as neutrophils (Figure 3.6D, D1). The Ly6G- cells were different subtypes of monocytes which were differentiated on the basis of their Ly6C expression (Figure 3.6D, D2-4). Cells with low expression of Ly6C were the non-classical (resident) monocytes (D2) and those with high expression of Ly6C were the classical (inflammatory) monocytes (D4). The population with intermediate expression of Ly6C were likely monocytes undergoing conversion between the two different subtypes (D3).



C1	**Resident alveolar macrophage** CD45+ CD11c+ CD11b- F4/80+
C2	**Conventional dendritic cells (cDCs)** CD45+ CD11c+ F4/80-
D1	**Neutrophils** CD45+ CD11c- CD11b+ Ly6G+
D2-4	**Monocytes (classical to inflammatory)** CD45+ CD11c- CD11b+ Ly6G- Ly6C low/intermediate/high

Figure 3.6 - Lung leukocyte gating strategy using flow cytometry.

(A) CD45 positive (CD45+) cells were gated; (B) Cells were separated based on CD11c and CD11b expression; (C) CD11c+ cells gated based on their F4/80 expression into alveolar macrophages (C1) and conventional dendritic cells (cDCs, C2); (D) CD11b+ cells gated based on Ly-6G and Ly-6C expression into neutrophils (D1), and monocytes subsets (non-classical, intermediate, and classical, D2-D4).

Identification of pulmonary epithelial cells is less well defined than leukocytes. To identify pulmonary epithelial cells, leukocytes (CD45+) and endothelial cells (CD31+) were excluded (Figure 3.7A, B). The remaining CD45-, CD31- cells were then separated into three different subtypes of epithelial cells based on their EpCAM (epithelial cell adhesion molecule) and T1α/Podoplanin expression (Figure 3.7C, C1-3).

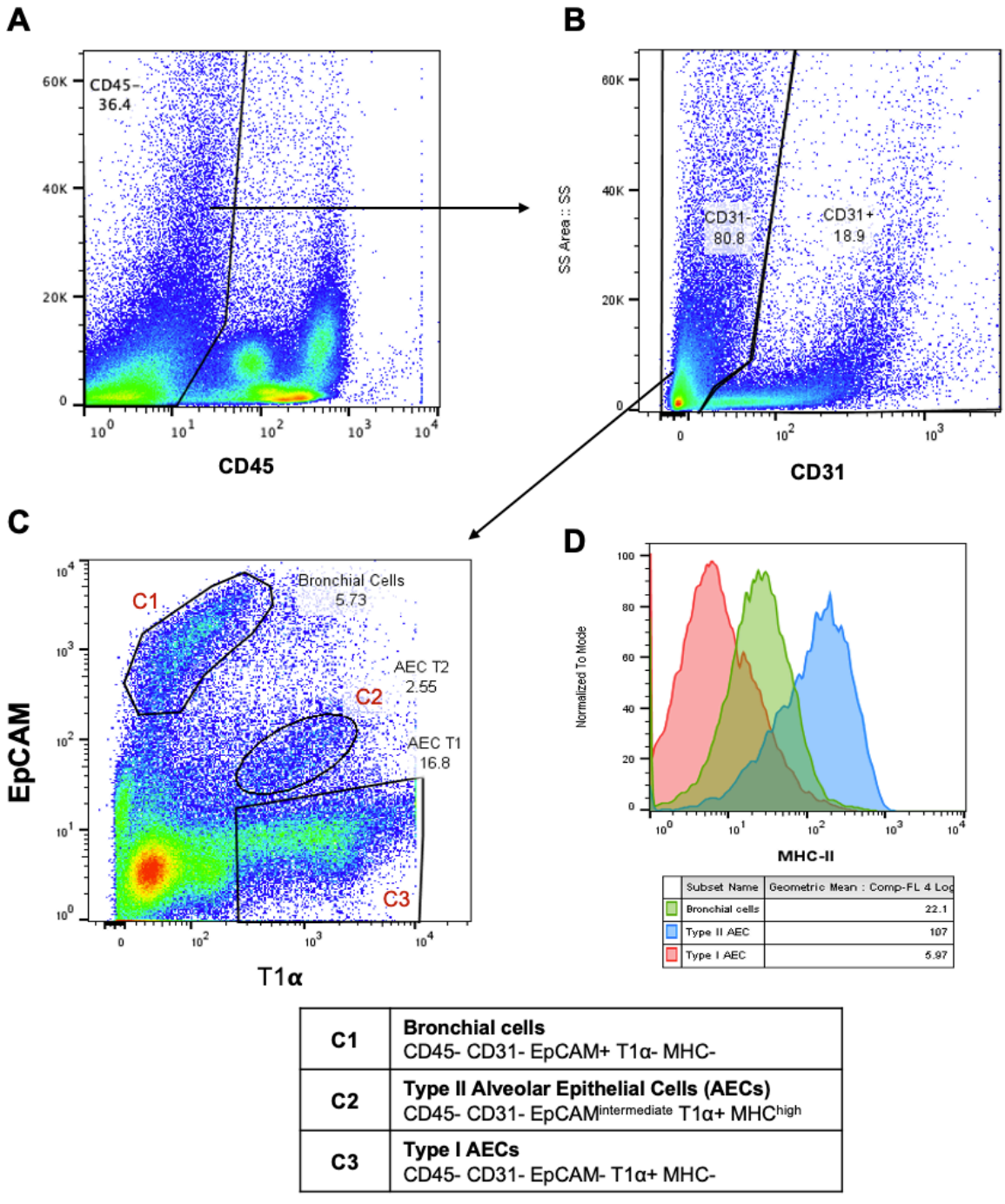
Cells that were EpCAM+ and T1α- (Figure 3.7C, C1) were identified as bronchial epithelial cells; these cells lack any alveolar-specific epithelial markers and this phenotyping was consistent with the findings reported by McQualter et al (339). The remaining two populations of interest were both T1α+ (Figure 3.7C, C2 and C3). Within the lung, type I alveolar epithelial cells (AECs) are the major expressing cell of T1α. However, cells transdifferentiating from type II AECs into type I AECs can also express T1α (340). Therefore, an additional marker had to be used to validate this gating. While pro-surfactant protein C (pro-SP-C) is typically considered a type II AEC specific marker, this protein is expressed intracellularly, and cells need to be permeabilised in order for staining and identification to be performed. However, because the main aim of this set of experiments was to measure surface expression of CD147 on different pulmonary epithelial cells, permeabilisation of cells was not feasible. Therefore, I sought to develop a gating strategy that would allow me to differentiate between type I and II AECs using only surface markers.

A paper recently published by Hasegawa et al reported the use of surface identification markers EpCAM and major histocompatibility complex class II (MHC-II) to classify murine distal lung epithelial cells (341). In keeping with my findings, this group found that there was a range of EpCAM expression among distal lung cells, with the highest levels detected in ciliated bronchiolar cells, intermediate levels in type II AECs, and lowest levels in type I AECs. Further, they found homogenous and specific expression of MHC-II in only type II AECs. The identification of these MHC-II+ cells were confirmed by alternative staining showing that 99%

of pro-SP-C cells were positive for MHC-II expression and that pro-SP-C negative cells had no detectable expression of MHC-II. When I applied this gating strategy, I found cells corresponding to each phenotype (Table 3.1).

Table 3.1 - Surface expression markers T1α, EpCAM, and MHC-II used to differentiate distal lung cells.

	T1α	EpCAM	MHC-II
Ciliated bronchial cells (C1)	–	High	–
Type I AEC (C3)	+	Low	–
Type II AEC (C2)	+	Intermediate	+



C1	**Bronchial cells** CD45- CD31- EpCAM+ T1α- MHC-
C2	**Type II Alveolar Epithelial Cells (AECs)** CD45- CD31- EpCAM^{intermediate} T1α+ MHC^{high}
C3	**Type I AECs** CD45- CD31- EpCAM- T1α+ MHC-

Figure 3.7 - Lung epithelial cell gating strategy using flow cytometry.

(A) CD45 negative (CD45-) cells were gated to exclude leukocytes; (B) CD31- cells were gated to exclude endothelial cells; (C) three epithelial cell sub-populations (C1-C3) were identified using markers EpCAM and T1α as described in the table. (D) Type II AECs expressed a high level of surface MHC-II but not bronchial cells or type I AECs.

3.5.6 CD147 during ventilator-induced lung injury

During the course of VILI, CD147 expression on surface of different pulmonary cells was assessed using flow cytometry (Figure 3.8). In response to high V_T ventilation, CD147 was upregulated on type I and II AECs, alveolar macrophages, and pulmonary capillary endothelial cells. This was observed at an early time point, peaking at 1 hour.

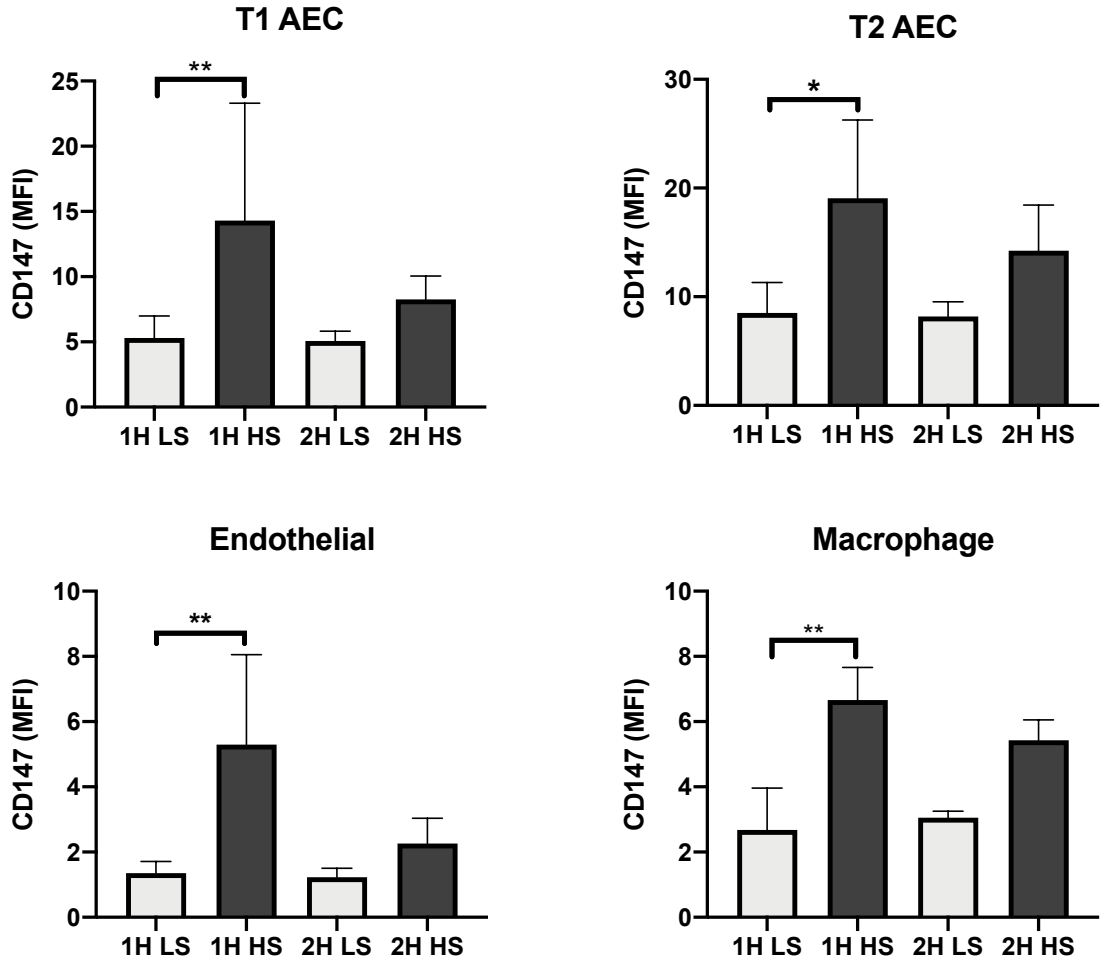


Figure 3.8 – CD147 expression is upregulated on the surface of pulmonary cells following 1 hour of high stretch ventilation.

*CD147 expression following 1 hour and 2 hours of low and high stretch ventilation on type I and II alveolar epithelial cells (AEC), alveolar macrophages, and endothelium. Data shown as mean ± SD. N=4-5. *p<0.05, **p<0.01. Kruskal-Wallis test with Dunn's multiple comparisons test.*

3.5.7 Extracellular CypA is significantly increased in ARDS patients

A total of 32 ARDS patient samples and 6 healthy volunteers BAL samples were analysed. To date, there have not been any studies exploring the involvement of CypA in human ALI or ARDS. For the first time, we have demonstrated a substantial 5-fold increase in levels of extracellular CypA in ARDS patients compared with healthy controls.

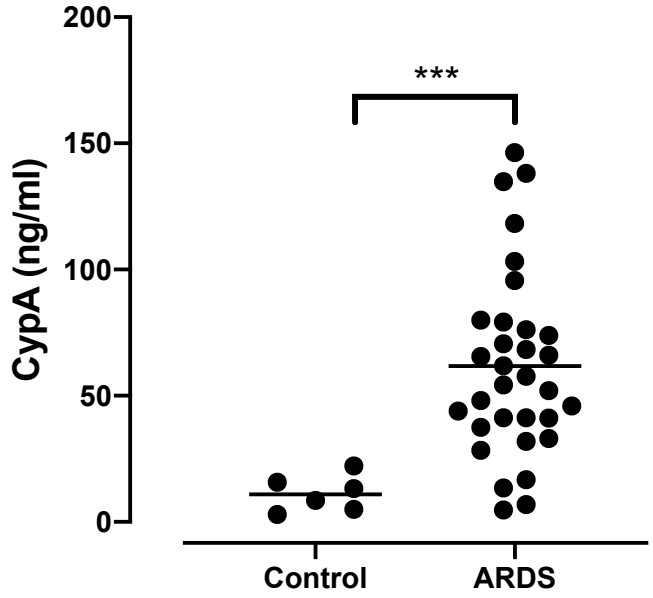


Figure 3.9 – Extracellular CypA is substantially increased in ARDS patients compared with healthy controls.

*Levels of CypA detected in ARDS patient cohort was 5.5-fold higher than in healthy volunteers (control: 11.3 ± 7.2 ng/mL vs ARDS: 61.8 ± 36.7 ng/mL). Data were normally distributed and shown as scatter dot plot with line representing mean. ***p<0.001. Data were evaluated by Mann-Whitney test despite normality to account for the difference in group sizes.*

3.6 Discussion

There has been a growing body of evidence to suggest that extracellular CypA and its receptor CD147 are involved in key processes underlying inflammatory diseases. The aim of this chapter was to investigate the expression of components of the CypA:CD147 axis in the pathogenesis of VILI.

3.6.1 BAL levels of CypA are dramatically increased during VILI

Following high V_T ventilation, there is a marked (over 100-fold) increase in CypA in BAL compared with untreated controls. This increase becomes even more impressive when it is taken into account that the process of performing a lung lavage can introduce up to a 120-fold dilution of the alveolar lining fluid (342-345), giving insight into the large amounts of CypA present *in situ.* This is the first time that VILI has been shown to lead to an upregulation of CypA release within the lungs.

3.6.2 CypA is produced locally in the alveolus

During VILI, epithelial injury or dysfunction leads to loss of the normal barrier function of the pulmonary epithelium and endothelium. This increase in alveolar capillary barrier permeability leads to flooding of protein-rich fluid containing albumin, immunoglobulin (e.g. high molecular weight IgM), fibrin, and complement from the vascular to the alveolar space. To explore the possibility that CypA might be one of the many proteins that gains access to the alveolar space due to barrier breakdown, levels of CypA in the plasma were also evaluated. There were no significant changes in the levels of plasma CypA over the 3 hours regardless of ventilation strategy. More importantly, plasma levels were also consistently lower than that in BAL. While the mean level of CypA in the plasma was ~500 pg/mL, the mean level in BAL following 3 hours of high V_T ventilation was ~6,000 pg/mL. This comparison does not take into account the dilutional effect of performing a BAL, which would have further highlighted the difference between plasma and BAL levels. Given that the levels in BAL were consistently several fold

greater than in plasma, it is apparent that the increase of CypA in the alveolar space cannot be explained by a leak from the systemic circulation following alveolar-capillary barrier damage. Thus, CypA must be produced locally within the alveolar space during VILI. This is also relevant mechanistically as it suggests that any role that CypA may play during the pathogenesis of VILI is likely to be primarily intra-alveolar.

3.6.3 CypA in VILI, cause or consequence of injury?

From our data, it was clear that CypA was increased dramatically following 3 hours of high V_T ventilation compared with untreated (unventilated) controls. However, from this alone, it is unclear if the increase was a cause (i.e. a potential therapeutic target) or a consequence (i.e. a potential biomarker) of VILI.

To address this, experiments were terminated at earlier time points (1 and 2 hours), before physiological dysfunction was expected to have developed. Levels of CypA in BAL from animals in the low V_T and high V_T groups were then evaluated and compared. The use of low V_T ventilation instead of untreated animals as a control better accounts for other potential confounding factors that could have also caused an inflammatory response, including the invasive surgical procedures, anaesthesia, and ventilation in a supine position.

From this set of experiments, we demonstrated that levels of CypA is significantly higher in the high V_T group compared with the low V_T group following just 2 hours of ventilation. This was early in the course of VILI, and importantly, before other signs of lung injury were observed. At 2 hours, there were no significant differences in BAL protein and PaO_2 levels between groups. This suggests that the integrity of the alveolar-capillary barrier was still intact, and no physiological dysfunction was present. This early increase of CypA and its presence in the alveolar space at substantial levels when other markers of injury were absent makes a physiological role in the pathogenesis of VILI highly feasible.

However, some aspects of the data do suggest that CypA could be released as a consequence of VILI. At 2 hours, there was a corresponding significant increase in sRAGE. sRAGE is a secreted isoform of the full-length membrane-bound RAGE (346). It retains the same V-type and C-type regions found in RAGE but lacks the transmembrane domain and cytoplasmic tail (346). RAGE is constitutively expressed at high levels in the lung, where it serves as one of the pattern-recognition receptors of the innate immune system (347). It is primarily located on the basal membrane of type I AECs, but is also constitutively expressed at low levels in multiple pulmonary cells, including the bronchiolar epithelium, type II AECs, alveolar macrophages, and vascular endothelial cells (348-350). sRAGE is either produced following proteolytic cleavage of the membrane-bound RAGE by specific sheddases or represents the alternative spliced isoform of RAGE, known as endogenous secreted RAGE (esRAGE) (348, 351). esRAGE is believed to act as a decoy receptor, blocking signals through surface RAGE.

As sRAGE is located on the basal membrane of type I AECs, it is thought that damage to alveolar cells would result in release of sRAGE into the pulmonary fluid. Thus, it has been widely considered to be a biomarker for type I alveolar epithelial cell injury and has also been demonstrated to correlate with the severity of ALI (350, 352-355). The simultaneous upregulation of both CypA and sRAGE at 2 hours and the strong positive correlation between levels of BAL CypA and sRAGE suggest an association between the processes underlying CypA release and epithelial injury.

Correlations between CypA and other markers of lung injury, including W/D weight ratio, BAL protein, and PaO_2, were also assessed. This revealed a positive correlation between CypA and BAL protein and a negative correlation between CypA and PaO_2. These results suggest that an increase in CypA is associated with an increase in the level of lung injury.

With the data available at this point, it was not possible to determine if lung injury was the cause or consequence of the increase in CypA; this question will be addressed in Chapter 5. It does, however, highlight that CypA undoubtedly features in VILI.

3.6.4 CD147 upregulation during VILI

Alongside an increase in BAL CypA following high V_T ventilation, CD147, the primary receptor for extracellular CypA, was also upregulated on the surfaces of pulmonary cells including both type I and II AECs, endothelial cells, and alveolar macrophages. On all these cell types, levels of CD147 appeared to peak at 1 hour before the upregulation of CypA at 2 hours. This supports the potential role of a CypA:CD147 signalling axis in VILI; if CypA was indeed shown to be a mediator of lung injury, the early increase in expression of its partner CD147 would mean it has an increased number of potential binding sites as soon as it enters the extracellular milieu.

This upregulation of CD147 following cell stretch is in keeping with findings from a rat VILI study conducted by Foda et al (169). Using a combination of haematoxylin-eosin (H&E) staining and *in situ* hybridisation, they demonstrated an early increase in the amount of CD147 mRNA in airway epithelial cells and alveolar macrophages after 1-hour of high-volume ventilation (V_T: 20 mL/kg, PEEP: 0 cmH_2O, RR: 25 bpm, 4 hours) (169).

There have also been a number of studies which suggest that the degree of CD147 expression contributes to an increase in cell response to CypA. Trachtenberg et al demonstrated a direct correlation between CD147 expression and the magnitude of chemotactic response of HeLa cells to extracellular CypA, and proposed that CD147 may be the rate-limiting component in the CypA-responding receptor complex (356). CD147 overexpression on macrophage-like and fibroblast-like synoviocytes in rheumatoid arthritis has been implicated in enhancing MMP secretion and activation, thus promoting invasion of the articular cartilage (251). CD147

overexpression is also widely implicated in cancer. Elevated levels of CD147 have been reported in a range of malignant tumours and have been shown to correlate with tumour progression (193, 231, 357-361). Dysregulation of CD147 is linked tightly to induction of MMPs, which promotes increased tissue destruction and facilitates tumour invasion and metastasis (196, 362, 363).

While we do observe a decrease in the absolute levels of CD147 expression from 1 hour of high V_T ventilation to 2 hours of high V_T ventilation, this decrease was not found to be significant on any cell type. There are two possible reasons to account for this slight decrease in surface levels of CD147.

Firstly, cleavage of the CD147 receptor by MMPs. Both a disintegrin and metalloproteinase (ADAM)-12 and membrane type 1 matrix metalloproteinase (MT1-MMP/MMP-14) have been observed to cleave CD147, releasing a 22-kDa fragment in the process (364, 365). This fragment contains the N-terminal Ig-like domain which is known to be functionally important for MMP induction. Indeed, in an *in vitro* study, these cleavage fragments were demonstrated to be functionally active and retained the ability to promote MMP-2 expression in human fibroblasts. This is thought to occur through homophilic interactions with retained surface CD147 and allows cleaved CD147 to reach distant target cells that may be difficult or otherwise impossible for the bigger, intact form of CD147 (364).

Although there is no literature available for the recognition site for the anti-CD147 antibody used in these experiments, it is plausible that the antibody recognises an antigen within the cleave N-terminal Ig-like domain. Thus, the decrease in MFI observed on flow cytometry might be due to a failure to recognise the proteolytically altered CD147. Of importance, however, the binding site for CypA on CD147 (Pro211) is unaffected by this cleavage. The truncated CD147 receptor retains its biological activity; cleavage of the N-terminal fragment is thought to

downregulate only its function as an MMP inducer. Thus, this suggests that CypA would still be able to bind to and signal through CD147 that has undergone proteolytic cleavage.

Secondly, the decrease in CD147 could be due to agonist-induced receptor shedding. For instance, this has been shown with TNF-induced TNFR shedding as a regulatory mechanism (366, 367). It is therefore feasible that CypA could also regulate CD147 expression through a similar mechanism.

Lastly, in light of the very promising findings presented in this chapter wherein we demonstrate that inhibition of extracellular CypA in an *in vivo* mouse model of VILI results in impressive and physiologically relevant protection, it was important to demonstrate the relevance of this novel mediator in human disease. Currently, very little is known about CypA human lung disease; at the time of writing, there were only two published studies, both investigating CypA in chronic obstructive pulmonary disease (COPD). In the first, serum levels of CypA were shown to be increased in convalescent COPD patients compared to healthy controls (convalescent COPD: 4.02 ± 0.63 vs healthy: 3.36 ± 0.51 ng/mL, n=88-93), and further upregulated in patients with an acute exacerbation (4.97 ± 0.68 ng/mL) (368). Although this was reported to be significant in the study, the absolute increase in CypA levels were fairly small, which makes its relevance slightly questionable. In the second, CypA was identified as one of 40 proteins upregulated in COPD in a 2D-PAGE proteomic study investigating BAL fluid protein profiles of COPD patients (369). In both studies, no further investigations into the mechanisms underlying its upregulation or implications of it were conducted.

To date, there have been no studies looking at CypA in ALI/ARDS. This is, therefore, the first time that a significant increase in CypA in ARDS patients compared with healthy controls have been demonstrated. Additionally, the increase is both statistically significant and clear, with a 5.5-fold difference between the groups. These encouraging results further support

extracellular CypA as a promising potential therapeutic target during VILI. Importantly, we showed that CypA levels are substantially elevated at baseline. This is crucial as it suggests that CypA is indeed an early mediator of ARDS and thus would be amenable to prophylactic blockade prior to commencement of mechanical ventilation in patients.

Unfortunately, at the time of writing, the clinical data for this cohort of patients was not yet made available to us. However, it would be very interesting and informative to analyse the data for potential correlations between the levels of CypA and several clinical parameters, including severity of ARDS and patient outcomes as there appears to be a spread in the levels of CypA values. These analyses will be performed once the clinical data is released to us.

3.7 Concluding remarks

For the first time, we have demonstrated the involvement of CypA in VILI. The substantive increase in BAL CypA despite relatively low plasma levels and a strong correlation with sRAGE suggest that CypA is produced locally within the lungs through a process related to epithelial injury. While the upregulation of both CypA and CD147 before any markers of lung injury are present makes a pathogenic role highly likely, there is currently insufficient data to conclude if CypA is present in the alveolar space as a cause or effect of lung injury. The findings in this chapter will form the basis of subsequent experiments presented in chapter 5. Lastly, we show, for the first time, the presence of extracellular CypA in BAL samples from patients with ARDS. Crucially, CypA was present at significantly elevated levels at baseline, making CypA a promising potential therapeutic target for VILI.

4 Source of Cyclophilin A

4.1 Abstract

In chapter 3, we showed that substantial amounts of CypA is released into the alveolar space during VILI. In contrast, plasma concentrations remained unchanged. These findings suggest that CypA was likely to be released from cells facing the alveolar space, rather than leaking in from the circulation following injury to the alveolar-capillary barrier. Further, CypA was found to correlated strongly with epithelial injury marker, sRAGE, implicating epithelial cells as a source for CypA within the alveolar space.

Our preliminary studies evaluating and comparing CypA levels in two additional models of ALI revealed a significant upregulation during acid-induced lung injury but not following LPS-induced lung injury. Acid models are known to involve a substantial degree of epithelial insult whereas intratracheal LPS is initially a more macrophage driven model. Additionally, sRAGE was also found to be significantly increased following acid but not LPS-induced lung injury, further suggesting that CypA release is likely associated with epithelial injury. By staining the lungs following VILI in vivo, we showed a significant decrease in the intracellular levels of CypA in epithelial cells but not in alveolar macrophages.

Using an in vitro stretch model, we investigated the effects of cyclic stretch on both epithelial cells and macrophages in isolation. Mechanical stretch induced release of CypA from human primary alveolar epithelial cells. This increase in CypA content in cell supernatants was not associated with an increase in cell death as measured as 7-AAD staining or in the levels of lactase dehydrogenase, suggesting that CypA is actively secreted by cells and not merely present as a consequence of damage to the integrity of cell membranes. Mechanical stretch of macrophages (RAW cells) did not induce CypA release. However, further stretch experiments on primary cells were not performed. The findings presented in this chapter implicate AECs as a source of extracellular CypA during ALI. While it appears that macrophages are not a significant contributor of CypA, we cannot confidently exclude macrophage involvement in the absence of further data.

4.2 Introduction

In the previous chapter, we demonstrated that CypA is upregulated early during the course of VILI. The substantive increase in BAL levels despite relatively low plasma levels, and its close correlation with sRAGE suggests that CypA is produced locally within the lungs through a process related to epithelial injury. However, the source of CypA and the mechanism of its release into the extracellular space remain unknown.

CypA has been shown to be secreted in response to inflammatory stimuli, hypoxia, and oxidative stress (201, 279, 286, 293). Perhaps the most well studied cell type in terms of its CypA release is the VSMC where CypA has been consistently shown to be secreted following ROS. Here its release has been demonstrated to occur following post-translational modification (acetylation) of the protein through a vesicular pathway (286). Alternatively, it has also be suggested that CypA is released passively from dead or dying cells due to membrane permeabilisation (285).

To date there have been no studies that have demonstrated the release of CypA from AECs or alveolar macrophages. Further, no studies have investigated the effect of mechanical stretch on CypA secretion. Given that mechanical stretch is known to evoke oxidative stress pathway and generate reactive oxygen species (ROS) (370-373), it is reasonable to suspect that active secretion of CypA may result. In this chapter, we explore the source of CypA during VILI using a combination of different *in vivo* and *in vitro* methodologies.

4.3 Aim

The work within this chapter focuses on the investigation of CypA release during VILI using *in vivo* mechanical ventilation and *in vitro* stretch models. The aims included:

1) Identification of the cellular source(s) of extracellular CypA during VILI.
2) Determining if the process of CypA release in response to mechanical stretch was passive or active.

4.4 Protocols

4.4.1 LPS-induced lung injury model

C57BL/6 mice were anaesthesised with an intraperitoneal injection of a combined dose of ketamine (60 mg/mL) and xylazine (6 mg/mL). A fine catheter was passed into the trachea between the vocal cords via the mouth. 50 µg LPS in 50 µL sterile PBS or PBS alone was instilled. Mice were then placed in a custom-made recovery box until the effects of the anaesthetic had fully worn off. Three hours post instillation, mice were euthanised and tracheostomised to perform a bronchoalveolar lavage (BAL) to recover samples.

4.4.2 Acid-induced lung injury model

Our lab has developed an acute model of acid aspiration induced lung injury (374). Mice were anaesthetised, tracheostomised for mechanical ventilation, and left carotid artery cannulated. After an initial recruitment manoeuvre to standardise the volume history of lungs for the effects of surgery and anaesthesia, an inspiratory pause was performed to measure baseline respiratory mechanics. Subsequently, mice were briefly disconnected from the ventilator pneumotach to allow instillation of 2 mL/kg (approximately 50 µL) of 0.15M hydrochloric acid (HCl) via the endotracheal tube. The mice were then reconnected to the ventilator and a recruitment manoeuvre was immediately performed to ensure even acid distribution throughout the lungs. Mice were then ventilated for 3 hours at low tidal volume (V_T: 8 mL/kg, respiratory rate [RR]: 120 bpm, peak end-expiratory pressure [PEEP]: 3.0 cmH_2O, 100% O_2) settings. Recruitment manoeuvres were performed at 30-minute intervals. Three hours post acid instillation, mice were euthanised and tracheostomised to perform BAL and recover BAL fluid samples.

4.4.3 *In vivo* alveolar macrophage depletion

To deplete resident alveolar macrophages, mice underwent laryngoscopy under anaesthesia as described in the LPS-induced lung injury model above. Mice then received either 50 µL of clodronate-containing liposomes (7 mg/mL, 50 µL) or sterile saline. 48 hours after, mice were ventilated at high V_T (V_T 35-40 mL/kg, PEEP 3 cmH_2O, RR 80 bpm, 96% O_2 / 4% CO_2) for 150 minutes or until surrogate mortality markers were reached (as detailed in Chapter 2.3.1). Macrophage depletion was assessed in lung single cell suspensions by flow cytometry. Alveolar macrophages were identified as CD45+, CD11c+, CD11b-, F4/80+ cells.

4.4.4 *In vivo* intracellular CypA staining

Intracellular CypA was measured using an adapted flow cytometry based staining protocol. Lungs were harvested from untreated mice and mice that were ventilated at high V_T (V_T 35-40 mL/kg, PEEP 3 cmH_2O, RR 80 bpm, 96% O_2 / 4% CO_2) for 3 hours and processed to obtain a single cell suspension. Cells were permeabilised with BD Cytofix/Cytoperm for 20 minutes at 4ºC. Subsequently, a three-step staining procedure was performed: (1) 1-hour incubation with primary anti-cyclophilin A antibody (10 µg/mL) at 4ºC; (2) 30-minute incubation with rabbit IgG APC-conjugated antibody (80 ng/mL) at 4ºC; (3) 30-minute incubation with surface antigen antibody panels for parenchymal cells and leukocytes (see Chapter 2.9 for details) at 4ºC. Samples were washed twice with permeabilisation wash buffer (PWB; 0.2% saponin, 0.5% BSA, and 0.1% sodium-azide in PBS) between each step. After staining was complete, samples were washed again and re-suspended in PWB for analysis using flow cytometry.

4.4.5 Cell stretching *in vitro*

A number of different cells were used in these *in vitro* cell stretch experiments including cell lines MLE-12 (mouse lung epithelial cells), RAW 264.7 (murine monocyte/macrophage-like cells), A549 (human type II pulmonary epithelial cells), and primary human alveolar epithelial cells (H-AECs).

All cells were seeded onto flexible bottomed 6-well BioFlex® culture plates coated with type I collagen (Flexcell International) with the appropriate medium supplemented with 10% foetal bovine serum (FBS) at least 24 hours prior to stretching. Cells were then left to reach 90-100% confluence, assessed by light microscopy, for 24 hours at 37ºC in a humidified 5% CO_2 atmosphere. Once 90% confluence was achieved, existing media was removed and replaced with fresh low-serum media (5% FBS) immediately before stretch experiments were commenced.

Cells were exposed to cyclic mechanical stretch at 0.25 Hz (equivalent of 15 breaths per minute), at a duty cycle of 33.3% (inspiratory:expiratory ratio of 1:2) using a computer-controlled vacuum strain apparatus (Flexcell Tension System) with a vacuum pressure sufficient to generate a maximum of 20% elongation. For the duration of the experiment, cells were placed in an incubator maintained at 37ºC in a humidified 5% CO_2 atmosphere. Static control cells were also seeded and cultured on the same BioFlex® culture plates and placed into the same incubator for the same stretch exposure time.

Sample collection

At the end of stretch experiments, conditioned culture media were collected and centrifuged at 300 x g for 5 minutes at 4ºC to yield cell-free supernatants. These were stored in aliquots at -80ºC for future analyses. Wells were rinsed twice with phosphate buffered saline (PBS) and cells were detached from the surface of the wells using Cell Dissociation Buffer and gentle pipetting. Cells were washed with FACS wash buffer (FWB) before undergoing antibody staining for analysis by flow cytometry.

Flow cytometry analysis

Cells were then identified using specific surface markers on flow cytometry. Any noise and cell debris were excluded based on auto-fluorescent and size. MLE-12 cells were identified based on their expression of T1α (Figure 4.1A); A549 cells were identified based on their expression of EpCAM (Figure 4.1B); primary human AECs were identified based on their expression of EpCAM (Figure 4.1C); and RAW cells were identified based on their expression of CD45. Cell surface expression of CD147 and activation markers, including ICAM-1, MHC-II, and CD86, were also measured.

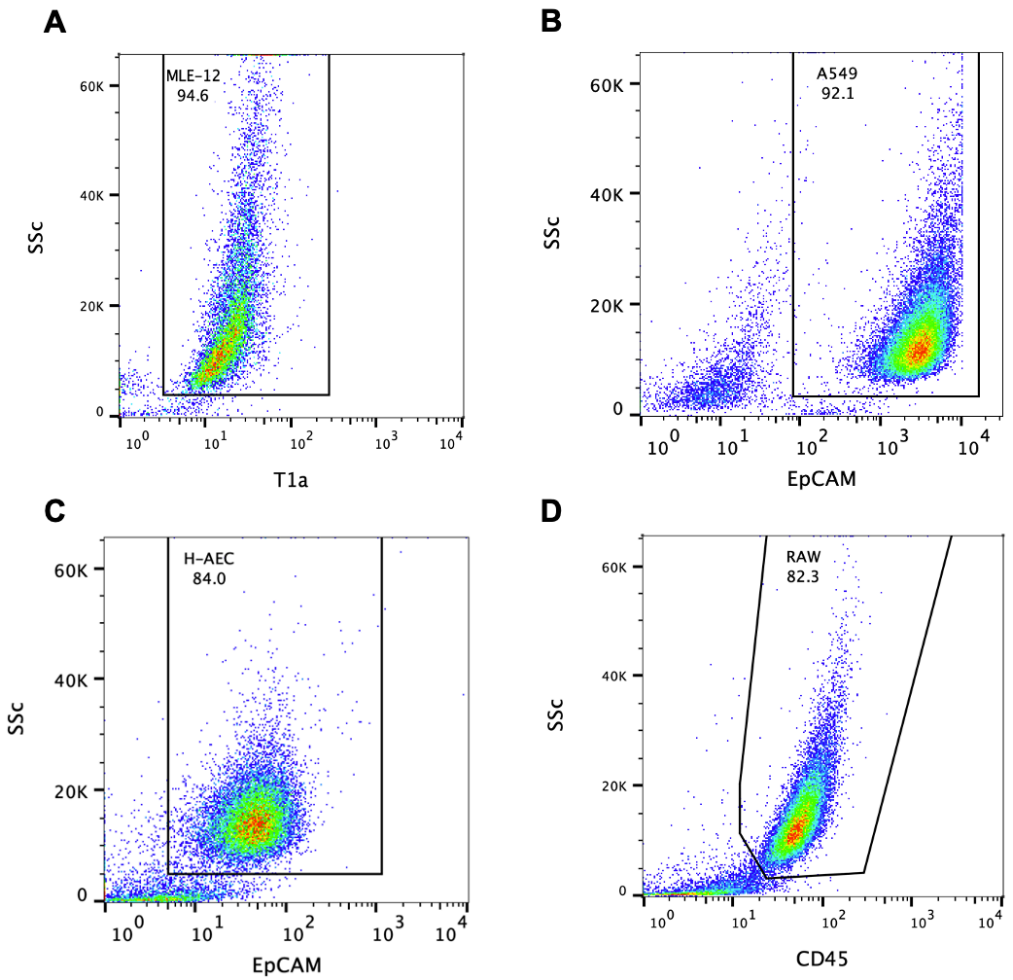


Figure 4.1 – Identification of epithelial cells by flow cytometry.

(A) MLE-12 cells were identified by their T1α expression, (B) A549 cells and (C) primary human alveolar epithelial cells (H-AEC) were identified by their EpCAM expression, and RAW cells were identified by their CD45 expression.

Cell viability: 7-AAD

Cell viability was assessed by flow cytometry analysis. After cells were processed and stained with antibodies, 5 µL of 7-Amino-Actinomycin D (7-AAD) was added to each FACS tube and incubated for 5 minutes at room temperature with minimal light exposure before analysis of flow cytometry. 7-AAD is a membrane impermeant fluorescent dye that has a strong affinity for DNA. While it is generally excluded from viable cells, permeabilisation or disruption of the cell membranes in dying or dead cells allows 7-AAD to enter the cell and bind to double stranded DNA by intercalating between base pairs in G-C rich regions (375). 7-AAD/DNA complexes are excited at 488 nm and detected at an emission of 645 nm.

Cell viability: Lactate-dehydrogenase

Cell viability was also assessed by measuring the activity of lactate dehydrogenase (LDH) in conditioned media. LDH is a stable enzyme, present in a wide variety of organisms. Upon damage to the plasma membrane of cells, LDH is rapidly released into the extracellular space. Since it is a fairly stable enzyme, it is widely used to evaluate the presence of cell damage and cytotoxicity.

Levels of LDH in conditioned media were measured using a commercially available colorimetric assay kit. This colorimetric assay used relies on the oxidoreductase activity of LDH, which converts NAD (nicotinamide adenine dinucleotide) to its reduced form – NADH. NADH then interacts with a specific probe to produce a colour measured at a wavelength of 450 nm.

The assays were conducted as per manufacturer's instructions. In brief, 50µL of NADH standards (0 – 12.5 nmol) and samples (conditioned media diluted 1 in 2 to fit the standard curve readings) were prepared and added to 96-well plates. For every plate assayed, a positive control provided within the kit was included. 50 µL of LDH substrate mix was then

added to all wells and mixed. The plates were then immediately placed in a microplate reader (Biotek ELx800) and the absorbance was measured at 450 nm in kinetic mode, every 2-3 minutes, for 60 minutes at 37ºC protected from light. All samples were analysed in duplicates.

To calculate the LDH activity of samples, a standard curve was generated in Graphpad Prism. The activity of LDH in test samples was calculated as per instructions in the kit protocol and expressed as mU/mL where 1 unit LDH is equal to the amount of enzyme that catalyses the conversion of lactate to pyruvate to generate 1.0 µmol of NADH per minute at pH 8.8 at 37ºC.

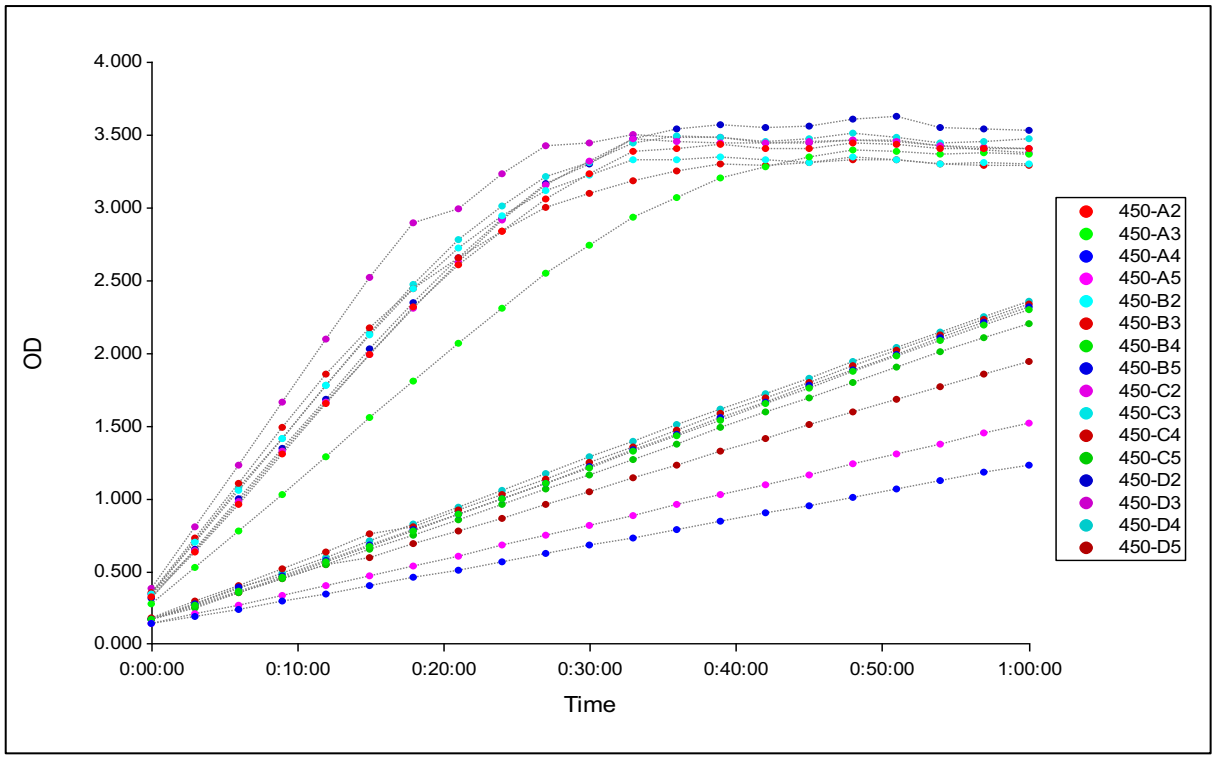


Figure 4.2 - Representative absorbance curves generated over 1 hour following assay kit protocol.

The top cluster of lines are the readings from the NADH standard curve; the reaction in these wells begin to plateau from 30 minutes onwards. The bottom cluster of lines are the readings from sample wells. To calculate LDH activity, two time points in the linear range (T1 and T2) where chosen and the difference in absorbances were calculated (A1 subtracted from A2).

4.4.6 ELISA

Colorimetric ELISAs were performed on BAL samples collected from *in vivo* LPS-induced lung injury and acid-induced lung injury model to measure murine CypA and sRAGE content. Colorimetric ELISAs were also performed on supernatants of stretched and static cells to measure the IL-6, IL-8, and murine CypA content. All assays were conducted as per manufacturer's instructions.

4.4.7 Bradford assay

The protein concentration of cell-free conditioned media was measured using the Bradford assay. Protein (bovine serum albumin) standards were prepared in PBS at the following concentrations: 2 mg/mL, 1.5 mg/mL, 1 mg/mL, 0.75 mg/mL, 0.5 mg/mL, 0.125 mg/mL, 0 mg/mL. 5 µL of standard and samples (appropriately diluted in saline where necessary) were added to a 96-well plate. Bradford dye (250 µL) was added to each well and wells were mixed with a microplate shaker for 30 seconds. The samples were then incubated at room temperature for 10 minutes before absorbances was measured at 595 nm. Samples and standards were assayed in duplicates and the averages were used to determine the protein concentration of samples.

4.4.8 Western blotting

Equal volumes of cell-free supernatants were loaded on NuPAGE 12% Bis-Tris gels, separated by sodium dodecyl sulphate-polyacrylamide gel electrophoresis (SDS-PAGE), and transferred to nitrocellulose membranes. Membranes were blocked with 5% non-fat milk in Tris-buffered saline with 0.1% Tween-20 (TBS-T) for 1 hour at room temperature with gentle agitation. Membranes were washed three times with TBS-T and incubated with anti-cyclophilin A antibody (1:500) in TBS-T overnight at 4ºC.

The following day, membranes were rinsed in TBS-T three times before incubation with anti-rabbit HRP-conjugated secondary antibody (1:1000) for 1 hour. Membranes were washed three times for 5 minutes each and blots were visualised with Luminol reagent (Santa Cruz Biotechnology). Blots were captured with GeneSnap (Syngene) and analysed with GeneSnap (Syngene) or ImageJ (National Institutes of Health).

4.5 Results

4.5.1 Cyclophilin A levels are markedly increased in acid-induced lung injury – an epithelial insult dominant model

As our previous findings implicate AECs as a source of extracellular CypA during VILI, we decided to first explore this by conducting some preliminary experiments to compare the levels of CypA in two additional models of acute lung injury – acid- and LPS-induced lung injury (Figure 4.3A). The acid-induced lung injury model is known to involve a substantial degree of epithelial insult (374, 376). In contrast, intratracheal LPS-induced lung injury tends to be, at least in its acute phase, a predominantly macrophage driven model (374, 377, 378). Thus, levels of CypA in BAL of mice following 3 hours of acid or LPS stimulation were measured and compared to unventilated controls and mice that were subjected to 3 hours of high V_T ventilation (Figure 4.3A).

Following LPS-induced lung injury there was a trend towards an increase in CypA compared with untreated mice. While this was not statistically significant, we did observe a fairly large numerical increase in the absolute values of CypA, with nearly a 30-fold increase compared with untreated controls. However, in the acid model, there was an impressive increase in CypA, with levels 480-fold greater respectively than in the untreated group.

These findings suggest that CypA involvement is most apparent when there is a significant degree of epithelial insult. To investigate this further, levels of soluble RAGE, an established marker of epithelial injury was also measured in all three models of lung injury (Figure 4.3B). This revealed a significant increase in both the acid and VILI model, supporting the hypothesis that CypA release is likely associated with epithelial damage.

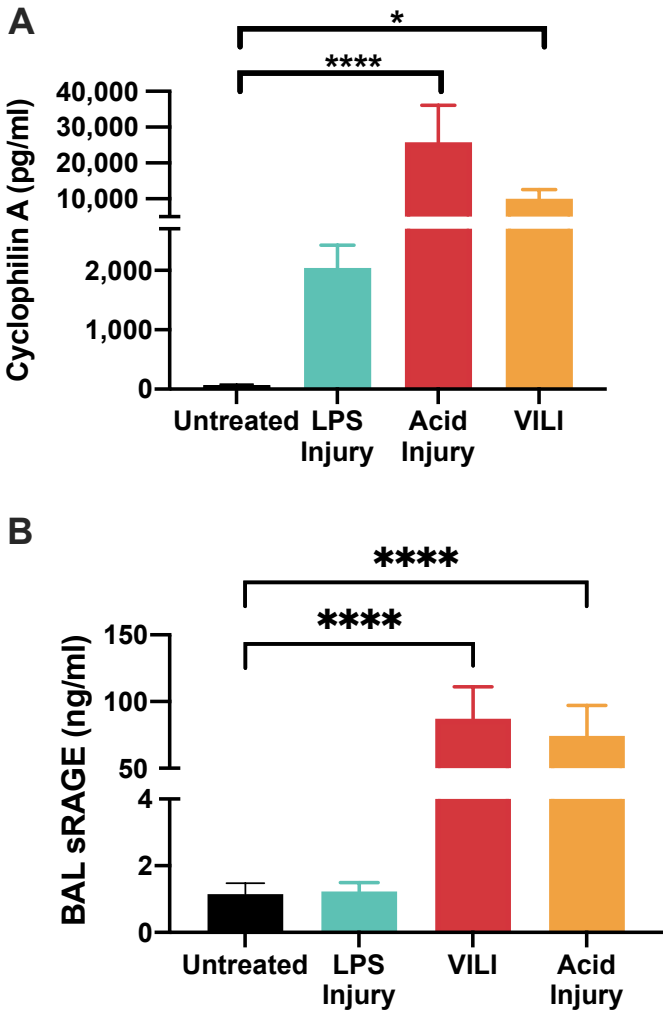


Figure 4.3 - Levels of CypA and sRAGE in BAL of untreated mice and mice subjected to 3 hours LPS challenge, acid-induced lung injury, or VILI.

*(A) No significant increase in BAL CypA seen 3 hours after LPS (50 µg) administration compared with untreated mice (untreated: 53.6 ± 25.3 pg/mL vs. LPS: 1,564.1 ± 869.8 pg/mL). An impressive increase was seen in response to acid injury (acid: 25,721.7 ± 10,332.9 pg/mL). (B) Levels of soluble RAGE were significantly increased following injurious ventilation (untreated: 1.2 ± 0.3 ng/mL vs. VILI: 87.2 ± 24.0 ng/mL) and acid injury (acid: 73.3 ± 22.8 ng/mL) but LPS (1.2 ± 0.3 ng/mL). Data were normally distributed and shown as mean ± SD. N=6. * p<0.05, ****p<0.0001. Data were evaluated by an ordinary one-way ANOVA with Sidak's multiple comparisons test.*

4.5.2 Optimisation of *in vivo* depletion of alveolar macrophages

Given our preliminary findings were suggestive of AECs being a source of CypA, we next sought to design experiments to investigate the contribution of alveolar macrophages to extracellular CypA by carrying out *in vivo* depletion of alveolar macrophages before ventilation at high V_T to induce VILI. We hypothesised that levels of CypA released into the alveolar space would remain relatively unchanged following macrophage depletion.

In vivo depletion of alveolar macrophages

To achieve maximal depletion of alveolar macrophages, two different routes of administration (intranasal vs intratracheal) and dosing durations (48 and 72 hours) were trialled. Macrophage depletion was assessed in lung single cell suspensions by flow cytometry. Alveolar macrophages were identified as CD45+, CD11c+, CD11b-, F4/80+ cells (Figure 4.4).

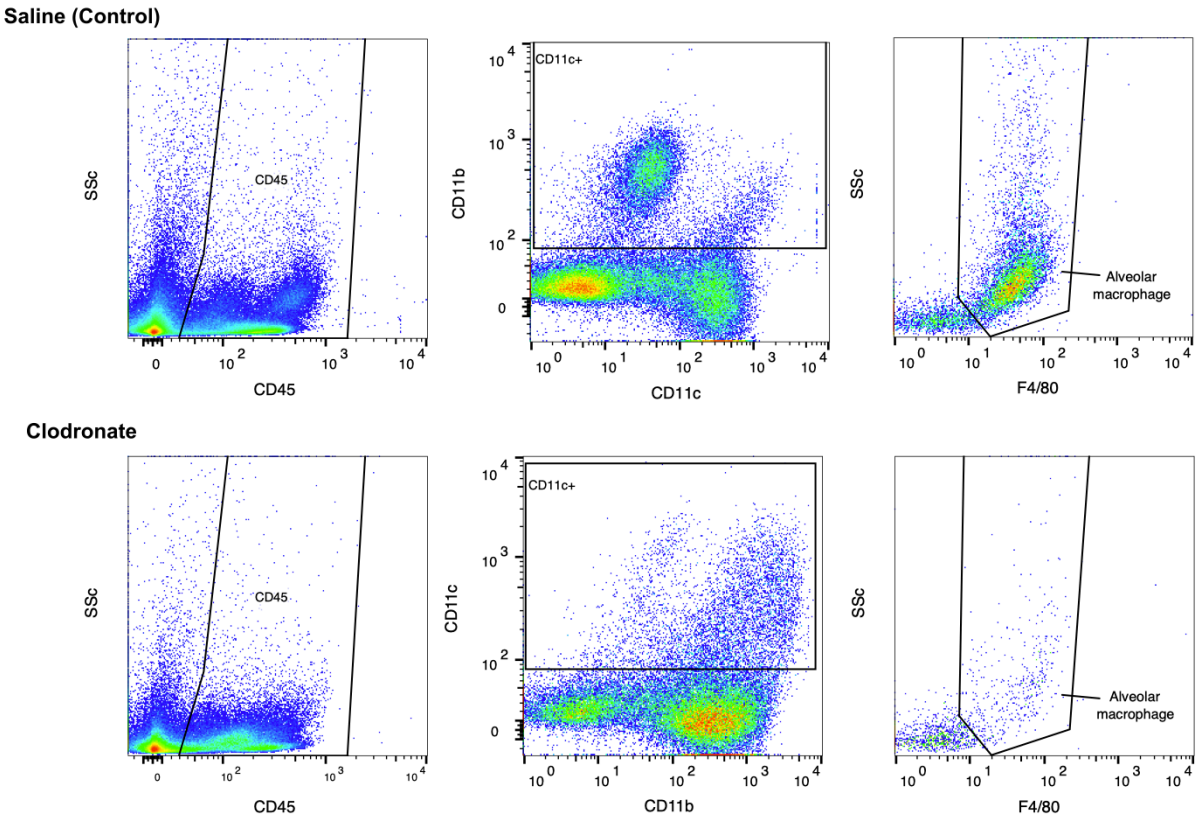


Figure 4.4 - Flow cytometric analysis of alveolar macrophages depletion following intratracheal clodronate treatment.

Resident alveolar macrophage in lung single cell suspensions were identified as CD45+, CD11c+, CD11b-, F4/80+ cells. Intra-tracheal instillation of clodronate liposomes led to a depletion of alveolar macrophages.

From these preliminary experiments, it was determined that intratracheal delivery of clodronate liposomes led to more effective macrophage depletion than intranasal (Figure 4.5A). At 48 hours, alveolar macrophage counts reached the lowest levels, before returning to baseline at 72 hours (Figure 4.5B). However, an influx of neutrophils was also observed at 48 hours, which returned to baseline at 72 hours. As the main aim of these experiments was to assess the contribution of alveolar macrophages to extracellular CypA during VILI, 48 hours was chosen as the dosing duration. For all subsequent experiments, alveolar macrophages were depleted via intratracheal instillation of clodronate liposomes 48 hours before. Consistent with previous findings (248), evaluation of alveolar macrophage counts 48 hours after clodronate administration using flow cytometry demonstrated an 80-90% depletion of the resident AM population (Figure 4.5C).

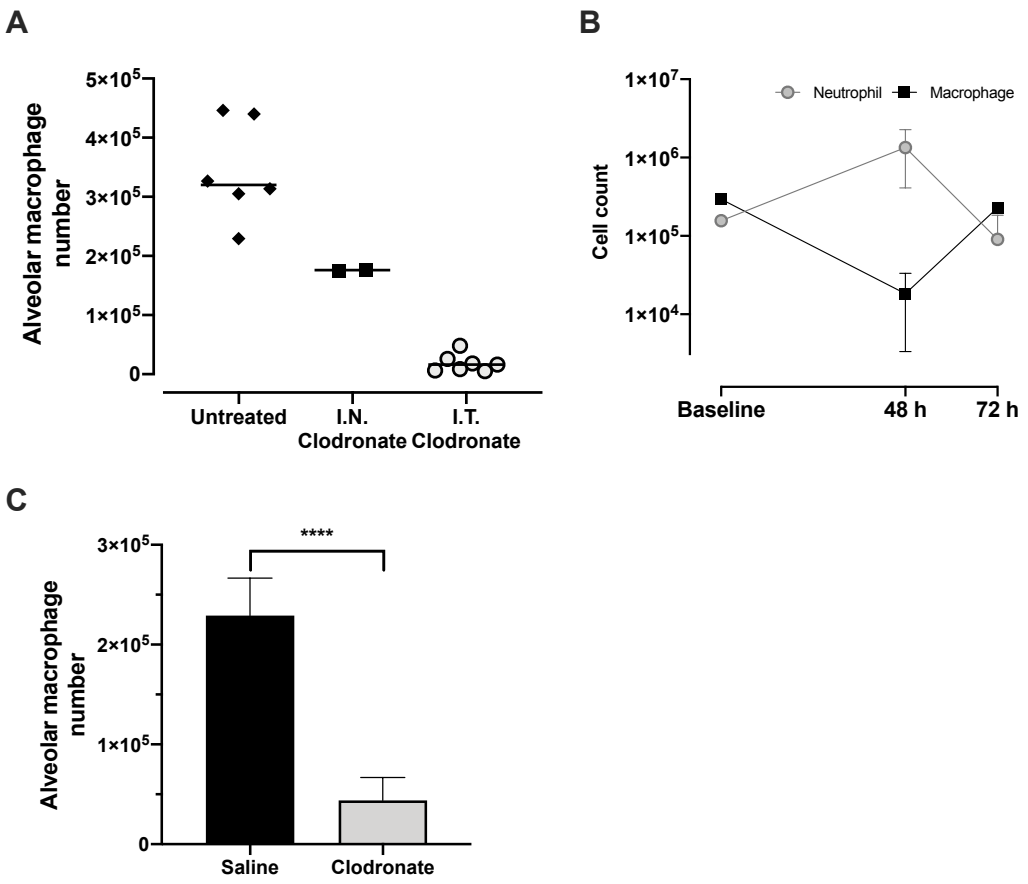


Figure 4.5 – Comparison of alveolar macrophage depletion by clodronate liposomes using different routes of administration.

*(A) Comparison of alveolar macrophage depletion achieved using different routes of administration. Administration of clodronate liposomes intranasally (i.n.) achieved ~50% decrease in alveolar macrophages within lungs; Intratracheal (i.t.) delivery of clodronate liposomes led to a greater decrease, reducing alveolar macrophages numbers by ~90%. There is only an N=2 in the i.n. group as it was apparent that it was less effective than clodronate delivered i.t. and no further Ns were required. (B) Alveolar macrophage and neutrophil counts were evaluated at 48 hours and 72 hours post-clodronate treatment and compared with baseline (untreated). Alveolar macrophage counts reached their lowest levels 48 hours post-clodronate treatment before returning to baseline at 72 hours. Conversely, neutrophil counts peaked at 48 hours but also returned to baseline at 72 hours. (C) 48 hours after intratracheal clodronate liposomes, lung alveolar macrophage counts decreased by 80-90% compared with saline controls. Data in (A) shown as scatter dot plot with lines representing median values. Data in (B) shown as line graph of means ± SD. N=2-6. Data in (C) shown as mean ± SD. N=6. ****p<0.0001. Unpaired t-test.*

4.5.3 Optimisation of alveolar macrophage depletion experiments

As stated above, the aim of these experiments was to investigate the contribution of alveolar macrophages to extracellular CypA by carrying out *in vivo* depletion of alveolar macrophages before VILI. However, the design of this set of experiments had to be carefully considered. It is well established that depletion of alveolar macrophages results in a significant decrease in the severity of lung injury during VILI. The results presented in the previous chapter strongly suggest that CypA levels in BAL strongly correlated with the degree of lung injury. Thus, in order to interpret any potential data from these experiments, we would need to first identify a time point where the severity of injury was effectively the same in both control (saline) and clodronate-depleted mice.

Given our previous data, this time point would need to be after 120 minutes (when we first observed an upregulation in CypA levels in BAL) and before 150 minutes as animals begin to rapidly deteriorate beyond 150 minutes when ventilated with the parameters used in our VILI model. Thus, pilot experiments where both groups of mice were ventilated for up to 150 minutes were conducted. Respiratory mechanics and markers of lung injury were measured and evaluated.

4.5.4 Alveolar macrophage depletion attenuates VILI

As expected, depletion of alveolar macrophages led to an attenuation of lung injury when mice were subsequently ventilated with high V_T. This was indicated by respiratory mechanics and other markers of lung injury. At the onset of ventilation, peak inspiratory pressure (PIP) was virtually identical in both groups and continued to remain similar for the first 105 minutes (Figure 4.6A). From 120 minutes onwards, PIP increased rapidly in control animals, and was consistently significantly higher than in clodronate treated animals at all time points beyond this. Respiratory system elastance (Ers) followed a similar pattern (Figure 4.6B). While the values of both groups were virtually identical from 0 – 90 minutes, the trajectories of Ers values begin to diverge from 105 minutes. At 135 minutes and 150 minutes, Ers in the saline treated controls was significantly increased compared with clodronate treated group.

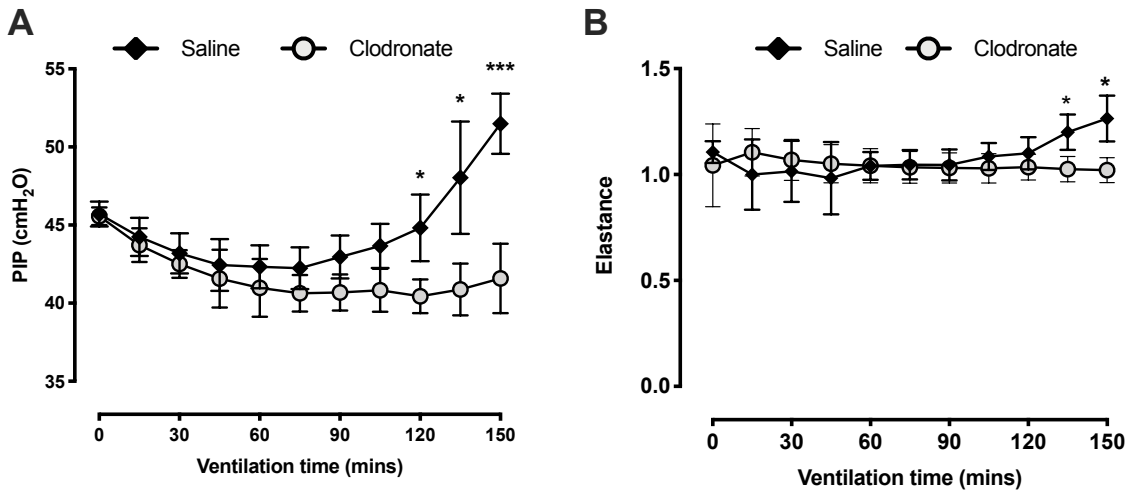


Figure 4.6 – Physiological parameters show protective effects of alveolar macrophage depletion with clodronate treatment following 150 minutes of injurious high V_T ventilation.

(A) Time course of peak inspiratory pressure (PIP) change during high V_T ventilation. PIP was found to be significantly higher in clodronate group compared with saline controls from 120 minutes onwards, indicating ongoing lung injury. (B) Respiratory system elastance (Ers) was also found to be significantly increased in the saline treated group at 135 and 150 minutes.

*Data shown as mean ± SD. N=6. ****p<0.0001. Two-way ANOVA with Sidak's multiple comparisons test*

At 150 minutes, clodronate treated animals displayed significantly less injury than saline treated animals. AM depletion attenuated the development of alveolar-capillary barrier permeability (BAL protein) (Figure 4.7A), pulmonary oedema (lung wet/dry weight ratio) (Figure 4.7B), and alveolar epithelial injury assessed by levels of soluble receptor for advanced glycation end products (sRAGE) in BAL fluid (Figure 4.7C).

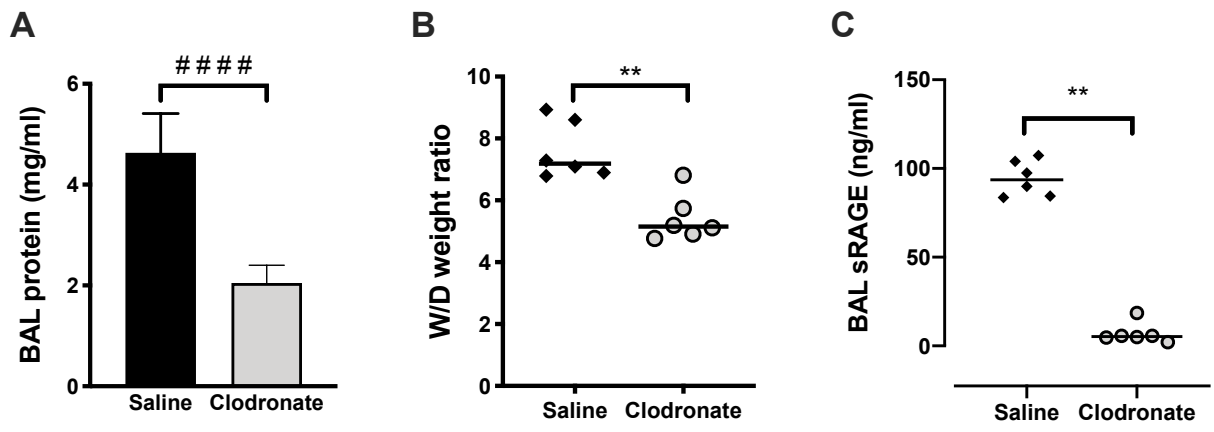


Figure 4.7 – Markers of lung injury decreased at 150 minutes following clodronate depletion of alveolar macrophages.

*At 150 minutes, it was apparent that the severity of injury was lower in the clodronate treated group. (A) alveolar-capillary permeability (BAL protein), (B) pulmonary oedema (W/D weight ratio), and (C) epithelial injury (BAL soluble RAGE) were significantly attenuated by clodronate treatment. N=6. Data in (A) shown as mean ± SD. N=6. # # # # p<0.0001. Unpaired t-test. Data in (B) and (C) were non-parametrically distributed and displayed as scatter dot plots with lines representing medians. **p<0.01. Mann-Whitney test.*

At 120 minutes, no differences in alveolar-capillary permeability as assessed by BAL protein was observed. However, lung wet/dry weight ratio was significantly lower in the clodronate

treated group, suggesting that injury was already beginning to develop in animals treated with saline.

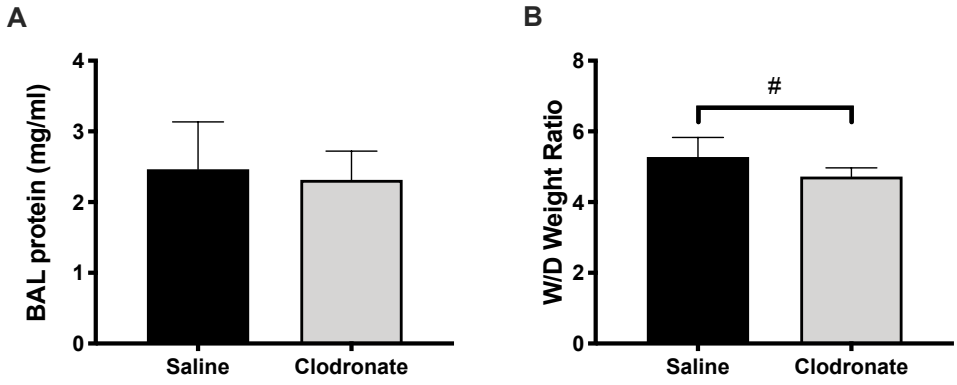


Figure 4.8 – Markers of lung injury at 120 minutes suggest the beginnings of lung injury in saline treated animals.

At 120 minutes, there were no differences in alveolar-capillary permeability (BAL protein) between groups (A). However, W/D weight ratio was found to be significantly lower in clodronate treated animals, suggesting that lung injury was already started to develop at this time point. Data shown as mean ± SD. N=6. # p<0.05. Unpaired t-test.

Since we know that CypA correlates with the degree of injury, we had to identify a time point where the severity of injury was the same so we could stop the experiment to measure BAL CypA levels and determine if macrophages were producing CypA. However, upon assessment of the data at 120 minutes and 150 minutes, it became apparent that at even as early as 120 minutes, there was already differences in the degree of lung injury between groups. Clodronate treated animals were protected from deterioration of respiratory mechanics and development of lung injury following high V_T ventilation. As mentioned above, ventilation for any durations shorter than 120 minutes was unlikely to provide a clear answer as CypA is only significantly upregulated at 120 minutes.

Unfortunately, this meant that this clodronate mediated macrophage depletion model could not be used to assess the relative contributions of AECs and alverolar macrophages to extracellular CypA during VILI. While we could have tried to adjust the ventilation parameters such that it did not produce injury within such a short time frame, we decided, with hindsight, that the substantial neutrophil influx introduced too much uncertainty into the model; Even if we were able to identify a time point where the degree of injury was identical in both groups, we would still have to contend with interpretation of the data in light of the significant neutrophilia in the clodronate treated group. Thus, we decided to investigate our hypotheses using alternative methodologies.

4.5.5 Intracellular levels of CypA decrease in only epithelial cells during VILI

Since clodronate depletion was not a viable method, an alternative method was used to investigate the source of CypA during *in vivo* ventilation. Flow cytometry was utilised to determine intracellular expression (mean fluorescent intensity) of CypA in whole lung single cell suspension. Intracellular levels of CypA in lungs harvested from untreated controls and mice ventilated for 3 hours with high V_T – the time point where highest levels of extracellular CypA were detected in previously experiments – were compared (Figure 4.9).

This revealed a significant decrease in the MFI of CypA in EpCAM+T1α– epithelial cells (control: MFI 63.4 ± 9.5 vs. 3H HS: 48.4 ± 11.0; Figure 4.9A) and EpCAM–T1α+ epithelial cells (control: MFI 30.0 ± 9.0 vs. 3H HS 19.4 ± 5.4; Figure 4.9B) but not in alveolar macrophages (control: MFI 61.4 ± 15.7 vs. 3H HS: 52.1 ± 17.5; Figure 4.9C), supporting our hypothesis that AECs are a likely source of CypA following stretch.

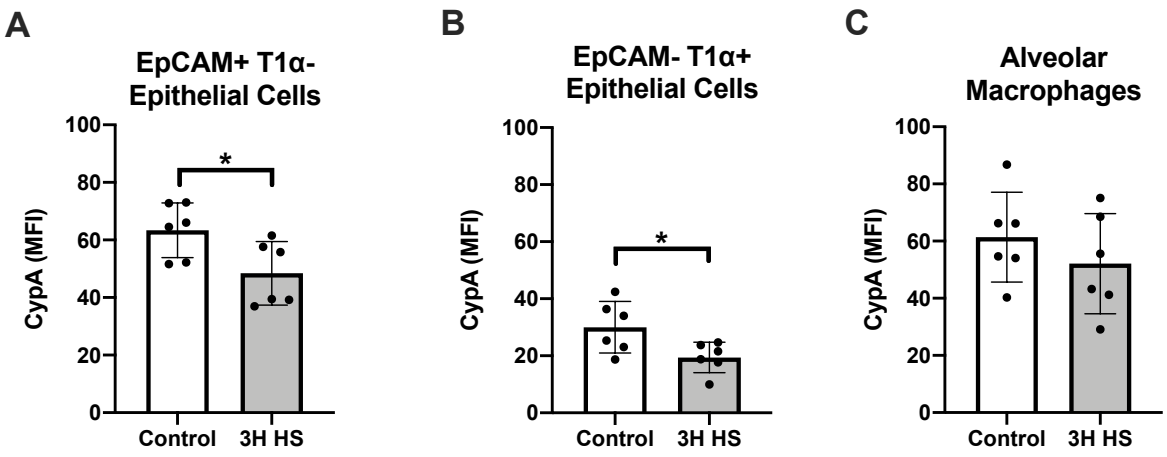


Figure 4.9 – Intracellular expression of CypA decrease in epithelial cells but not alveolar macrophages following 3 hours of high V_T ventilation.

*Levels (measured and expressed as mean fluorescent intensity [MFI]) of intracellular CypA analysed by flow cytometry were decreased significant in both EpCAM+T1α- (A) and EpCAM-T1α+ (B) epithelial cells but remained unchanged in alveolar macrophages (C). Data shown as mean ± SD. N=6. *p<0.05. Unpaired t-test.*

4.5.6 *In vitro* cell stretching – alveolar epithelial cells

To validate the *in vivo* findings and to determine if alveolar macrophages are involved in secretion of CypA from AECs, an *in vitro* cell stretch system was developed. This system would allow for investigation of each pulmonary cell type in isolation to dissect the contribution of each cell to the production of CypA following stretch.

As we hypothesised that AECs are a likely source of extracellular CypA, we begun by exploring the effects of stretch on mouse lung epithelial (MLE-12) cells. Our first steps with these *in vitro* stretch experiments were to (1) establish that our stretch protocol was leading cell activation, and (2) identify readouts that would allow us to assess the cells' response to stretch.

MLE-12 cells were subjected to either low stretch (4% elongation) or high stretch (20% elongation) cyclic stretching for 6 hours. The decision to use low stretch as a control instead of static cells was made on the basis that being held static is an unnatural state for lung epithelial cells. Instead, 4% elongation – the estimated linear distension of the basement membrane of the alveolus caused by volume fluctuations during normal tidal breathing (379-382) – was chosen as a potentially more physiologically relevant control. From our *in vivo* experiments, we had a rough estimation of when CypA would be released, with the earliest time point being 2 hours and perhaps more substantially at 3 hours. However, cells were stretched for 6 hours for a number of reasons. Firstly, as we wanted to first establish that cells were activated by stretch, we chose a time point where others had previously detected epithelial cell activation in response to stretch. In one of the few studies reporting the effects of *in vitro* stretch on MLE-12 cells, cyclic stretch at a similar degree of elongation (18%) was shown to induce a significant increase in release of the pro-inflammatory cytokine, IL-6, at 6 hours (383). In another study, Hu et al demonstrated that stretch-induced ICAM-1 expression peaked at 6 hours (384). Secondly, as we suspected that CypA secretion was induced by oxidative stress, it was crucial that the duration of our stretch protocol would be long enough to allow for the potential ROS production and downstream signalling events. Chapman et al subjected epithelial cells (16HBE and A549 cells) to mechanical strain at 20% elongation and found that intracellular superoxide (O_2^-) production was significantly increased at 2 hours and achieved the maximal response at 6 hours (370). Therefore, with a 6-hour stretch protocol we could be confident that there would be sufficient time for upstream signalling events to occur and for adequate upregulation of subsequent cell activation markers.

Following 6 hours of mechanical stretch, cell phenotype and viability of cells in both groups were assessed and compared. Cell surface expression of ICAM-1 and CD147 was not upregulated following high stretch (Figure 4.10A, B). Cell viability remained over 85-90% in

both group with no differences in 7-AAD positive (dead) cells between low stretch and high stretch (Figure 4.10C).

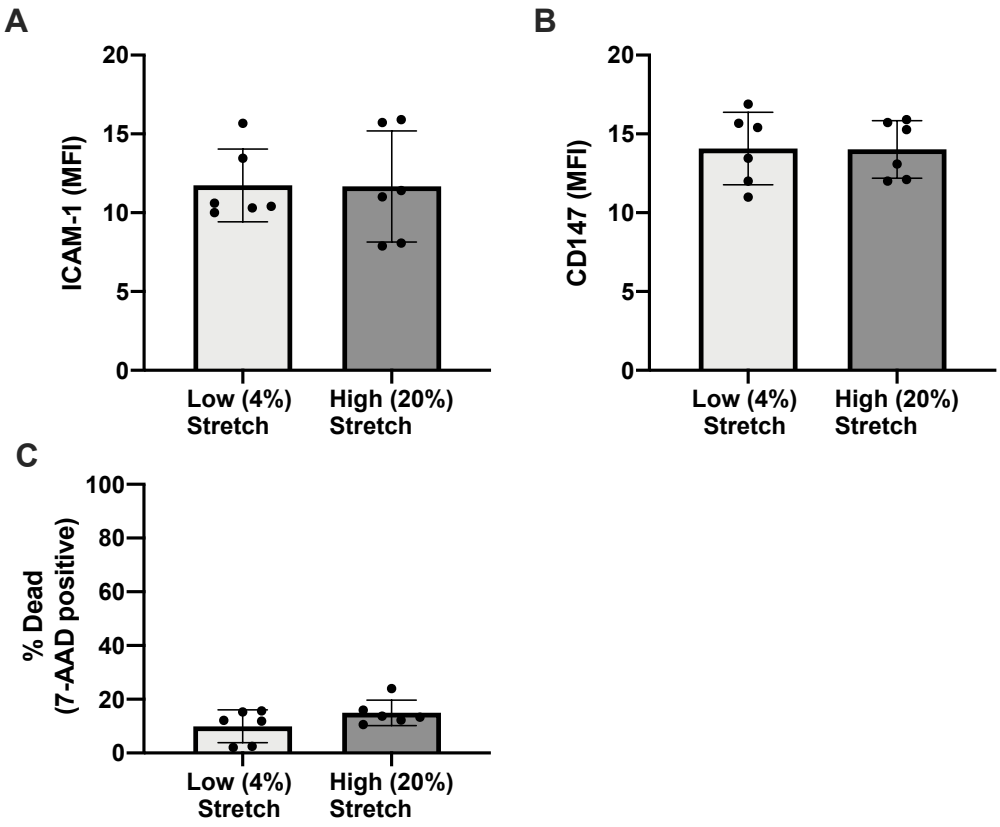


Figure 4.10 – No differences were observed in cell surface markers and viability of MLE-12 cells following 6 hours of low (4%) and high (20%) *in* vitro stretch.

High stretch did not induce an upregulation of activation marker ICAM-1 (A) or CypA receptor, CD147 (B). Cell viability was assessed by 7-AAD staining and the percentage of dead cells in both groups were similar (C). N=6. Data shown as mean ± SD. NS. Unpaired t-test.

Cell supernatants from low and high stretch cells were evaluated for IL-6 and CypA. Following high stretch, there was a significant increase in IL-6 in cell supernatants but only by a small (6 pg/mL) increment (Figure 4.11A). High stretch did not induce CypA release from MLE-12 cells. In half of the repeats (N=3) for both groups no CypA was detected at all. Further, large levels of variability were observed (Figure 4.11B).

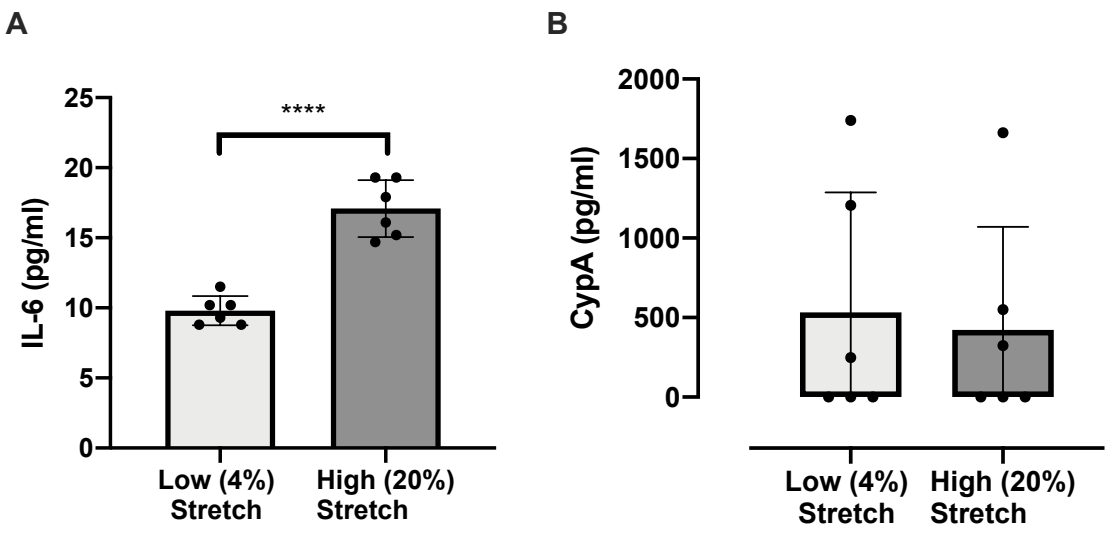


Figure 4.11 - Comparison of IL-6 and levels of CypA in release from MLE-12 cells following 6 hours of low (4%) and high (20%) *in vitro* stretch.

*While cells subjected to high stretch released a significantly greater amount of IL-6 (A), the absolute increase in concentration was only ~6 pg/mL compared with cells subjected to low stretch. No differences were observed in levels of CypA (B). N=6. Data shown as mean ± SD. **** p<0.0001. Unpaired t-test.*

From the results above, we were not fully convinced that cells were responding to the *in vitro* stretch. We next tried a static control instead of the low stretch control. However, even when cells subjected to high (20%) stretch were compared with static controls, no changes in expression of surface markers ICAM-1 (Figure 4.12A) or CD147 (Figure 4.12B) were observed. Cell supernatants were evaluated for IL-6 (Figure 4.12D) and CypA (Figure 4.12C), but no significant differences were found between groups. Levels of CypA remained highly variable between experiments. Cell viability remained between 80-93% for all experiments (Figure 4.12D).

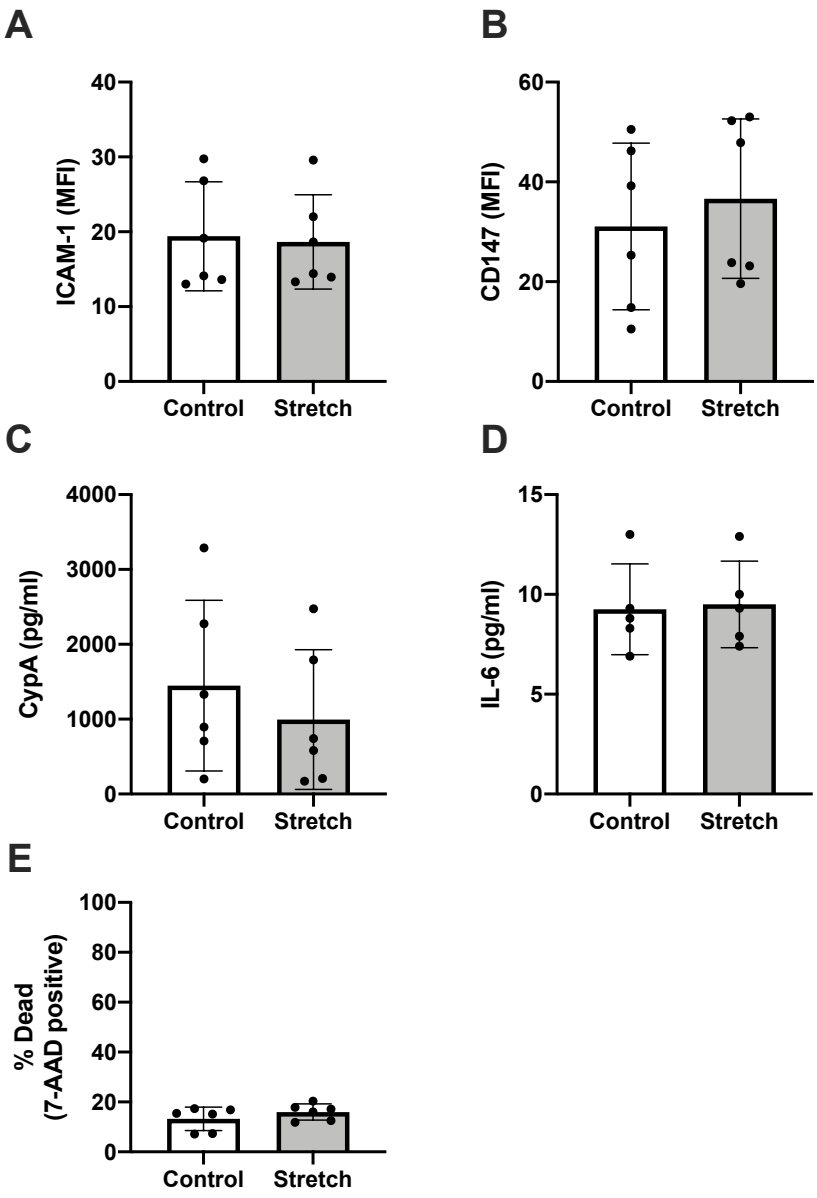


Figure 4.12 - No differences observed between MLE-12 cells held static (control) or subjected to *in vitro* stretch for 6 hours.

Surface markers ICAM-1 (A) and CD147 (B) show no differences between control and stretched cells. Culture media was evaluated for CypA (C) and soluble mediator IL-6 (D) content and again, no differences between control and stretched cells were detected. Lastly, viability (E) assessed using percentage of dead (7-AAD positive) cells in control and stretch groups were also not significantly different. Data shown as mean ± SD. N=6. NS. Mann-Whitney test.

In light of these results, we hypothesised that this lack of response to stretch could be due to three different variables: (1) stretch protocol, (2) cells, (3) readouts used to determine if cells were activated.

The first reason for the lack of response to stretch could be the stretch protocol, specifically the parameters used. A number of different factors including, duration of stretch, magnitude of stretch applied (% elongation), and frequency of stretch (Hz) were potentially crucial. It was possible that the protocol we were using was not injurious enough. In particular, literature suggests that the magnitude of stretch defined by the % elongation, was especially important factors for cell activation (385). Unfortunately, the stretch system that we had available to us was only able to generate a maximum of 20% elongation, which eliminated the option of investigating the effects of higher magnitudes of stretch. While some studies have used protocols which subject cells to stretch for up to 48 hours, we were hesitant to extend the duration of our protocol as it would no longer be a model investigating the acute effects of stretch.

The second possible reason was the cell line. The epithelial cells stretched in these experiments were MLE-12 cells – a tumour cell line, which led to two points of concern. Firstly, MLE-12 cells did not appear to display contact inhibition. Thus, instead of a uniform, confluent monolayer, the cells grew in multi-layers over the surface of the stretch plate. Initially, to address this issue, lower seeding densities were tested but this only led to a patchier growth of cells. As such, it was likely that cells were exposed to very variable degrees of stretch (linear elongation) and we suspected that this might be the cause for the large variability in results.

The third variable could be the readouts that were chosen to assess cell activation. The readouts that were assessed in this set of experiments were by no means exhaustive, thus it

is possible had we assessed other markers such as, intracellular calcium levels, F-actin distribution, or activity of NFκB pathway, we might have detected cell activation.

Stretching A549s

Since using a static control did not appear to address the large variability in levels of CypA, we decided to address the next variable that was thought to be a contributing factor to the large variability: the lack of contact inhibition. To do so, a different cell line – the human lung adenocarcinoma A549 cell line, was stretched. While A549 cells are also a cancer cell line, they grow more uniformly and have been more frequently used in cyclic stretch experiments than MLE-12 cells. Visual inspection of these cells with light microscopy immediately prior to stretch when cells were >90% confluent revealed that cells grew in a confluent monolayer.

As before, the first step was to establish whether cells were responding to the stretch. To assess cell activation, levels of IL-8, a cytokine frequently reported to be increased following mechanic stretch, in conditioned media were analysed. Previous studies investigating mechanical stretch with A549 cells have reported an increase in IL-8 levels following 4 to 24 hours of stretch (386-391). Thus, A549s were exposed to high (20%) stretch for 4, 6, 8, or 24 hours and IL-8 content in conditioned media were assessed using ELISA. IL-8 was not increased with exposure to high stretch at any time point (Figure 4.13). ICAM-1 and CD147 expression was assessed but showed no increase with mechanical stretch (data not shown). Cell viability remained over 90% in all experiments. As there was no evidence of cell activation following mechanical stretch, cell supernatants were not evaluated for CypA.

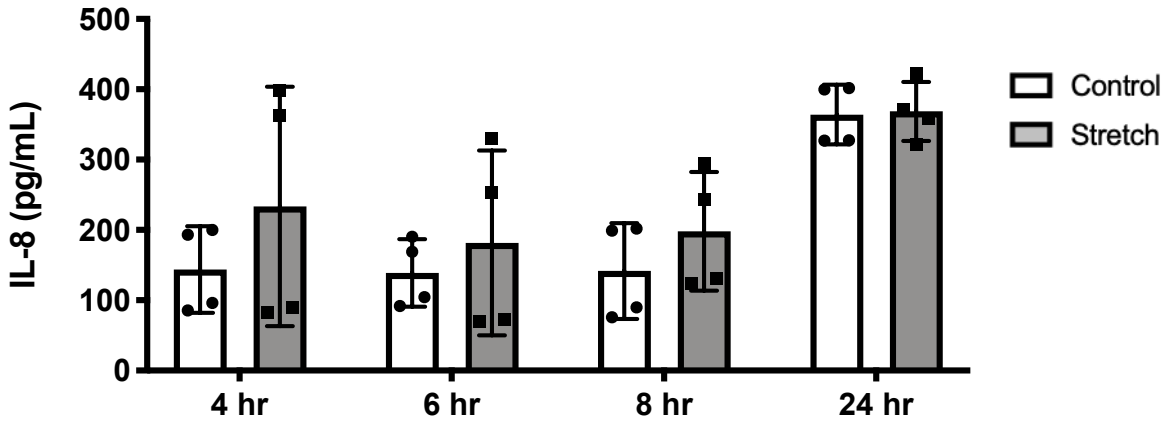


Figure 4.13 – Levels of IL-8 in conditioned media of A549 cells that were kept static (control) or stretched (20% elongation) for various time periods.

No significant increase in IL-8 following 4, 6, 8, or 24 hours (hr) of high stretch. N=4. Data shown as mean ± SD. NS. Two-way ANOVA.

Stretching primary human alveolar epithelial cells

As the A549 cells did not appear to be activated by stretch, we decided to stretch primary cells. Both MLE-12 and A549 cells were cancer cell lines. While this makes them easy to culture and maintain, it was a concern that the mechanical transduction pathways might be disrupted, rendering them irresponsive to stretch of the magnitude that we can deliver. Primary human alveolar epithelial cells (H-AECs) were cultured in the same Flexcell plates. Visual inspection of these cells with light microscopy immediately prior to stretch when cells were >90% confluent revealed that cells grew in a confluent monolayer.

H-AECs were then stretched (20% elongation) or held static as a control for 6 hours. No significant changes in expression of surface markers ICAM-1 and CD147 were observed when cells were stretched (Figure 4.14A, B). However, IL-8 release was significantly higher in stretched cells (control: 36.8 ± 5.5 pg/ml vs 20% stretch: 55.4 ± 8.6 pg/ml) (Figure 4.14C).

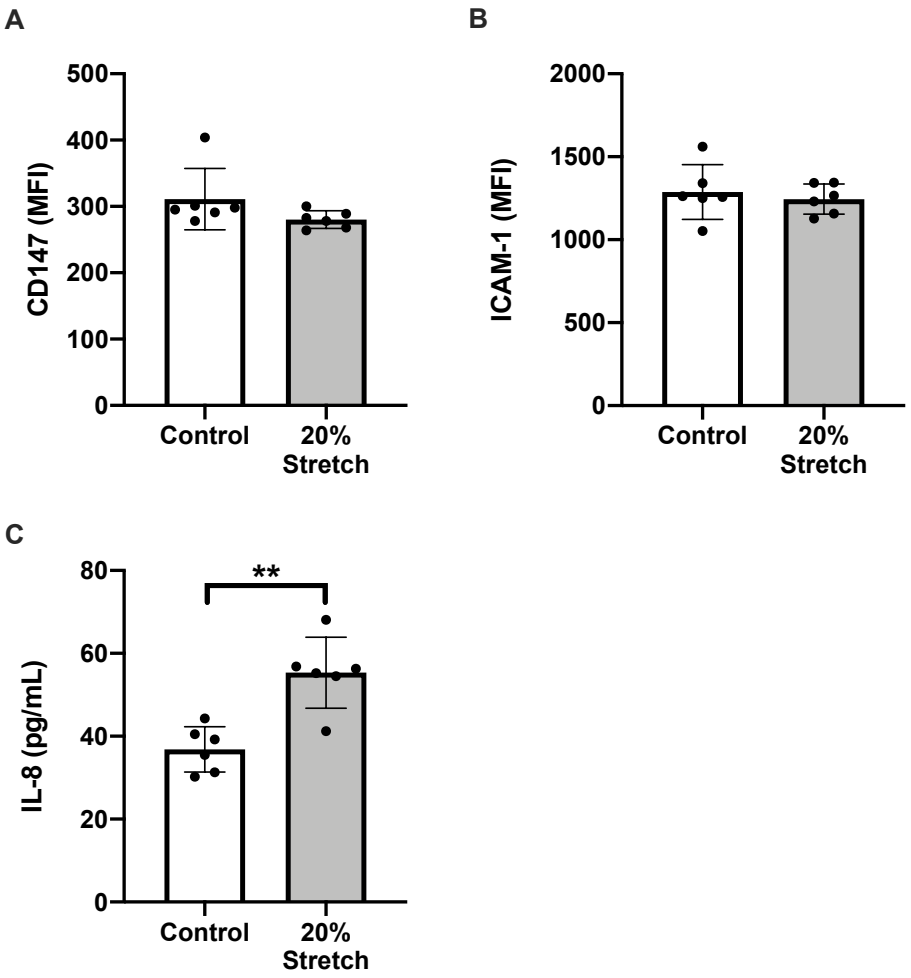


Figure 4.14 – Comparison of expression of ICAM-1 and CD147, and IL-8 release in H-AECs that were held static (control) or subjected to 20% stretched cells for 6 hours.

*No differences observed between control and stretched cell expression of CD147 (A) and ICAM-1 (B). IL-8 levels (C) in conditioned media were evaluated and found to be significant increased with stretch at 6 hours. Data shown as mean ± SD. N=6. ** p<0.01. Unpaired t-test.*

Since H-AECs appeared to be activated following mechanical stretch, cell supernatants were also evaluated for CypA. At this point, we did not have a validated human CypA ELISA kit (only mouse samples were analysed using ELISA). However, we did have a validated antibody that was previously used for *in vivo* staining of CypA in mouse lung with human cross-reactivity. Thus, cell-free conditioned media from control and stretched cells were analysed for CypA using western blotting.

As the samples assayed were cell-free supernatants, conventional loading control proteins (e.g. β-actin) could not be used to ensure equal protein loading across wells or as a reference point for data normalisation. Instead, equal volumes (16.25 µL) of supernatants were loaded into each lane for electrophoresis. A protein assay was performed to measure the protein concentration in supernatants and found to be virtually identical in control and stretched cells (Figure 4.16A). After each stretch experiments, cells were detached from all wells and counted using flow cytometry to ensure that cell counts were consistent across experiments (Figure 4.15B).

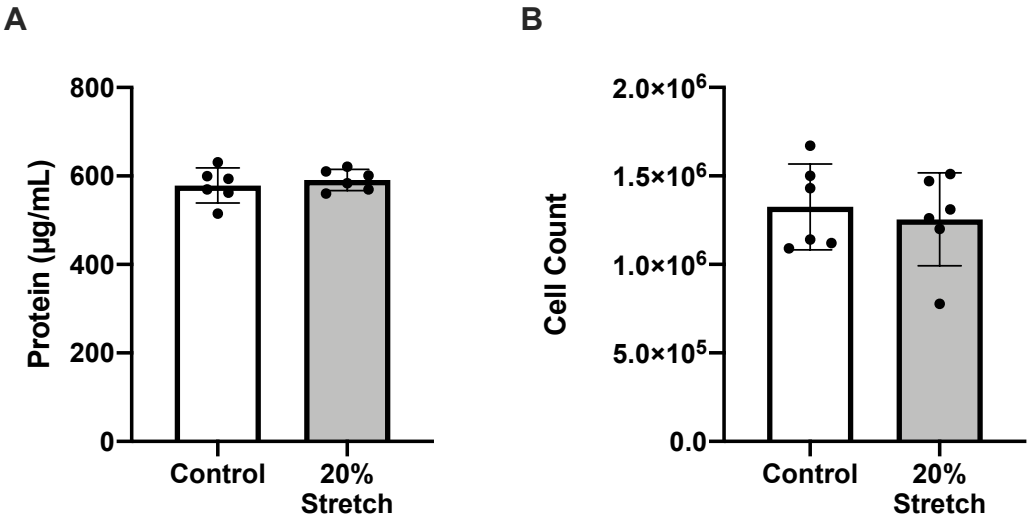


Figure 4.15 – Comparison of protein concentration of supernatants and cell counts between H-AECs that were held static (control) or subjected to 20% stretched cells for 6 hours.

(A) Protein concentration of conditioned supernatants, analysed using Bradford assay, was found to be virtually identical in control and stretched cells. (B) Cell counts (cells per well in stretch plate) were determined using flow cytometry after each experiment and also found to be consistent across both groups for all experiments. Data shown as mean ± SD. NS. Unpaired t-test.

To allow comparison between gels, an internal standard – a sample known to contain high levels of CypA – was loaded onto every gel. This density of this sample was given an arbitrary unit of 1 and the density of all bands were expressed as a value relative to it.

Levels of CypA was significantly increased in conditioned media of stretched human AECs (Figure 4.16A, B), adding further data to support our hypothesis that epithelial cells are the primary source of extracellular CypA during VILI.

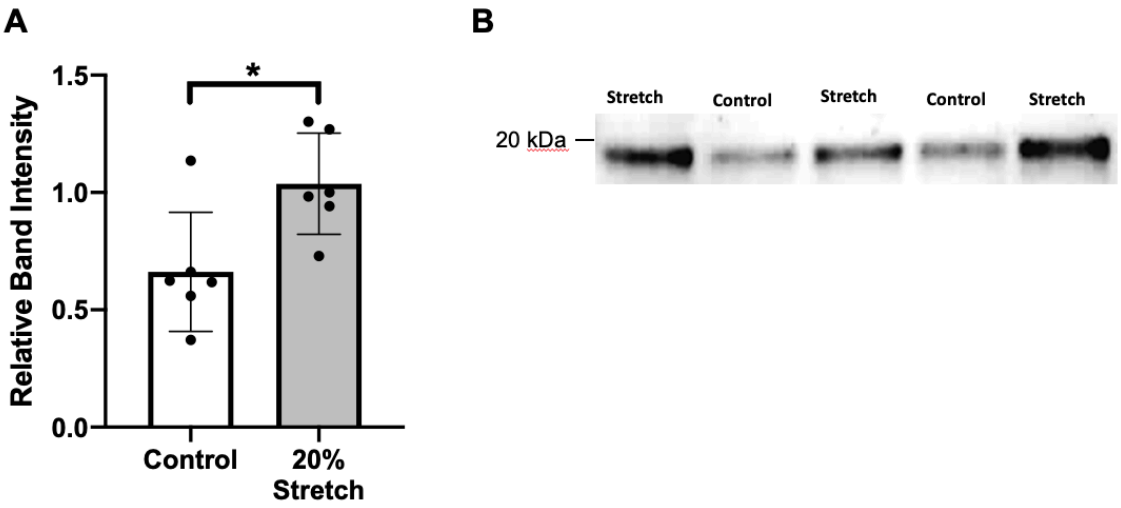


Figure 4.16 – CypA released is increased following 6 hours of 20% stretch.

(A) Densitometry of CypA (18 kDa) from the western blots revealed a significant increase in CypA se following 6 hours of stretch. The density of protein in an 'internal standard' (a sample known to contain high levels of CypA) was loaded onto every gel and used as a standard to compare relative densities in other bands. All results are expressed as a value relative to the standard (1 arbitrary unit). (B) Representative western blot of supernatants collected from unstretched controls and stretched (20% elongation) human AECs using a rabbit anti-cyclophilin A antibody.

Cell viability was evaluated using two different methods. Firstly, as before, cells were analysed for 7-AAD staining using flow cytometry (Figure 4.17A). The proportion of dead cells in control and stretched experiments were not significantly different and low in both groups (control: 1.98

± 4.25% vs 20% stretch: 4.58 ± 5.6%). Secondly, levels of LDH in cell-free supernatants from both groups were measured (Figure 4.17B). No increase in LDH was observed in stretched cells compared with control cells. These data suggest that CypA release is not merely a passive process that occurs following damage to the cell membrane on application of mechanical stretch.

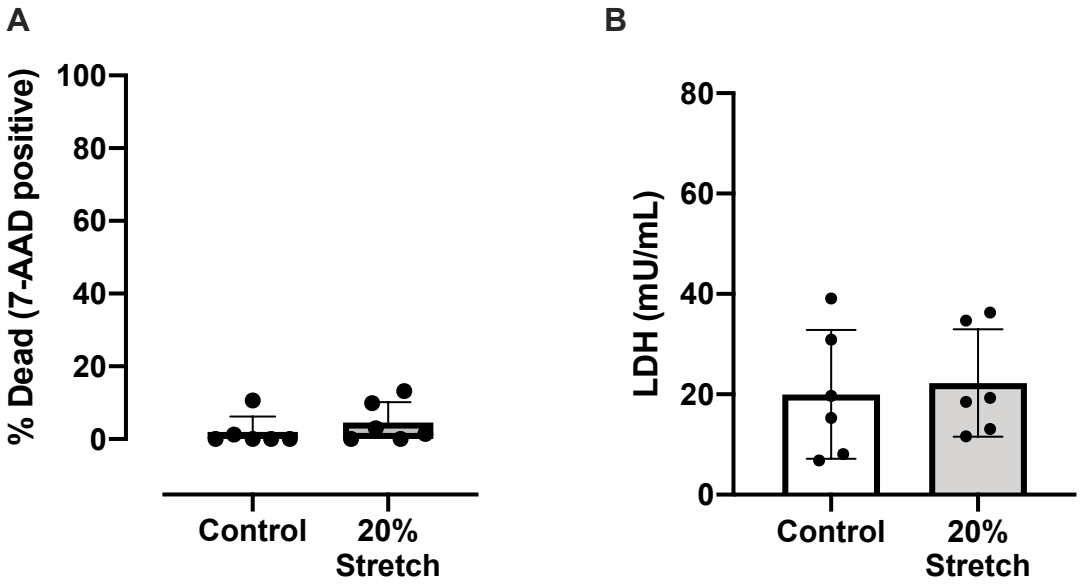


Figure 4.17 - Assessment of viability in H-AEC cells that were held static (control) or subjected to 20% stretched cells for 6 hours.

The percentage of cells staining positive for 7-AAD (i.e. non-viable cells) assessed using flow cytometry was not significantly increased with stretch. (B) Similarly, levels of lactate dehydrogenase (LDH) were virtually identical in control and stretched cells. Data shown as mean ± SD. N=6. NS. Unpaired t-test.

4.5.7 In vitro cell stretching – alveolar macrophages

It is unclear if alveolar macrophages would directly experience stretch *in vivo*. For pilot experiments, we explored the effects of stretch on RAW cells – a murine monocyte/macrophage-like cell line. Although it would have been ideal to use primary alveolar macrophages, the recovery rates of alveolar macrophages in lungs of mice are low. In our

hands, a typical yield of alveolar macrophage cells per mouse is roughly 2-5 x 10^5 cells. While this low yield would be addressed by scaling down the experiments (e.g. using a 48-well plate instead of a 6-well plate), the only plate format compatible with our stretch machine was a 6-well plate. Therefore, the low macrophage yield per mouse would have meant that up to 2 mice would have to be sacrificed to harvest enough cells for one well of a 6-well stretch plate, which we felt was not justified in the first instance.

Thus, RAW cells were subjected to stretch (20% elongation) for 6 hours and compared with static controls. Stretch had no effect on expression of surface activation markers ICAM-1, MHC-II and CD86 (Figure 4.18A), cell viability as assessed by 7-AAD staining (Figure 4.18B), or secretion of pro-inflammatory cytokine IL-6 (Figure 4.18C). Culture supernatants of both controls and stretched cells were assayed for CypA but was not detected (levels were below the detection range of the ELISA kit – 0.16 – 10 ng/mL).

Following these pilot experiments with RAW cells, our aim was to investigate the effects of stretch on primary macrophages. As primary human alveolar macrophages are very difficult to obtain, our intentions were to (1) stretch human monocyte-derived macrophages which can be isolated from the peripheral blood mononuclear cells obtained from healthy volunteers (as described in Chapter 6) and possibly (2) stretch primary mouse alveolar macrophages. Unfortunately, I did not have time to complete these subsequent experiments.

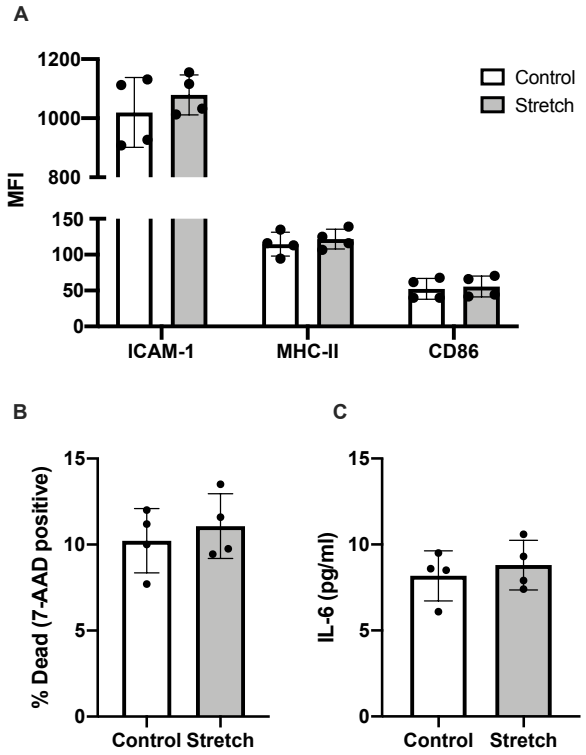


Figure 4.18 – Assessment of cell activation markers, viability, and IL-6 release from RAW cells following 6 hours of *in vitro* stretch.

(A) Surface expression of activation markers ICAM-1, MHC-II, and CD86 unchanged following stretch. (B) No differences in viability, assessed by % dead (7-AAD positive), and (C) IL-6 levels between control and stretched cells. N=6. Data shown as mean ± SD. NS. Unpaired t-test.

As a series of pilot positive control, RAW 246.7 cells, primary mouse alveolar macrophages, and primary mouse bone marrow derived macrophages were stimulated with high doses of LPS (100 ng/mL) for 4 hours. The aim of these experiments was to assess if there was potential for CypA release from these macrophages using a stimuli (LPS) that has been previously shown to induce CypA secretion from macrophages (279). However, no CypA was detected in the conditioned media when assessed by ELISA (N=3 per cell type, levels were all below the detection range of the ELISA kit – 0.16 – 10 ng/mL).

Thus, while our current data suggests that macrophages are unlikely to be as important a contributor of extracellular CypA during VILI, we still remain uncertain and are unable to exclude their involvement.

4.6 Discussion

The results presented in this chapter suggest that AECs are a likely source of CypA following mechanical stretch. However, whether alveolar macrophages also contribute to extracellular CypA release during VILI is still unclear; the data that we have at present is insufficient to rule out that possibility.

At the beginning of this chapter, the potential contributors to extracellular CypA during VILI were narrowed down to two cell types: AECs and alveolar macrophages. Although pulmonary endothelial cells would have also been exposed to considerable stretching during high V_T ventilation and have been shown to be capable of releasing chemokines such as IL-8 and MCP-1 in response to cyclic stretch *in vitro* (392, 393), they were not investigated in this chapter; The results presented in Chapter 3 suggested that CypA was produced locally within the alveolar space and not leaking in from the bloodstream, further circulating plasma levels did not show any changes following VILI. Together, these data suggest that endothelial cells are an unlikely source of CypA observed in the alveolar space.

Between AECs and alveolar macrophages, we hypothesised that AECs would be the more likely candidate as they almost definitely experience greater levels of distension during mechanical ventilation. Thus, our first approach was to conduct a set of preliminary experiments comparing the levels of CypA production in two more different ALI models - acid- and LPS-induced lung injury. In the acid-induced lung injury model, where there is known to be a substantial degree of epithelial injury, there was an impressive nearly 500-fold increase in CypA in BAL when compared with untreated controls. In contrast, in the macrophage driven LPS injury model, we did not observe a significant increase in CypA compared with untreated animals. Following acid injury, a significant increase in sRAGE was also observed. Together, these data suggest that CypA is not a VILI-specific marker and instead is likely to released following general epithelial insult.

Although CypA has previously been implicated in LPS-induced lung inflammatory in a study conducted by Gwinn et al (335), there were no significant differences in the levels of CypA between the LPS and untreated group in our model. While the increase was not statistically significant, the numerical increase was fairly substantial – a 25-fold increase in mean CypA levels, suggesting that CypA was still present at much higher levels following LPS treatment. The lack of statistical significance could be due to the large variability in CypA levels within the group and/or being included in an ANOVA tests with the acid model where CypA was present at much greater levels. While it would have been informative to compare the values of CypA detected in our model with those found by Gwinn et al, they used Western blots to analyse the levels of CypA present in BAL. Therefore, while it is possible that similar levels of CypA were present, the lack of quantitative data precludes any comparisons.

Since our preliminary experiments suggest that CypA was significantly upregulated in the acid model where epithelial insult forms a significant component of injury seen but not in the macrophage driven LPS model, our first approach was to eliminate alveolar macrophage and assess the effect of this on CypA secretion during VILI. Unfortunately, we were unable to identify a time point after 120 minutes – when CypA was previously shown to be upregulated in our VILI model – where the severity of injury was similar groups. As CypA was previously shown to be correlated with the degree of injury, the difference in severity of lung injury at as early as 120 minutes meant that we would be unable to interpret extracellular CypA levels if they were evaluated. Furthermore, there was substantial neutrophilia in the clodronate treated animals that would have added even more uncertainty to the interpretation of the results.

There are alternative methods of alveolar macrophage depletion which circumvent the neutrophilia that occurs with clodronate liposome administration. Roberts et al devised a protocol using CD11c.DOG mice (a newer diphtheria toxin (DT) receptor transgenic mice) treated with DT to deplete alveolar macrophages and reported near complete depletion of

alveolar macrophage after 24 hours (394). While they did also observe a significant increase in neutrophils after DT treatment, they found that waiting 5 days would allow neutrophils to dissipate while still maintaining >90% depletion of alveolar macrophages (394). However, they also warn that alveolar macrophage depletion with DT was accompanied by many other changes to the cytokine milieu and cellular composition to the lung that potentially impact innate immune response. Thus, we decided to investigate our hypothesis using alternative methodologies.

We continued with an *in vivo* approach and measured intracellular levels of CypA using flow cytometry. Following *in vivo* high V_T ventilation, we observed a significant decrease in intracellular levels of CypA in epithelial cells but not in alveolar macrophages. This decrease in intracellular CypA is consistent with the corresponding increase in extracellular CypA detected in BAL during VILI. Despite the relatively small decrease in MFI, given that it is such an abundant cytosolic protein (making up 0.1-0.6% total cytosolic protein), we believe that our ability to even detect a decrease in signal is consistent with the substantial increase in extracellular CypA following high VT ventilation. One possible way to further this line of investigation would have been to use a fluorescence quantification kit designed to estimate antibodies bound per cell (e.g. BD Quantibrite™ beads, BD Biosciences). However, this kit has been designed for use with PE-labelled monoclonal antibodies; Our protocol utilised a polyclonal anti-CypA antibody that is secondarily conjugated with APC for detection. We were unsure how these factors would affect quantitation and therefore decided not to attempt to quantify the amount of CypA released. Despite the absence of quantification, these results do support our hypothesis that AECs are the primary source of CypA.

Since it was difficult to dissect out the contribution of AECs and alveolar macrophages to CypA *in vivo*, we developed an *in vitro* stretch protocol which allowed us to study each cell type in isolation. We began by stretching alveolar epithelial cells, starting with MLE-12s. Following

stretch, no changes in cell phenotype or viability was observed. A small increase in IL-6 was observed following 6 hours of high stretch when compared to low stretch controls, suggesting that MLE-12 cells were capable of responding to mechanical stretch. Two other research groups have reported an increase in IL-6 secretion following stretch (18% elongation) at as early as 6 hours and at 48 hours (383, 395). At 6 hours, this increase was found to be minimal (10 pg/mL), in keeping with our results (383). However, when cell supernatants were evaluated for CypA, no differences were observed between high stretch and static or low stretch controls. Further, levels of CypA detected were very variable between experiments.

As we believed that a possible reason for the large variability was the absence of contact inhibition between MLE-12 cells leading to multi-layered cell growth, the human pulmonary epithelial cell line, A549, was stretched instead. This cell line has been most frequently used to study signalling in response to stretch in the literature and grows more uniformly than MLE-12 cells. To assess cell activation, levels of IL-8 in conditioned media of static controls and stretched cells were evaluated at 4, 6, 8, and 24 hours. However, we did not find a significant increase in IL-8 at any of these time points.

While there is some evidence to suggest that IL-8 is increased following various periods of *in vitro* stretch ranging from 4 to 48 hours (396-398), there is also evidence to suggest otherwise (399, 400). Interesting, two studies have observed that smaller deformation (amplitudes of 20% strain) produced no consistent increase in IL-8, similar to what we found in our system (390, 401, 402). Only when stretch was increased to an amplitude of 30% to 40% did cells release significantly greater amounts of IL-8 compared with static controls (390, 401, 402). The lack of definitive increase in IL-8 made it impossible to determine if the A549 cells were responding to stretch, thus supernatants were not evaluated for CypA.

While cell lines, such as MLE-12 and A549, are easier to culture and maintain than primary cells, it is known that they can behave differently. Therefore, we decided that it would be necessary to investigate the effects of stretch on primary H-AECs before concluding that stretch of epithelial cells alone does not promote CypA secretion. Although changes in expression of surface markers were not observed, there was a significant increase in IL-8 concentration in the supernatants of cells following 6 hours of stretch (20%) suggesting that cells were activated. CypA secretion was evaluated by western blotting of supernatants and found to significantly increased in stretched cells compared with static controls. In another study, exposure of fibroblasts to a necroptosis-inducing stimulus increased release of CypA, an effect attributed to passive release following cell membrane permeabilisation (285). To determine if increased CypA levels in stretched cells was a result of passive release following damage to the cell membrane, we measured cell viability by both 7-AAD staining and LDH assay. In both instances, there was no difference in viability of stretched cells compared with control cells, suggesting that in response to mechanical stretch, CypA is actively secreted by AECs and not a consequence of damage to the integrity of epithelial cells.

Having demonstrated release of CypA from epithelial cells, we proceeded to investigate the effect of stretch on macrophages. No changes in their phenotype or secretion of IL-6 or CypA were detected following 6 hours of cyclic stretch. To the best of my knowledge, no studies have looked at the effects of *in vitro* stretch on this specific cell line (RAW 264.7). Other studies looking at the response of macrophages to stretch have produced mixed results. Pugin et al stretched primary human alveolar macrophages using a “plastic lung” model ventilated with an inspiratory plateau pressure of 70 cmH_2O (corresponds to a mean stretch of 12%) and found that they secreted IL-8, with maximal response seen 8 hours after initiation of mechanical stress (403). Mechanical ventilation alone did not induce TNF-α and IL-6 but synergises with bacterial endotoxin (LPS) to stimulate the secretion of these mediators. In the same study, they also stretched human monocyte-derived macrophages and found a similar

patterns of cytokine secretion to that of primary alveolar macrophages. In contrast, Lang et al reported that mechanical stretch alone did not induce the production or secretion of CINC-1 (a chemoattractant with close sequence homology to IL-8 in rat alveolar macrophages). But they echoed that physical strain enhanced the cells' secretion of TNF-α and IL-6 to LPS (404).

Unfortunately, I was unable to complete further experiments evaluating the effects of stretch on primary macrophages. However, stimulation of primary mouse alveolar macrophages, and primary mouse bone marrow derived macrophages with high doses of LPS (100 ng/mL) for 4 hours failed to induce any CypA secretion. While LPS has been previously shown to stimulate CypA release, the incubation time used as significantly longer than ours (16 hours). This may suggest that CypA may not be secreted in the acute phase of a macrophage's inflammatory response. Whether this would have also been true if the stimuli was stretch instead of LPS is unclear.

4.7 Concluding remarks

In this chapter, we present a number of findings that implicate AECs as a source of CypA following lung injury. Firstly, we demonstrate a significant increase in BAL CypA during acid-induced lung injury – a model known to involve substantial epithelial injury – but not LPS-induced lung injury – a model driven by macrophages in its acute phase. Additionally, using a flow cytometry-based method, we show a significant decrease in intracellular CypA levels in epithelial cells but not alveolar macrophages following *in vivo* high V_T ventilation. Lastly, using an *in vitro* cyclical stretch model, we also show that CypA is secreted from H-AECs following stretch. In contrast, macrophages exposed to the same degree and duration of mechanical stretch did not show increases in CypA secretion.

To gain insight into the mechanism of CypA secretion in response to mechanical strain, we also performed assessments of cell viability of both static and stretched cells. There was no significant decrease in cell viability following stretch, thus suggesting that CypA is actively secreted by AECs rather than passively leaking out of an injured epithelium.

Together, our data seems to suggest that AECs are a potential source of CypA in response to stretch. While the data available suggests that macrophages do not secrete CypA directly in response to *in vitro* stretch, we cannot rule out the possibility that they do secrete CypA or are involved in the process of CypA secretion *in vivo.* Further experiments are needed, e.g. stretching primary macrophages and stretching co-cultures of AECs and macrophages.

5 Inhibition of CypA in ventilator-induced lung injury

5.1 Abstract

In previous chapters, CypA was shown to be significantly upregulated in the alveolar space early in the course of VILI. AECs were implicated as a likely source of extracellular CypA, which appeared to be secreted actively following mechanical stretch. However, in the absence of further data, it was impossible to delineate its role in VILI: is it a causative agent (i.e. a potential therapeutic target), or is it released as a consequence of injury (i.e. a potential biomarker of epithelial cell stress)? In this chapter, we addressed this question by investigating the effects of inhibiting extracellular CypA in our *in vivo* VILI model.

The experiments demonstrated that administration of extracellular CypA inhibitor (MM-284) prior to injurious mechanical ventilation appears to attenuate VILI. Animals treated with MM-284 showed improved survival rates, attenuated respiratory mechanics, preserved arterial oxygenation, decreased pulmonary oedema, and alveolar-capillary membrane permeability. Together, these results suggest that CypA plays an important mediator role in the development of VILI.

Exploration of the mechanisms through which MM-284 leads to protection from VILI suggests that dampening the activation of key players in the alveolar space – AECs and alveolar macrophages – may be involved. Further, CypA inhibition may also negatively regulate CD147-mediated MMP secretion and activation, leading to decreased levels of MMP activity in the alveolar space, and decreased barrier permeability.

5.2 Introduction

Despite 'lung protective' ventilation strategies, mortality rates in ARDS remain high, suggesting that there are other contributory factors left unaddressed. One of the main damaging consequences caused by mechanical ventilation is the inflammatory response to the non-physiological patterns of stretch. In the absence of macro- and microscopic lung damage, Slutsky et al have proposed that mechanical ventilation can still induce molecular and cell-mediated events, coining the term 'biotrauma' to encapsulate this hypothesis (67). The biotrauma hypothesis proposes that the mechanical forces imposed on lungs during ventilation leads to a biological response involving the release of various mediators. These circulating mediators then cause local lung injury and, if disseminated into the systemic circulation, distal organ dysfunction (67).

Although many potential inflammatory mediators/pathways have been proposed, inhibition of these pathways have not shown clinical benefit when evaluated in clinical trials despite initially showing therapeutic effects in experimental animal models of ARDS. As such, there are currently no effective pharmacological therapies for ARDS/VILI, and identification of plausible pharmacological targets continues.

In the previous chapters, cyclophilin A (CypA) was shown to be significantly upregulated in the alveolar space during the course of VILI. The early release of substantial amounts of CypA following initiation of high V_T ventilation makes a physiological role plausible. AECs were identified as the main source of extracellular CypA, which appeared to be actively secreted following mechanical stretch. However, in the absence of further data, it was impossible to determine if its presence was a cause or consequence of VILI. In this chapter, we addressed this by investigating the effects of inhibiting extracellular CypA in our *in vivo* VILI model.

CypA is best known for being the primary intracellular protein target for the immunosuppressive drug, cyclosporin A (CsA). CsA exerts its effect by binding with high affinity to intracellular cyclophilins, especially CypA, forming a ternary complex (405). This CsA-CypA complex associates with calcineurin, inhibits its phosphatase activity and consequently, prevents the dephosphorylation of nuclear factor of activated T-cells (NF-ATc). Phosphorylated NF-ATc is unable to enter the nucleus and cannot bind to its nuclear component, blocking the synthesis of cytokines such as IL-2, ultimately resulting in a restricted activation of T-cells (76). However, while CsA is a tight-binding inhibitor of CypA, it is a promiscuous drug and does not distinguish between extracellular and intracellular CypA. Studies using fluorescent-tagged CsA have demonstrated that the high affinity of the drug predisposes its sequestration into intercellular space, leaving little amounts of it available in the extracellular compartment to interact with any released CypA (406).

Instead of CsA, inhibition of CypA in these experiments was achieved with a structurally simplified cyclosporin A (CsA) benzimidazole derivative known as MM-284. Similar to its parent CsA, MM-284 retains potent CypA inhibitory activity; its inhibitory constant (*K*i) value also falls in the nanomolar range indicating that it is also a tight binding inhibitor of CypA (407). Upon binding to the active site of CypA, it inhibits its peptidyl-prolyl *cis-trans* isomerase (PPIase) activity (406). Through the use of active site mutants of CypA, Yurchenko et al demonstrated that preservation of enzymatic activity was crucial for its signalling activity through CD147; Mutants which retain less than 1% of the wild-type catalytic activity failed to initiate ERK activation downstream of CD147 signalling (290). In accordance with these findings, Bahmed et al conducted a comparative analysis of the biological activities induced by CypA on multiple cancerous cell lines using luciferase reporter assay (408). Focusing on the most highly upregulated luciferase reporter induced by CypA in each cell line (IL-6, IL-8 and IL-5), they found that stimulation of cells with a CypA active site mutant (PPIA R55A) led

to markedly reduced biological activity in all cell lines compared to that of the wild type CypA, confirming an important role of the CypA active site and its PPIase activity (408).

Unlike CsA, MM-284 is restricted to the extracellular space due to the introduction of an anionic group in the 5 position of the benzimidazole ring, thus ensuring that inhibition is limited to only the extracellular fraction of CypA (407). As the compound is no longer cell permeable, it does not complex with intracellular CypA to inhibit calcineurin phosphatase activity and hence does not possess any immunosuppressive effects (406, 407). As MM-284 is non-immunosuppressive and selective for extracellular CypA, it is particularly well suited for the investigation of the role of extracellular cyclophilins in our *in vivo* VILI model.

5.3 Aims

The aim of this chapter was to assess whether CypA inhibition during *in vivo* ventilation attenuates VILI and to investigate the possible mechanisms behind any observed protective effects.

5.4 Protocols

5.4.1 Cyclophilin A inhibition experiments

To confirm a role for CypA during VILI, we explored the impact of *in vivo* CypA inhibition using MM-284, a CsA derivative selective for extracellular cyclophilins that has been demonstrated to have powerful antagonistic effects on CypA activity (406, 407).

The protocol used was similar to that detailed in Chapter 2 with slight alterations as shown in Figure 5.1. Mice were placed on the ventilator on low V_T ventilation settings (8 mL/kg, PEEP 3 cmH_2O, respiratory rate (RR) 120 bpm, 100% O_2). Mice were randomly allocated to receive 50 µL of either vehicle (10% DMSO diluted in saline) or MM-284 (0.67 mM; kind gift from Dr Malesevic at Martin Luther University). Mice were briefly disconnected from the ventilator and the vehicle/drug was delivered intratracheally via the endotracheal tube. Immediately after, mice were re-attached to the ventilator and recruitment manoeuvres (3 x 30 cmH_2O, 5 seconds) were performed to aid distribution of fluid. Mice were then maintained at low V_T for 30 minutes with recruitment manoeuvres performed every 15 minutes. After this initial 30-minute equilibration period, V_T was increased 30-35 mL/kg to reach a standardised peak inspiratory pressure (PIP) of 40 cmH_2O (PEEP 3 cmH_2O, RR 80 bpm, 96% O_2 + 4% CO_2). Ventilation at these settings were continued for 3 hours or until mortality surrogates (blood pressure <50 mmHg or PIP increased >20%) were reached.

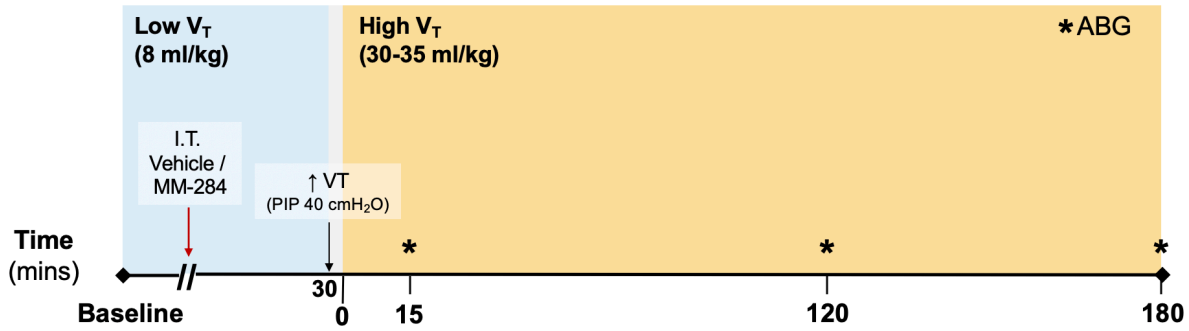


Figure 5.1 - In vivo VILI protocol for inhibition experiments

To measure respiratory mechanics, inspiratory pauses were performed at baseline, post-instillation, 15 minutes, 30 minutes, and then every 15 minutes once high V_T ventilation begun. Arterial blood gas samples (denoted as * on Figure 5.1) were collected after initiation of high V_T ventilation at 15 minutes, 120 minutes and at the end of the protocol.

5.4.2 MM-284 – mechanism of action and dose

Currently, there are only a handful of studies which have utilised MM-284. Most of these explore the effects of the drug in models of chronic conditions and this is reflected in their dosing regimen. In a study assessing the drug in the context of myocarditis, Heinzmann et al administered the drug intraperitoneally every second day over the course of 28 days at a dose of 10 mg/kg (409). In a study of allergic lung inflammation, Ditiatkovski and colleagues also delivered the drug via an intraperitoneal injection every second day but over a longer period of 6 weeks at a dose of 6.6 mg/kg (410). There is no study that uses this particular CypA inhibitor in the setting of acute lung injury. However, its parent drug, CsA, has been investigated in the context of acute lung injury and inflammation. Both drugs are reported to have a similar half maximal inhibitory concentration (IC50) of ~10 nM (unpublished data from Dr Malesevic), thus making it possible to draw comparisons between dosages. CsA has been administered at doses ranging from 10 mg/kg to 50 mg/kg (411, 412). However, in almost every study, CsA is administered systemically (via an intravenous or intraperitoneal injection), and usually as multiple doses over the course of 48 hours to 72 hours before exposure to the injurious stimuli (411-414). As our intentions were to administer the drug locally (intratracheally) and as a single dose before ventilation, deciding on the dose of the drug to be administered was based on two main factors: the solubility of the drug, and the concentration of CypA present in the BAL (as shown in Chapter 3).

MM-284 was supplied in a solid form which had to be dissolved before use. The compound is poorly soluble in water or saline, which is why DMSO was chosen as a vehicle for the drug.

However, given the cytotoxic effects of DMSO, we tried to limit it to as low a percentage as possible while still ensuring that the drug did not precipitate out of solution. This compromise was found by first dissolving the drug in 100% DMSO before then diluting it 10-fold in saline to reach a final solution that was 10% DMSO. Following this protocol, we achieved an intermediate MM-284 solution in 100% DMSO at a concentration of 6.69 mM, and a final solution in 10% DMSO at 0.67 mM. The final dose administered was 1.9 mg/kg; this was constrained by our route of administration – intratracheal, which limits the volume delivered to 50 µL.

Although our dose was lower than that used in literature, we believed it was still appropriate based on the concentrations of MM-284 to CypA in BAL. A 1.9 mg/kg dose in an average sized 25g mouse equates to 44.2 µg of MM-284 per dose. In Chapter 3, we showed that the concentration of CypA present in BAL in the VILI model was 5,918.5 ± 3,036.3 pg/mL in an average of 600 µL of BAL. The maximum amount of CypA detected at 3 hours during VILI is therefore approximately 5 µg. At the dose of MM-284 used, it was 8.8-fold more abundant than CypA suggesting that the dose was unlikely to be too low. Furthermore, our drug was delivered directly to the intended site of action instead of systemically, therefore we did not have to worry about whether enough of the drug would reach the lungs and it reduced the likelihood of significant systemic clearance during the 3-hour protocol.

5.4.3 Post-experiment sample processing and analyses

At the end of the 3-hour protocol, animals were euthanised. BAL was sampled for analysis of protein concentration, inflammatory cytokines (IL-6, KC/CXCL-1, IL-1β), sRAGE, and leukocyte counts. The right lower lobe of lungs was removed to determine wet/dry (W/D) weight ratio. The remaining right lobes were snap-frozen and stored at -80ºC for analyses with gelatin zymography or western blotting at a later date. The left lobe of the lung was homogenised using a GentleMACS tissue dissociator to produce a single-cell suspension for

antibody staining and subsequent flow cytometric leukocyte counts and analyses of surface ICAM-1 expression.

5.4.4 Homogenisation of lung samples

Frozen right lung lobes were mechanically homogenised in 200 µL of ice-cold PBS in Precelly's homogeniser tubes at 500 rpm, 1 minute. Homogenised samples were then incubated with 100 µL of cell lysate buffer (RIPA buffer, protease inhibitor, phosphatase inhibitor, EDTA, PMSF prepared in deionised water) for 30 minutes on ice. Samples were vortex intermittently to ensure thorough lysis of cells. Samples were then centrifuged at 14,000 x *g* for 10 mins at 4ºC to pellet any cell debris and supernatants were collected for analyses with western blotting or gelatin zymography. The protein content of supernatants was also quantified using the Bradford protein assay.

5.4.5 Gelatin Zymography

One of the main roles of CypA's primary receptor, CD147, is to regulate matrix metalloproteinases (MMPs). Therefore, it was of interest to investigate the potential effects of CypA inhibition on MMP activity, which were likely mediated through CD147. To detect MMP presence and activity in lung homogenate and BAL fluid, samples were analysed using gelatin zymography.

Gelatin zymography was used instead of western blotting for two main reasons. Firstly, zymography is much more sensitive than western blot, enabling detection of gelatinolytic bands at MMP levels as low as 10 pg (415). Secondly, we wanted to evaluate the enzymatic activity of MMPs within the sample. Zymography allows for the detection of enzymatic activity while western blot does not. This is because in SDS-PAGE, the protein is denatured and negatively charged so that protein can be separated by molecular weight. In zymography, there is no protein denaturation or addition of reducing agent, and separation during PAGE

occurs on the basis of charge. This preserves the enzymatic activity of the protein of interest which can then be detected by incubating the substrate co-polymerised gel in an appropriate buffer after PAGE and staining the gel in a suitable staining solution to visualise the proteolytic bands.

Samples were prepared in 1X Novex™ Tris-Glycine SDS Sample Buffer (Invitrogen) and diluted appropriately in deionised water to make a final volume of 25 µL. Equal quantities of protein (100 µg) of lung homogenates or equal volumes of BAL fluid (12.5 µL) were prepared 1X Novex™ Tris-Glycine SDS Sample Buffer and topped up with deionised water where necessary to make a final volume of 25 µL. When BAL is assayed, equal volume loading is commonly used to avoid normalisation of secreted protein (416-418). Samples were loaded into 10% gelatin protein gels for electrophoresis separation under non-reducing conditions. After, gels were washed with renaturing buffer and then incubated overnight in developing buffer to induce digestion of gelatin by any MMP-2 and MMP-9 present in the samples. Gels were then stained with colloidal blue to allow visualisation of denatured areas. To allow comparison between gels, an internal standard – a sample known to contain high levels of MMPs – was loaded on to every gel. This density of this sample was given an arbitrary unit of 1 and the density of all bands were expressed as a value relative to it. All analyses of gels were performed using ImageJ software.

5.4.6 Western blotting

Equal amounts of protein (100 µg) of lung homogenates were loaded on NuPAGE 12% Bis-Tris (Invitrogen) gels, separated by SDS-PAGE, and transferred to nitrocellulose membranes. Membranes were blocked with 5% non-fat milk in Tris-buffered saline with 0.1% Tween-20 (TBS-T) for 1 hour at room temperature with gentle agitation. Membranes were washed three times with TBS-T and incubated with anti-occludin antibody (1:250) or the loading control rabbit anti-β-actin (1:1000) in TBS-T overnight at 4ºC. The following day, membranes were

rinsed in TBS-T three times before incubation with anti-rabbit HRP-conjugated secondary antibody (1:1000) for 1 hour. Membranes were washed three times for 5 minutes each and blots were visualised with Luminol reagent (Santa Cruz Biotechnology). Blots were captured and analysed with GeneSnap/Syngene software. Protein band intensity was expressed as a relative intensity to β-actin.

5.4.7 Statistics

Given that the *in vivo* inhibition studies were very early exploratory studies, we estimated group sizes of approximately 5-7 would be sufficient to achieve 80% power at 0.05 alpha based on our previous power calculations (see section 3.4.5) performed for preliminary experiments looking at CypA levels. Group N numbers may vary between groups due to technical loss, e.g. failure of blood gas sampling, flow cytometry or BAL sampling procedure. No outliers were removed, and no animals died unexpectedly.

5.5 Results

5.5.1 Optimisation of inhibitor administration

In vivo inhibition of CypA with MM-284 has been explored in a number of models. However, as briefly discussed above, there are a number of key differences between these models and ours. Firstly, previous studies have largely been aimed at assessing the effects CypA inhibition in the setting of chronic illness/inflammation. Therefore, the majority of experimental set-ups deliver the drug intraperitoneally or intravenously, administering several doses over the course of an extended period of time. However, our model was aimed at assessing CypA inhibition in the acute setting of VILI. Furthermore, we wanted to design a model that best simulates how this inhibitor might be used in a clinical setting, i.e. where the drug would likely only be administered a shortly before initiation of mechanical ventilation. Lastly, instead of intraperitoneal or intravenous injection, the drug was delivered intratracheally. This ensured that the drug was rapidly available in the lungs and any potential confounding off-target effects that might arise from systemic administration were reduced.

The instillation of fluid into the lungs via the trachea inevitably leads to transient deteriorations in respiratory mechanics, as seen by the immediate increase in peak inspiratory pressure (PIP), elastance (Ers) and resistance (Rrs) in both vehicle and MM-284 treated groups (Figure 5.2). To allow for distribution and/or clearance of the administered drug or vehicle within/from the lungs, animals were maintained at low V_T ventilation during the initial 30-minute equilibration period. This allowed respiratory mechanics to return to close to baseline levels (before any fluid was introduced into the lungs). During this 30-minute period, there were no significant differences in respiratory mechanics (PIP, Ers, and Rrs) between the groups, suggesting that the drug itself had no immediate impact, either positive or negative, on the lungs. This was important as one of the solvents used for high-performance liquid chromatography purification of the drug compound contained trifluoroacetic acid (TFA). Whilst

only a small quantity remained in the final compound, it was a concern that the TFA could have had an immediate problematic effect – however, these data strongly suggest that it did not.

After 30 minutes, high V_T ventilation was commenced. Animals in both groups were ventilated with a standardised starting PIP of 40 cmH_2O which produced effectively identical V_T (vehicle: 32.0 ± 0.9 mL/kg vs. MM-284: 31.8 ± 1.7 mL/kg; N=7-8). The similarities in tidal volumes achieved suggests that distribution of the vehicle and drug within the lungs was very closely matched in both groups.

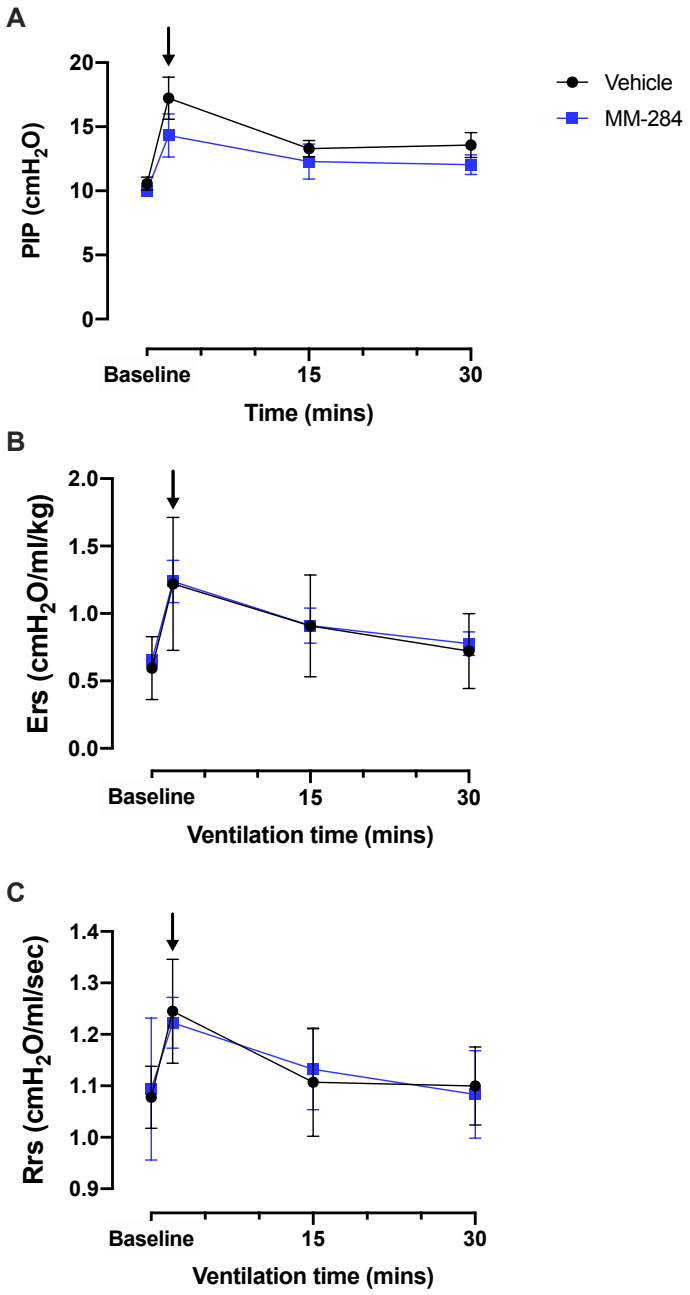


Figure 5.2 - Respiratory mechanics in vehicle and MM-284 treated groups at baseline to 30 minutes post instillation of drug.

(A) Peak inspiratory pressure (PIP), (B) Elastance (Ers), and (C) Resistance (Rrs) both show immediate increase after intratracheal instillation of drug (marked on graphs with an arrow). Data shown as mean ± SD. N=7-8. No significant difference in respiratory mechanics between groups. Interaction (group x time) assessed by two-way ANOVA with Sidak's multiple comparisons test.

5.5.2 Treatment with MM-284 prior to high V_T ventilation attenuates VILI

Animals were ventilated with high V_T for 180 minutes or until mortality surrogates (blood pressure <50 mmHg or PIP increased >20%) were reached. Animals in the MM-284-treated groups were protected from the development of VILI, with a remarkable 100% survival in this group compared with 50% in the vehicle-treated group (Figure 5.3A).

Arterial blood pressure was well maintained (>75 mmHg) in both groups up to 120 minutes (Figure 5.3B). After which, it began to fall substantially in a number of animals in the vehicle group. In 50% of the vehicle group, animals reached the 50 mmHg cut off point for haemodynamic stability, from as early as 150 minutes. In contrast, all animals in the MM-284 group maintained blood pressures >50 mmHg for the entirety of the 180 minute ventilation protocol.

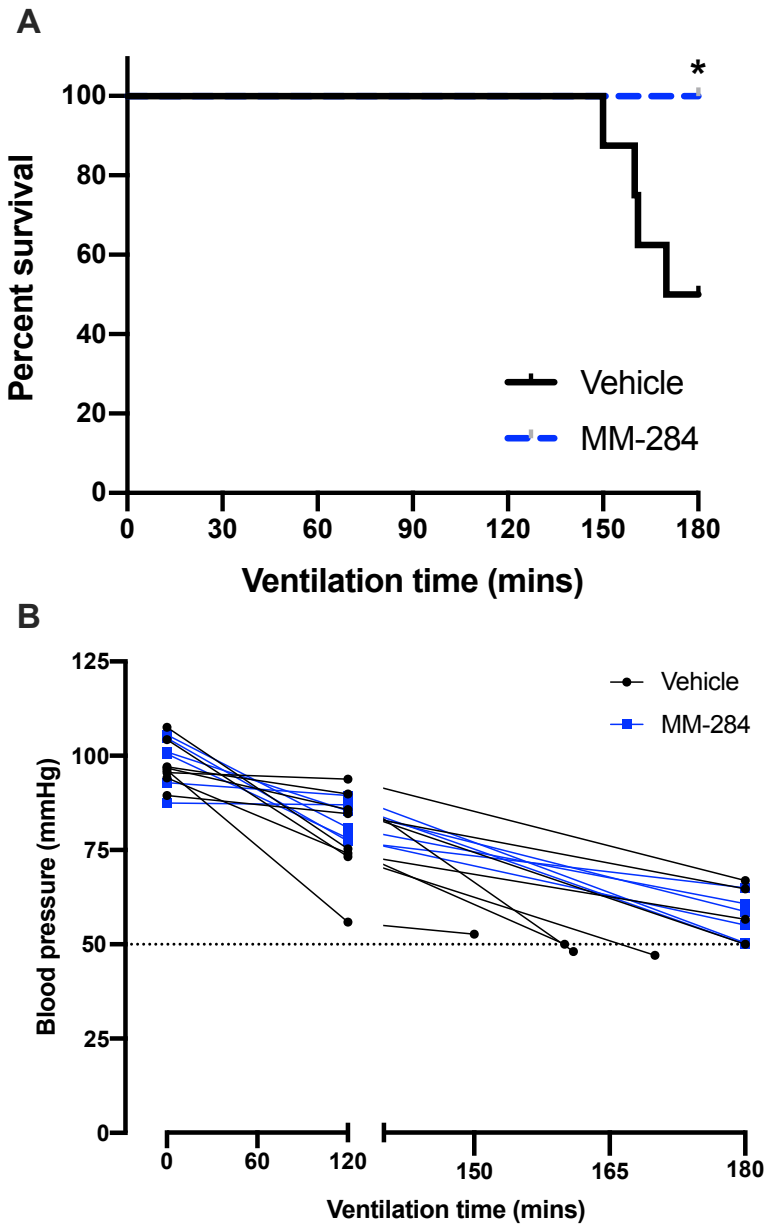


Figure 5.3 – (A) Kaplan-Meier survival curve and (B) blood pressures of animals in both vehicle and MM-284 treated groups over the course of 3 hours of high V_T ventilation.

*(A) Kaplan-Meier survival curve showing 100% survival in the MM-284-treated group compared with 50% survival in the vehicle-treated group. Survival in these experiments was based on the blood pressure (<50 mmHg) or lung injury proxy marker (>20% increase in PIP from start). (B) Blood pressures of animals in both groups showing 50% of the animals in vehicle group meeting the 50 mmHg mortality surrogate cut-off point (displayed as dotted line) before the 180-minute time point. N=7-8. *p<0.05. Significance determined by log-rank test.*

5.5.3 Improved physiological markers of injury following MM-284

Respiratory mechanics

This attenuation of injury was reflected in the respiratory mechanics (Figure 5.4A-C). In both groups, there was an initial small decrease in PIP corresponding to lung recruitment during high V_T ventilation, after which PIP then remained stable for approximately 120 minutes, as would be expected in this VILI model (Figure 5.4A); It is usually only after the 120-minute time point that any derangement of respiratory mechanics tends to become apparent. Indeed, from 120 minutes onwards, the trajectories of the groups began to diverge, with PIP in the vehicle-treated group showing an upward pattern as ventilation time increased. In contrast, PIP in the MM-284-treated group remained stable for the duration of the entire experiment, reaching a significantly lower final PIP (vehicle: 46.3 ± 3.7 cmH_2O vs. MM-284: 37.9 ± 1.2 cmH_2O), which was 6% below that of baseline values (Figure 5.4A). Respiratory system elastance followed a similar pattern, also displaying a statistically significant difference in the response to ventilation following the MM-284 treatment (Figure 5.4B). At the start of the protocol, elastance of both groups were virtually identical, but over the course of the 3-hour protocol, only the vehicle group showed increases in elastance from 120 minutes onwards, suggestive of signs of ongoing injury. Similarly, respiratory system resistance displayed initial decreases in both groups, however, while resistance remained low for the MM-284 group, there was a gradual increase in vehicle group (Figure 5.4C).

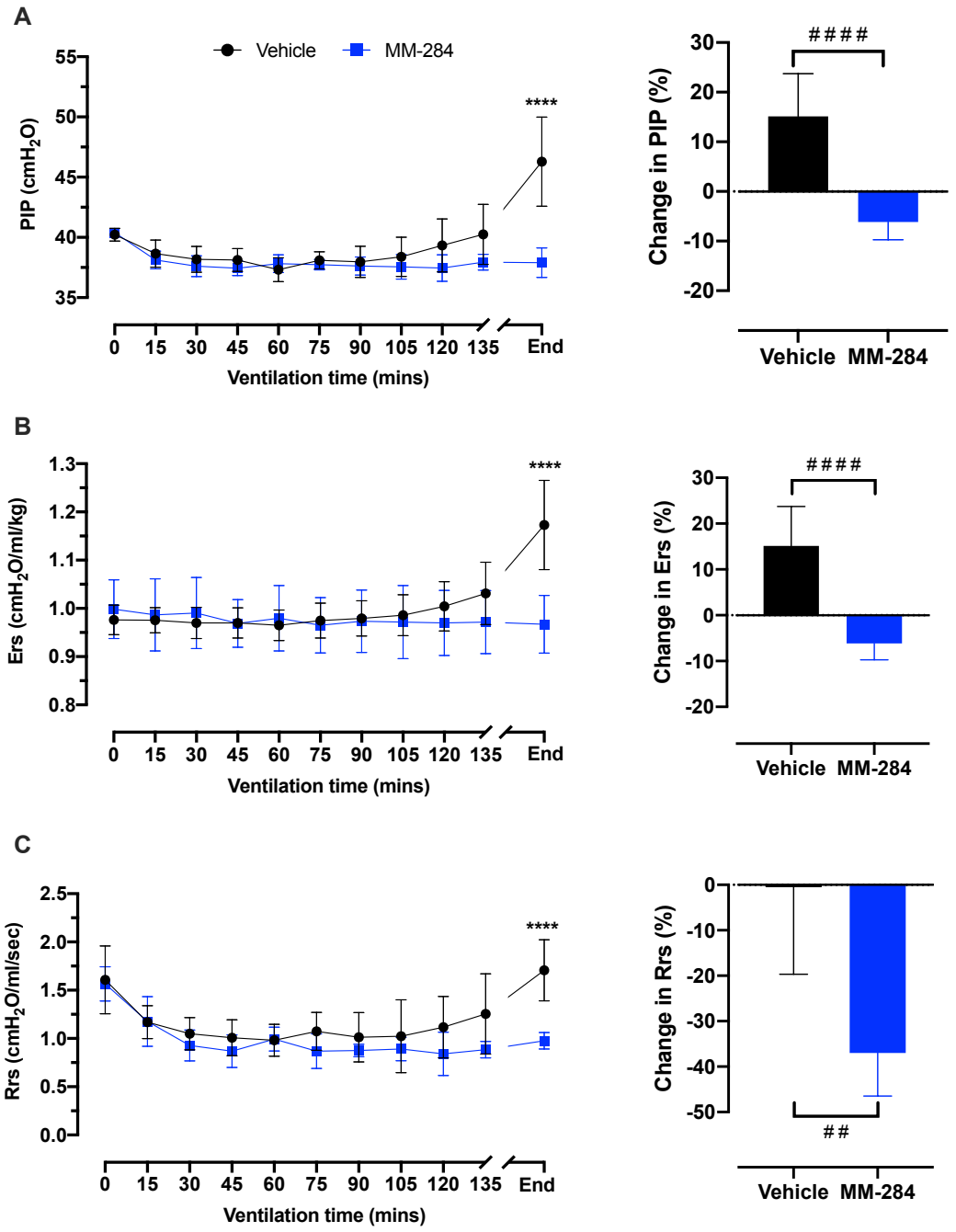


Figure 5.4 - Time course of respiratory mechanics over the course of 3 hours of high V_T ventilation in both treatment groups.

*(A) Peak inspiratory pressure (PIP), (B) Elastance (Ers), and (C) Resistance (Rrs) over ≥ 3 hours of high V_T ventilation in vehicle and MM-284 treatment group during VILI. Data shown as mean ± SD. N=7-8. ****p<0.0001. Interaction (time x group) was assessed by two-way*

ANOVA with Sidak's multiple comparisons test for time course data. $^{\#\#}$ *p<0.01,* $^{\#\#\#\#}$ *p<0.0001. Unpaired t-test performed for % change in respiratory mechanics.*

Arterial blood gas analysis

Arterial blood gas sampling was performed at three time points: 15 minutes after the initiation of high V_T ventilation, 120 minutes, and at the end of protocol (180 minutes or when surrogate mortality markers were reached). Arterial oxygenation was preserved in both groups up to 120 minutes of high V_T ventilation (Figure 5.5). After this point, there was a sharp decrease in oxygenation in the vehicle group reaching PaO_2/FiO_2 ratios that would have constituted moderate to severe clinical ARDS (i.e. <200) in 50% of the group. In contrast, arterial oxygenation was preserved in the MM-284-treated group, showing minimal decreases from baseline measurements and none reaching mild ARDS (i.e. all PaO_2/FiO_2 ratio >300). Arterial carbon dioxide was not significant different between groups.

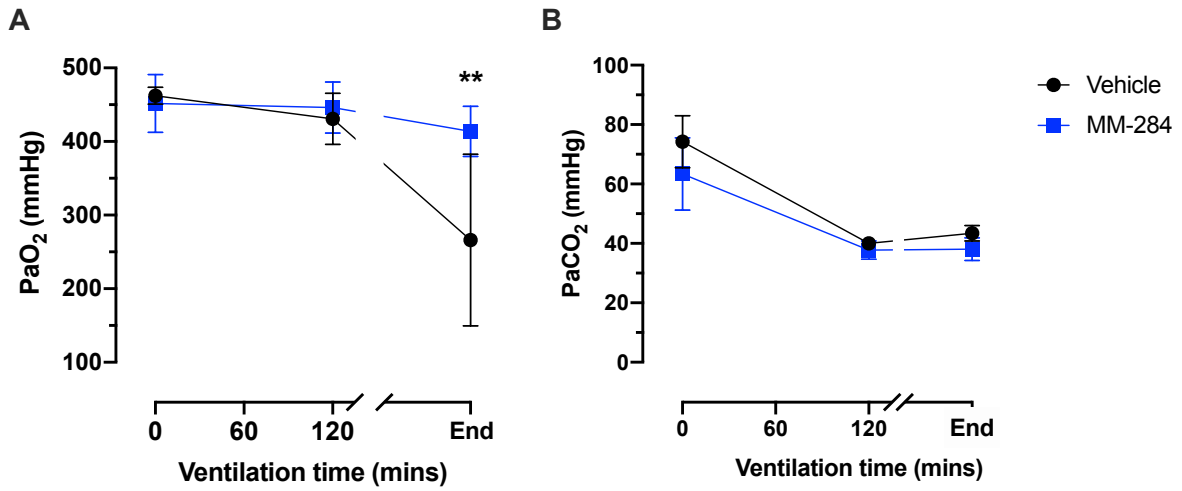


Figure 5.5 - Time course of (A) arterial oxygenation (PaO_2) and (B) arterial carbon dioxide ($PaCO_2$) during 3 hours of high V_T ventilation in both treatment groups.

*(A) MM-284 treatment significantly attenuated deterioration of arterial oxygenation during VILI. (B) No significant difference in arterial carbon dioxide. Data shown as mean ± SD. N=6-8. **p<0.01. Two-way ANOVA with Sidak's multiple comparisons test.*

Pulmonary oedema & alveolar-capillary membrane permeability

To evaluate the extent of pulmonary oedema and alveolar-capillary barrier permeability, lung wet:dry weight ratios and BAL protein content were determined in both groups. The wet-dry weight ratio of the lungs from the vehicle treated group was significantly higher than that of the MM-284 treated lungs, suggesting the development of pulmonary oedema (Figure 5.6A). In the MM-284 treated group, wet:dry weight ratios remained at a value that would be expected in an unventilated, untreated mouse (~4.5). BAL protein was also found to be significantly higher in the vehicle treated group compared with the MM-284 group, suggesting that MM-284 treatment was protective against development of alveolar-capillary membrane permeability during VILI. (Figure 5.6B).

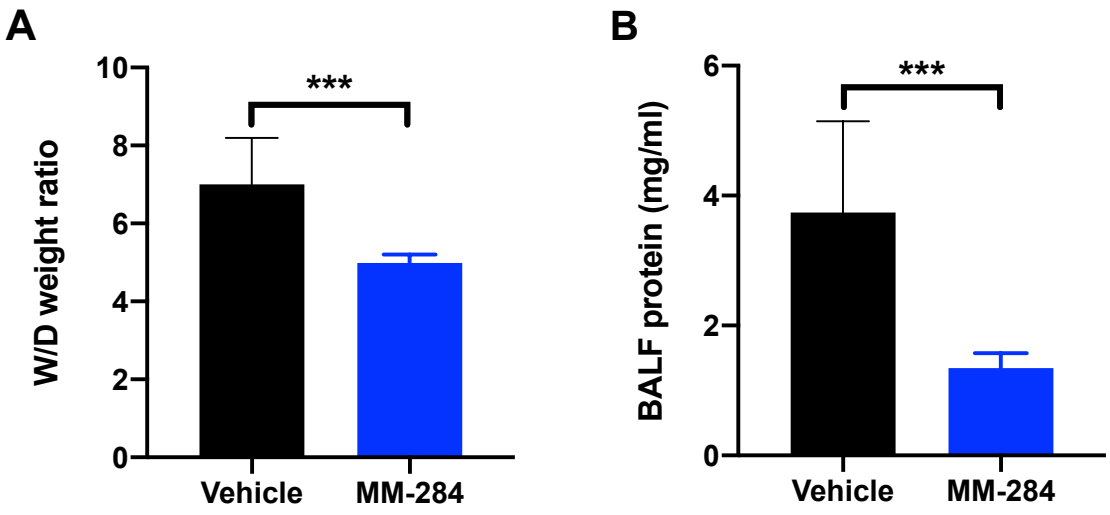


Figure 5.6 - Assessment of alveolar-capillary membrane permeability in both vehicle and MM-284 treated groups at the end of 3 hours of high V_T ventilation.

*(A) Wet:dry (W/D) weight ratio and (B) BAL fluid protein concentration in MM-284 treated group was significantly lower than in vehicle group. Data shown as mean ± SD. N=7. ***p<0.001. Unpaired t-test.*

5.5.4 Mechanistic investigation of cyclophilin A inhibition

Following observations of an attenuation of VILI in the MM-284 treated group, we explored a number of possible mechanisms/factors that could explain the protection conferred by the CypA inhibitor, MM-284.

Inflammatory cytokines/chemokines

Given that CypA is known for its chemotactic effects on leukocytes, soluble levels of inflammatory cytokines/chemokines in BAL fluid were evaluated first (Figure 5.7). Only levels of KC/CXCL-1, a neutrophil chemotactic agent, was significantly lower in the MM-284 treated group. Levels of IL-6 and IL-1β were not significantly different between the two groups.

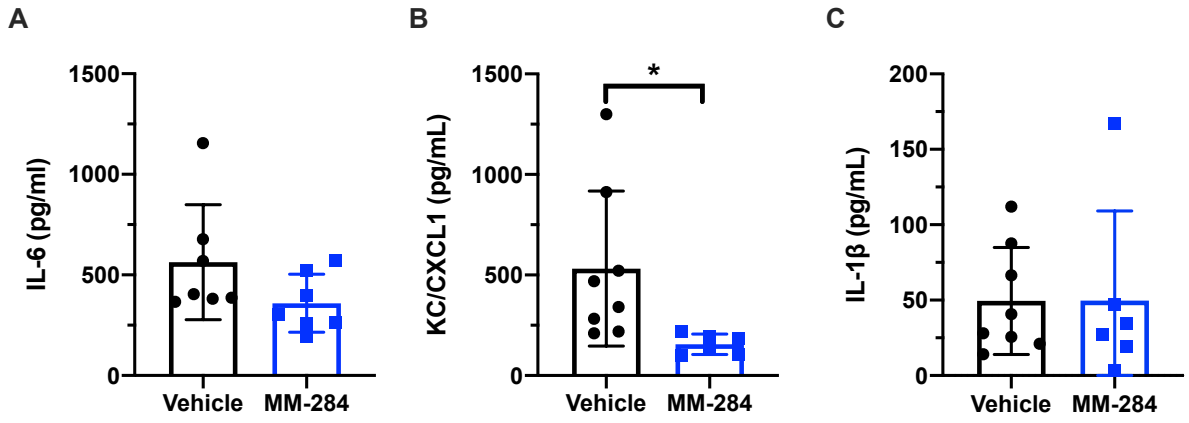


Figure 5.7 – BAL cytokines/chemokines in vehicle- and MM-284-treated groups following 3 hours of high V_T ventilation.

*No change in levels of (A) IL-6 and (C) IL-1β; Decreased levels of (B) KC / CXCL-1 in the MM-284 group compared with vehicle group. Data shown as mean ± SD. *p<0.05. Unpaired t-test.*

Leukocyte recruitment

Leukocyte infiltration into the lung tissue and BAL was also assessed by flow cytometry. Given the attenuation of KC/CXCL-1 release in the MM-284 treated group, we had expected neutrophils counts to also be decreased, which might account in part for the protective effects observed. Surprisingly, our data showed that MM-284 treatment had minimal impact on influx of neutrophils and Ly6C^{high} 'inflammatory' monocytes in the lung tissue and presence in BAL fluid (Figure 5.8A, B). Numbers of alveolar macrophages and Ly6C^{low} 'classical' monocytes also remained unchanged between treatment groups.

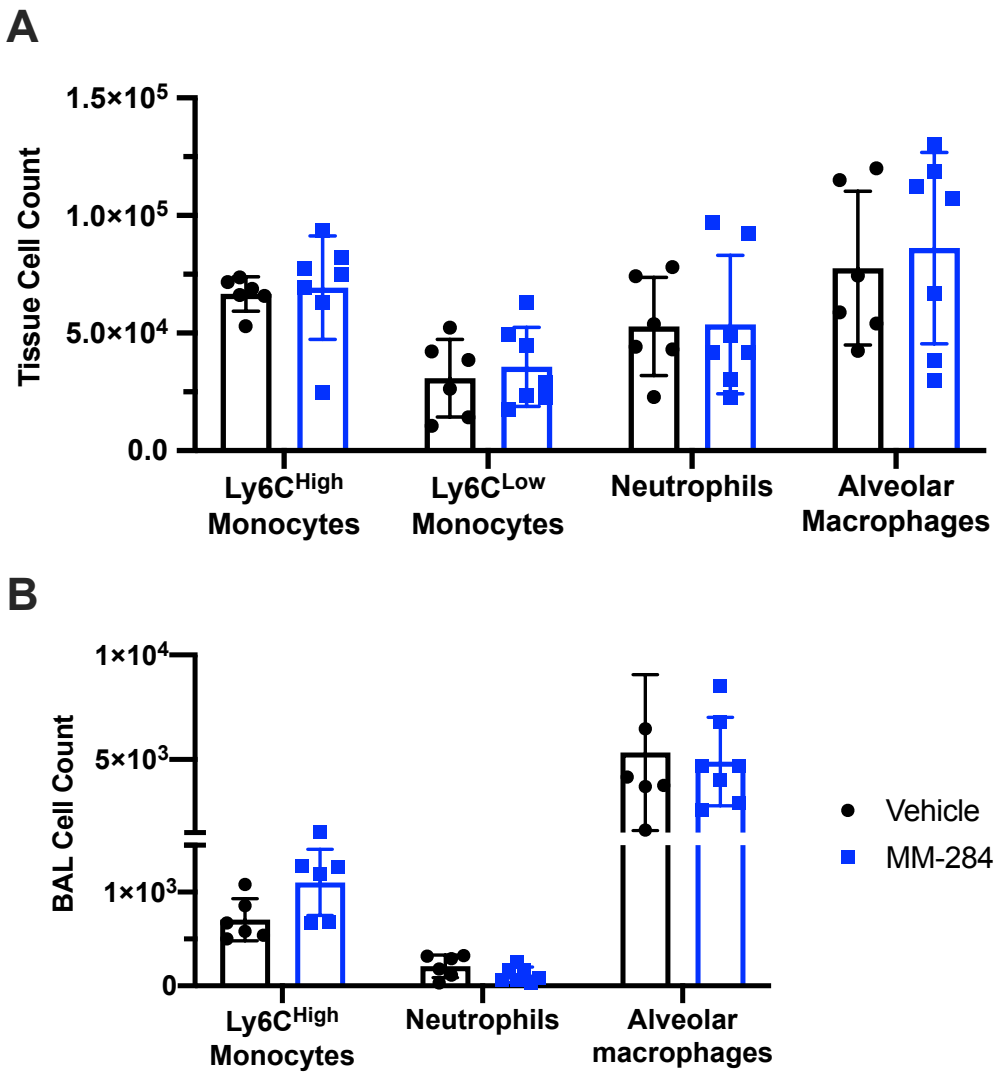


Figure 5.8 - Protective effect of MM-284 treatment appears to be independent to lung leukocyte recruitment during VILI.

(A) Tissue cell count and (B) BAL cell count (total number) show no significant differences between vehicle and MM-284 treated groups. Data displayed as scatter dot plot showing mean ± SD. Not significant. Two-way ANOVA with Sidak's multiple comparisons test.

Pulmonary cell activation

To assess the degree of pulmonary cell activation, surface expression on ICAM-1 on the local pulmonary cells – alveolar epithelial cells (AECs), resident alveolar macrophages, and endothelial cells (ECs) – were measured (Figure 5.9A-C). MM-284 treatment led to significant downregulation of ICAM-1 expression on AECs and alveolar macrophages but not ECs.

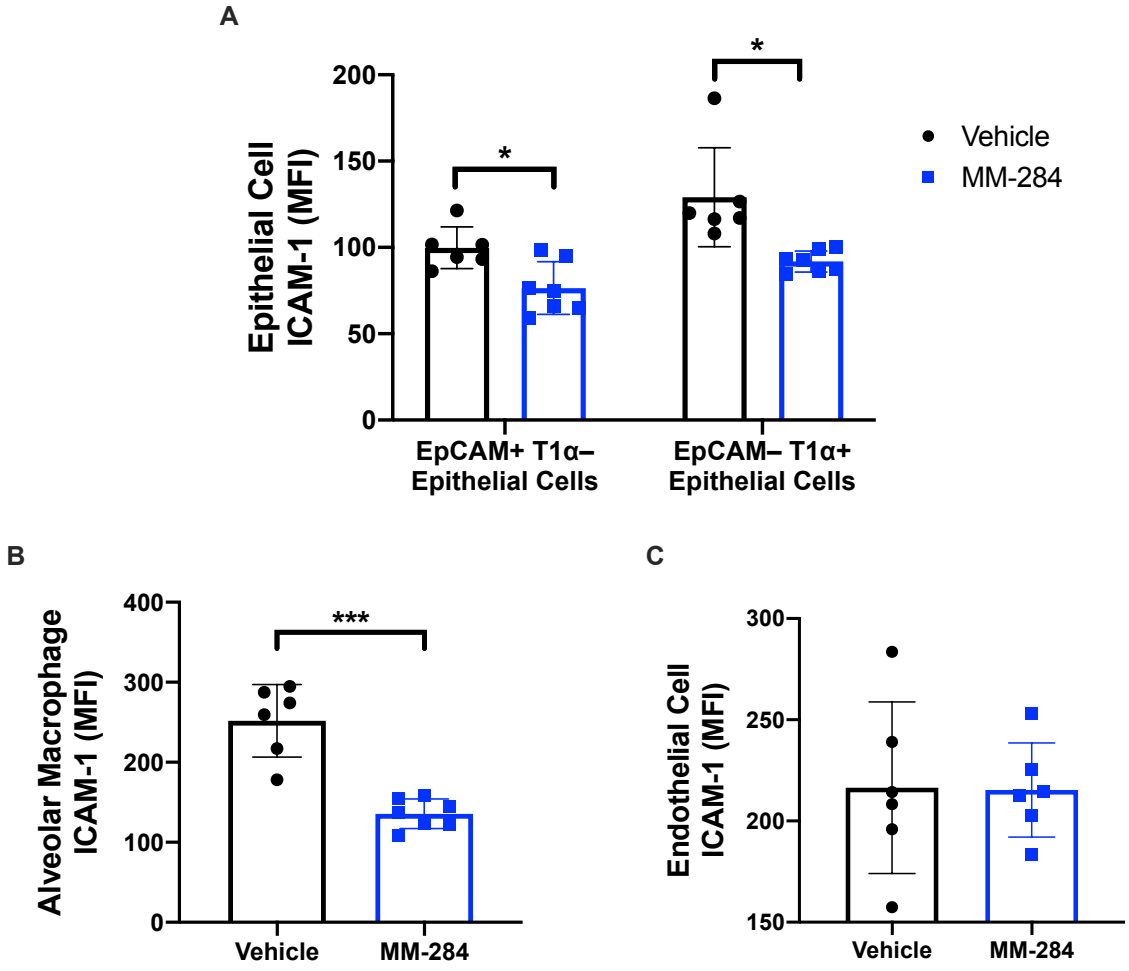


Figure 5.9 - Assessment of pulmonary cell activation during VILI *in vivo* using surface expression of activation marker, ICAM-1, on (A) AECs, (B) alveolar macrophages, and (C) endothelial cells (ECs).

*ICAM-1 expression was significantly lower on epithelial cells and alveolar macrophages but not endothelial cells. Data shown as mean ± SD. N=6-7. *p<0.05, ***p<0.001. Multiple t-test with multiple comparison correction using the Holm-Sidak method.*

Epithelial injury

In chapter 3, our findings suggested that CypA release was closely related to epithelial injury. Therefore, we measured BAL levels of sRAGE, an established epithelial injury marker, and found that it was significantly decreased in the MM-284 treated group.

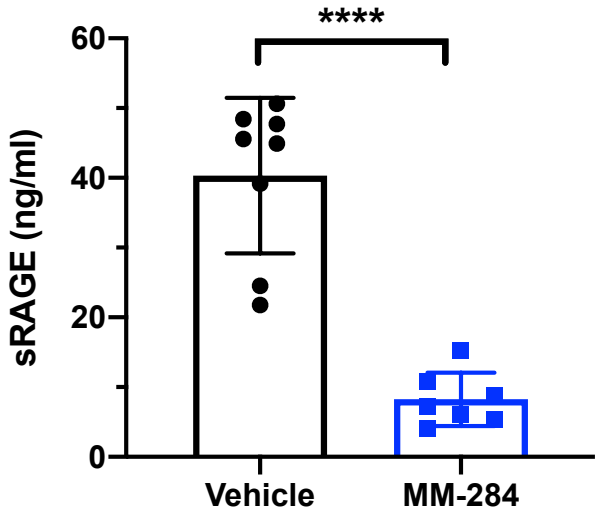


Figure 5.10 – BAL sRAGE levels was significantly decreased in the MM-284 treatment during *in vivo* VILI.

*BAL levels of sRAGE was significantly decreased in the MM-284 treated group (vehicle: 8.3 ± 3.8 ng/mL vs MM-284: 40.3 ± 11.2 ng/mL). Data shown as mean ± SD. N= 6-7. ****p<0.001. Unpaired t-test.*

Matrix metalloproteinase

CD147, the main receptor for CypA, has been well established as an upstream regulator of MMP activation, secretion, and activity (170). In chapter 3, upregulation of CD147 in response to high V_T ventilation was demonstrated. To investigate the effects of CypA inhibition on MMP activity, which might be mediated through CD147, we measured the activity of latent and active forms of MMP-2 and MMP-9 in lung homogenate and BAL by gelatin zymography.

In lung homogenate, no differences were observed in the activity of either MMP between control and MM-284 group (Figure 5.11). In BAL fluid, there was a trend towards an increase in gelatinolytic bands of activity at 72 kDa (pro MMP-2) and significantly higher levels of 62 kDa (active MMP-2) in the vehicle group compared with the MM-284 group (Figure 5.12, Figure 5.13). No differences in bands at 92 kDa (pro MMP-9) or 82 kDa (active MMP-9) were detected between the groups. However, of note, the only instances where bands corresponding to either form of MMP-9 was detected was in the vehicle group.

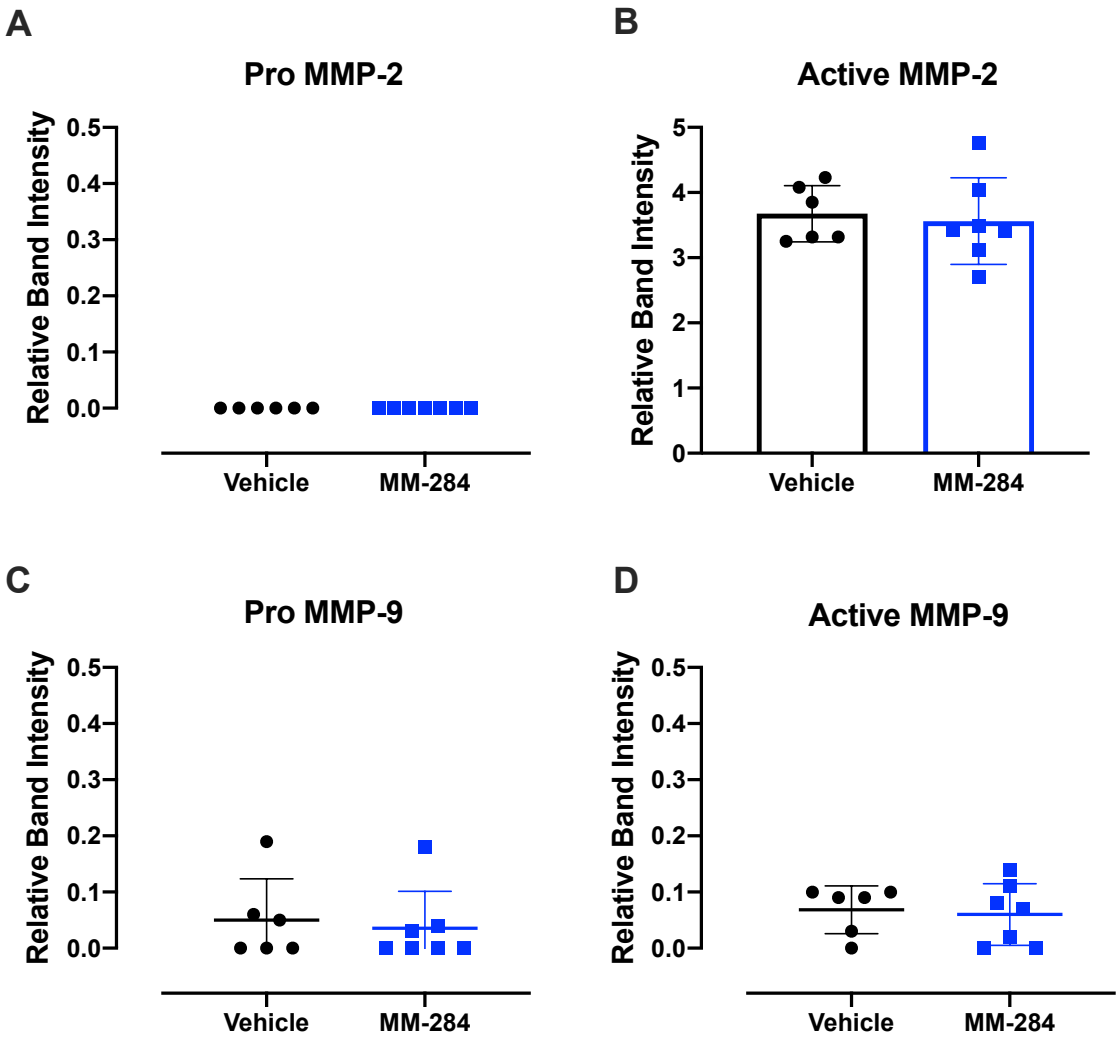


Figure 5.11 - Assessment of matrix metalloproteinases in lung homogenates from both vehicle and MM-284 treated groups following *in vivo* VILI using gelatin zymography.

(A) No pro MMP-2 was detected in either group. (B) Active MMP-2 was present but no differences were observed between vehicle and MM-284 group. Both (C) pro-MMP-9 and (D) active MMP-9 were also not significantly different between groups. All results are expressed as a value relative to the internal standard (which was given an arbitrary unit of 1). Data shown as mean ± SD. NS. Unpaired t-test.

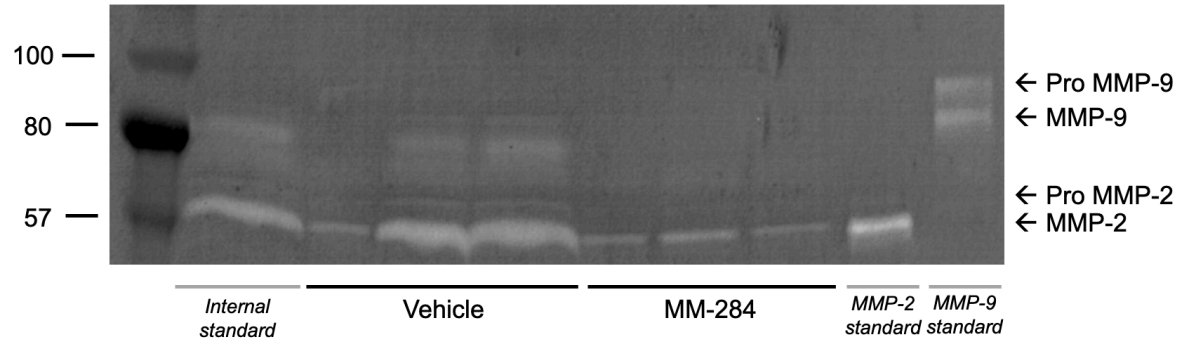


Figure 5.12 – Representative gelatin zymography gel for MMP-2 and MMP-9 activity in the BAL of vehicle and MM-284 treated animals following *in vivo* VILI.

MMP activity was visualised as clear bands against a dark stained background. On each gel, molecular weight markers and MMP-2 and -9 standards were used to identity the pro and active forms of MMPs. To enable comparisons between gel, an internal standard (a sample containing relatively high amounts of MMPs) was loaded on to every gel and used to compare relative densities in other bands.

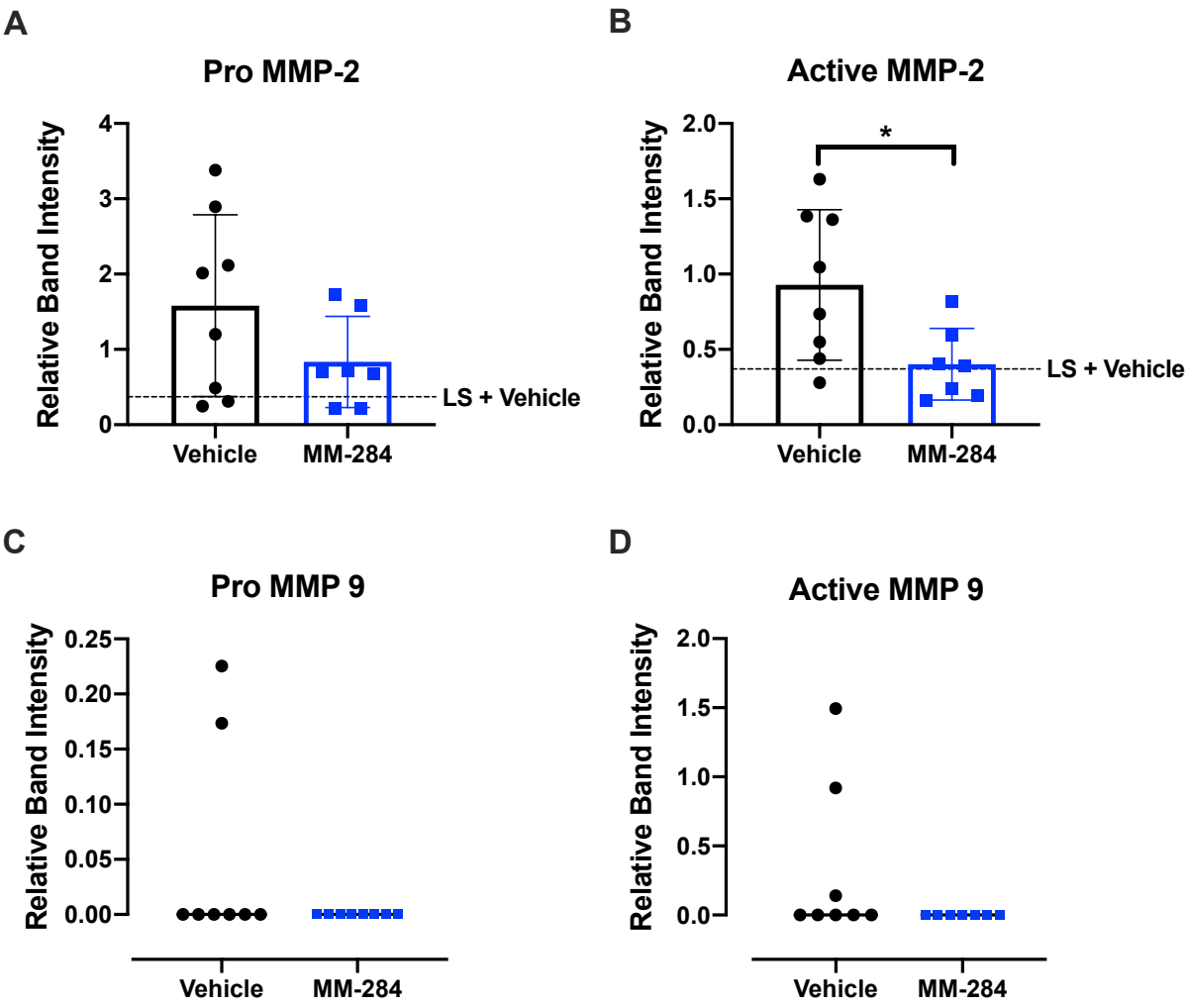


Figure 5.13 - Assessment of matrix metalloproteinases in BAL fluid from both groups following 3 hours of high V_T ventilation using gelatin zymography.

*(A) Pro MMP-2 showed a trend (p=0.12) towards lower levels in MM-284 treated group. (B) Active MMP-2 was significantly lower in MM-284 group. Dotted lines in these graphs represent levels of MMPs measured in mice that were ventilated with the vehicle at low V_T (8 mL/kg, 3 hours). (C) Pro MMP-9 and (D) active MMP-9 were not significantly different between groups. All results are expressed as a value relative to the internal standard (which was given an arbitrary unit of 1). Data shown as mean ± SD (A and B) or scatter dot plot with line representing median (C and D). *p<0.5. Unpaired t-test.*

Tight junctions (occludin)

To investigate if increased MMP-2 activity had an effect on tight junction proteins, protein levels of occludin in whole lung homogenates were assessed using western blots (Figure 5.14). Two different molecular weights of occludin were detected – ~65 kDa and ~58 kDa. The band at ~65 kDa corresponds to the published molecular weight of occludin. An additional band at ~58 kDa was also detected and likely represents the cleaved form of occludin. No differences were found in occludin expression between the MM-284 and control group.

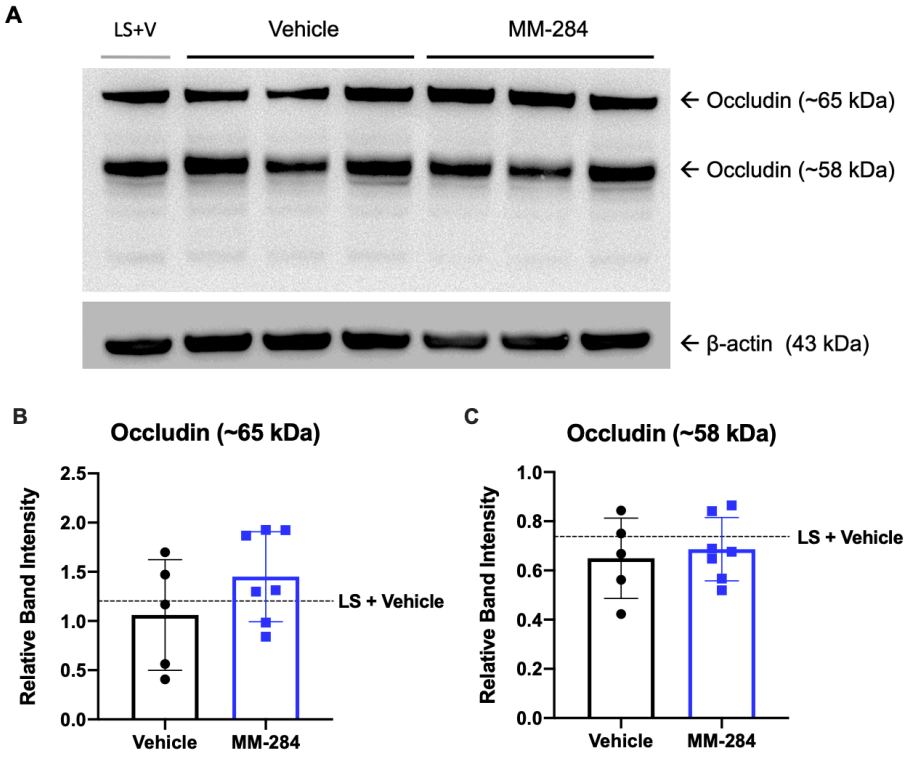


Figure 5.14 – No differences in lung occludin expression was observed in MM-284 treated mice compared with vehicle treated controls following 3 hours of high V_T ventilation.

(A) Representative western blot of occludin in lung homogenates of mice ventilated at high V_T. Occludin was detected at two molecular weights – 65 kDa and 58 kDa. (B) Densitometry analysis of occludin expression revealed no differences between MM-284 and control group.

Dotted line represents occludin expression in a sample that was treated with the vehicle control and ventilated at low V_T. Data shown as mean ± SD. N=5-7. NS. Unpaired t-test.

5.6 Discussion

In Chapter 3, we demonstrated the early significant increase in CypA in the alveolar space during VILI. By inhibiting extracellular CypA during high V_T ventilation, we sought to expand on our previous findings and investigate its role in the pathogenesis of VILI – is it a mediator or a consequence of injury?

The results from this chapter demonstrated, for the first time, that treatment with an extracellular CypA inhibitor (MM-284) prior to initiation of injurious mechanical ventilation attenuates VILI. All animals in the MM-284 treated group survived the full 180-minute protocol in contrast to 50% in the vehicle treated group, with all the survivors in the vehicle group displaying substantial signs of injury. Mice that received MM-284 also had improved physiological parameters, displaying lower PIP, minimal deteriorations in respiratory mechanics, preserved arterial oxygenation, less pulmonary oedema, and decreased alveolar-capillary membrane permeability. Together, these results indicate that CypA plays an important mediator role in the development of VILI. Although we did not definitively confirm that the reduction in injury observed following MM-284 treatment was due to CypA antagonism, we believe it is likely. Previous studies have shown that MM-284 specifically inhibits the peptidyl-prolyl *cis-trans* isomerase activity of extracellular CypA (406, 407).

To explore potential mechanisms underlying these protective effects, we first evaluated leukocyte recruitment into lung tissue and cellularity in BAL. Most studies investigating the role of CypA in inflammatory diseases have focused on its potent chemotactic abilities and its role in recruiting effector cells into the tissue of interest (409, 419, 420). In the only study involving CypA in acute lung injury, Arora et al reported that *in vivo* blockade of CypA (using a non-immunosuppressive CsA analogue SDZNIM811) significantly reduces extravasation and accumulation of neutrophils in lungs in response to LPS-induced lung inflammation (291).

Surprisingly, despite attenuation of KC/CXCL-1, a neutrophil chemoattractant, levels following MM-284 treatment, we found no differences in leukocyte counts (neutrophils and monocytes) in either lung tissue or BAL between vehicle and MM-284 treated mice. This suggests that in our model, protection conferred by CypA inhibition is leukocyte independent, at least during the early phases of injury. The discrepancy between our findings and those reported by Arora et al is most likely due to the different time points studied – 3 hours post-VILI in our study vs 18 hours post-LPS in theirs (291). Further, LPS-induced lung injury is a very 'neutrophil-driven' injury, whereas VILI involves other factors. During VILI, it is believed that one of the important drivers of neutrophil recruitment is the generation of a chemotactic gradient (89). This is dependent on the release of inflammatory mediators and chemokines (e.g. CXCL1/KC, CXCL2/MIP-2, CXCL8/IL-8) following activation and injury to local pulmonary cells, such as AECs, pulmonary endothelium and AMs (89). It is likely that 3 hours, a relatively early time point, might be too early for any significant chemokine-driven neutrophil recruitment. However, this does not exclude the involvement of extracellular CypA in the recruitment of neutrophils and/or monocytes as lung injury progresses. It also remains possible that despite no changes in leukocyte numbers, leukocyte functionality might have been altered (e.g. decreased reactive oxygen species (ROS) production, release of neutrophil extracellular traps or elastases). CypA has been shown to substantially increase oxidised low density lipoprotein (LDL)-induced cytosolic ROS production from monocyte differentiated macrophages (421). However, this was not investigated.

Interestingly, CXCL-1/KC has also been implicated in inducing lung permeability independently of neutrophils. *In vitro* stimulation of isolated pulmonary endothelial cells with recombinant CXCL-1 has been shown to induce cytoskeletal rearrangement in a manner that enhances vascular permeability (422). After 5 minutes of incubation, endothelial cells displayed a significant increase in F-actin-positive stress fibres, especially at intercellular borders. After 120 minutes, cells were observed to have a polygonal, retracted morphology,

resulting in a marked increase in inter-endothelial gaps. Therefore, it is possible that in our VILI model, CXCL-1 was involved in the promotion of increased barrier permeability. Consistent with the possible role of CXCL-1 in mediating lung permeability, we observed a decrease in permeability (decreased BAL protein concentration and W/D weight ratio) in the MM-284 treated group compared with vehicle controls where CXCL-1 levels were lower.

Since the protection conferred by treatment with the extracellular CypA inhibitor MM-284 in our model of VILI appeared to be neutrophil-independent, it suggests that CypA had an intra-alveolar role rather than a direct chemotactic role. Therefore, we explored whether protection could be explained by decreased activation of local pulmonary cells, such as AECs, alveolar macrophage, and pulmonary endothelium. We previously demonstrated that all three cell types express the primary CypA receptor, CD147, which was shown to be upregulated following high stretch ventilation. To evaluate the activation status of these cells, surface expression of ICAM-1 was evaluated. ICAM-1 has been frequently studied in the context of lung injury and there is evidence to suggest that it is involved specifically in VILI. *In vitro,* application of cyclic stretch to endothelial cells has been shown to induce ICAM-1 expression compared with cells under static conditions (423). Mechanical strain has also been shown to cause upregulation of ICAM-1 protein and mRNA levels in alveolar epithelial cells (A549 cells) in a manner that is both frequency and duration dependent (384). *In vivo*, Imanaka et al observed rapid upregulation of surface adhesion markers CD11b and ICAM-1 on alveolar macrophages of rats ventilated for just 40 minutes at high pressures (45 cmH_2O) compared with low pressures (7 cmH_2O) (424). Bertok et al showed that blockade of intra-alveolar p55 TNF receptor led to substantial attenuation of VILI and was associated with significantly decreased expression of ICAM-1 on alveolar macrophages (425).

Following CypA inhibition, we observed significant downregulation of cell surface activation marker, ICAM-1, on both alveolar-facing pulmonary cells – AECs and Alveolar macrophage –

but not on ECs in the MM-284 group compared with the vehicle group. This is consistent with the idea that even though CD147 is also expressed on endothelial cells, CypA appears to be working solely in the alveolar space rather than leaking out into the vasculature. This suggest that CypA plays a role in the activation of AECs and alveolar macrophages.

In chapter 4, we demonstrated that following *in vivo* high V_T ventilation and *in vitro* cyclic stretch, CypA is released primarily by AECs. Therefore, we hypothesised that AEC-derived CypA is most likely to have a direct effect on alveolar macrophages and events downstream of macrophage activation. This directionality of signalling (i.e. from AECs to alveolar macrophages) have been suggested by others. An *in vivo* study conducted by Woods et al demonstrated that in response to injurious ventilation, AECs displayed signs of activation before alveolar macrophages (426). They postulated that parenchymal cells are likely to be the cells within the lungs that initiate the inflammatory response to stretch, which is then communicated to other cells, such as alveolar macrophages. These cells then become activated and are then able to propagate downstream signalling.

Many studies have confirmed that alveolar macrophages play a crucial role in the development of VILI. It is assumed that as the resident immune cell of the lung, alveolar macrophages are the main source of pro-inflammatory mediators. Indeed, in a study conducted by Frank et al, depletion of alveolar macrophages from lungs of rats before ventilation at high V_T led to significantly lower plasma levels of the CXCL-1 compared with ventilated controls that had not undergone macrophage depletion (427). The decrease in CXCL-1 is particularly interesting as it suggests that alveolar macrophages are the major source of this neutrophil chemokine, which is in keeping of our observation of significantly decreased CXCL-1 following a dampening of macrophage activation.

As well as being a source of inflammatory cytokines, alveolar macrophages also contribute to the development of alveolar epithelial permeability and pulmonary oedema. In studies where alveolar macrophages are depleted prior to high tidal volume ventilation, animals have been observed to develop significantly less lung injury, in particular, reduced pulmonary oedema and decrease alveolar epithelial and lung endothelial permeability (427, 428). One of the ways that alveolar macrophages could contribute to alveolar barrier dysfunction and subsequently pulmonary oedema during VILI is through stimulating the production and secretion of MMPs. MMPs have been associated with the degradation and remodelling of components of the extracellular matrix (ECM) (429, 430). Dysregulation of their activity in ARDS and VILI has been linked to damage of the alveolar-capillary barrier through degradation of protein components including intercellular junction proteins, the alveolar basement membrane, and proteins involved in anchoring cells to the basement membrane (429-432). In particular, MMP-2 and -9, which are capable of metabolising a wide variety of ECM proteins including: gelatin, type I, IV, and V collagen, and elastin, has been implicated in ALI in several animal and human studies (168, 429, 433-437). Increase in these MMPs are often associated with an increase in features of lung injury including increased W/D weight ratios, deteriorating in arterial oxygenation, and an increase in BAL cellularity (435). Alveolar macrophages have frequently been identified as the main source of MMP-2 while MMP-9 is known to also be produced by neutrophils (438-442).

Since alveolar macrophages are known to secrete MMPs and CD147, the main receptor for CypA, is known to play a crucial role in MMP activity (170), we hypothesised that one of the downstream effects of CypA stimulation of alveolar macrophages is likely to be related to MMPs. Therefore, we assessed levels of MMP activity in lung homogenates and BAL fluid from mice in both vehicle- and MM-284-treated groups. In lung homogenate, no differences were observed in the activity of either MMP-2 or -9 between control and MM-284 group. In BAL fluid, however, pro-MMP-2 showed a trend towards lower levels in the MM-284 treated

group and active MMP-2 was significantly lower. Levels of pro and active MMP-9 were not significantly different.

The lack of MMP-9 in our model might be explained by the kinetics of MMP release noted by a number of studies, where MMP-2 often peaks before MMP-9 (433, 435). We found no significant differences in both the pro and active form of MMP-9 between the groups but did find instances of increased levels of MMP-9 only in the vehicle treated group. It is plausible that, had the injury been allowed to proceed beyond the 3-hour protocol, we would have observed increased MMP-9 too. Although we did not localised the source of MMP secretion, other studies have reported localisation of MMP-2 to alveolar macrophages and MMP-9 to neutrophils (435, 436). Therefore, the lack of neutrophil infiltration, as discussed above, might also account for the MMP-2 dominant profile we saw.

We then proceeded to investigate potential downstream consequences of increased MMP levels. A number of studies have linked CypA-mediated MMP activation to the disruption of tight junction proteins. In one study investigating the mechanisms that drive blood-brain-barrier (BBB) dysfunction, CypA was implicated as a component of a human apolipoprotein E isoform 4 (APOE4)-activated CypA-NFκB-MMP-9 pathway in pericytes (443). Activation of this pathway led to BBB breakdown and a corresponding decrease in several proteins that are crucial for normal BBB integrity, including collagen IV and tight junction proteins ZO-1, occludin, and claudin 5. (443). In a related study, Main et al demonstrated that treatment of mice with CypA antagonist CsA attenuated the MMP-9 response and enhanced BBB repair after traumatic brain injury by stabilising the expression of tight junction proteins (zonula occludens-1, occludin, and claudin-5) (444). During VILI, disruption of tight junction proteins has been shown to lead to increased alveolar-capillary barrier permeability. Cavanaugh et al demonstrated that subjecting primary rat alveolar epithelial cells to *in vitro* cyclic biaxial stretch (37% change in surface area) for 1 hour resulted in significant decreases in the

immunofluorescent staining intensity of peripheral occludin, total cellular occludin content, and the degree of cell-cell attachment (445). Gu et al reported that exposing MLE-12 cells to 20% cyclic stretch for 4 hours induced degradation of E-cadherin, p120 and occludin, reducing protein levels by up to 60% (446). Using immunofluorescence, they performed quantitative analyses of the co-localization of junction proteins and stretch-induced gap formation and found that the total gap area after 4 hours of cyclic stretches was increased significantly compared with static controls (446).

Therefore, we investigated the expression of the epithelial tight junction protein occludin, which is also known to be a substrate of MMP-2 (447). However, no differences in occludin protein levels in total lung homogenate between the groups were found. It is possible that CypA inhibition could have had an effect on the distribution of occludin away from its peri-junctional location (e.g. by internalisation of the protein) such that its ability to bind cells was compromised. However, we could not investigate this with our samples as they were homogenised. Additionally, occludin is only one of the many adherens and tight junction proteins that contribute to the integrity of the alveolar epithelial barrier. Other proteins including ZO-1, p120, and claudins, have been shown to be affected during cyclic stretch and may have been implicated in our model. However, we did not perform any further western blots to assess protein levels of these other proteins as we thought investigation in an *in vitro* setting where both expression and distribution of these proteins could be assessed would have provided more conclusive results.

Although we think it is more likely that AEC-derived CypA would primarily affect alveolar macrophages, we cannot rule out that CypA may also have a direct effect on AECs. As discussed above, we also observed signs of decreased AEC activation following CypA inhibition. AEC surface expression of ICAM-1 was downregulated in the MM-284 group compared with the vehicle group. BAL fluid levels of the epithelial injury marker, sRAGE, was

also significantly lower levels in the MM-284 group. However, in an *in vivo* setting, it was impossible to determine if this decrease in AEC activation was due to blocking the direct effect of CypA on AECs or if it was a secondary consequence of decreased macrophage activation and therefore any subsequent macrophage related AEC activation.

5.7 Concluding remarks

In this chapter, we showed that animals treated with an extracellular CypA inhibitor (MM-284) prior to injurious mechanical ventilations sustained substantially less physiological dysfunction. We observed a significant decrease in mortality rates, attenuated derangement of respiratory mechanics, and substantial improvement in alveolar capillary permeability, oxygenation, and pulmonary oedema. Although we did not provide direct evidence to show that the protective effects following MM-284 treatment were due to CypA antagonism, we believe that this is likely given what is described of the drug's mechanism of action in the literature. These findings suggest that CypA is present in the alveolar space as a mediator with a role in the pathogenesis of VILI instead of a general cellular inflammatory marker released as a consequence of VILI.

Surprisingly, protection from VILI conferred by MM-284 treatment appears to be leukocyte independent in our model, at least during the early phases of injury. Instead, we propose that dampening the activation of key players in the alveolar space – AECs and alveolar macrophages – may be one of the mechanisms through which CypA inhibition leads to protection from VILI. It is possible that decreased macrophage activation following CypA blockade may have also contributed to the decrease in cytokine (CXCL-1/KC) secretion. Furthermore, we demonstrated a decrease in MMP-2 activity in the alveolar space following MM-284 treatment. This suggests that the drug may have also attenuated CD147-mediated MMP secretion and activation. Given that MMPs are often implicated in the degradation of barrier proteins, this decrease in MMP-2 activity may account for the lack of increase in alveolar capillary barrier permeability that is typical of VILI and observed in the vehicle treated group.

6 Exploration of CypA stimulation *in vitro*

6.1 Abstract

In chapter 5, we demonstrated that inhibition of CypA *in vivo* attenuated responses in both alveolar epithelial cells (AECs) and alveolar macrophages. However, it was impossible to determine if these were primary or secondary responses to CypA inhibition. In this chapter, both AECs and alveolar macrophages were separately stimulated *in vitro* with recombinant CypA to investigate downstream cellular effects.

CD147 expressing murine bone marrow-derived macrophages, human monocyte-derived macrophages, and A549s (human epithelial cell line) were incubated with recombinant CypA. In macrophages, we observed a significant upregulation in pro-inflammatory markers ICAM-1, MHC-II, and CD86, as well as an increase in nitric oxide and IL-6 release. However, no signs of cell activation were displayed following stimulation of epithelial cells.

Together, the data suggest a directionality in the CypA signalling in the alveolar space. It appears that CypA is secreted into the extracellular space following epithelial injury, such as mechanical stretch or acid, where it then primarily targets local alveolar macrophages, promoting cell activation and propagation of local inflammatory responses.

6.2 Introduction

There is a growing body of literature covering the many cellular functions and signalling events induced by extracellular CypA. In pathological contexts, it has been shown to induce inflammatory signalling, cell migration, reactive oxygen species (ROS) production, matrix degradation, cell proliferation, and apoptosis. All these downstream effects of CypA stimulation has been shown to play a crucial role in the pathogenesis of a wide range of inflammatory diseases.

Pro-inflammatory signalling following CypA stimulation appears to be dependent on the activation of the NF-κB pathway, which then propagate downstream events. In endothelial cells (ECs), this includes upregulation of adhesion molecules E-selectin and VCAM-1 (297); In macrophages, NF-κB activation leads to the production and secretion of cytokines/chemokines such as TNF-α, IL-8, MCP-1, and IL-1β (294). In both instances, the downstream consequences of CypA stimulation contribute to the recruitment and influx of leukocytes to the site(s) of injury. CypA also acts as a chemoattractant to various leukocytes subsets including monocytes, neutrophils, eosinophils, and T-cells (292, 301). Additionally, CypA can also act a synergistic co-factor with other chemokines such as MIP-2 and CXCR4 leading to an augmentation in cell proliferation and migration (288). CypA also contributes to inflammation by promoting matrix degradation through stimulation of matrix metalloproteinase (MMP) activity. When stimulated with recombinant CypA, the monocyte/macrophage cell line (THP-1) has been shown to express greater levels of MMP-9 (299, 301, 448). This upregulation in MMP expression is also associated with increased activity of gelatinases (MMP-2 and MMP-9) (297, 449). CypA has also been reported to induce apoptosis in both a cell and dose dependent manner. In VSMCs, CypA appears to act as a growth factor, stimulating extracellular signal-regulated kinases (ERK1/2 also known as p42/44 mitogen-activate protein kinases [MAPKs]) activity to promoting cell proliferation, increase DNA synthesis and inhibit apoptosis. In ECs, the effects of CypA varies with the dose at which it is

administered. At low concentrations, CypA appears to stimulate EC proliferation (449). However, at high concentrations, CypA leads to a decrease in EC viability, inducing apoptosis by increase expression of cleaved caspade-3 and stimulating pro-apoptotic pathways including c-Jun N-terminal kinase (JNK) pathway and p38 MAPK (450). Lastly, CypA is also capable of inducing ROS production, thus propagating a positive feedback loop on its own oxidative stress-induced secretion, further potentiating the activation of inflammatory pathways involved (451).

The exact mechanism through which extracellular CypA mediates its functions still remains elusive. CD147, its primary cell surface signalling receptor, has been proposed as a crucial signalling mediator. *In vitro*, the presence of anti-CD147 antibody has been shown to significantly decrease CypA-mediated neutrophil and monocyte chemotaxis (291, 448). The role of CypA-CD147 interactions in disease pathogenesis such as acute pulmonary embolism, myocardial ischemia and reperfusion, subarachnoid haemorrhage, pulmonary arterial hypertension, and rheumatoid arthritis has also been demonstrated in several *in vivo* studies (314, 452-455). In these studies, both CypA and CD147 were found to be upregulated in pathological states, leading to activation of similar downstream signalling pathways (e.g. ERK and NF-κB), and attenuation of injury was observed following inhibition of either/both mediator(s). In two of these studies, the effects of inhibiting both CypA and CD147 was investigated and compared with the effects following blockade of a single mediator. Both studies revealed that inhibition of both did not yield any further significant protection, suggesting that these mediators were indeed part of one common pathway (453, 454).

While most effects of CypA appear to be mediated through CD147, there is also evidence to suggest that some extracellular CypA activity may be dependent on other receptors apart from CD147. Bahmed et al demonstrated that knockdown of CD147 in a monocytic cell line (U937) did not prevent CypA-mediated induction of IL-8 (408). Xue et al also reported that

'multiple signals' activated by extracellular CypA in VSMC and EC were unaffected by knockdown of CD147, although no further details were provided in that study (308).

While some effects of CypA stimulation of macrophages have been recorded, including secretion of pro-inflammatory cytokines secondary to NF-κB activation and increased expression of MMP (as discussed above), there have been no studies looking at the effects of CypA stimulation on lung epithelial cells.

In the previous chapter, we demonstrated that inhibition of CypA *in vivo* attenuated responses in both alveolar epithelial cells (AECs) and alveolar macrophages. However, it was impossible to determine if these were primary or secondary responses to CypA inhibition. Therefore, this chapter, both AECs and alveolar macrophages were separately stimulated with recombinant CypA *in vitro* to investigate downstream cellular effects.

6.3 Aims

In the previous chapter, we observed that attenuation of VILI following CypA inhibition *in vivo* seemed to be associated with a dampening of cell activation. this chapter seeks to explore the mechanisms through which extracellular CypA contributes to the pathogenesis of VILI using *in vitro* methods, by:

1. Investigating the effects of stimulation of AEC with recombinant CypA
2. Investigating the effects of stimulation of macrophages with recombinant CypA

6.4 Protocols

6.4.1 Isolation of murine bone-marrow-derived macrophage

While the optimal choice of cells for these experiments would have been alveolar macrophages, the relatively low numbers of alveolar macrophages present in the lungs of mice posed an issue. In our hands, a typical yield of alveolar macrophage cells per mouse is roughly 2-5 x 10^5 cells; this is consistent with reports from others (456-458). This low yield per mouse often means there are insufficient cells for experimental assays. To acquire sufficient numbers of alveolar macrophages, we would have had to sacrifice large numbers of mice to provide sufficient cells. As an alternative – which we felt was more in line with the 3Rs of animal research – we decided to first investigate our hypotheses with murine bone marrow derived macrophages (BMDM).

Tissue macrophages are derived from monocytes or from local proliferation of tissue-resident macrophage colony-forming unit cells (459). Monocytes, themselves, originate from progenitor cells in the bone marrow (460, 461). This protocol involves the isolation of bone marrow-derived progenitor cells which are then stimulated with macrophage-colony stimulating factor (M-CSF), a growth factor that encourages the propagation and differentiation of committed precursor cells into a fairly homogenous population of macrophages (462). Due to the abundance of progenitor cells in the bone marrow, this technique produces significantly higher yields (roughly 7-10 x 10^7 macrophages) of differentiated macrophages from a single mouse within a few days.

To isolate bone marrow cells, C57BL/6 mice were sacrificed, and trunks/legs of animals were sprayed with 70% ethanol solution. Both femurs were isolated, and a 27-G needle attached to a syringe containing 1 mL of sterile RPMI 1640 media was inserted into the bone marrow cavity of the femur. To extract bone marrow cells, the bone cavity was flushed with 2-5 mL of

sterile media until the bone appears white. This cell-containing media was then filtered through 40 µm filters and resuspended in a total of 10 mL of fresh RPMI, 10% FCS, 1% PSG, supplemented with 50 ng/mL recombinant macrophage colony-stimulating factor (M-CSF) (PeproTech, New Jersey, USA). Cells were seeded into 55 cm^2 sterile plastic petri dishes and cultured for five days in incubators maintained at 37ºC in a humidified 5% CO_2 atmosphere. Media was replaced every other day and any non-adherent cells were discarded.

6.4.2 Human monocyte-derived macrophage isolation

Ethics

Ethical permission was granted by the local ethics committee (REC reference 15/LO/1764) for obtaining peripheral venous blood from healthy, non-medicated volunteers. Informed consent was obtained for all participants. For peripheral blood mononuclear cells (PBMCs) isolation, venous blood was collected in EDTA-containing BD Vacutainer tubes and processed immediately.

Isolation of peripheral blood mononuclear cells

50 mL Leucosep tubes containing 15 mL Histopaque-1077 (Sigma-Aldrich) were centrifuged at 1,300 x *g* for 1 minute at room temperature (RT). Blood was collected from healthy volunteers in EDTA containing BD Vacutainer tube. To each Leucosep tube, 20 mL of blood was added and centrifuged at 1,300 x *g* for 15 minutes at RT. Following separation, whole blood should be separated into layers: plasma, peripheral blood mononuclear cells (PBMCs), followed by red blood cells (RBCs) and granulocytes. The top plasma layer was removed and discarded using a Pasteur pipette and the middle layer made up of PBMCs was gently aspirated and transferred to a new 50 mL Falcon tube.

PBMCs were washed by addition of cold sterile PBS to a final volume of 50 mL and centrifuged at 300 x *g* for 10 minutes at 4ºC. After the first centrifugation, supernatant was removed and discarded. Another 50 mL of cold sterile PBS was then added and the wash step was repeated. After the second centrifugation, the supernatant was removed, discarded, and the final cell pellet was resuspended in 1 mL of cell sorting buffer (PBS, 1% FCS, 2 mM EDTA, 1% penicillin-streptomycin).

10 µL of cells were transferred to a FACS tube containing 10 µL AccuCheck counting beads (ThermoFisher Scientific) for a cell count using flow-cytometry. Different cell populations were identified based on their characteristic forward scatter (FCs) and side scatter (SSc) (Figure 6.1). Cell counts were determined.

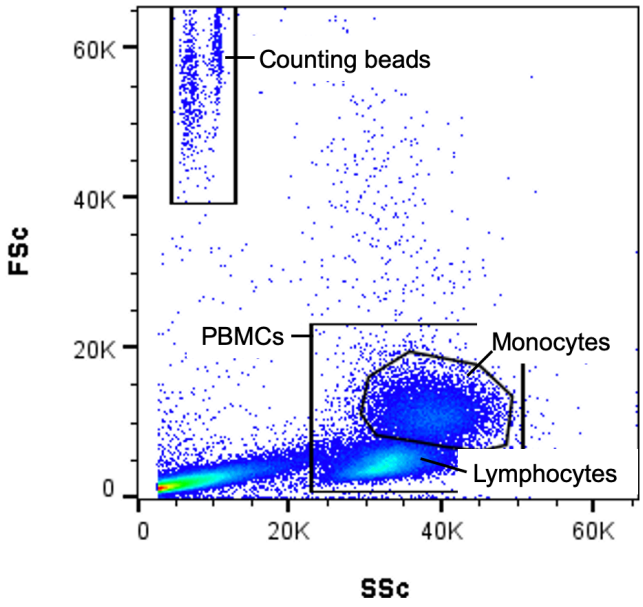


Figure 6.1 - Representative flow cytometry plot of PBMCs isolated from peripheral blood.

Monocytes, lymphocytes were identified based on their characteristic forward scatter (FSc) and side scatter (SSc). Equivolume of counting beads (10 µL) was also added to the sample to determine cell counts.

Isolation of monocytes from PBMCs

A pan-monocyte isolation kit (Miltenyi Biotec) was used to isolate monocytes from PBMCs. This kit is an indirect magnetic labelling system that allows users to obtain a population of highly pure, unlabelled monocytes, including classical ($CD14^{++}/CD16^{-}$), non-classical ($CD16^{++}/CD14^{+}$), and intermediate ($CD16^{+}/CD14^{++}$) monocytes, by depletion of magnetically labelled non-monocyte PMBCs.

Briefly, the magnetic-activated cell sorting (MACS) separation system used in this chapter can be broken down into three main steps. Step one involves the labelling of non-monocytes with a cocktail of biotin-conjugated monoclonal antibodies. In step two, anti-biotin monoclonal antibodies conjugated to magnetic microbeads are added. These bind to the biotin on the primary labelling reagent, completing the indirect magnetic labelling of non-monocytes cells. In step three, the mixed population of cells is placed in an external magnetic field (MACS Separator) within a MACS® Column. The magnetically labelled non-monocyte cells are retained on the column, while the unlabelled monocytes pass through for collection.

The protocol was performed as manufacturer's instructions. The PBMC pellet was first resuspended in sorting buffer with addition of FC receptor (FcR) Blocking Reagent and Pan-Monocyte Biotin-Antibody Cocktail (containing a cocktail of biotin-conjugated monoclonal antibodies against antigens that are not expressed on human monocytes) for 5 minutes before a 10-minute secondary incubation with Anti-Biotin Microbeads. Magnetic cell separation was then performed using appropriately sized MACS Separator and MACS Columns determined based on the number of labelled and total cells. The cell suspension was applied onto the column and flow-through containing unlabelled, enriched monocyte cells were collected. A 10 µL aliquot of cells were stained with CD16 (FITC) and CD14 (PerCP) to check for cell purity and MACS sorting yield using flow cytometry (Figure 6.2). Cell loss was also calculated after magnetic separation and was consistently < 5%.

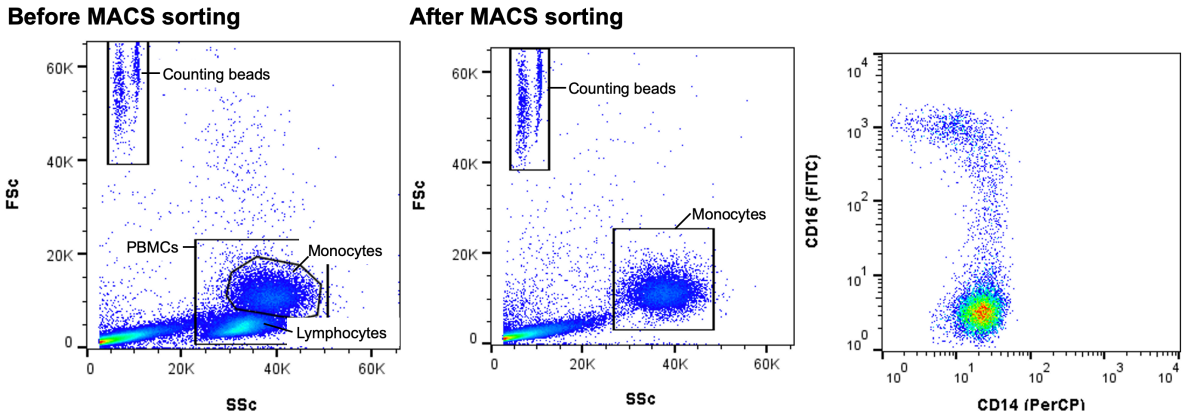


Figure 6.2 - Comparison of flow cytometry plots before and after MACS sorting.

Monocytes were isolated from PBM Cs by magnetic bead separation (negative selection) and stained with anti-CD16 and anti-CD14 antibodies.

Monocytes were then centrifuged at 300 x *g* for 5 minutes at 4ºC. The cell pellet was resuspended in RPMI, 10% FCS, 1% PSG supplemented with 20 ng/mL recombinant granulocyte-macrophage colony-stimulating factor (GM-CSF) and macrophage colony-stimulating factor (M-CSF) (PeproTech, New Jersey, USA), seeded into 55 cm^2 dishes, and cultured in incubators maintained at 37ºC in a humidified 5% CO_2 atmosphere. Media was first replaced on day 3, and then every other day subsequently. Any non-adherent cells were discarded. Cells were ready for use from day 7 onwards.

Both M-CSF and GM-CSF was used in culture media to induce differentiation of monocytes into a mixed population of M1 (classically activated) and M2 (alternatively activated) macrophages. A recent study by Mitsi et al reported the majority of human adult AM express high levels of both M1 (CD80, CD86, CD64) and M2 (CD206 and CD163) markers simultaneously, conferring a hybrid M1/M2 phenotype which does not fit the classic macrophage classification (463). While it may be argued that it would have been better to differentiated monocytes into MDMs without any growth factors leading to a so-called M0 (naïve) phenotype, in our hands we found that monocytes failed to adhere to the culture

surface and did not survive and differentiate when growth factors were not present; This is consistent with findings from other groups (464, 465).

On day seven, the cells were characterised according to their surface markers using flow cytometry (Figure 6.3). MDMs expressed high levels of macrophage markers CD16 and CD11b. MDMs were also evaluated for the M1 and M2 markers CD86 and CD206, respectively. MDMs were characterised as $CD206^{+}$ and $CD86^{+}$. This pattern of hybrid M1 and M2 surface marker expression by MDMs on day 7 were similar to that found by Mitsi et al in human Alveolar macrophage (463).

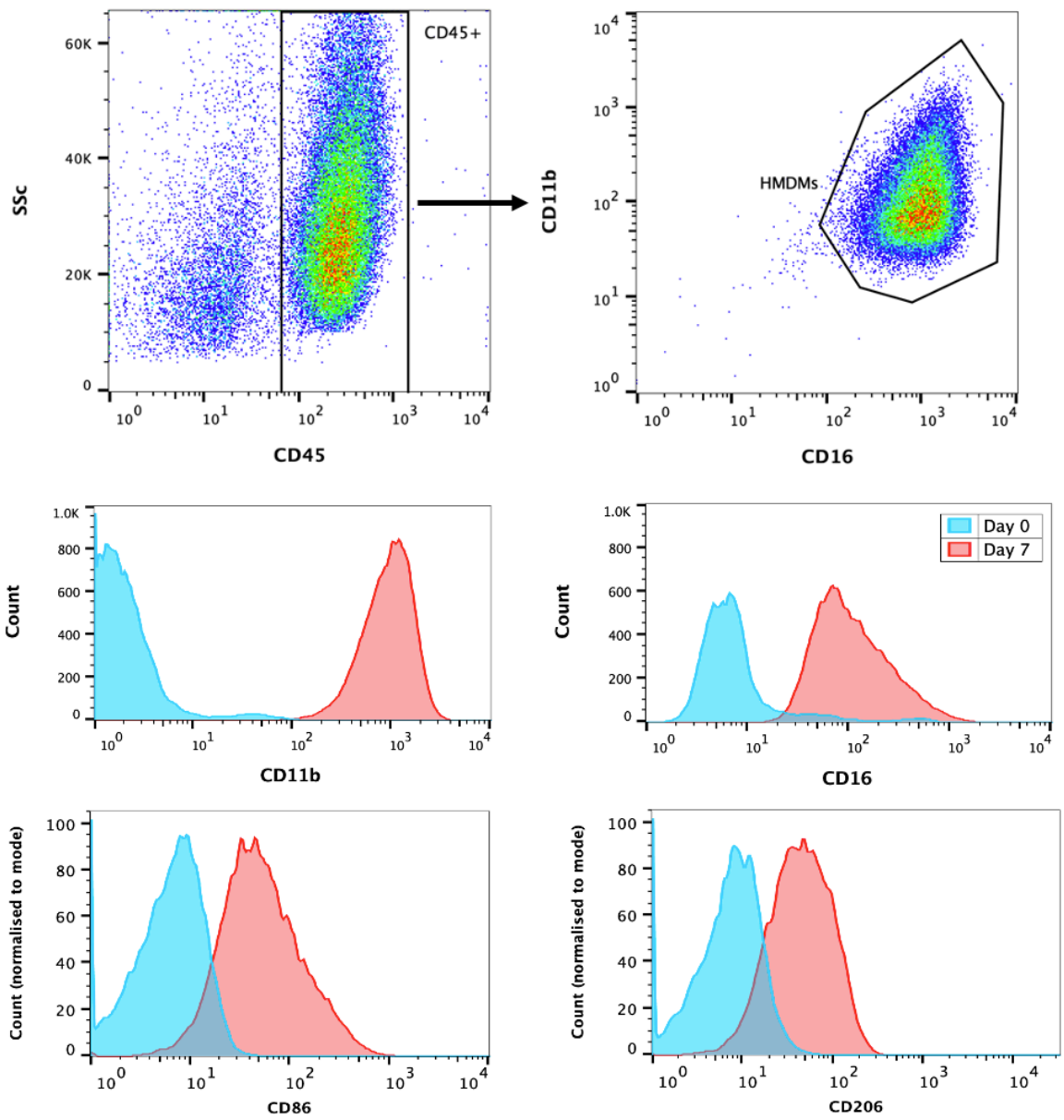


Figure 6.3 - Characterisation of HMDMs after seven days in culture.

Cells were first gated on the basis of their CD45 expression. CD45+ cells expressed both macrophage markers CD11b and CD16. Upregulation of markers CD11b, CD16, CD86 (M1 marker) and CD206 (M2 marker) from day 0 of culture to day seven.

6.4.3 Stimulating cells with recombinant cyclophilin A

Dose of recombinant cyclophilin A

For these experiments, an *E. coli*-derived recombinant human CypA protein (R&D Systems) was used. At the time that these experiments were performed, recombinant mouse CypA protein was not commercially available.

To determine the dose of recombinant CypA to use for the *in vitro* stimulation experiments, we referred back to the concentrations of CypA detected previous in our *in vivo* models of ALI. In chapter 3, we reported that the mean concentrations of CypA in BAL in following VILI and acid-induced lung injury was 5.9 ng/mL and 25.7 ng/mL respectively. In human ARDS samples, the mean concentration of CypA was 61.8 ng/mL. As the process of performing a BAL dilutes the epithelial lining fluid by a factor of 50- to 120-fold (342, 345), this was also taken into account in our calculations (Table 6.1).

Table 6.1 - An estimation of the concentration of CypA in the alveolar space based on the mean concentration of BAL CypA found *in vivo* and estimated BAL dilution factors

	VILI	Acid-induced lung injury	Human ARDS
In vivo BAL CypA concentration	5.9 ng/mL	25.7 ng/mL	61.8 ng/mL
Assuming a 50-fold dilution…	295.0 ng/mL	1.3 µg/mL	3.1 µg/mL
Assuming a 120-fold dilution…	708 ng/mL	3.1 µg/mL	7.4 µg/mL

In initial pilot experiments, a supra-physiological dose of CypA (90 µg/mL) was used to (1) determine if recombinant CypA was biologically activity and (2) identify readouts for subsequent experiments that were then carried out with a physiologically relevant dose of CypA (1 µg/mL).

For these recombinant CypA stimulation experiments, macrophages (BMDMs or HMDMs) or epithelial cells (A549) were seeded in 48-well plates as detailed in Table 6.2. Cells were allowed to adhere overnight. The following day, media was removed, and wells were gently washed with calcium free PBS. Cells were then incubated with serum-free media (control) or recombinant CypA for 8 hours.

Table 6.2 - Seeding densities and media of macrophages and epithelial cells for CypA stimulation experiments

Cell	Seeding density (cells/well)	Media
Macrophages		
Murine BMDM	9×10^4	RPMI, 10% FCS, 1% PSG
HMDM	9×10^4	RPMI, 10% FCS, 1% PSG
Epithelial cells		
A549	1×10^5	DMEM, 10% FCS, 1% PSG

After the incubation time, media was collected and centrifuged at 300 x *g* for 5 minutes at 4ºC to yield cell-free supernatant which were aliquoted and frozen at -80ºC for future analyses. Wells were rinsed twice with phosphate buffered saline (PBS) and cells were detached from the surface of the wells using Cell Dissociation Buffer (ThermoFisher Scientific) and gentle pipetting. Cells were washed with FACS wash buffer (FWB) before undergoing antibody staining for analysis by flow cytometry.

Cells were then identified using specific surface markers on flow cytometry. Any noise and cell debris were excluded based on auto-fluorescent and size. BMDMs were identified as CD45+, CD11b+, and F4/80+ cells. HMDMs were identified as CD45+, CD16+ cells. A549 cells were identified based on their expression of EpCAM. Cell surface expression of CD147 and activation markers, including ICAM-1, MHC-II, and CD86, were also measured.

6.4.4 Cell viability: 7-AAD

Cell viability was assessed by flow cytometry analysis. After cells were processed and stained with antibodies, 5 µL of 7-Amino-Actinomycin D (7-AAD) was added to each FACS tube and incubated for 5 minutes at room temperature before analysis of flow cytometry. 7-AAD is a membrane impermeant fluorescent dye that has a strong affinity for DNA. While it is generally excluded from viable cells, permeabilisation or disruption of the cell membranes in dying or dead cells allows 7-AAD to enter the cell and bind to double stranded DNA by intercalating between base pairs in G-C rich regions (375). 7-AAD/DNA complexes are excited at 488 nm and detected at an emission of 645 nm.

6.4.5 Nitric oxide assay

Nitric oxide is a molecular mediator of many physiology processes, and therefore measuring its levels in cell culture media is often of interest. In our case, it was used as a surrogate marker of macrophage activation. The kit used to analyse our samples utilises the Griess reaction to detect both nitrite, formed by the spontaneous oxidation of NO under physiological conditions, and nitrate that has been catalytically reduced to nitrite. The Griess reaction is summarised as the azo coupling between diazonium species, which are produced from sulphanilamide with NO_2, and naphthylethylenediamine, resulting in a colorimetric (540 or 570 nm) product proportional to the NO metabolite present.

The protocol was performed as per manufacturer's instructions. In brief, cell culture media was centrifuged at 1,000 x *g* for 15 minutes at 4ºC to remove any insoluble material. Supernatant was collected and used for assays. Standard curves for both NO_2 and NO_3 were generated by diluting appropriate amounts of provided standards with buffer solution. 50 µL of samples were added into four wells of a 96-well plate. Two wells were used for the NO_2^- detection and the other two were used for the [NO3- + NO_2^-] detection step. Buffer solution was added to wells to bring samples to a final volume of 100 µL for NO_2^- and 80 µL for [NO3-

+ NO_2^-] detection. In the wells for [NO3- + NO_2^-] detection, 10 µL of nitrate reductase solution and 10 µl of enzyme co-factors solution was added. the plate was then mixed using a horizontal plate shaker and incubated for two hours at 25ºc. After two hours, 50 µl of Griess reagent A was added to all wells, mixed, and incubated for 5 minutes at 25ºc. Then 50 µl of Griess reagent B was added to all wells, mixed, and incubated for 10 minutes at 25ºc. The plate was then read at 540 nm in a microplate reader.

6.4.6 Gelatin zymography

Equal volumes of conditioned media (12.5 µL) were prepared in 1X Novex™ Tris-Glycine SDS Sample Buffer. To ensure that equal volume loading allowed for comparisons across experiments, cells were seeded at the same density, stimulated in the same volume of media, and cell counts were determined at the end of every experiment to ensure that cell counts across experiments were virtually identical. Samples were loaded into 10% gelatin protein gels for electrophoresis separation under non-reducing conditions. After, gels were washed with renaturing buffer and then incubated overnight in developing buffer to induce digestion of gelatin by any MMP-2 and MMP-9 present in the samples. Gels were then stained with colloidal blue to allow visualisation of denatured areas. To allow comparison between gels, the same amount of recombinant MMP-2 and MMP-9 protein standards were loaded on to every gel. This density of standards was given an arbitrary unit of 1 and the density of all bands were expressed as a value relative to it using ImageJ.

6.5 Results

6.5.1 Bone marrow-derived macrophages express the CypA receptor CD147

After BMDMs were allowed to differentiate in cell culture, cell surface expression CD147, the primary receptor for CypA, was analysed using flow cytometry. BMDMs demonstrated surface expression of CD147 (Figure 6.4), thus confirming that recombinant CypA would have a receptor to bind to and signal through.

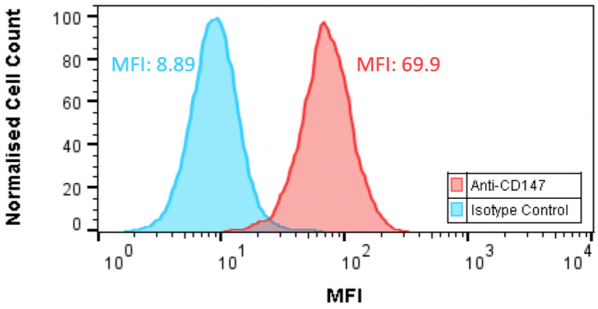


Figure 6.4 – Representative flow cytometry histogram showing BMDM expression of CD147 receptor

6.5.2 Effects of recombinant CypA on mouse BMDMs

Most previous studies have looked at the effects of CypA stimulation and reported various effects after 12 hours or 24 hours. Here, BMDMs were stimulated for 8 hours (12-hour incubation was logistically difficult to perform) and 24 hours with a supra-physiological dose (90 µg/mL) of human recombinant CypA (Figure 6.5). This high dose was used to determine this recombinant protein had any bioactivity *in vitro.* At the time that these experiments were performed, only human recombinant protein was commercially available. While the gene encoding mouse CypA was reported to be 92.48% similar (based on nucleic acid comparisons) (466), we were uncertain if the protein was cross-reactive. Thus, we used a higher concentration to test the bioactivity of CypA and to determine what readouts would be helpful for assessing CypA-induced activation for following experiments.

At 8 hours, BMDMs stimulated with CypA demonstrated significant upregulation of ICAM-1 and MHC-II, no differences in CD86, and significant downregulation of CD206 compared with untreated controls. At 24 hours, no differences in any markers were observed.

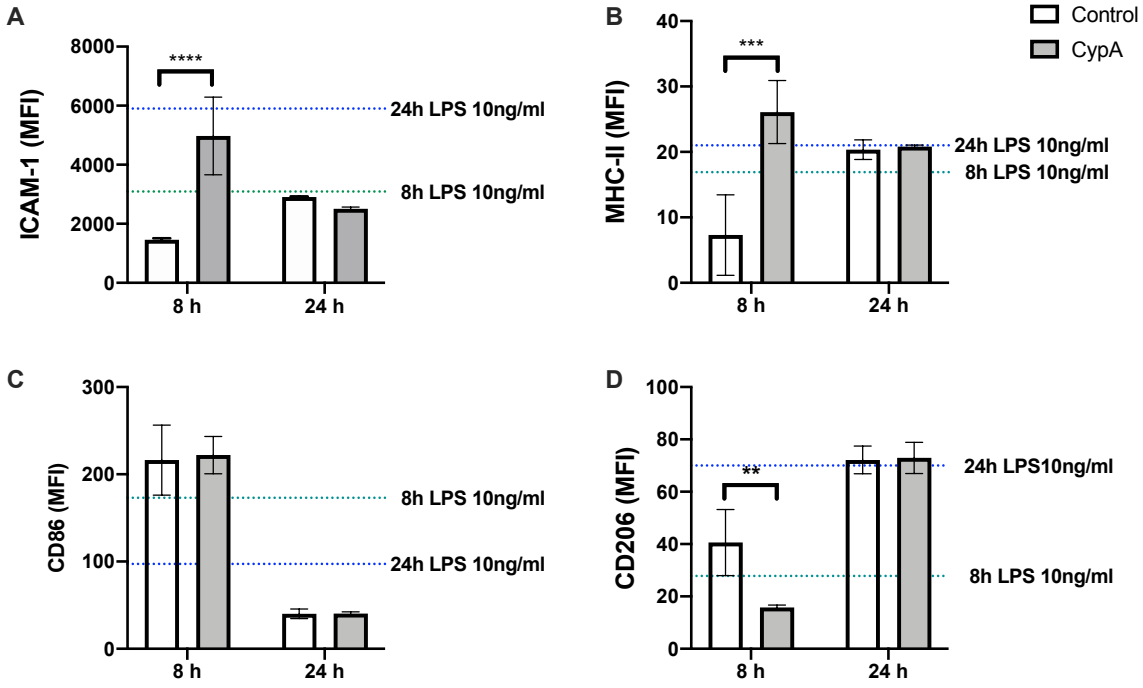


Figure 6.5 – Assessment of cell surface activation markers following an 8- and 24-hour incubation with recombinant CypA.

*At 8 hours, CypA induces an upregulation of ICAM-1 (A) and MHC-II (B), no change in CD86 (C), and downregulation of CD206 (D). At 24 hours, no changes in surface markers were observed following CypA stimulation. As a positive control, cells were also stimulated with 10 ng/mL LPS and these are shown as dotted lines. Data shown as mean ± SD. N=4 for 8-hour data and N=2 for 24-hour data. **p<0.01, ***p<0.001, ****p<0.0001. Two-way ANOVA with Sidak's multiple comparisons test.*

At 8-hours, cell viability was also assessed by measuring 7-AAD staining using flow cytometry. The percentage of cells staining positive for 7-AAD (non-viable) was significantly higher

following in the CypA treated group compared with untreated controls (Figure 6.6A). Conditioned media from 8-hour stimulation experiments were also evaluated for nitric oxide (NO) concentration and IL-6 (Figure 6.6B, C). CypA stimulation induces a significant increase in NO production and IL-6 release.

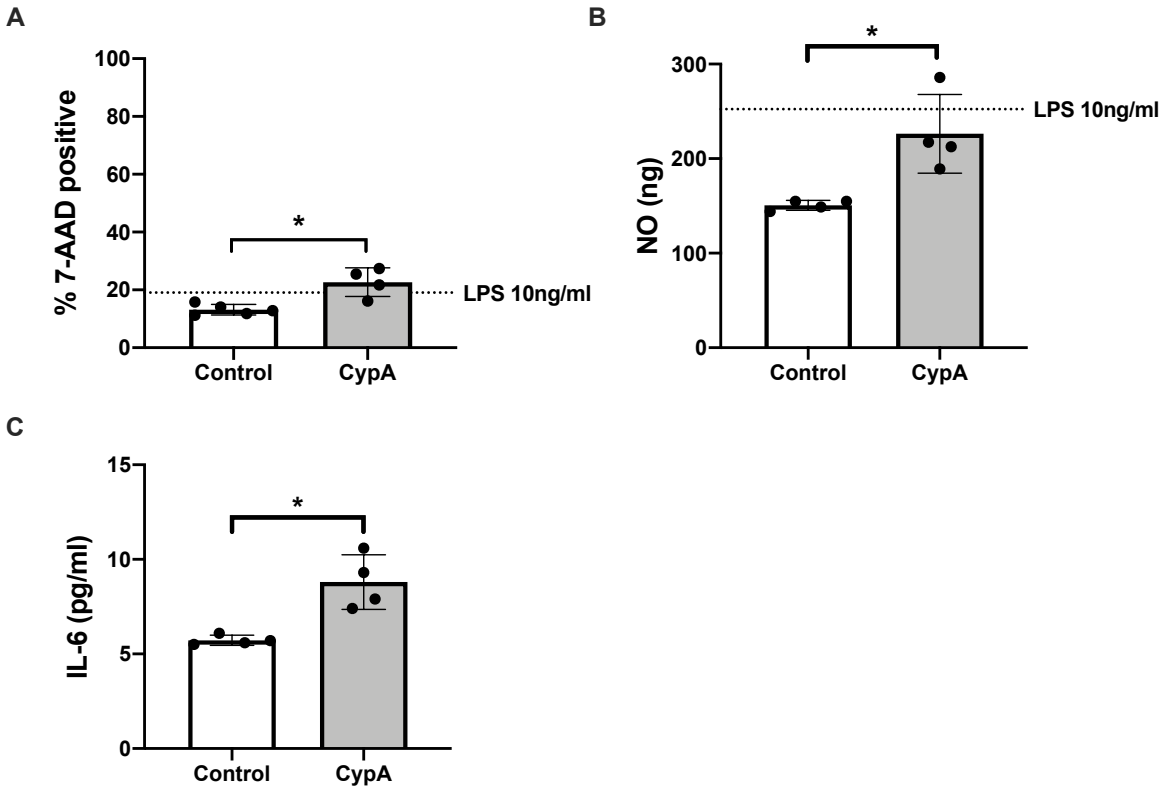


Figure 6.6 – 8-hour stimulation with recombinant CypA leads to increased cell death (A), nitric oxide production (B), and IL-6 release (C).

*(A) The percentage of cells staining positive for 7-AAD (% non-viable) assessed by flow cytometry was significantly higher following CypA stimulation. (B, C) Conditioned media from the 8-hour stimulation experiments were evaluated. BMDMs produced significantly more nitric oxide (NO) and also released significantly greater amounts of IL-6 following recombinant CypA stimulation. As a positive control, cells were also stimulated with 10 ng/mL LPS and these are shown as dotted lines. Data shown as mean ± SD. *p<0.05. Mann-Whitney test.*

Conditioned media from the 8-hour stimulation experiments were also evaluated for activity of MMP-2 and MMP-9 using gelatin zymography. No gelatinolytic bands of activity were

detected in media from untreated controls and CypA-stimulated cells, suggesting that neither pro or active MMP-2 or MMP-9 were present (N=4, gels not shown).

Having shown that recombinant human CypA shows bioactivity and is able to activate murine BMDMs, cells were stimulated with a lower, physiologically relevant concentration of CypA. A dose titration experiment was performed. Cells were stimulated with 0.1 – 1.0 μg/mL, covering the range of CypA previously detected in *in vivo* VILI model (Figure 6.7). At these lower concentrations of CypA, changes in ICAM-1, MHC-II and CD206 that were previously observed were not found. Although it is possible to conclude from this data that stimulation of macrophages with physiologically relevant doses does not lead to cell activation, it was also possible that the lack of response was due to a decreased sensitivity of mouse macrophages to the human recombinant CypA.

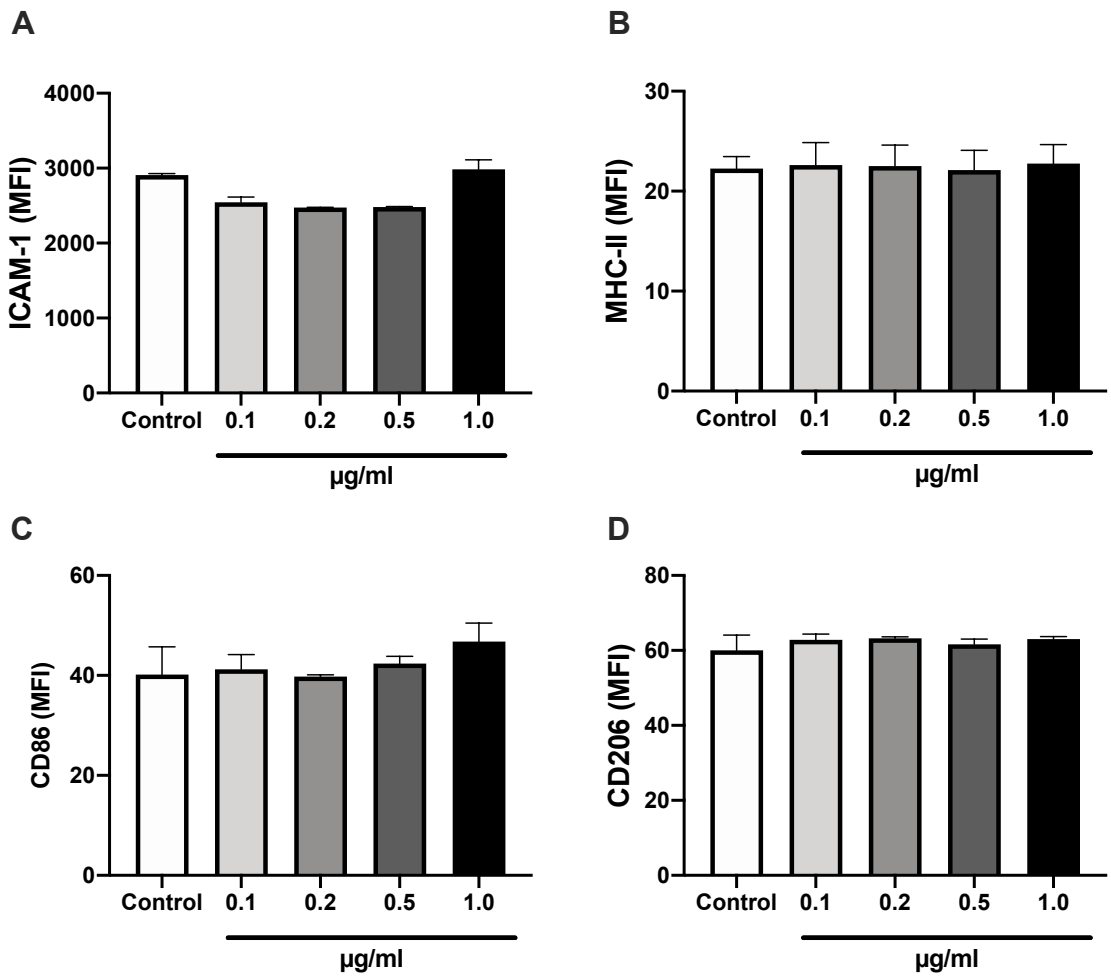


Figure 6.7 – Dose titration of recombinant CypA.

8-hour stimulation of BMDMs with lower, physiologically relevant concentrations of CypA failed to reproduce changes in surface markers that were previously observed when BMDMs were stimulated with a supraphysiological (90 µg/mL) dose of CypA. Data shown as mean ± SD. N=2.

6.5.3 HMDMs also express the CypA receptor CD147

To thoroughly assess whether recombinant CypA leads to activation of macrophages *in vitro*, human monocyte-derived macrophages were isolated from peripheral blood mononuclear cells. This eliminated any potential issues related with cross-species reactivity of the recombinant CypA protein. As above, cell surface expression CD147, the primary receptor for

CypA, was analysed using flow cytometry. HMDMs also demonstrated surface expression of CD147 (Figure 6.8).

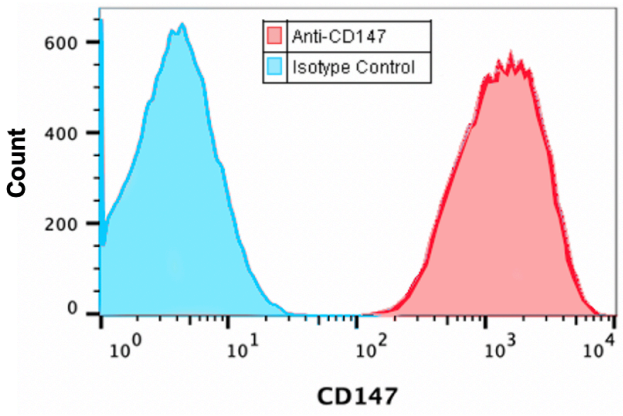


Figure 6.8- Representative flow cytometry histogram showing BMDM expression of CD147 receptor

6.5.4 Effects of recombinant CypA on HMDMs

HMDMs were stimulated for 8 hours with a physiologically relevant dose of recombinant CypA (1 µg/mL). CypA induced a significant upregulation of activation markers ICAM-1 and CD86 compared with untreated controls (Figure 6.9A, B). No differences in MHC-II and CD206 were observed (Figure 6.9C, D). Cell viability of untreated controls and CypA treated cells was high in both instances and virtually identical (Figure 6.9E). Cell supernatants were also evaluated for NO content, but no differences were detected between control and CypA treated groups. There was, however, a significant increase in IL-6 release following CypA stimulation (Figure 6.9F).

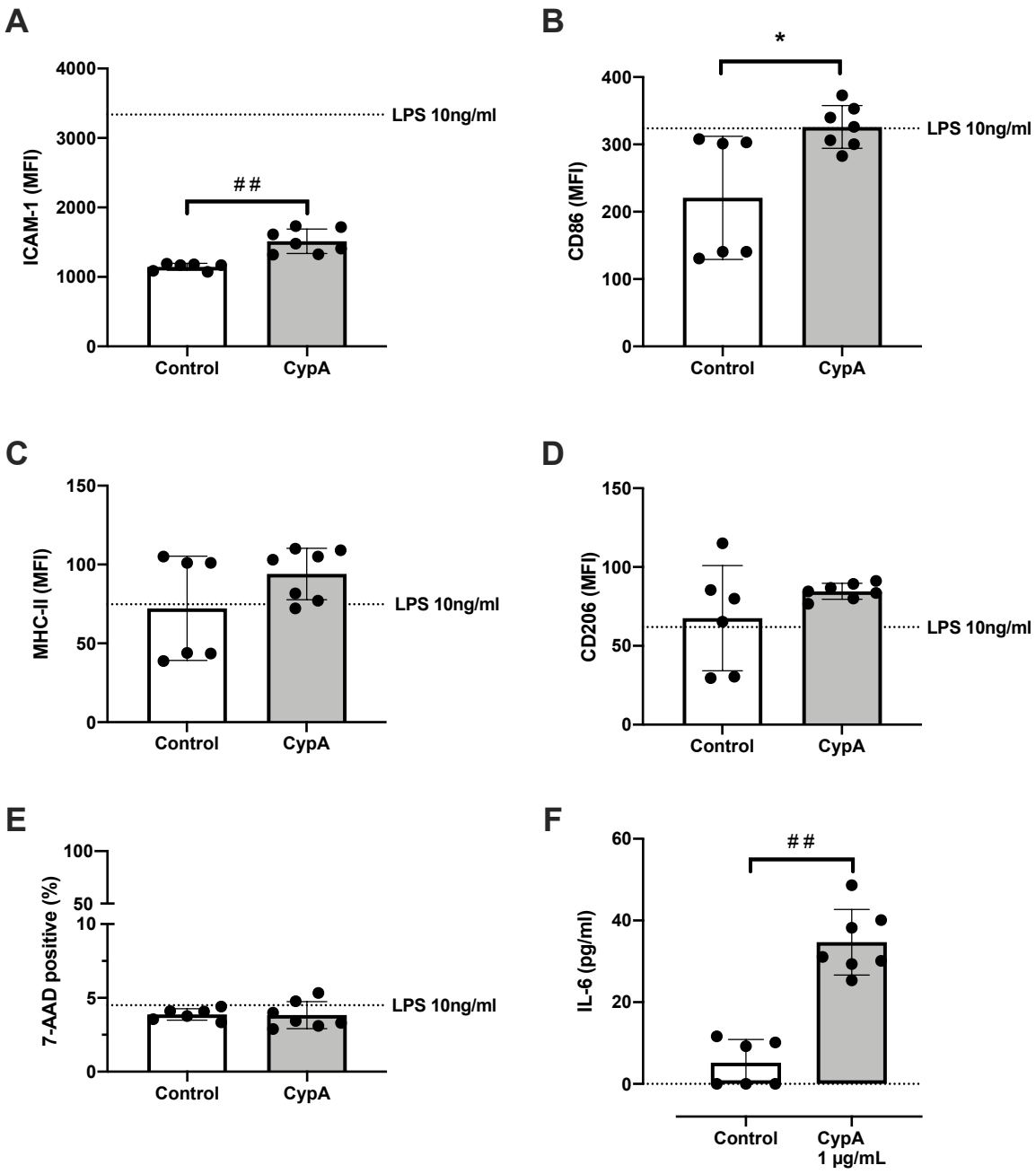


Figure 6.9 – 8-hour incubation of HMDMs with recombinant CypA leads to cell activation.

At 8 hours, CypA (1 µg/mL) induces an upregulation of ICAM-1 (A) and CD86 (B) compared with untreated controls. No changes in MHC-II (C) or CD206 (D) expression was observed. Cell viability was also unaffected by CypA treatment (E). A significant increase in the concentration of IL-6 in supernatants of CypA stimulated cells was detected (F). As a positive control, cells were also stimulated with 10 ng/mL LPS for the same time period and these are

*shown as dotted lines. Data shown as mean ± SD. N=6-7. * p<0.05. Unpaired t-test. # # p<0.01. Mann-Whitney test.*

Conditioned media were evaluated for activity of MMP-2 and MMP-9 using gelatin zymography. Gelatinolytic bands of activity were detected at 72 kDa (pro-MMP-2) in supernatants from both untreated (–) and CypA stimulated (+) HMDMs. However, there appears to be no differences in levels of pro-MMP-2 between the groups (untreated 0.40 ± 0.021 vs CypA 0.43 ± 0.017 relative band intensity, N=3-4). No bands were detected at 62 kDa (MMP-2). Instead of two separate gelatinolytic bands at 92 kDa (pro MMP-9) and 82 kDa (active MMP-9), there was a thick, merged band that made it impossible analyse the two forms of MMP-9 separately. The data is therefore for the band intensity of the merged bands and expressed as an absolute band intensity instead of relative band intensity to the MMP-9 standard. Similarly, there appears to be no differences in levels of total MMP-9 activity between the groups (control 40,415 ± 5, 465 vs CypA 40,537 ± 7,922 absolute band intensity, N=3-4).

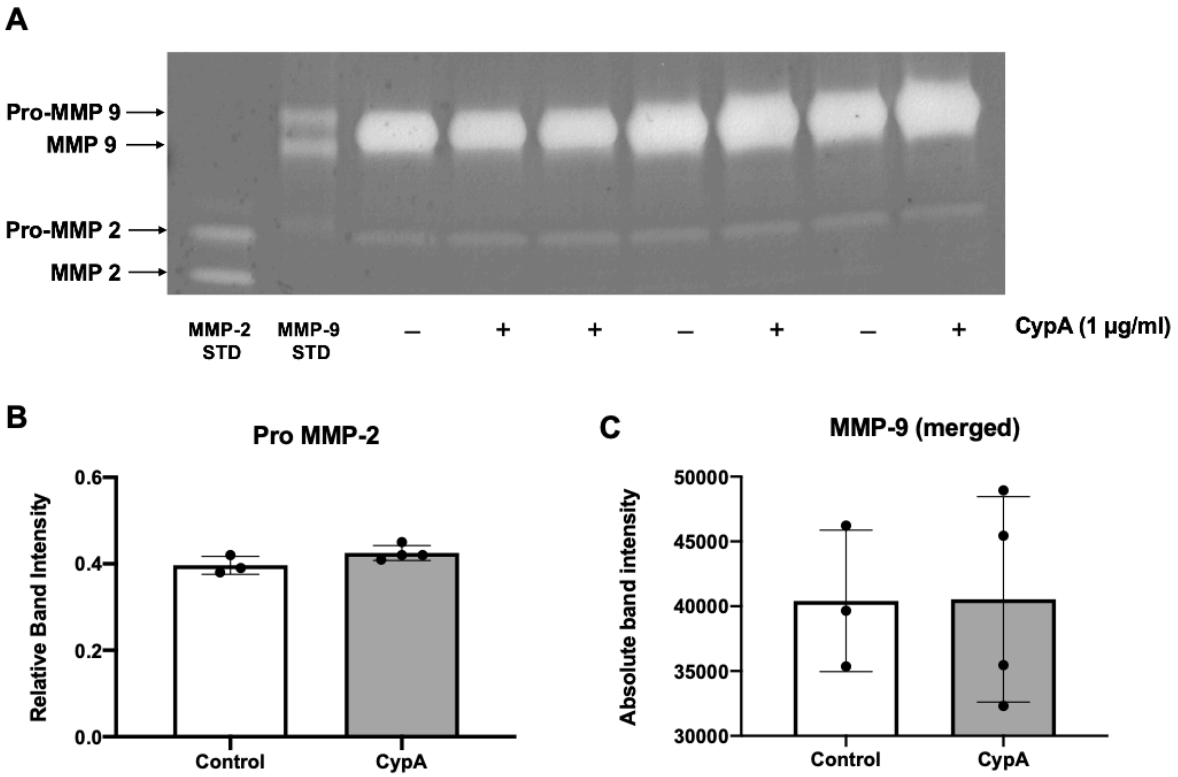


Figure 6.10 – Assessment of MMP activity in conditioned media from HMDMs stimulated with CypA.

(A) A representative gelatin zymography gel for MMP-2 and MMP-9 activity in the conditioned media of untreated controls (–) and CypA (1 µg/mL) treated (+) HMDMs. On each gel, MMP-2 and MMP-9 standards were used to identify the pro and active forms of MMPs and for comparisons of relative band densities between gel. MMP-9 bands were merged on this gel and thus processed as total MMP-9 activity and results expressed as absolute band intensity as relative band intensity calculations against the standard would not have been appropriate. (B) Pro-MMP-2 (72 kDa) was detected in both groups but did not appear to be different following CypA stimulation. (C) Total MMP-9 activity was also unchanged in the CypA stimulated cells. Data shown as mean ± SD. N=3-4.

6.5.5 Stimulation of A549 with recombinant CypA

To determine if CypA has a direct effect on AECs, A549 were also stimulated with the same physiological dose (1 µg/mL) of recombinant CypA for 8 hours. Cells were first confirmed to express the CD147 receptor (Figure 6.11).

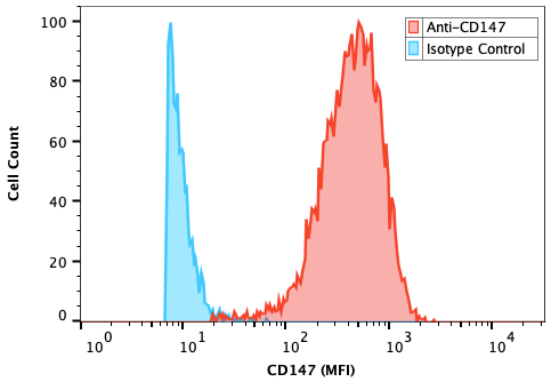


Figure 6.11 – Representative flow cytometry histogram showing BMDM expression of CD147 receptor.

Using flow cytometry, cell activation and viability were assessed through expression of the activation marker ICAM-1 and 7-AAD staining respectively. A549 cells did not show significant upregulation of ICAM-1 following CypA treatment (Figure 6.12A). Cell viability also remained unchanged following CypA stimulation (Figure 6.12B). Conditioned media from both control and CypA treated A549 cells were also analysed by ELISA for the presence of IL-6. However, the samples were found to contain no detectable levels of IL-6 (data not shown).

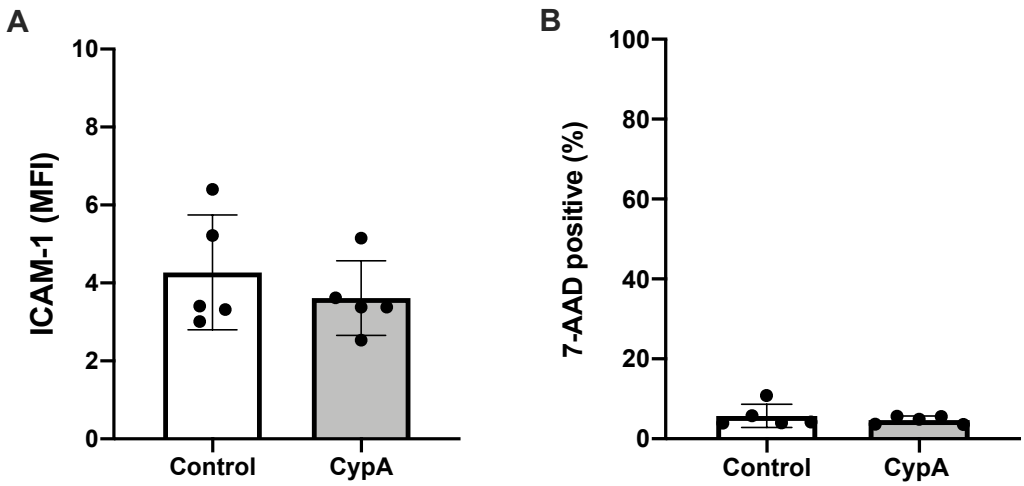


Figure 6.12 – A549 cells did not demonstrate signs of cellular activation following 8-hour stimulation recombinant CypA (1 µg/mL).

(A) ICAM-1 expression was not found to be increased following CypA stimulation. (B) Cell viability determined by 7-AAD staining on flow cytometry was also unchanged. Data shown as mean ± SD. NS. Unpaired t-test.

6.6 Discussion

To date, our understanding of whether and how extracellular CypA is involved in inflammatory processes within the lung remains very limited. In the previous chapter, we demonstrated that *in vivo* inhibition of extracellular CypA attenuated VILI. We proposed that the protective effects observed following CypA inhibition might due to a dampened activation of key players in the alveolar space, specifically the AECs and alveolar macrophages. However, in an *in vivo* setting, it was impossible to know if CypA was primarily affecting alveolar macrophages or AECs, and if it had a direct or indirect effect on either cell. Thus, in this chapter, we investigated the effect of CypA stimulation *in vitro*.

The first main finding presented within this chapter is that recombinant CypA has biological activity. Furthermore, incubation of CypA with macrophages leads to cell activation. In initial experiments, murine BMDMs were stimulated with a supraphysiological dose (90 μg/mL or ~5 μM) of CypA. Although this dose was indeed several fold greater than the concentration of CypA we had previously found *in vivo,* other investigators have used higher concentrations – up to 25 μM (408). In our experiments, CypA was shown to lead to activation of macrophages. This was demonstrated by the upregulation of M1 phenotype surface markers ICAM-1 and MHC-II, and a downregulation of M2 marker CD206, suggesting polarisation of macrophages towards a M1 pro-inflammatory phenotype. Additionally, CypA stimulation induced an increase in NO production, a recognised functional marker of macrophage activation. CypA also led to greater IL-6 release from macrophages but the absolute increase was relatively small (~2.5 pg/mL more than controls). Lastly, it appeared that CypA stimulation resulted in a small decrease in viability of BMDMs; A 10% increase of cell death was detected in CypA treated cells compared with controls. When murine BMDMs were stimulated with a lower, physiologically relevant concentration of recombinant human CypA, no signs of cell activation that were previously observed were present.

However, stimulation of HMDM with physiological relevant doses of CypA lead to cell activation, suggesting that the lack of response with the same dose in murine BMDM was likely due to a decreased sensitivity of mouse macrophages to the human recombinant CypA. The effects of CypA stimulation of HMDMs were similar to those found in BMDMs. CypA induced an increase in classical M1 markers ICAM-1 and CD86, once again indicative of polarisation of macrophages towards a pro-inflammatory phenotype. Additionally, an increase in pro-inflammatory marker IL-6 was also observed.

Of note, no changes in MMP expression, secretion, or activity was detected in response to CypA. This was surprising as we had previously observed a significant decrease in active MMP-2 in BAL following CypA inhibition *in vivo*. Additionally, there have been previous studies which had all reported increased macrophage secretion of either or both MMP-2 and MMP-9 in response to *in vitro* stimulation with CypA.

However, there are a few possible reasons for this discrepancy in findings. Firstly, all of these previous studies had investigated the effects of CypA on different types of macrophages to those used in this chapter. Wang et al used the THP-1 cells – a monocytic-like cell line (299); Seizer et al used monocyte-derived macrophages which were then subsequently differentiated to foam cells through the addition of acetylated low density lipoprotein (320); and although Yang et al also used HMDMs, they had harvested monocytes from the peripheral blood of patients with rheumatoid arthritis (301).

Secondly, the absence of MMP in our experiments could be due to the dose of recombinant CypA used. In the studies conducted by these other groups, the dose of CypA varied from 100 ng/mL to 2 µg/mL. CypA dependent induction of MMP secretion appears to be dose-dependent, with the optimal dose varying between cell types. This is supported by the study conducted by Wang et al where they demonstrated a peak in MMP-2 and -9 secretion at 100

ng/mL, which then subsequently decreased with increasing CypA concentration (299). Therefore, it is possible that although the concentration of recombinant CypA used in these experiments (1 μg/mL) was closely matched to the levels we had previous found *in vivo*, it might not be the optimal concentration for investigating the effects of MMP induction in *in vitro* studies. This would have been investigated through a dose-response studies using an appropriately constructed concentration-response curve. The response of cells to recombinant CypA would have been assessed over at least two orders of magnitude on a logarithmic scale of recombinant CypA concentration to produce a sigmoid curve. This would have allowed us to determine the threshold dose of CypA required to observe a response.

Finally, all these experiments stimulated cells with CypA for 24 hours. In contrast, our incubation period was a lot shorter, lasting only 8 hours. Thus, it might have been too early for significant MMP induction, expression and secretion to have occurred. Again, this would have to be verified by performing future experiments with matched incubation time.

The second main finding is that CypA stimulation of A549 cell line (human epithelial cells) did not appear to result in any cell activation. Although we had previously observed a decrease in ICAM-1 expression on epithelial cells in response to CypA inhibition *in vivo*, direct stimulation of AECs with recombinant CypA *in vitro* did not appear to lead to cell activation. No differences in activation marker ICAM-1 was observed, cell viability remained unchanged, and no IL-6 was detected in conditioned media. These results suggest that CypA might not have a direct effect on AECs, supporting a process whereby CypA is released following epithelial insult and then subsequently targets primarily local macrophages.

However, we do also recognise that there are several possible reasons for this lack of AEC activation following CypA stimulation. Firstly, it could be that responses that we failed to detect are mediated through other receptors/pathways. As discussed in the introduction of this

chapter, the presence of other receptors apart from CD147 has been suggested by others; these have yet to be identified. While we did confirm that CD147 was expressed on all the cell types, we do not know if these alternative receptors were also expressed. Secondly, it is likely that *E.coli* expressed proteins may not be as biologically active as native proteins. Indeed, there are studies which provide evidence to suggest that post-translational modification (acetylation) of CypA *in vivo* enhances its biological activity (450, 467, 468).

Unfortunately, due to time constraints and COVID-19 related lab closures, there were a number of experiments that I had initially planned but was unable to perform. These will be discussed in further detail in the 'Future studies' section of chapter 7. In brief, these include:

1) *In vitro* stimulation of primary human AEC to determine if these cells would be more sensitive to recombinant CypA than the A549 cells were.
2) Further investigations into the potential effects of stimulating of cells with different forms of CypA, including endogenous CypA derived from conditioned media from stretched AEC cells and acetylated CypA.
3) Evaluation of the contribution of the CD147 receptor to any observed CypA-induced responses.

6.7 Concluding remarks

The main findings presented within these chapter are that recombinant CypA has biological activity *in vitro*. Incubation of macrophages with physiologically relevant concentrations of CypA leads to polarisation of cells towards an M1 pro-inflammatory phenotype and secretion of pro-inflammatory cytokine IL-6. In contrast, we detected no signs of cell activation when epithelial cells were stimulated with CypA, suggesting that CypA does not have a direct effect on the epithelium.

Overall, the data present in this chapter support a process whereby CypA is secreted into the alveolar space following pulmonary epithelial insult (e.g. mechanical stretch or acid injury). Once in the extracellular space, it primarily targets local alveolar macrophages, promoting cell activation and propagation of local inflammatory responses (e.g. release of pro-inflammatory cytokines).

7 Final discussion

Acute respiratory distress syndrome (ARDS) remains a significant cause of mortality and morbidity within the Intensive Care Unit. Despite progress in the past 50 years in our understanding of the pathogenesis of the disease, management remains purely supportive with mechanical ventilation forming the mainstay of treatment. However, mechanical ventilation itself can worsen pre-existing ARDS, and even cause damage in previously uninjured lungs, a phenomenon known as ventilator-induced lung injury (VILI). Since exposure to mechanical ventilation remains largely unavoidable, it is important that clinicians are able to limit the damage, in particular the inflammatory response, that occurs when patients are ventilated.

Pharmacotherapies aimed at mitigating the inflammatory component of VILI have always been an attractive approach. With VILI, clinicians have the unique opportunity to administer a pharmacological intervention before the inciting cause of injury (mechanical ventilation) is commenced and potentially completely prevent any downstream consequences. Despite the attractiveness of this approach, pharmacological strategies are not yet part of the clinical arsenal for prevention and/or treatment for ARDS/VILI. However, this is not for lack of trying.

Over the past few decades, numerous preclinical studies investigating the effects of blocking various inflammatory pathways have been conducted. Disappointingly, none of these have been shown to have effective therapeutic effects in subsequent phase II and phase III clinical trials. This suggests that there are still gaps in our understanding of the disease, in particular the biological response that occurs following exposure to mechanical stretch and strain. In 2003, the National Heart, Lung, and Blood Institute working group was convened to identify future directions in research in ALI/ARDS. One of their recommendations was that further studies investigating the mechanistic/pathogenic pathways of ALI was crucial to forming the basis of any future clinical trials (469).

7.1 Aims of this work

The main aim of this thesis was to investigate a novel pathogenic pathway of VILI, specifically the CypA:CD147 axis. This overarching aim was further broken down into two sub-aims. The first aim was to extend our understanding of the basic biological effects of CypA:CD147 in the context of pulmonary inflammatory and injury using *in vitro* methodologies. This was primarily addressed in chapters 4 and 6. The second aim was to thoroughly evaluate the effects of CypA:CD147 interactions during *in vivo* ventilation. This was addressed in chapters 3 and 5.

7.2 Summary of findings

CypA is upregulated early in the course of VILI

In chapter 3, we show, for the first time, the involvement of the novel mediator, CypA, in VILI. Following high V_T ventilation, we observed a marked (over 100-fold) elevation in CypA levels in BAL compared with untreated controls. When the substantial dilutional effects introduced by the process of performing a lung lavage are taken into account (up to 120-fold dilution of epithelial lining fluid (342-345)), we can begin to appreciate the significant quantities of CypA present *in situ*.

Investigation of the kinetics of CypA levels over the course of VILI revealed a significant upregulation of BAL levels of CypA at as early as 2 hours. Crucially, this was before any significant lung injury had occurred. This early increase suggests that CypA might play role in the pathogenesis of VILI as oppose to merely being a marker of injury. However, we also observed correlations between CypA and injury markers PaO_2, BAL protein, and BAL sRAGE. The particularly strong correlation with sRAGE, an established marker of epithelial injury, suggests an association between the processes underlying CypA release and damage of the alveolar epithelium. While it was difficult to conclude if CypA is present in the alveolar space

as a cause or consequence of VILI, the findings presented within this chapter does highlight that CypA undoubtedly features in VILI.

CypA is produced locally within the lungs

Interestingly, evaluation of plasma content of CypA revealed no significant changes over the 3-hour protocol, regardless of ventilation strategies. Additionally, the levels seen in plasma were consistently several folds lower than that in BAL fluid. This almost certainly indicates that the upregulation of CypA in the alveolar space was a result of increased local production and not the consequence of an overspill from the systemic circulation following damage to the alveolar capillary barrier. Thus, this also suggests that any role that CypA may play during the pathogenesis of VILI is likely to be primarily intra-alveolar.

Upregulation of the CypA receptor CD147 also occurs at an early time point

Lastly, in chapter 3, we also reported a corresponding upregulation in the expression of the CD147 receptor on the surfaces of pulmonary cells including type I and II AECs, alveolar macrophages, and endothelial cells. Levels of CD147 expression also peaked early in the course of VILI (at 1 hour), providing further support for a potential involvement of the CypA:CD147 axis in the pathogenesis of VILI.

Alveolar epithelial cells are likely to be the primary source of CypA

To date, very little is known about the basic biology of CypA within the lungs. Prior to this project, it was only known that intranasal LPS increases intra-alveolar CypA levels but no attempts to identify its source were made (291). Having established the involvement of CypA during VILI, we proceeded to investigate the source of extracellular CypA following mechanical stretch.

In chapter 3, we established that CypA was produced locally within the alveolar space, therefore eliminating endothelial cells as a cellular source. Between AECs and alveolar macrophages, we hypothesised that AECs was the most likely source of CypA. Firstly, the alveolar epithelium is exposed to the greatest deformation during mechanical ventilation. Secondly, we had observed a strong correlation between CypA and sRAGE, an epithelial marker of injury. To explore this, we utilised a combination of different *in vivo* and *in vitro* methodologies.

The first approach we took was an evaluation of CypA concentrations in two different models of acute lung injury: LPS- and acid-induced lung injury. These models were specifically selected as intratracheal LPS is a predominantly macrophage driven model whereas acid-induced lung injury is known to involve a substantial degree of epithelial insult. CypA was not significantly increased following LPS administration. In contrast, there was an impressive increase in CypA in response to acid insult, with levels 480-fold greater than that observed in the untreated group, providing further evidence to suggest upregulation of CypA is most apparent when epithelial insult is involved. Returning to the VILI model, we utilised a flow cytometry protocol to demonstrate a significant downregulation of intracellular levels of CypA in epithelial cells but not alveolar macrophages. This was consistent with a secretion of CypA from the epithelium but not macrophages following injurious ventilation. Taken together, these *in vivo* findings suggest that epithelial cells are the most likely candidate for CypA secretion, albeit without ruling out the possible contribution of macrophages.

To investigate this further, we developed and optimised an *in vitro* stretch protocol. This allowed us to investigate the different pulmonary cells in isolation to dissect out the contribution of each to the production of CypA following cyclical mechanical stretch. Using western blotting, we identified CypA in the supernatants of stretched primary human AECs, confirming that the epithelium is a source of CypA. Although it is unclear if alveolar macrophages are directly

exposed to deformative forces *in vivo*, we did subject RAW cells to the same stretch stimuli but failed to detect any signs of cell activation. Evaluation of cell supernatants also failed to detect any CypA, suggesting that macrophages are unlikely to secrete CypA in response to stretch alone.

CypA secretion from epithelial cells appears to be an active process

The mechanism of CypA secretion is another aspect its basic biology that remains unclear. While a study investigating CypA in vascular smooth muscle cells suggest that its secretion is an active process which proceeds via a vesicular secretory pathway (286), others have proposed that CypA is released in a passive manner during early stages of necroptosis as a consequence of cell membrane permeabilisation (285). It is possible that CypA secretion differs in different cell types. Given that it is such an abundant intracellular protein, it would certainly be plausible that its presence in the extracellular milieu is a good biomarker of necrotic cell death as proposed by Christofferson and Yuan (285).

Although we did not thoroughly investigate the mechanistic pathway of CypA secretion in response to stretch, we did assess the viability of static and stretched cells following *in vitro* stretch. Here, we found that lactate dehydrogenase levels and the percentage of cells staining positive for 7-AAD were virtually identical, indicating that viability following stretch was unchanged and remained high. These results strongly suggest that release of CypA from stretched cells occurs via an active process of secretion as opposed to a passive leakage from damaged/dead cells.

Inhibition of extracellular CypA in vivo leads to significant attenuation of VILI

At the end of chapter 3, we were unable to conclude if CypA was present in the alveolar space as a cause or consequence of VILI, so we investigated this further in chapter 5. To do so, we performed an *in vivo* inhibition experiment, utilising an extracellular specific CypA inhibitor,

MM-284, to selectively target extracellular CypA during VILI. Administration of the drug 30 minutes before initiation of high V_T ventilation led to remarkable results. Blockade of CypA using MM-284 effectively attenuated all physiological signs of VILI; mice displayed lower end-point peak inspiratory pressures, minimal deteriorations in respiratory mechanics, preserved arterial oxygenation, less development pulmonary oedema and alveolar-capillary membrane permeability. Treatment with MM-284 also conferred an impressive survival benefit, with 100% of animals managing to complete the full 3-hour ventilatory protocol compared with only 50% in the vehicle treated group. Furthermore, there were also signs of less physiological injury; sRAGE levels were substantially lower in the treatment group. Together, these results strongly suggest that CypA does play an important mediator role in the development of VILI.

Protection appears to involve dampened cell activation

Exploration of the potential mechanisms underlying these protective effects yielded some unexpected results. Given that most studies investigating the role of CypA in inflammatory diseases have been largely focused on its role as a potent chemoattractant, it was surprising to find no differences in leukocyte counts in both lung tissue and BAL between vehicle and MM-284 treated mice. This suggests that in our model, protection conferred by CypA inhibition is leukocyte independent, at least during the early phases of injury.

Instead, we observed significant attenuation of pro-inflammatory cytokine KC/CXCL-1, downregulation of surface activation marker ICAM-1 on epithelial cells and, to a greater extent, on alveolar macrophages, and finally, a significant reduction in intra-alveolar MMP-2 activity. Together, these results are highly suggestive that extracellular CypA, which is primarily derived from AECs following stretch, then proceeds to affect macrophage function. However, it was impossible to determine if the effects observed in AECs and alveolar macrophages were a primary or secondary response to CypA inhibition.

In vitro, recombinant CypA promotes activation of macrophages but not epithelial cells

To expand on the findings in chapter 5 and clarify the effects of CypA on each cell, we returned to *in vitro* studies. AECs and macrophages were separately stimulated with recombinant CypA to determine if CypA had a direct effect on either cell.

There were two main findings from these studies. Firstly, stimulation of macrophages with recombinant CypA leads to cell activation. We demonstrated a polarisation of macrophages towards an M1 pro-inflammatory phenotype. The cells displayed significant upregulation of ICAM-1, MHC-II, CD86 and downregulation of the M2 marker CD206. Additionally, secretion of pro-inflammatory cytokine IL-6 was increased, and conditioned supernatants from murine bone marrow-derived macrophages were also found to contain elevated levels of nitric oxide, consistent with increased cell activation. Secondly, incubation of epithelial cells with recombinant CypA failed to result in any cell activation. Similar markers were assessed but unlike macrophages, no increase in ICAM-1 expression or IL-6 secretion was observed in A549 cells. Together, the findings presented within chapter 6 supports a directionality of cell signalling whereby CypA is secreted by AECs and then proceeds to target local alveolar macrophages, promoting cell activation.

Extracellular CypA is significantly increased in ARDS patients

Finally, we demonstrate, for the first time, that extracellular levels of CypA are substantially increased in BAL samples obtained from ARDS patients at baseline (i.e. within 48 to 72 hours of intubation). These data confirm the involvement of CypA in human disease, providing further encouraging evidence to support the novel mediator CypA as a promising therapeutic target amenable to prophylactic blockade.

The findings presented within this thesis certainly makes CypA an attractive therapeutic target in VILI. However, in light of the overwhelmingly negative track record of the translation of targeted pharmacological interventions from experimental studies to clinical trials, we need to

ask ourselves the important question of whether this mediator is a plausible therapeutic target. Wilson and Takata proposed that a mediator's likely usefulness may be evaluated based on three main criteria: (1) How 'upstream' it is within that pathway, (2) Whether it plays a key regulatory role in the pathogenesis of VILI, and (3) How impressive the effects of modulating the target mediator are (470). Based on these criteria, we propose that CypA is a plausible target. In Chapter 3, we demonstrated that CypA is released early into the alveolar space early in the course of VILI before significant signs of lung injury are present. Importantly, we show that patients with ARDS also had substantially elevated BAL levels of CypA at baseline (i.e. when patients present for treatment). As an early mediator, CypA would be amenable to prophylactic blockade before clinicians commence mechanical ventilation. Furthermore, in this chapter, we show that inhibition of CypA results in impressive, objective, and physiologically relevant attenuation of VILI, which suggests that CypA does play a key regulatory role in the pathogenesis of VILI as opposed to being part of the general cellular inflammatory machinery.

Proposed pathway of CypA:CD147 signalling during VILI

Putting everything together, we propose the following pathway by which the CypA:CD147 mediates pro-inflammatory signalling during VILI. In response to pulmonary insult, such as mechanical ventilation, there is an upregulation of surface expression of CD147. At the same time, CypA is secreted by AECs into the alveolar space via an active process. Once within the extracellular space, CypA then interacts with its receptor, CD147, on alveolar macrophages. This promotes cell activation and propagation of downstream inflammatory, which may include secretion of pro-inflammatory cytokines and MMPs.

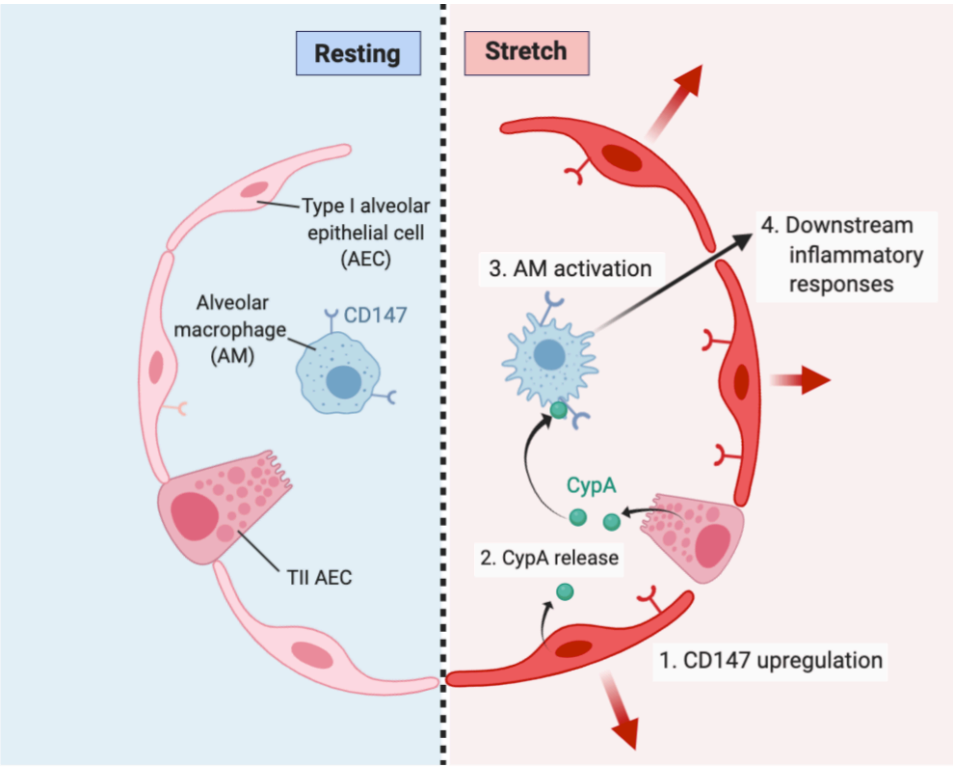


Figure 7.1 - Propose schematic for the CypA:CD147 signalling pathway during VILI

7.3 Limitations of work in this thesis

The work presented in this thesis is not without its limitations.

7.3.1 VILI model

The model we used throughout this thesis was also a 'pure' one-hit VILI model. While these high stretch models are generally crucial for understanding the biological mechanisms, it may be argued that it fails to fully reflect the clinical picture of ARDS patients who are often ventilated in the presence of a pre-existing lung injury. Another aspect of the model to consider is the age of the mice used. Here, all animals were aged between 7-14 weeks old (i.e. young adults). We know, however, that advanced age is associated with increased mortality in ARDS patients (471). Thus, it might be more appropriate to perform our investigations with older animals.

7.3.2 Utilisation of different techniques to determine the source of CypA during VILI

Although we did attempt to use several approaches to determine the source of CypA during VILI, the majority of these were flow cytometry based. One of the key limitations of this work is therefore not using alternative strategies with different techniques to answer the research question posed. In attempting to identify the source of CypA, a number of other techniques should have been considered, including:

a) Using quantitative real-time PCR to measure mRNA expression levels of CypA in each respective cell type, including AECs, alveolar macrophages and endothelial cells to look at upregulation of CypA at a messaging level.
b) Using imaging techniques to localise areas of upregulated CypA expression at the protein level, such as immunohistochemical staining or confocal immunofluorescence microscopy.

The above methods could have been used in conjunction with either our *in vivo* model by analysing frozen lung sections or our *in vitro* stretch model.

7.3.3 MM-284 target engagement data

In Chapter 5, we ascribed the effects of MM-284 to CypA antagonism based on what is reported of its pharmacological activities in the literature. However, the data in this chapter would have been more convincing if we had included evidence of target engagement. This could have been demonstrated by measuring the peptidyl prolyl *cis/trans* isomerase activity of recombinant CypA with and without MM-284.

7.4 Future work

1) To what extent is CD147 involved in CypA mediated inflammatory signalling during VILI?

As yet, we have not identified a mechanistic pathway for CypA signalling and its downstream effects. One of the key questions here is the extent to which CypA signalling is dependent on CD147. As discussed previously, there is also evidence to suggest that CypA may mediate its effects through receptors apart from CD147.

In our *in vivo* experiments, we had assumed that CD147 was involved on the basis that the CypA inhibitor (MM-284) used in the experiments works by inhibiting its peptidyl-prolyl *cis-trans* isomerase (PPIase) activity which is crucial for signalling through CD147. However, we did not provide direct evidence to show that CD147 is involved. Therefore, additional experiments where the CD147 receptor is blocked may provide further insight into its role. This could be clarified *in vivo* using an anti-CD147 antibody. Further, we could also evaluate the effects of using both a CypA and CD147 inhibitor. If simultaneous blockade of both CypA and CD147 does not result in additional protection, this may suggest that they are involved in the same pathway. Additionally, further *in vitro* experiments exploring the contribution of CD147 to any observed CypA-induced responses in different cell types may also be informative. Again, this can be achieved through the use of an anti-CD147 antibody or by siRNA knockdown of CD147.

2) Is endogenously secreted CypA different from recombinant CypA? If so, how does one compare against the other?

We are beginning to appreciate that the form in which proteins are secreted or delivered to cells has a crucial impact on its effects. For instance, our laboratory has recently showed that the form in which pro-inflammatory cytokine tumour necrosis factor (TNF) is secreted has a

crucial impact on its *in vivo* effect (472). To do so, we performed experiments where the biological effects of two different forms of TNF – recombinant TNF and TNF packaged within microvesicles (MVs) – were compared. Intratracheal instillation of the different forms of TNF produced vastly different effects. While MV enclosed TNF cause a significant increase in inflammatory monocyte recruitment, CXCL1 release, alveolar epithelial cell activation, and increase in lung permeability, no signs of inflammation were seen with soluble recombinant TNF.

Interestingly, there is also evidence to suggest that recombinant CypA may behave differently to endogenous CypA. Arora et al have made preliminary observations that intranasal delivery of recombinant CypA alone is not sufficient to initiate leukocytes influx into tissues. They hypothesised that the contribution of extracellular CypA during inflammatory responses is dependent on a primed, pro-inflammatory environment such as that which would have been provided by LPS, or the presence of other endogenous factors released during the inflammatory response. However, Sherry et al have previously demonstrated significant neutrophil influx when CypA was injected into footpads of mice (279). Crucially, chromatographically purified CypA from LPS stimulated primary murine macrophages and not recombinant CypA was used in this study.

While it is probable that the environment in which CypA is “seen” by cells is important, we hypothesis that the native form of CypA might actually possess different biological effects to recombinant CypA. A relatively straight-forward way of investigating this hypothesis would be to compare the effects of the following stimuli: recombinant CypA, supernatants from stretch human AECs known to contain CypA, and perhaps even BAL collected from animals subjected to high V_T ventilation ± CypA inhibitor.

This also leads to the question of how endogenous CypA is different to recombinant CypA. Could CypA also be packaged into MVs? As CypA is known to be a ubiquitously distributed intracellular protein and it has been identified in extracellular vesicles (473), it would certainly be feasible. In preliminary experiments, we examine the contents of MVs released during *in vivo* VILI for CypA. While we found that CypA was indeed present in MVs which were released early (at 1 hour) in the course of injury, further analyses revealed that only a relatively small proportion of total CypA was packaged into MVs. Additionally, we did not observe any MV release in response to cyclical stretching of primary human AECs *in vitro*.

Another potential explanation for the difference between endogenous and recombinant CypA and the difference for their biological activities is the occurrence of post-translational modifications. Others have demonstrated that CypA does undergo phosphorylation (474), glutathionylation (475), and acetylation (450, 468, 476). Many studies have suggested these post-translational modifications of CypA regulate key functions of CypA by modulating signal transduction and protein-protein interactions, affording it the ability to mediate diverse roles within and outside the cell.

In an *in vitro* study, it was found that large proportion (between 38-50%) of endogenous CypA in human cells (HeLa and Jurkat T cells) were acetylated (468). In another, acetylation was shown to be crucial for the secretion of CypA from vascular smooth muscles cells (450). Furthermore, there have been suggestions that oxidative stress regulates the acetylation and subsequent secretion of CypA (477). Given that mechanical stretch is known to evoke oxidative stress pathway and generate reactive oxygen species (ROS) (370-373), it is reasonable to suspect that CypA may also undergo acetylation in response to stretch. Interestingly, acetylated CypA has been shown to be more functionally active than native CypA. In an *in vitro* study, Soe et al stimulated vascular smooth muscle cells and endothelial

cells with both native and acetylated CypA and demonstrated significantly increased inflammation, cell proliferation, and cell death in response to the latter (450).

Given the growing body of evidence to suggest the importance of acetylation of CypA and its association with oxidative stress, further investigation into whether (1) it is involved in stretch induced CypA secretion, and (2) if it has any downstream biological consequences, is merited.

3) How else does extracellular CypA promote epithelial injury during VILI?

So far, we have demonstrated that blockade of CypA leads to a decrease in pulmonary cell activation and intra-alveolar MMP activity. However, these findings only partly answer why CypA inhibition leads to such impressive attenuation of VILI. Further investigation into the mechanisms through which extracellular CypA promotes epithelial injury are required to fully understand its role during VILI. Plausible avenues of investigation include:

i) Whether CypA contributes epithelial permeability, e.g. through alterations of epithelial tight junction protein expression, or modulation of cell cytoskeleton.

ii) Whether CypA leads to epithelial activation/injury indirectly, i.e. through first activating of alveolar macrophages, causing a release of pro-inflammatory mediators/signalling that subsequently contributes to epithelial activation. This could be assessed by:

   (a) Comparing the effects of stimulating cells with: recombinant CypA alone, supernatants from naïve macrophages, supernatants from macrophages pre-incubated with CypA ± MM-284.

   (b) Performing CypA stimulation experiments in a co-culture of AECs and alveolar macrophages. This model would have been particular useful due to the known *in situ* proximity of these two cell types and extensive interactions between the cell types.

iii) Investigation into the ability of CypA to promote apoptosis or necroptosis signalling. This could be determined by measuring caspase-3, -7 and/or staining cells for annexin V in

conjunction with propidium iodide to separate cells into healthy, early apoptotic, late apoptotic, and necroptotic cell populations.

4) Is extracellular CypA a potential therapeutic target?

The ultimate purpose of this thesis is to gain some insight into the mechanistic/pathogenic pathways of ALI with the hopes of identifying potential therapeutic targets. While the findings are very promising, further experiments are crucial in order to determine if inhibition of extracellular CypA can be translated from bench to the bedside. One of the reasons that inhibition of so many mediators/pathways have failed when trials move from the experimental to clinical phase may be the lack of translational animal models that truly mimic the clinical situation.

Therefore, assessment of CypA inhibition could be made more robust if it was assessed using a two-hit injury model. Our lab has recently demonstrated the use of such a model (478). In brief, we first induced acute lung injury by intranasal administration of endotoxin (LPS). Once ARDS was clinically established, we administered therapeutic treatment just prior to commencement of ventilation. If CypA inhibitors are still able to attenuate VILI in this model, then we could be more confident of its efficacy in a more clinically relevant scenario.

8 References

1. Ashbaugh D, Boyd Bigelow D, Petty T, Levine B. Acute Respiratory Distress in Adults. The Lancet. 1967;290(7511):319-23.

2. Bernard GR, Artigas A, Brigham KL, Carlet J, Falke K, Hudson L, et al. The American-European Consensus Conference on ARDS. Definitions, mechanisms, relevant outcomes, and clinical trial coordination. Am J Respir Crit Care Med. 1994 Mar;149(3 Pt 1):818-24. PubMed PMID: 7509706. Epub 1994/03/01. eng.

3. Ranieri VM, Rubenfeld GD, Thompson BT, Ferguson ND, Caldwell E, Fan E, et al. Acute respiratory distress syndrome: the Berlin Definition. Jama. 2012 Jun 20;307(23):2526-33. PubMed PMID: 22797452. Epub 2012/07/17. eng.

4. Ferguson ND, Meade MO, Hallett DC, Stewart TE. High values of the pulmonary artery wedge pressure in patients with acute lung injury and acute respiratory distress syndrome. Intensive Care Med. 2002 Aug;28(8):1073-7. PubMed PMID: 12185427. Epub 2002/08/20. eng.

5. Wheeler AP, Bernard GR, Thompson BT, Schoenfeld D, Wiedemann HP, deBoisblanc B, et al. Pulmonary-artery versus central venous catheter to guide treatment of acute lung injury. N Engl J Med. 2006 May 25;354(21):2213-24. PubMed PMID: 16714768. Epub 2006/05/23. eng.

6. Pham T, Rubenfeld GD. Fifty Years of Research in ARDS.The Epidemiology of Acute Respiratory Distress Syndrome. A 50th Birthday Review. American Journal of Respiratory and Critical Care Medicine. 2017 2017/04/01;195(7):860-70.

7. Sweatt AJ, Levitt JE. Evolving epidemiology and definitions of the acute respiratory distress syndrome and early acute lung injury. Clin Chest Med. 2014 Dec;35(4):609-24. PubMed PMID: 25453413. Epub 2014/12/03. eng.

8. Thompson BT, Chambers RC, Liu KD. Acute Respiratory Distress Syndrome. N Engl J Med. 2017 Aug 10;377(6):562-72. PubMed PMID: 28792873. Epub 2017/08/10. eng.

9. Bellani G, Laffey JG, Pham T, Fan E, Brochard L, Esteban A, et al. Epidemiology, Patterns of Care, and Mortality for Patients With Acute Respiratory Distress Syndrome in Intensive Care Units in 50 Countries. JAMA. 2016;315(8):788-800.

10. Summers C, Singh NR, Worpole L, Simmonds R, Babar J, Condliffe AM, et al. Incidence and recognition of acute respiratory distress syndrome in a UK intensive care unit. Thorax. 2016 Nov;71(11):1050-1. PubMed PMID: 27552782. PMCID: PMC5099179. Epub 2016/08/24. eng.

11. Matthay MA, Zemans RL, Zimmerman GA, Arabi YM, Beitler JR, Mercat A, et al. Acute respiratory distress syndrome. Nature Reviews Disease Primers. 2019 2019/03/14;5(1):18.

12. Meyer NJ, Li M, Feng R, Bradfield J, Gallop R, Bellamy S, et al. ANGPT2 genetic variant is associated with trauma-associated acute lung injury and altered plasma

angiopoietin-2 isoform ratio. American journal of respiratory and critical care medicine. 2011;183(10):1344-53. PubMed PMID: 21257790. Epub 2011/01/21. eng.

13. Meyer NJ, Feng R, Li M, Zhao Y, Sheu C-C, Tejera P, et al. IL1RN Coding Variant Is Associated with Lower Risk of Acute Respiratory Distress Syndrome and Increased Plasma IL-1 Receptor Antagonist. American Journal of Respiratory and Critical Care Medicine. 2013 2013/05/01;187(9):950-9.

14. Reutershan J, Ley K. Bench-to-bedside review: acute respiratory distress syndrome - how neutrophils migrate into the lung. Crit Care. 2004 Dec;8(6):453-61. PubMed PMID: 15566616. PMCID: PMC1065041. Epub 2004/11/30. eng.

15. Crosby LM, Waters CM. Epithelial repair mechanisms in the lung. Am J Physiol Lung Cell Mol Physiol. 2010 Jun;298(6):L715-31. PubMed PMID: 20363851. PMCID: PMC2886606. Epub 2010/04/07. eng.

16. Christie JD, Wurfel MM, Feng R, O'Keefe GE, Bradfield J, Ware LB, et al. Genome wide association identifies PPFIA1 as a candidate gene for acute lung injury risk following major trauma. PloS one. 2012;7(1):e28268-e. PubMed PMID: 22295056. Epub 2012/01/25. eng.

17. Moss M, Bucher B, Moore FA, Moore EE, Parsons PE. The role of chronic alcohol abuse in the development of acute respiratory distress syndrome in adults. Jama. 1996 Jan 3;275(1):50-4. PubMed PMID: 8531287. Epub 1996/01/03. eng.

18. Calfee CS, Matthay MA, Kangelaris KN, Siew ED, Janz DR, Bernard GR, et al. Cigarette Smoke Exposure and the Acute Respiratory Distress Syndrome. Crit Care Med. 2015 Sep;43(9):1790-7. PubMed PMID: 26010690. PMCID: PMC4737582. Epub 2015/05/27. eng.

19. Reilly JP, Zhao Z, Shashaty MGS, Koyama T, Christie JD, Lanken PN, et al. Low to Moderate Air Pollutant Exposure and Acute Respiratory Distress Syndrome after Severe Trauma. American Journal of Respiratory and Critical Care Medicine. 2019;199(1):62-70. PubMed PMID: 30067389.

20. Dancer RCA, Parekh D, Lax S, D'Souza V, Zheng S, Bassford CR, et al. Vitamin D deficiency contributes directly to the acute respiratory distress syndrome (ARDS). Thorax. 2015;70(7):617-24.

21. Ryb GE, Cooper C. Race/ethnicity and acute respiratory distress syndrome: a National Trauma Data Bank study. J Natl Med Assoc. 2010 Oct;102(10):865-9. PubMed PMID: 21053700. Epub 2010/11/09. eng.

22. Erickson SE, Shlipak MG, Martin GS, Wheeler AP, Ancukiewicz M, Matthay MA, et al. Racial and ethnic disparities in mortality from acute lung injury. Crit Care Med. 2009 Jan;37(1):1-6. PubMed PMID: 19050621. PMCID: PMC2696263. Epub 2008/12/04. eng.

23. Matthay MA, Zemans RL. The acute respiratory distress syndrome: pathogenesis and treatment. Annu Rev Pathol. 2011;6:147-63. PubMed PMID: 20936936. PMCID: PMC3108259. Epub 2010/10/13. eng.

24. Mackay A, Al-Haddad M. Acute lung injury and acute respiratory distress syndrome. Continuing Education in Anaesthesia Critical Care & Pain. 2009;9(5):152-6.

25. Katzenstein AL, Bloor CM, Leibow AA. Diffuse alveolar damage--the role of oxygen, shock, and related factors. A review. The American journal of pathology. 1976;85(1):209-28. PubMed PMID: 788524. eng.

26. Ichikado K, Muranaka H, Gushima Y, Kotani T, Nader HM, Fujimoto K, et al. Fibroproliferative changes on high-resolution CT in the acute respiratory distress syndrome predict mortality and ventilator dependency: a prospective observational cohort study. BMJ Open. 2012;2(2):e000545.

27. Papazian L, Doddoli C, Chetaille B, Gernez Y, Thirion X, Roch A, et al. A contributive result of open-lung biopsy improves survival in acute respiratory distress syndrome patients. Critical care medicine. 2007 2007/03//;35(3):755-62. PubMed PMID: 17255856. eng.

28. Martin C, Papazian L, Payan MJ, Saux P, Gouin F. Pulmonary fibrosis correlates with outcome in adult respiratory distress syndrome. A study in mechanically ventilated patients. Chest. 1995 Jan;107(1):196-200. PubMed PMID: 7813276. Epub 1995/01/01. eng.

29. Wiedemann HP, Wheeler AP, Bernard GR, Thompson BT, Hayden D, deBoisblanc B, et al. Comparison of two fluid-management strategies in acute lung injury. N Engl J Med. 2006 Jun 15;354(24):2564-75. PubMed PMID: 16714767. Epub 2006/05/23. eng.

30. Griffiths MJD, McAuley DF, Perkins GD, Barrett N, Blackwood B, Boyle A, et al. Guidelines on the management of acute respiratory distress syndrome. BMJ Open Respiratory Research. 2019;6(1):e000420.

31. Bernard GR, Luce JM, Sprung CL, Rinaldo JE, Tate RM, Sibbald WJ, et al. High-dose corticosteroids in patients with the adult respiratory distress syndrome. N Engl J Med. 1987 Dec 17;317(25):1565-70. PubMed PMID: 3317054. Epub 1987/12/17. eng.

32. Duggal A, Ganapathy A, Ratnapalan M, Adhikari NK. Pharmacological treatments for acute respiratory distress syndrome: systematic review. Minerva Anestesiol. 2015 May;81(5):567-88. PubMed PMID: 24937499. Epub 2014/06/18. eng.

33. Kor DJ, Erlich J, Gong MN, Malinchoc M, Carter RE, Gajic O, et al. Association of prehospitalization aspirin therapy and acute lung injury: results of a multicenter international observational study of at-risk patients. Crit Care Med. 2011 Nov;39(11):2393-400. PubMed PMID: 21725238. PMCID: PMC3196806. Epub 2011/07/05. eng.

34. Simonis FD, de Iudicibus G, Cremer OL, Ong DSY, van der Poll T, Bos LD, et al. Macrolide therapy is associated with reduced mortality in acute respiratory distress syndrome

(ARDS) patients. Ann Transl Med. 2018 Jan;6(2):24. PubMed PMID: 29430441. PMCID: PMC5799146. Epub 2018/02/13. eng.

35. Walkey AJ, Wiener RS. Macrolide antibiotics and survival in patients with acute lung injury. Chest. 2012 May;141(5):1153-9. PubMed PMID: 22116799. PMCID: PMC3342785. Epub 2011/11/26. eng.

36. McAuley DF, Cross LM, Hamid U, Gardner E, Elborn JS, Cullen KM, et al. Keratinocyte growth factor for the treatment of the acute respiratory distress syndrome (KARE): a randomised, double-blind, placebo-controlled phase 2 trial. Lancet Respir Med. 2017 Jun;5(6):484-91. PubMed PMID: 28526233. Epub 2017/05/21. eng.

37. Paine R, 3rd, Standiford TJ, Dechert RE, Moss M, Martin GS, Rosenberg AL, et al. A randomized trial of recombinant human granulocyte-macrophage colony stimulating factor for patients with acute lung injury. Crit Care Med. 2012 Jan;40(1):90-7. PubMed PMID: 21926600. PMCID: PMC3242850. Epub 2011/09/20. eng.

38. Mac Sweeney R, McAuley DF. Mesenchymal stem cell therapy in acute lung injury: is it time for a clinical trial? Thorax. 2012 Jun;67(6):475-6. PubMed PMID: 22504891. Epub 2012/04/17. eng.

39. Matthay MA, Calfee CS, Zhuo H, Thompson BT, Wilson JG, Levitt JE, et al. Treatment with allogeneic mesenchymal stromal cells for moderate to severe acute respiratory distress syndrome (START study): a randomised phase 2a safety trial. Lancet Respir Med. 2019 Feb;7(2):154-62. PubMed PMID: 30455077. Epub 2018/11/21. eng.

40. Bernard GR, Wheeler AP, Arons MM, Morris PE, Paz HL, Russell JA, et al. A trial of antioxidants N-acetylcysteine and procysteine in ARDS. The Antioxidant in ARDS Study Group. Chest. 1997 Jul;112(1):164-72. PubMed PMID: 9228372. Epub 1997/07/01. eng.

41. Zeiher BG, Artigas A, Vincent JL, Dmitrienko A, Jackson K, Thompson BT, et al. Neutrophil elastase inhibition in acute lung injury: results of the STRIVE study. Crit Care Med. 2004 Aug;32(8):1695-702. PubMed PMID: 15286546. Epub 2004/08/03. eng.

42. McAuley DF, Laffey JG, O'Kane CM, Perkins GD, Mullan B, Trinder TJ, et al. Simvastatin in the Acute Respiratory Distress Syndrome. New England Journal of Medicine. 2014;371(18):1695-703. PubMed PMID: 25268516.

43. Matthay MA, Brower RG, Carson S, Douglas IS, Eisner M, Hite D, et al. Randomized, placebo-controlled clinical trial of an aerosolized β_2-agonist for treatment of acute lung injury. Am J Respir Crit Care Med. 2011 Sep 1;184(5):561-8. PubMed PMID: 21562125. PMCID: PMC3175548. Epub 2011/05/13. eng.

44. Gates S, Perkins GD, Lamb SE, Kelly C, Thickett DR, Young JD, et al. Beta-Agonist Lung injury TrIal-2 (BALTI-2): a multicentre, randomised, double-blind, placebo-controlled trial and economic evaluation of intravenous infusion of salbutamol versus placebo in patients with

acute respiratory distress syndrome. Health Technol Assess. 2013 Sep;17(38):v-vi, 1-87. PubMed PMID: 24028755. PMCID: PMC4781532. Epub 2013/09/14. eng.

45. Anzueto A, Baughman RP, Guntupalli KK, Weg JG, Wiedemann HP, Raventós AA, et al. Aerosolized Surfactant in Adults with Sepsis-Induced Acute Respiratory Distress Syndrome. New England Journal of Medicine. 1996;334(22):1417-22. PubMed PMID: 8618579.

46. Shari G, Kojicic M, Li G, Cartin-Ceba R, Alvarez CT, Kashyap R, et al. Timing of the Onset of Acute Respiratory Distress Syndrome: A Population-Based Study. Respiratory Care. 2011;56(5):576-82.

47. Xiong B, Wang C, Tan J, Cao Y, Zou Y, Yao Y, et al. Statins for the prevention and treatment of acute lung injury and acute respiratory distress syndrome: A systematic review and meta-analysis. Respirology. 2016;21(6):1026-33.

48. Yadav H, Kor DJ. Platelets in the pathogenesis of acute respiratory distress syndrome. Am J Physiol Lung Cell Mol Physiol. 2015 Nov 1;309(9):L915-23. PubMed PMID: 26320157. PMCID: PMC4628982. Epub 2015/09/01. eng.

49. Respirator Lung Syndrome. Can Fam Physician. 1967;13(9):57-9. PubMed PMID: PMC2280710. eng.

50. Macklin MT, Macklin CC. Malignant interstitial emphysema of the lungs and mediastinum as an important occult complication in many respiratory diseases and other conditions: an interpretation of the clinical literature in the light of laboratory experiment. Medicine. 1944;23(4).

51. Webb HH, Tierney DF. Experimental pulmonary edema due to intermittent positive pressure ventilation with high inflation pressures. Protection by positive end-expiratory pressure. Am Rev Respir Dis. 1974 Nov;110(5):556-65. PubMed PMID: 4611290. Epub 1974/11/01. eng.

52. Cooper JA, van der Zee H, Line BR, Malik AB. Relationship of end-expiratory pressure, lung volume, and 99mTc-DTPA clearance. J Appl Physiol (1985). 1987 Oct;63(4):1586-90. PubMed PMID: 3320010. Epub 1987/10/01. eng.

53. Egan EA, 2nd. Effect of lung inflation on alveolar permeability to solutes. Ciba Found Symp. 1976 (38):101-14. PubMed PMID: 1047637. Epub 1976/01/01. eng.

54. Egan EA. Response of alveolar epithelial solute permeability to changes in lung inflation. J Appl Physiol Respir Environ Exerc Physiol. 1980 Dec;49(6):1032-6. PubMed PMID: 7440291. Epub 1980/12/01. eng.

55. Parker JC, Townsley MI, Rippe B, Taylor AE, Thigpen J. Increased microvascular permeability in dog lungs due to high peak airway pressures. J Appl Physiol Respir Environ Exerc Physiol. 1984 Dec;57(6):1809-16. PubMed PMID: 6511554. Epub 1984/12/01. eng.

56. Dreyfuss D, Soler P, Basset G, Saumon G. High inflation pressure pulmonary-edema - respective effects of high airway pressure, high tidal volume, and positive end-expiratory pressure. Am Rev Respir Dis. 1988 May;137(5):1159-64. PubMed PMID: WOS:A1988N412300031. English.

57. Dreyfuss D, Saumon G. Barotrauma is volutrauma, but which volume is the one responsible? Intensive Care Med. 1992;18(3):139-41. PubMed PMID: 1644960. Epub 1992/01/01. eng.

58. Gattinoni L, Pesenti A. The concept of "baby lung". Intensive Care Med. 2005 Jun;31(6):776-84. PubMed PMID: 15812622. Epub 2005/04/07. eng.

59. Slutsky AS. Lung injury caused by mechanical ventilation. Chest. 1999 Jul;116(1 Suppl):9s-15s. PubMed PMID: 10424561. Epub 1999/07/29. eng.

60. Albert RK. The role of ventilation-induced surfactant dysfunction and atelectasis in causing acute respiratory distress syndrome. Am J Respir Crit Care Med. 2012 Apr 1;185(7):702-8. PubMed PMID: 22227381. Epub 2012/01/10. eng.

61. Mead J, Takishima T, Leith D. Stress distribution in lungs: a model of pulmonary elasticity. J Appl Physiol. 1970 May;28(5):596-608. PubMed PMID: 5442255. Epub 1970/05/01. eng.

62. Uhlig S, Ranieri M, Slutsky AS. Biotrauma hypothesis of ventilator-induced lung injury. Am J Respir Crit Care Med. 2004 Jan 15;169(2):314-5; author reply 5. PubMed PMID: 14718244. Epub 2004/01/14. eng.

63. Slutsky AS, Tremblay LN. Multiple System Organ Failure. American Journal of Respiratory and Critical Care Medicine. 1998 1998/06/01;157(6):1721-5.

64. Kawano T, Mori S, Cybulsky M, Burger R, Ballin A, Cutz E, et al. Effect of granulocyte depletion in a ventilated surfactant-depleted lung. J Appl Physiol (1985). 1987 Jan;62(1):27-33. PubMed PMID: 3558186. Epub 1987/01/01. eng.

65. Matzinger P. The danger model: a renewed sense of self. Science. 2002 Apr 12;296(5566):301-5. PubMed PMID: 11951032. Epub 2002/04/16. eng.

66. Bianchi ME. DAMPs, PAMPs and alarmins: all we need to know about danger. J Leukoc Biol. 2007 Jan;81(1):1-5. PubMed PMID: 17032697. Epub 2006/10/13. eng.

67. Tremblay L, Valenza F, Ribeiro SP, Li J, Slutsky AS. Injurious ventilatory strategies increase cytokines and c-fos m-RNA expression in an isolated rat lung model. J Clin Invest. 1997 Mar 1;99(5):944-52. PubMed PMID: 9062352. PMCID: PMC507902. Epub 1997/03/01. eng.

68. Whitehead TC, Zhang H, Mullen B, Slutsky AS. Effect of mechanical ventilation on cytokine response to intratracheal lipopolysaccharide. Anesthesiology. 2004 Jul;101(1):52-8. PubMed PMID: 15220771. Epub 2004/06/29. eng.

69. Chu EK, Whitehead T, Slutsky AS. Effects of cyclic opening and closing at low- and high-volume ventilation on bronchoalveolar lavage cytokines. Crit Care Med. 2004 Jan;32(1):168-74. PubMed PMID: 14707576. Epub 2004/01/07. eng.
70. Bailey TC, Martin EL, Zhao L, Veldhuizen RA. High oxygen concentrations predispose mouse lungs to the deleterious effects of high stretch ventilation. J Appl Physiol (1985). 2003 Mar;94(3):975-82. PubMed PMID: 12571129. Epub 2003/02/07. eng.
71. von Bethmann AN, Brasch F, Nüsing R, Vogt K, Volk HD, Müller KM, et al. Hyperventilation induces release of cytokines from perfused mouse lung. Am J Respir Crit Care Med. 1998 Jan;157(1):263-72. PubMed PMID: 9445308. Epub 1998/01/28. eng.
72. Ricard JD, Dreyfuss D, Saumon G. Production of inflammatory cytokines in ventilator-induced lung injury: a reappraisal. Am J Respir Crit Care Med. 2001 Apr;163(5):1176-80. PubMed PMID: 11316656. Epub 2001/04/24. eng.
73. Cheng KC, Zhang H, Lin CY, Slutsky AS. Ventilation with negative airway pressure induces a cytokine response in isolated mouse lung. Anesth Analg. 2002 Jun;94(6):1577-82, table of contents. PubMed PMID: 12032030. Epub 2002/05/29. eng.
74. Held HD, Boettcher S, Hamann L, Uhlig S. Ventilation-induced chemokine and cytokine release is associated with activation of nuclear factor-kappaB and is blocked by steroids. Am J Respir Crit Care Med. 2001 Mar;163(3 Pt 1):711-6. PubMed PMID: 11254529. Epub 2001/03/20. eng.
75. Ranieri VM, Suter PM, Tortorella C, De Tullio R, Dayer JM, Brienza A, et al. Effect of mechanical ventilation on inflammatory mediators in patients with acute respiratory distress syndrome: a randomized controlled trial. Jama. 1999 Jul 7;282(1):54-61. PubMed PMID: 10404912. Epub 1999/07/15. eng.
76. Ranieri VM, Giunta F, Suter PM, Slutsky AS. Mechanical ventilation as a mediator of multisystem organ failure in acute respiratory distress syndrome. Jama. 2000 Jul 5;284(1):43-4. PubMed PMID: 10872010. Epub 2000/06/29. eng.
77. Ventilation with Lower Tidal Volumes as Compared with Traditional Tidal Volumes for Acute Lung Injury and the Acute Respiratory Distress Syndrome. New England Journal of Medicine. 2000;342(18):1301-8. PubMed PMID: 10793162.
78. Meduri GU, Kohler G, Headley S, Tolley E, Stentz F, Postlethwaite A. Inflammatory cytokines in the BAL of patients with ARDS. Persistent elevation over time predicts poor outcome. Chest. 1995 Nov;108(5):1303-14. PubMed PMID: 7587434. Epub 1995/11/01. eng.
79. Wolthuis EK, Vlaar AP, Choi G, Roelofs JJ, Juffermans NP, Schultz MJ. Mechanical ventilation using non-injurious ventilation settings causes lung injury in the absence of pre-existing lung injury in healthy mice. Crit Care. 2009;13(1):R1. PubMed PMID: 19152704. PMCID: PMC2688111. Epub 2009/01/21. eng.

80. Vaneker M, Halbertsma FJ, van Egmond J, Netea MG, Dijkman HB, Snijdelaar DG, et al. Mechanical ventilation in healthy mice induces reversible pulmonary and systemic cytokine elevation with preserved alveolar integrity: an in vivo model using clinical relevant ventilation settings. Anesthesiology. 2007 Sep;107(3):419-26. PubMed PMID: 17721244. Epub 2007/08/28. eng.

81. Hauber HP, Karp D, Goldmann T, Vollmer E, Zabel P. Effect of low tidal volume ventilation on lung function and inflammation in mice. BMC Pulm Med. 2010;10:21-. PubMed PMID: 20409304. eng.

82. Bein T, Weber-Carstens S, Goldmann A, Müller T, Staudinger T, Brederlau J, et al. Lower tidal volume strategy (≈3 ml/kg) combined with extracorporeal CO2 removal versus 'conventional' protective ventilation (6 ml/kg) in severe ARDS: the prospective randomized Xtravent-study. Intensive Care Med. 2013 May;39(5):847-56. PubMed PMID: 23306584. PMCID: PMC3625408. Epub 2013/01/12. eng.

83. Terragni PP, Del Sorbo L, Mascia L, Urbino R, Martin EL, Birocco A, et al. Tidal volume lower than 6 ml/kg enhances lung protection: role of extracorporeal carbon dioxide removal. Anesthesiology. 2009 Oct;111(4):826-35. PubMed PMID: 19741487. Epub 2009/09/11. eng.

84. Dreyfuss D, Ricard JD, Saumon G. On the physiologic and clinical relevance of lung-borne cytokines during ventilator-induced lung injury. Am J Respir Crit Care Med. 2003 Jun 1;167(11):1467-71. PubMed PMID: 12770853. Epub 2003/05/29. eng.

85. Dreyfuss D, Rouby JJ. Mechanical ventilation-induced lung release of cytokines: a key for the future or pandora's box? Anesthesiology. 2004 Jul;101(1):1-3. PubMed PMID: 15220762. Epub 2004/06/29. eng.

86. Tremblay LN, Slutsky AS. Pathogenesis of ventilator-induced lung injury: trials and tribulations. Am J Physiol Lung Cell Mol Physiol. 2005 Apr;288(4):L596-8. PubMed PMID: 15757952. Epub 2005/03/11. eng.

87. Wilson MR, Choudhury S, Goddard ME, O'Dea KP, Nicholson AG, Takata M. High tidal volume upregulates intrapulmonary cytokines in an in vivo mouse model of ventilator-induced lung injury. J Appl Physiol (1985). 2003 Oct;95(4):1385-93. PubMed PMID: 12807894. Epub 2003/06/17. eng.

88. Wilson MR, Choudhury S, Takata M. Pulmonary inflammation induced by high-stretch ventilation is mediated by tumor necrosis factor signaling in mice. Am J Physiol Lung Cell Mol Physiol. 2005 Apr;288(4):L599-607. PubMed PMID: 15489373. Epub 2004/10/19. eng.

89. Belperio JA, Keane MP, Burdick MD, Londhe V, Xue YY, Li K, et al. Critical role for CXCR2 and CXCR2 ligands during the pathogenesis of ventilator-induced lung injury. The Journal of Clinical Investigation. 2002 12/01/;110(11):1703-16.

90. Bersten AD, Edibam C, Hunt T, Moran J. Incidence and mortality of acute lung injury and the acute respiratory distress syndrome in three Australian States. Am J Respir Crit Care Med. 2002 Feb 15;165(4):443-8. PubMed PMID: 11850334. Epub 2002/02/19. eng.

91. Montgomery AB, Stager MA, Carrico CJ, Hudson LD. Causes of mortality in patients with the adult respiratory distress syndrome. Am Rev Respir Dis. 1985 Sep;132(3):485-9. PubMed PMID: 4037521. Epub 1985/09/01. eng.

92. Valta P, Uusaro A, Nunes S, Ruokonen E, Takala J. Acute respiratory distress syndrome: frequency, clinical course, and costs of care. Crit Care Med. 1999 Nov;27(11):2367-74. PubMed PMID: 10579250. Epub 1999/12/01. eng.

93. Del Sorbo L, Slutsky AS. Acute respiratory distress syndrome and multiple organ failure. Current Opinion in Critical Care. 2011;17(1):1-6. PubMed PMID: 00075198-201102000-00002.

94. Lin CY, Zhang H, Cheng KC, Slutsky AS. Mechanical ventilation may increase susceptibility to the development of bacteremia. Crit Care Med. 2003 May;31(5):1429-34. PubMed PMID: 12771614. Epub 2003/05/29. eng.

95. Murphy DB, Cregg N, Tremblay L, Engelberts D, Laffey JG, Slutsky AS, et al. Adverse ventilatory strategy causes pulmonary-to-systemic translocation of endotoxin. Am J Respir Crit Care Med. 2000 Jul;162(1):27-33. PubMed PMID: 10903215. Epub 2000/07/21. eng.

96. Nahum A, Hoyt J, Schmitz L, Moody J, Shapiro R, Marini JJ. Effect of mechanical ventilation strategy on dissemination of intratracheally instilled Escherichia coli in dogs. Crit Care Med. 1997 Oct;25(10):1733-43. PubMed PMID: 9377891. Epub 1997/10/23. eng.

97. Terragni PP, Rosboch G, Tealdi A, Corno E, Menaldo E, Davini O, et al. Tidal hyperinflation during low tidal volume ventilation in acute respiratory distress syndrome. Am J Respir Crit Care Med. 2007 Jan 15;175(2):160-6. PubMed PMID: 17038660. Epub 2006/10/14. eng.

98. Amato MB, Meade MO, Slutsky AS, Brochard L, Costa EL, Schoenfeld DA, et al. Driving pressure and survival in the acute respiratory distress syndrome. N Engl J Med. 2015 Feb 19;372(8):747-55. PubMed PMID: 25693014. Epub 2015/02/19. eng.

99. Miller RR, 3rd, MacIntyre NR, Hite RD, Truwit JD, Brower RG, Morris AH. Point: should positive end-expiratory pressure in patients with ARDS be set on oxygenation? Yes. Chest. 2012 Jun;141(6):1379-82. PubMed PMID: 22670017. PMCID: PMC4349296 conflicts of interest: Dr MacIntyre has been a consultant for CareFusion Corporation since 1985. Dr Hite currently is a National Institutes of Health-funded investigator for studies related to ARDS. He also serves as a consultant (data safety and monitoring board chair) for a clinical trial sponsored by Cumberland Pharmaceuticals Inc and is a shareholder in Discovery Laboratories, Inc (both unrelated to the content of this article). Dr Hite has been an unfunded

speaker on the subject of mechanical ventilation and ARDS, which is relevant to the content of this article. Dr Truwit has received National Institutes of Health grant funding in ARDS and an ARDS-surfactant grant from PneumoPartners. Drs Miller, Brower, and Morris have reported that no potential conflicts of interest exist with any companies/organizations whose products or services may be discussed in this article. Epub 2012/06/07. eng.

100. Schmidt GA. Counterpoint: should positive end-expiratory pressure in patients with ARDS be set based on oxygenation? No. Chest. 2012 Jun;141(6):1382-4. PubMed PMID: 22670018. Epub 2012/06/07. eng.

101. Crotti S, Mascheroni D, Caironi P, Pelosi P, Ronzoni G, Mondino M, et al. Recruitment and Derecruitment during Acute Respiratory Failure. American Journal of Respiratory and Critical Care Medicine. 2001 2001/07/01;164(1):131-40.

102. VillagrÁ ANA, OchagavÍA ANA, Vatua S, Murias G, Del Mar FernÁNdez M, Aguilar JL, et al. Recruitment Maneuvers during Lung Protective Ventilation in Acute Respiratory Distress Syndrome. American Journal of Respiratory and Critical Care Medicine. 2002 2002/01/15;165(2):165-70.

103. Grasso SMD, Mascia LMD, Del Turco MMD, Malacarne PMD, Giunta FMD, Brochard LMD, et al. Effects of Recruiting Maneuvers in Patients with Acute Respiratory Distress Syndrome Ventilated with Protective Ventilatory Strategy. Anesthesiology: The Journal of the American Society of Anesthesiologists. 2002;96(4):795-802.

104. Mercat A, Richard JC, Vielle B, Jaber S, Osman D, Diehl JL, et al. Positive end-expiratory pressure setting in adults with acute lung injury and acute respiratory distress syndrome: a randomized controlled trial. Jama. 2008 Feb 13;299(6):646-55. PubMed PMID: 18270353. Epub 2008/02/14. eng.

105. Meade MO, Cook DJ, Guyatt GH, Slutsky AS, Arabi YM, Cooper DJ, et al. Ventilation strategy using low tidal volumes, recruitment maneuvers, and high positive end-expiratory pressure for acute lung injury and acute respiratory distress syndrome: a randomized controlled trial. Jama. 2008 Feb 13;299(6):637-45. PubMed PMID: 18270352. Epub 2008/02/14. eng.

106. Brower RG, Lanken PN, MacIntyre N, Matthay MA, Morris A, Ancukiewicz M, et al. Higher versus lower positive end-expiratory pressures in patients with the acute respiratory distress syndrome. N Engl J Med. 2004 Jul 22;351(4):327-36. PubMed PMID: 15269312. Epub 2004/07/23. eng.

107. Briel M, Meade M, Mercat A, Brower RG, Talmor D, Walter SD, et al. Higher vs lower positive end-expiratory pressure in patients with acute lung injury and acute respiratory distress syndrome: systematic review and meta-analysis. Jama. 2010 Mar 3;303(9):865-73. PubMed PMID: 20197533. Epub 2010/03/04. eng.

108. Fan E, Del Sorbo L, Goligher EC, Hodgson CL, Munshi L, Walkey AJ, et al. An Official American Thoracic Society/European Society of Intensive Care Medicine/Society of Critical Care Medicine Clinical Practice Guideline: Mechanical Ventilation in Adult Patients with Acute Respiratory Distress Syndrome. American Journal of Respiratory and Critical Care Medicine. 2017 2017/05/01;195(9):1253-63.

109. Talmor D, Sarge T, Malhotra A, O'Donnell CR, Ritz R, Lisbon A, et al. Mechanical ventilation guided by esophageal pressure in acute lung injury. N Engl J Med. 2008 Nov 13;359(20):2095-104. PubMed PMID: 19001507. PMCID: PMC3969885. Epub 2008/11/13. eng.

110. Beitler JR, Sarge T, Banner-Goodspeed VM, Gong MN, Cook D, Novack V, et al. Effect of Titrating Positive End-Expiratory Pressure (PEEP) With an Esophageal Pressure-Guided Strategy vs an Empirical High PEEP-Fio2 Strategy on Death and Days Free From Mechanical Ventilation Among Patients With Acute Respiratory Distress Syndrome: A Randomized Clinical Trial. Jama. 2019 Mar 5;321(9):846-57. PubMed PMID: 30776290. PMCID: PMC6439595. Epub 2019/02/19. eng.

111. O'Gara B, Fan E, Talmor DS. Controversies in the Management of Severe ARDS: Optimal Ventilator Management and Use of Rescue Therapies. Semin Respir Crit Care Med. 2015 Dec;36(6):823-34. PubMed PMID: 26595042. Epub 2015/11/26. eng.

112. Goligher EC, Kavanagh BP, Rubenfeld GD, Adhikari NK, Pinto R, Fan E, et al. Oxygenation response to positive end-expiratory pressure predicts mortality in acute respiratory distress syndrome. A secondary analysis of the LOVS and ExPress trials. Am J Respir Crit Care Med. 2014 Jul 1;190(1):70-6. PubMed PMID: 24919111. Epub 2014/06/12. eng.

113. Grasso S, Mascia L, Del Turco M, Malacarne P, Giunta F, Brochard L, et al. Effects of recruiting maneuvers in patients with acute respiratory distress syndrome ventilated with protective ventilatory strategy. Anesthesiology. 2002 Apr;96(4):795-802. PubMed PMID: 11964585. Epub 2002/04/20. eng.

114. Lim SC, Adams AB, Simonson DA, Dries DJ, Broccard AF, Hotchkiss JR, et al. Intercomparison of recruitment maneuver efficacy in three models of acute lung injury. Crit Care Med. 2004 Dec;32(12):2371-7. PubMed PMID: 15599138. Epub 2004/12/16. eng.

115. Cavalcanti AB, Suzumura É A, Laranjeira LN, Paisani DM, Damiani LP, Guimarães HP, et al. Effect of Lung Recruitment and Titrated Positive End-Expiratory Pressure (PEEP) vs Low PEEP on Mortality in Patients With Acute Respiratory Distress Syndrome: A Randomized Clinical Trial. Jama. 2017 Oct 10;318(14):1335-45. PubMed PMID: 28973363. PMCID: PMC5710484 Form for Disclosure of Potential Conflicts of Interest. All authors received grant support from Program to Support Institutional Development of Universal

System (PROADI) from the Brazilian Ministry of Health to conduct the study. Dr Amato also received grants from Timpel S. A. and Medtronic. No other disclosures are reported. Epub 2017/10/04. eng.

116. Brower RG, Morris A, MacIntyre N, Matthay MA, Hayden D, Thompson T, et al. Effects of recruitment maneuvers in patients with acute lung injury and acute respiratory distress syndrome ventilated with high positive end-expiratory pressure. Crit Care Med. 2003 Nov;31(11):2592-7. PubMed PMID: 14605529. Epub 2003/11/08. eng.

117. Goligher EC, Hodgson CL, Adhikari NKJ, Meade MO, Wunsch H, Uleryk E, et al. Lung Recruitment Maneuvers for Adult Patients with Acute Respiratory Distress Syndrome. A Systematic Review and Meta-Analysis. Annals of the American Thoracic Society. 2017 2017/10/01;14(Supplement_4):S304-S11.

118. Ferguson ND, Cook DJ, Guyatt GH, Mehta S, Hand L, Austin P, et al. High-frequency oscillation in early acute respiratory distress syndrome. N Engl J Med. 2013 Feb 28;368(9):795-805. PubMed PMID: 23339639. Epub 2013/01/24. eng.

119. Gattinoni L, Taccone P, Carlesso E, Marini JJ. Prone position in acute respiratory distress syndrome. Rationale, indications, and limits. Am J Respir Crit Care Med. 2013 Dec 1;188(11):1286-93. PubMed PMID: 24134414. Epub 2013/10/19. eng.

120. Gattinoni L, Carlesso E, Taccone P, Polli F, Guérin C, Mancebo J. Prone positioning improves survival in severe ARDS: a pathophysiologic review and individual patient meta-analysis. Minerva Anestesiol. 2010 Jun;76(6):448-54. PubMed PMID: 20473258. Epub 2010/05/18. eng.

121. Guérin C, Reignier J, Richard J-C, Beuret P, Gacouin A, Boulain T, et al. Prone Positioning in Severe Acute Respiratory Distress Syndrome. New England Journal of Medicine. 2013;368(23):2159-68. PubMed PMID: 23688302.

122. Mauri T, Cambiaghi B, Spinelli E, Langer T, Grasselli G. Spontaneous breathing: a double-edged sword to handle with care. Ann Transl Med. 2017 Jul;5(14):292. PubMed PMID: 28828367. PMCID: PMC5537122. Epub 2017/08/23. eng.

123. Arnal JM, Chatburn R. Paying attention to patient self-inflicted lung injury. Minerva Anestesiol. 2019 Sep;85(9):940-2. PubMed PMID: 31064175. Epub 2019/05/09. eng.

124. Beitler JR, Sands SA, Loring SH, Owens RL, Malhotra A, Spragg RG, et al. Quantifying unintended exposure to high tidal volumes from breath stacking dyssynchrony in ARDS: the BREATHE criteria. Intensive Care Medicine. 2016 2016/09/01;42(9):1427-36.

125. Guervilly C, Bisbal M, Forel JM, Mechati M, Lehingue S, Bourenne J, et al. Effects of neuromuscular blockers on transpulmonary pressures in moderate to severe acute respiratory distress syndrome. Intensive Care Med. 2017 Mar;43(3):408-18. PubMed PMID: 28013329. Epub 2016/12/26. eng.

126. Papazian L, Forel J-M, Gacouin A, Penot-Ragon C, Perrin G, Loundou A, et al. Neuromuscular Blockers in Early Acute Respiratory Distress Syndrome. New England Journal of Medicine. 2010;363(12):1107-16. PubMed PMID: 20843245.
127. Early Neuromuscular Blockade in the Acute Respiratory Distress Syndrome. New England Journal of Medicine. 2019;380(21):1997-2008. PubMed PMID: 31112383.
128. Günther A, Siebert C, Schmidt R, Ziegler S, Grimminger F, Yabut M, et al. Surfactant alterations in severe pneumonia, acute respiratory distress syndrome, and cardiogenic lung edema. Am J Respir Crit Care Med. 1996 Jan;153(1):176-84. PubMed PMID: 8542113. Epub 1996/01/01. eng.
129. Verbrugge SJ, Vazquez de Anda G, Gommers D, Neggers SJ, Sorm V, Böhm SH, et al. Exogenous surfactant preserves lung function and reduces alveolar Evans blue dye influx in a rat model of ventilation-induced lung injury. Anesthesiology. 1998 Aug;89(2):467-74. PubMed PMID: 9710406. Epub 1998/08/26. eng.
130. Haitsma JJ, Uhlig S, Lachmann U, Verbrugge SJ, Poelma DL, Lachmann B. Exogenous surfactant reduces ventilator-induced decompartmentalization of tumor necrosis factor alpha in absence of positive end-expiratory pressure. Intensive Care Med. 2002 Aug;28(8):1131-7. PubMed PMID: 12185437. Epub 2002/08/20. eng.
131. Welk B, Malloy JL, Joseph M, Yao LJ, Veldhuizen AW. Surfactant treatment for ventilation-induced lung injury in rats: effects on lung compliance and cytokines. Exp Lung Res. 2001 Sep;27(6):505-20. PubMed PMID: 11558967. Epub 2001/09/18. eng.
132. Zambelli V, Bellani G, Amigoni M, Grassi A, Scanziani M, Farina F, et al. The effects of exogenous surfactant treatment in a murine model of two-hit lung injury. Anesth Analg. 2015 Feb;120(2):381-8. PubMed PMID: 25502842. Epub 2014/12/17. eng.
133. Willson DF, Thomas NJ, Markovitz BP, Bauman LA, DiCarlo JV, Pon S, et al. Effect of exogenous surfactant (calfactant) in pediatric acute lung injury: a randomized controlled trial. Jama. 2005 Jan 26;293(4):470-6. PubMed PMID: 15671432. Epub 2005/01/27. eng.
134. Boet A, Brat R, Aguilera SS, Tissieres P, De Luca D. Surfactant from neonatal to pediatric ICU: bench and bedside evidence. Minerva Anestesiol. 2014 Dec;80(12):1345-56. PubMed PMID: 24504167. Epub 2014/02/08. eng.
135. Lewis SR, Pritchard MW, Thomas CM, Smith AF. Pharmacological agents for adults with acute respiratory distress syndrome. Cochrane Database Syst Rev. 2019 Jul 23;7(7):Cd004477. PubMed PMID: 31334568. PMCID: PMC6646953 known Andrew F Smith: none known. Epub 2019/07/25. eng.
136. Meng SS, Chang W, Lu ZH, Xie JF, Qiu HB, Yang Y, et al. Effect of surfactant administration on outcomes of adult patients in acute respiratory distress syndrome: a meta-

analysis of randomized controlled trials. BMC Pulm Med. 2019 Jan 9;19(1):9. PubMed PMID: 30626363. PMCID: PMC6325713. Epub 2019/01/11. eng.

137. Weg JG, Balk RA, Tharratt RS, Jenkinson SG, Shah JB, Zaccardelli D, et al. Safety and potential efficacy of an aerosolized surfactant in human sepsis-induced adult respiratory distress syndrome. Jama. 1994 Nov 9;272(18):1433-8. PubMed PMID: 7933425. Epub 1994/11/09. eng.

138. Spragg RG, Lewis JF, Walmrath HD, Johannigman J, Bellingan G, Laterre PF, et al. Effect of recombinant surfactant protein C-based surfactant on the acute respiratory distress syndrome. N Engl J Med. 2004 Aug 26;351(9):884-92. PubMed PMID: 15329426. Epub 2004/08/27. eng.

139. Peek GJ, Mugford M, Tiruvoipati R, Wilson A, Allen E, Thalanany MM, et al. Efficacy and economic assessment of conventional ventilatory support versus extracorporeal membrane oxygenation for severe adult respiratory failure (CESAR): a multicentre randomised controlled trial. Lancet. 2009 Oct 17;374(9698):1351-63. PubMed PMID: 19762075. Epub 2009/09/19. eng.

140. Patroniti N, Zangrillo A, Pappalardo F, Peris A, Cianchi G, Braschi A, et al. The Italian ECMO network experience during the 2009 influenza A(H1N1) pandemic: preparation for severe respiratory emergency outbreaks. Intensive Care Medicine. 2011 2011/07/06;37(9):1447.

141. Australia T, Investigators* NZEMOI. Extracorporeal Membrane Oxygenation for 2009 Influenza A(H1N1) Acute Respiratory Distress Syndrome. JAMA. 2009;302(17):1888-95.

142. Noah MA, Peek GJ, Finney SJ, Griffiths MJ, Harrison DA, Grieve R, et al. Referral to an extracorporeal membrane oxygenation center and mortality among patients with severe 2009 influenza A(H1N1). Jama. 2011 Oct 19;306(15):1659-68. PubMed PMID: 21976615. Epub 2011/10/07. eng.

143. Combes A, Hajage D, Capellier G, Demoule A, Lavoué S, Guervilly C, et al. Extracorporeal Membrane Oxygenation for Severe Acute Respiratory Distress Syndrome. New England Journal of Medicine. 2018;378(21):1965-75. PubMed PMID: 29791822.

144. Hardin CC, Hibbert K. ECMO for Severe ARDS. New England Journal of Medicine. 2018;378(21):2032-4. PubMed PMID: 29791819.

145. Fanelli V, Ranieri MV, Mancebo J, Moerer O, Quintel M, Morley S, et al. Feasibility and safety of low-flow extracorporeal carbon dioxide removal to facilitate ultra-protective ventilation in patients with moderate acute respiratory distress sindrome. Crit Care. 2016 Feb 10;20:36. PubMed PMID: 26861596. PMCID: PMC4748548. Epub 2016/02/11. eng.

146. Combes A, Fanelli V, Pham T, Ranieri VM. Feasibility and safety of extracorporeal CO(2) removal to enhance protective ventilation in acute respiratory distress syndrome: the

SUPERNOVA study. Intensive Care Med. 2019 May;45(5):592-600. PubMed PMID: 30790030. Epub 2019/02/23. eng.

147. Fitzgerald M, Millar J, Blackwood B, Davies A, Brett SJ, McAuley DF, et al. Extracorporeal carbon dioxide removal for patients with acute respiratory failure secondary to the acute respiratory distress syndrome: a systematic review. Critical Care. 2014 2014/05/15;18(3):222.

148. Parker JC, Ivey CL, Tucker JA. Gadolinium prevents high airway pressure-induced permeability increases in isolated rat lungs. J Appl Physiol (1985). 1998 Apr;84(4):1113-8. PubMed PMID: 9516173. Epub 1998/05/09. eng.

149. Saldías FJ, Lecuona E, Comellas AP, Ridge KM, Rutschman DH, Sznajder JI. beta-adrenergic stimulation restores rat lung ability to clear edema in ventilator-associated lung injury. Am J Respir Crit Care Med. 2000 Jul;162(1):282-7. PubMed PMID: 10903255. Epub 2000/07/21. eng.

150. de Prost N, Dreyfuss D, Ricard JD, Saumon G. Terbutaline lessens protein fluxes across the alveolo-capillary barrier during high-volume ventilation. Intensive Care Med. 2008 Apr;34(4):763-70. PubMed PMID: 18097649. Epub 2007/12/22. eng.

151. Bertok S, Wilson MR, Morley PJ, de Wildt R, Bayliffe A, Takata M. Selective inhibition of intra-alveolar p55 TNF receptor attenuates ventilator-induced lung injury. Thorax. 2012 Mar;67(3):244-51. PubMed PMID: 22156959. PMCID: PMC3282043 and MT have no competing interests. Ethics approval: All protocols were approved by the ethical review board of Imperial College London as well as the GSK Policy on the Care, Welfare and Treatment of Laboratory Animals and carried out under the authority of the UK Home Office in accordance with the Animals (Scientific Procedures) Act 1986. Epub 2011/12/14. eng.

152. Uhlig U, Fehrenbach H, Lachmann RA, Goldmann T, Lachmann B, Vollmer E, et al. Phosphoinositide 3-OH kinase inhibition prevents ventilation-induced lung cell activation. Am J Respir Crit Care Med. 2004 Jan 15;169(2):201-8. PubMed PMID: 14578214. Epub 2003/10/28. eng.

153. Ren R, Mao Y, Ruan Z, Wang Y, Zhang Y, Du J, et al. Celastrol attenuates ventilator induced lung injury in mouse through inhibition of MAPK pathway. Int J Clin Exp Pathol. 2017;10(9):9302-9. PubMed PMID: 31966802. PMCID: PMC6965913. Epub 2017/09/01. eng.

154. Peng XQ, Damarla M, Skirball J, Nonas S, Wang XY, Han EJ, et al. Protective role of PI3-kinase/Akt/eNOS signaling in mechanical stress through inhibition of p38 mitogen-activated protein kinase in mouse lung. Acta Pharmacol Sin. 2010 Feb;31(2):175-83. PubMed PMID: 20139900. PMCID: PMC4002838. Epub 2010/02/09. eng.

155. Chimenti L, Luque T, Bonsignore MR, Ramírez J, Navajas D, Farré R. Pre-treatment with mesenchymal stem cells reduces ventilator-induced lung injury. European Respiratory Journal. 2012;40(4):939-48.
156. Lee J-W, Rocco PRM, Pelosi P. Mesenchymal stem cell therapy for acute respiratory distress syndrome: a light at the end of the tunnel? Anesthesiology. 2015;122(2):238-40. PubMed PMID: 25478942. eng.
157. Chen W, Epshtein Y, Ni X, Dull RO, Cress AE, Garcia JG, et al. Role of Integrin β4 in Lung Endothelial Cell Inflammatory Responses to Mechanical Stress. Sci Rep. 2015 Nov 17;5:16529. PubMed PMID: 26572585. PMCID: PMC4647208. Epub 2015/11/18. eng.
158. Müller HC, Hellwig K, Rosseau S, Tschernig T, Schmiedl A, Gutbier B, et al. Simvastatin attenuates ventilator-induced lung injury in mice. Crit Care. 2010;14(4):R143. PubMed PMID: 20673352. PMCID: PMC2945124. Epub 2010/08/03. eng.
159. Jiang JS, Wang LF, Chou HC, Chen CM. Angiotensin-converting enzyme inhibitor captopril attenuates ventilator-induced lung injury in rats. J Appl Physiol (1985). 2007 Jun;102(6):2098-103. PubMed PMID: 17317879. Epub 2007/02/24. eng.
160. Jerng JS, Hsu YC, Wu HD, Pan HZ, Wang HC, Shun CT, et al. Role of the renin-angiotensin system in ventilator-induced lung injury: an in vivo study in a rat model. Thorax. 2007 Jun;62(6):527-35. PubMed PMID: 17234658. PMCID: PMC2117227. Epub 2007/01/20. eng.
161. Matthay MA, McAuley DF, Ware LB. Clinical trials in acute respiratory distress syndrome: challenges and opportunities. Lancet Respir Med. 2017 Jun;5(6):524-34. PubMed PMID: 28664851. Epub 2017/07/01. eng.
162. Calfee CS, Delucchi K, Parsons PE, Thompson BT, Ware LB, Matthay MA. Subphenotypes in acute respiratory distress syndrome: latent class analysis of data from two randomised controlled trials. The Lancet Respiratory Medicine. 2014;2(8):611-20.
163. Calfee CS, Delucchi KL, Sinha P, Matthay MA, Hackett J, Shankar-Hari M, et al. Acute respiratory distress syndrome subphenotypes and differential response to simvastatin: secondary analysis of a randomised controlled trial. The Lancet Respiratory Medicine. 2018;6(9):691-8.
164. Wilson MR, Petrie JE, Shaw MW, Hu C, Oakley CM, Woods SJ, et al. High-Fat Feeding Protects Mice From Ventilator-Induced Lung Injury, Via Neutrophil-Independent Mechanisms. Crit Care Med. 2017 Aug;45(8):e831-e9. PubMed PMID: 28426531. PMCID: PMC5511730. Epub 2017/04/21.
165. Memtsoudis SG, Bombardieri AM, Ma Y, Walz JM, Chiu YL, Mazumdar M. Mortality of patients with respiratory insufficiency and adult respiratory distress syndrome after surgery:

the obesity paradox. J Intensive Care Med. 2012 Sep-Oct;27(5):306-11. PubMed PMID: 21778465. Epub 2011/07/23. eng.

166. De Jong A, Verzilli D, Jaber S. ARDS in Obese Patients: Specificities and Management. Critical Care. 2019 2019/03/09;23(1):74.

167. Sasabuchi Y, Yasunaga H, Matsui H, Lefor AT, Horiguchi H, Fushimi K, et al. The Dose-Response Relationship Between Body Mass Index and Mortality in Subjects Admitted to the ICU With and Without Mechanical Ventilation. Respir Care. 2015 Jul;60(7):983-91. PubMed PMID: 25691767. Epub 2015/02/19. eng.

168. Haseneen NA, Vaday GG, Zucker S, Foda HD. Mechanical stretch induces MMP-2 release and activation in lung endothelium: role of EMMPRIN. Am J Physiol Lung Cell Mol Physiol. 2003 Mar;284(3):L541-7. PubMed PMID: 12456388. Epub 2002/11/29. eng.

169. Foda HD, Rollo EE, Drews M, Conner C, Appelt K, Shalinsky DR, et al. Ventilator-induced lung injury upregulates and activates gelatinases and EMMPRIN: attenuation by the synthetic matrix metalloproteinase inhibitor, Prinomastat (AG3340). Am J Respir Cell Mol Biol. 2001 Dec;25(6):717-24. PubMed PMID: 11726397. Epub 2001/12/01.

170. Grass GD, Toole BP. How, with whom and when: an overview of CD147-mediated regulatory networks influencing matrix metalloproteinase activity. Biosci Rep. 2015 Nov 24;36(1):e00283. PubMed PMID: 26604323. PMCID: PMC4718507. Epub 2015/11/26.

171. Biswas C. Tumor cell stimulation of collagenase production by fibroblasts. Biochemical and Biophysical Research Communications. 1982 1982/12/15/;109(3):1026-34.

172. Altruda F, Cervella P, Gaeta ML, Daniele A, Giancotti F, Tarone G, et al. Cloning of cDNA for a novel mouse membrane glycoprotein (gp42): shared identity to histocompatibility antigens, immunoglobulins and neural-cell adhesion molecules. Gene. 1989 Dec 28;85(2):445-51. PubMed PMID: 2697642. Epub 1989/12/28. eng.

173. Biswas C, Zhang Y, DeCastro R, Guo H, Nakamura T, Kataoka H, et al. The human tumor cell-derived collagenase stimulatory factor (renamed EMMPRIN) is a member of the immunoglobulin superfamily. Cancer Res. 1995 Jan 15;55(2):434-9. PubMed PMID: 7812975. Epub 1995/01/15. eng.

174. Fadool JM, Linser PJ. 5A11 antigen is a cell recognition molecule which is involved in neuronal-glial interactions in avian neural retina. Dev Dyn. 1993 Apr;196(4):252-62. PubMed PMID: 8219348. Epub 1993/04/01. eng.

175. Finnemann SC, Marmorstein AD, Neill JM, Rodriguez-Boulan E. Identification of the retinal pigment epithelium protein RET-PE2 as CE-9/OX-47, a member of the immunoglobulin superfamily. Invest Ophthalmol Vis Sci. 1997 Oct;38(11):2366-74. PubMed PMID: 9344360. Epub 1997/10/31. eng.

176. Fossum S, Mallett S, Barclay AN. The MRC OX-47 antigen is a member of the immunoglobulin superfamily with an unusual transmembrane sequence. Eur J Immunol. 1991 Mar;21(3):671-9. PubMed PMID: 2009910. Epub 1991/03/01. eng.

177. Jiang JL, Zhou Q, Yu MK, Ho LS, Chen ZN, Chan HC. The involvement of HAb18G/CD147 in regulation of store-operated calcium entry and metastasis of human hepatoma cells. J Biol Chem. 2001 Dec 14;276(50):46870-7. PubMed PMID: 11591720. Epub 2001/10/10. eng.

178. Kasinrerk W, Fiebiger E, Stefanová I, Baumruker T, Knapp W, Stockinger H. Human leukocyte activation antigen M6, a member of the Ig superfamily, is the species homologue of rat OX-47, mouse basigin, and chicken HT7 molecule. J Immunol. 1992 Aug 1;149(3):847-54. PubMed PMID: 1634773. Epub 1992/08/01. eng.

179. Miyauchi T, Kanekura T, Yamaoka A, Ozawa M, Miyazawa S, Muramatsu T. Basigin, a new, broadly distributed member of the immunoglobulin superfamily, has strong homology with both the immunoglobulin V domain and the beta-chain of major histocompatibility complex class II antigen. J Biochem. 1990 Feb;107(2):316-23. PubMed PMID: 2361961. Epub 1990/02/01. eng.

180. Nehme CL, Cesario MM, Myles DG, Koppel DE, Bartles JR. Breaching the diffusion barrier that compartmentalizes the transmembrane glycoprotein CE9 to the posterior-tail plasma membrane domain of the rat spermatozoon. J Cell Biol. 1993 Feb;120(3):687-94. PubMed PMID: 8425897. PMCID: PMC2119531. Epub 1993/02/01. eng.

181. Schlosshauer B, Bauch H, Frank R. Neurothelin: amino acid sequence, cell surface dynamics and actin colocalization. Eur J Cell Biol. 1995 Oct;68(2):159-66. PubMed PMID: 8575462. Epub 1995/10/01. eng.

182. Seulberger H, Lottspeich F, Risau W. The inducible blood--brain barrier specific molecule HT7 is a novel immunoglobulin-like cell surface glycoprotein. Embo j. 1990 Jul;9(7):2151-8. PubMed PMID: 2357963. PMCID: PMC551936. Epub 1990/07/01. eng.

183. Spring FA, Holmes CH, Simpson KL, Mawby WJ, Mattes MJ, Okubo Y, et al. The Oka blood group antigen is a marker for the M6 leukocyte activation antigen, the human homolog of OX-47 antigen, basigin and neurothelin, an immunoglobulin superfamily molecule that is widely expressed in human cells and tissues. Eur J Immunol. 1997 Apr;27(4):891-7. PubMed PMID: 9130641. Epub 1997/04/01. eng.

184. Biswas C, Zhang Y, DeCastro R, Guo H, Nakamura T, Kataoka H, et al. The Human Tumor Cell-derived Collagenase Stimulatory Factor (Renamed EMMPRIN) Is a Member of the Immunoglobulin Superfamily. Cancer Research. 1995;55(2):434-9.

185. Kaname T, Miyauchi T, Kuwano A, Matsuda Y, Muramatsu T, Kajii T. Mapping basigin (BSG), a member of the immunoglobulin superfamily, to 19p13.3. Cytogenetic and Genome Research. 1993;64(3-4):195-7.
186. Belton RJ, Jr., Chen L, Mesquita FS, Nowak RA. Basigin-2 is a cell surface receptor for soluble basigin ligand. J Biol Chem. 2008 Jun 27;283(26):17805-14. PubMed PMID: 18434307. PMCID: PMC2440618. Epub 2008/04/25. eng.
187. Kaname T, Miyauchi T, Kuwano A, Matsuda Y, Muramatsu T, Kajii T. Mapping basigin (BSG), a member of the immunoglobulin superfamily, to 19p13.3. Cytogenet Cell Genet. 1993;64(3-4):195-7. PubMed PMID: 8404035. Epub 1993/01/01. eng.
188. Liao CG, Kong LM, Song F, Xing JL, Wang LX, Sun ZJ, et al. Characterization of basigin isoforms and the inhibitory function of basigin-3 in human hepatocellular carcinoma proliferation and invasion. Mol Cell Biol. 2011 Jul;31(13):2591-604. PubMed PMID: 21536654. PMCID: PMC3133368. Epub 2011/05/04. eng.
189. Liao C-G, Kong L-M, Song F, Xing J-L, Wang L-X, Sun Z-J, et al. Characterization of Basigin Isoforms and the Inhibitory Function of Basigin-3 in Human Hepatocellular Carcinoma Proliferation and Invasion. Molecular and Cellular Biology. 2011;31(13):2591-604.
190. Nehme CL, Fayos BE, Bartles JR. Distribution of the integral plasma membrane glycoprotein CE9 (MRC OX-47) among rat tissues and its induction by diverse stimuli of metabolic activation. Biochem J. 1995 Sep 1;310 (Pt 2)(Pt 2):693-8. PubMed PMID: 7654213. PMCID: PMC1135951. Epub 1995/09/01. eng.
191. Tang W, Chang SB, Hemler ME. Links between CD147 function, glycosylation, and caveolin-1. Mol Biol Cell. 2004 Sep;15(9):4043-50. PubMed PMID: 15201341. PMCID: PMC515339. Epub 2004/06/18. eng.
192. Yoshida S, Shibata M, Yamamoto S, Hagihara M, Asai N, Takahashi M, et al. Homo-oligomer formation by basigin, an immunoglobulin superfamily member, via its N-terminal immunoglobulin domain. Eur J Biochem. 2000 Jul;267(14):4372-80. PubMed PMID: 10880960. Epub 2000/07/06. eng.
193. Yan L, Zucker S, Toole BP. Roles of the multifunctional glycoprotein, emmprin (basigin; CD147), in tumour progression. Thromb Haemost. 2005 Feb;93(2):199-204. PubMed PMID: 15711733. Epub 2005/02/16. eng.
194. Sun J, Hemler ME. Regulation of MMP-1 and MMP-2 production through CD147/extracellular matrix metalloproteinase inducer interactions. Cancer Res. 2001 Mar 1;61(5):2276-81. PubMed PMID: 11280798. Epub 2001/03/31. eng.
195. Xiong L, Edwards CK, 3rd, Zhou L. The biological function and clinical utilization of CD147 in human diseases: a review of the current scientific literature. Int J Mol Sci. 2014 Sep 29;15(10):17411-41. PubMed PMID: 25268615. PMCID: PMC4227170. Epub 2014/10/01.

196. Yurchenko V, Constant S, Eisenmesser E, Bukrinsky M. Cyclophilin-CD147 interactions: a new target for anti-inflammatory therapeutics. Clin Exp Immunol. 2010 Jun;160(3):305-17. PubMed PMID: 20345978. PMCID: PMC2883100. Epub 2010/03/30.

197. Yurchenko V, Constant S, Bukrinsky M. Dealing with the family: CD147 interactions with cyclophilins. Immunology. 2006 Mar;117(3):301-9. PubMed PMID: 16476049. PMCID: PMC1782239. Epub 2006/02/16.

198. Pushkarsky T, Yurchenko V, Vanpouille C, Brichacek B, Vaisman I, Hatakeyama S, et al. Cell surface expression of CD147/EMMPRIN is regulated by cyclophilin 60. J Biol Chem. 2005 Jul 29;280(30):27866-71. PubMed PMID: 15946952. Epub 2005/06/11. eng.

199. DeCastro R, Zhang Y, Guo H, Kataoka H, Gordon MK, Toole B, et al. Human keratinocytes express EMMPRIN, an extracellular matrix metalloproteinase inducer. J Invest Dermatol. 1996 Jun;106(6):1260-5. PubMed PMID: 8752667. Epub 1996/06/01. eng.

200. Fossum SR, Mallett S, Neil Barclay A. The MRC OX-47 antigen is a member of the immunoglobulin superfamily with an unusual transmembrane sequence. European Journal of Immunology. 1991;21(3):671-9.

201. Seko Y, Fujimura T, Taka H, Mineki R, Murayama K, Nagai R. Hypoxia followed by reoxygenation induces secretion of cyclophilin A from cultured rat cardiac myocytes. Biochem Biophys Res Commun. 2004 Apr 23;317(1):162-8. PubMed PMID: 15047162. Epub 2004/03/30.

202. Clamp MF, Ochrietor JD, Moroz TP, Linser PJ. Developmental analyses of 5A11/Basigin, 5A11/Basigin-2 and their putative binding partner MCT1 in the mouse eye. Exp Eye Res. 2004 Apr;78(4):777-89. PubMed PMID: 15037112. Epub 2004/03/24. eng.

203. Tang W, Hemler ME. Caveolin-1 regulates matrix metalloproteinases-1 induction and CD147/EMMPRIN cell surface clustering. J Biol Chem. 2004 Mar 19;279(12):11112-8. PubMed PMID: 14707126. Epub 2004/01/07. eng.

204. Haug C, Lenz C, Díaz F, Bachem MG. Oxidized low-density lipoproteins stimulate extracellular matrix metalloproteinase Inducer (EMMPRIN) release by coronary smooth muscle cells. Arterioscler Thromb Vasc Biol. 2004 Oct;24(10):1823-9. PubMed PMID: 15319264. Epub 2004/08/21. eng.

205. Tang Y, Kesavan P, Nakada MT, Yan L. Tumor-stroma interaction: positive feedback regulation of extracellular matrix metalloproteinase inducer (EMMPRIN) expression and matrix metalloproteinase-dependent generation of soluble EMMPRIN. Mol Cancer Res. 2004 Feb;2(2):73-80. PubMed PMID: 14985463. Epub 2004/02/27. eng.

206. Chen Z, Mi L, Xu J, Yu J, Wang X, Jiang J, et al. Function of HAb18G/CD147 in invasion of host cells by severe acute respiratory syndrome coronavirus. J Infect Dis. 2005;191(5):755-60. PubMed PMID: 15688292. Epub 2005/01/25. eng.

207. Zucker S, Hymowitz M, Rollo EE, Mann R, Conner CE, Cao J, et al. Tumorigenic potential of extracellular matrix metalloproteinase inducer. The American journal of pathology. 2001;158(6):1921-8. PubMed PMID: 11395366. eng.

208. Michel RB, Ochakovskaya R, Mattes MJ. Antibody localization to B-cell lymphoma xenografts in immunodeficient mice: importance of using residualizing radiolabels. Clin Cancer Res. 2002 Aug;8(8):2632-9. PubMed PMID: 12171895. Epub 2002/08/13. eng.

209. Vetrivel KS, Zhang X, Meckler X, Cheng H, Lee S, Gong P, et al. Evidence that CD147 modulation of beta-amyloid (Abeta) levels is mediated by extracellular degradation of secreted Abeta. J Biol Chem. 2008 Jul 11;283(28):19489-98. PubMed PMID: 18456655. PMCID: PMC2443668. Epub 2008/05/06. eng.

210. Als AB, Dyrskjøt L, von der Maase H, Koed K, Mansilla F, Toldbod HE, et al. Emmprin and survivin predict response and survival following cisplatin-containing chemotherapy in patients with advanced bladder cancer. Clin Cancer Res. 2007 Aug 1;13(15 Pt 1):4407-14. PubMed PMID: 17671123. Epub 2007/08/03. eng.

211. Lim M, Martinez T, Jablons D, Cameron R, Guo H, Toole B, et al. Tumor-derived EMMPRIN (extracellular matrix metalloproteinase inducer) stimulates collagenase transcription through MAPK p38. FEBS Lett. 1998 Dec 11;441(1):88-92. PubMed PMID: 9877171. Epub 1999/01/07. eng.

212. Hagemann T, Wilson J, Kulbe H, Li NF, Leinster DA, Charles K, et al. Macrophages induce invasiveness of epithelial cancer cells via NF-kappa B and JNK. J Immunol. 2005 Jul 15;175(2):1197-205. PubMed PMID: 16002723. Epub 2005/07/09. eng.

213. Lee J, Banu SK, Subbarao T, Starzinski-Powitz A, Arosh JA. Selective inhibition of prostaglandin E2 receptors EP2 and EP4 inhibits invasion of human immortalized endometriotic epithelial and stromal cells through suppression of metalloproteinases. Mol Cell Endocrinol. 2011 Jan 30;332(1-2):306-13. PubMed PMID: 21111772. Epub 2010/11/30. eng.

214. Venkatesan B, Valente AJ, Reddy VS, Siwik DA, Chandrasekar B. Resveratrol blocks interleukin-18-EMMPRIN cross-regulation and smooth muscle cell migration. Am J Physiol Heart Circ Physiol. 2009 Aug;297(2):H874-86. PubMed PMID: 19561311. PMCID: PMC2724205. Epub 2009/06/30. eng.

215. Braundmeier AG, Fazleabas AT, Lessey BA, Guo H, Toole BP, Nowak RA. Extracellular matrix metalloproteinase inducer regulates metalloproteinases in human uterine endometrium. J Clin Endocrinol Metab. 2006 Jun;91(6):2358-65. PubMed PMID: 16522689. Epub 2006/03/09. eng.

216. Noguchi Y, Sato T, Hirata M, Hara T, Ohama K, Ito A. Identification and characterization of extracellular matrix metalloproteinase inducer in human endometrium

during the menstrual cycle in vivo and in vitro. J Clin Endocrinol Metab. 2003 Dec;88(12):6063-72. PubMed PMID: 14671212. Epub 2003/12/13. eng.

217. Xiao LJ, Diao HL, Ma XH, Ding NZ, Kadomatsu K, Muramatsu T, et al. Basigin expression and hormonal regulation in the rat uterus during the peri-implantation period. Reproduction. 2002 Aug;124(2):219-25. PubMed PMID: 12141934. Epub 2002/07/27. eng.

218. Kirk P, Wilson MC, Heddle C, Brown MH, Barclay AN, Halestrap AP. CD147 is tightly associated with lactate transporters MCT1 and MCT4 and facilitates their cell surface expression. Embo j. 2000 Aug 1;19(15):3896-904. PubMed PMID: 10921872. PMCID: PMC306613. Epub 2000/08/02. eng.

219. Philp NJ, Ochrietor JD, Rudoy C, Muramatsu T, Linser PJ. Loss of MCT1, MCT3, and MCT4 Expression in the Retinal Pigment Epithelium and Neural Retina of the 5A11/Basigin-Null Mouse. Investigative Ophthalmology & Visual Science. 2003;44(3):1305-11.

220. Yurchenko V, Pushkarsky T, Li J-H, Dai WW, Sherry B, Bukrinsky M. Regulation of CD147 Cell Surface Expression: INVOLVEMENT OF THE PROLINE RESIDUE IN THE CD147 TRANSMEMBRANE DOMAIN. Journal of Biological Chemistry. 2005 April 29, 2005;280(17):17013-9.

221. Igakura T, Kadomatsu K, Kaname T, Muramatsu H, Fan QW, Miyauchi T, et al. A null mutation in basigin, an immunoglobulin superfamily member, indicates its important roles in peri-implantation development and spermatogenesis. Dev Biol. 1998 Feb 15;194(2):152-65. PubMed PMID: 9501026. Epub 1998/03/17. eng.

222. Chen S, Kadomatsu K, Kondo M, Toyama Y, Toshimori K, Ueno S, et al. Effects of flanking genes on the phenotypes of mice deficient in basigin/CD147. Biochem Biophys Res Commun. 2004 Nov 5;324(1):147-53. PubMed PMID: 15464995. Epub 2004/10/07. eng.

223. Kuno N, Kadomatsu K, Fan QW, Hagihara M, Senda T, Mizutani S, et al. Female sterility in mice lacking the basigin gene, which encodes a transmembrane glycoprotein belonging to the immunoglobulin superfamily. FEBS Lett. 1998 Mar 27;425(2):191-4. PubMed PMID: 9559645. Epub 1998/04/29. eng.

224. Naruhashi K, Kadomatsu K, Igakura T, Fan QW, Kuno N, Muramatsu H, et al. Abnormalities of sensory and memory functions in mice lacking Bsg gene. Biochem Biophys Res Commun. 1997 Jul 30;236(3):733-7. PubMed PMID: 9245724. Epub 1997/07/30. eng.

225. Hori K, Katayama N, Kachi S, Kondo M, Kadomatsu K, Usukura J, et al. Retinal dysfunction in basigin deficiency. Invest Ophthalmol Vis Sci. 2000 Sep;41(10):3128-33. PubMed PMID: 10967074. Epub 2000/09/01. eng.

226. Gabison EE, Huet E, Baudouin C, Menashi S. Direct epithelial-stromal interaction in corneal wound healing: Role of EMMPRIN/CD147 in MMPs induction and beyond. Prog Retin Eye Res. 2009 Jan;28(1):19-33. PubMed PMID: 19056510. Epub 2008/12/06. eng.

227. Kato N, Kosugi T, Sato W, Ishimoto T, Kojima H, Sato Y, et al. Basigin/CD147 promotes renal fibrosis after unilateral ureteral obstruction. Am J Pathol. 2011 Feb;178(2):572-9. PubMed PMID: 21281789. PMCID: PMC3069835. Epub 2011/02/02. eng.

228. Yoon YW, Kwon HM, Hwang KC, Choi EY, Hong BK, Kim D, et al. Upstream regulation of matrix metalloproteinase by EMMPRIN; extracellular matrix metalloproteinase inducer in advanced atherosclerotic plaque. Atherosclerosis. 2005 May;180(1):37-44. PubMed PMID: 15823273. Epub 2005/04/13. eng.

229. Major TC, Liang L, Lu X, Rosebury W, Bocan TM. Extracellular matrix metalloproteinase inducer (EMMPRIN) is induced upon monocyte differentiation and is expressed in human atheroma. Arterioscler Thromb Vasc Biol. 2002 Jul 1;22(7):1200-7. PubMed PMID: 12117738. Epub 2002/07/16. eng.

230. Weidle UH, Scheuer W, Eggle D, Klostermann S, Stockinger H. Cancer-related issues of CD147. Cancer Genomics Proteomics. 2010 May-Jun;7(3):157-69. PubMed PMID: 20551248. Epub 2010/06/17. eng.

231. Nabeshima K, Iwasaki H, Koga K, Hojo H, Suzumiya J, Kikuchi M. Emmprin (basigin/CD147): matrix metalloproteinase modulator and multifunctional cell recognition molecule that plays a critical role in cancer progression. Pathol Int. 2006 Jul;56(7):359-67. PubMed PMID: 16792544. Epub 2006/06/24. eng.

232. Kataoka H, DeCastro R, Zucker S, Biswas C. Tumor cell-derived collagenase-stimulatory factor increases expression of interstitial collagenase, stromelysin, and 72-kDa gelatinase. Cancer Res. 1993 Jul 1;53(13):3154-8. PubMed PMID: 8319225. Epub 1993/07/01. eng.

233. Grass GD, Dai L, Qin Z, Parsons C, Toole BP. CD147: regulator of hyaluronan signaling in invasiveness and chemoresistance. Adv Cancer Res. 2014;123:351-73. PubMed PMID: 25081536. Epub 2014/08/02. eng.

234. Caudroy S, Polette M, Nawrocki-Raby B, Cao J, Toole BP, Zucker S, et al. EMMPRIN-mediated MMP regulation in tumor and endothelial cells. Clin Exp Metastasis. 2002;19(8):697-702. PubMed PMID: 12553375. Epub 2003/01/30. eng.

235. Guo H, Zucker S, Gordon MK, Toole BP, Biswas C. Stimulation of matrix metalloproteinase production by recombinant extracellular matrix metalloproteinase inducer from transfected Chinese hamster ovary cells. J Biol Chem. 1997 Jan 3;272(1):24-7. PubMed PMID: 8995219. Epub 1997/01/03. eng.

236. Grass GD, Bratoeva M, Toole BP. Regulation of invadopodia formation and activity by CD147. J Cell Sci. 2012 Feb 1;125(Pt 3):777-88. PubMed PMID: 22389410. PMCID: PMC3367836. Epub 2012/03/06. eng.

237. Huang W, Luo WJ, Zhu P, Tang J, Yu XL, Cui HY, et al. Modulation of CD147-induced matrix metalloproteinase activity: role of CD147 N-glycosylation. Biochem J. 2013 Jan 15;449(2):437-48. PubMed PMID: 23005037. Epub 2012/09/26. eng.

238. Yu XL, Hu T, Du JM, Ding JP, Yang XM, Zhang J, et al. Crystal structure of HAb18G/CD147: implications for immunoglobulin superfamily homophilic adhesion. J Biol Chem. 2008 Jun 27;283(26):18056-65. PubMed PMID: 18430721. Epub 2008/04/24. eng.

239. Zhao P, Zhang W, Wang SJ, Yu XL, Tang J, Huang W, et al. HAb18G/CD147 promotes cell motility by regulating annexin II-activated RhoA and Rac1 signaling pathways in hepatocellular carcinoma cells. Hepatology. 2011 Dec;54(6):2012-24. PubMed PMID: 21809360. Epub 2011/08/03. eng.

240. Dai JY, Dou KF, Wang CH, Zhao P, Lau WB, Tao L, et al. The interaction of HAb18G/CD147 with integrin alpha6beta1 and its implications for the invasion potential of human hepatoma cells. BMC Cancer. 2009 Sep 23;9:337. PubMed PMID: 19775453. PMCID: PMC2760576. Epub 2009/09/25. eng.

241. Berditchevski F, Chang S, Bodorova J, Hemler ME. Generation of monoclonal antibodies to integrin-associated proteins. Evidence that alpha3beta1 complexes with EMMPRIN/basigin/OX47/M6. J Biol Chem. 1997 Nov 14;272(46):29174-80. PubMed PMID: 9360995. Epub 1997/11/20. eng.

242. Tian X, Zhao C, Zhu H, She W, Zhang J, Liu J, et al. Hepatitis B virus (HBV) surface antigen interacts with and promotes cyclophilin a secretion: possible link to pathogenesis of HBV infection. J Virol. 2010 Apr;84(7):3373-81. PubMed PMID: 20089655. PMCID: PMC2838095. Epub 2010/01/22. eng.

243. Chen Z, Mi L, Xu J, Yu J, Wang X, Jiang J, et al. Function of HAb18G/CD147 in invasion of host cells by severe acute respiratory syndrome coronavirus. J Infect Dis. 2005 Mar 1;191(5):755-60. PubMed PMID: 15688292. PMCID: PMC7110046. Epub 2005/02/03. eng.

244. Chen J, Xia S, Yang X, Chen H, Li F, Liu F, et al. Human Cytomegalovirus Encoded miR-US25-1-5p Attenuates CD147/EMMPRIN-Mediated Early Antiviral Response. Viruses. 2017 Dec 1;9(12). PubMed PMID: 29194430. PMCID: PMC5744140. Epub 2017/12/02. eng.

245. Pushkarsky T, Zybarth G, Dubrovsky L, Yurchenko V, Tang H, Guo H, et al. CD147 facilitates HIV-1 infection by interacting with virus-associated cyclophilin A. Proceedings of the National Academy of Sciences. 2001;98(11):6360-5.

246. Coste I, Gauchat J-Fo, Wilson A, Izui S, Jeannin P, Delneste Y, et al. Unavailability of CD147 leads to selective erythrocyte trapping in the spleen. Blood. 2001;97(12):3984-8.

247. Schlosshauer B, Herzog KH. Neurothelin: an inducible cell surface glycoprotein of blood-brain barrier-specific endothelial cells and distinct neurons. J Cell Biol. 1990 Apr;110(4):1261-74. PubMed PMID: 2324198. PMCID: PMC2116095. Epub 1990/04/01. eng.
248. Jin R, Xiao AY, Chen R, Granger DN, Li G. Inhibition of CD147 (Cluster of Differentiation 147) Ameliorates Acute Ischemic Stroke in Mice by Reducing Thromboinflammation. Stroke. 2017;48(12):3356-65.
249. Miyauchi T, Masuzawa Y, Muramatsu T. The basigin group of the immunoglobulin superfamily: complete conservation of a segment in and around transmembrane domains of human and mouse basigin and chicken HT7 antigen. J Biochem. 1991 Nov;110(5):770-4. PubMed PMID: 1783610. Epub 1991/11/01. eng.
250. Wang CH, Dai JY, Wang L, Jia JF, Zheng ZH, Ding J, et al. Expression of CD147 (EMMPRIN) on neutrophils in rheumatoid arthritis enhances chemotaxis, matrix metalloproteinase production and invasiveness of synoviocytes. J Cell Mol Med. 2011 Apr;15(4):850-60. PubMed PMID: 20455995. PMCID: PMC3922672. Epub 2010/05/12. eng.
251. Zhu P, Lu N, Shi Z-g, Zhou J, Wu Z-b, Yang Y, et al. CD147 overexpression on synoviocytes in rheumatoid arthritis enhances matrix metalloproteinase production and invasiveness of synoviocytes. Arthritis Research & Therapy. 2006 2006/02/08;8(2):R44.
252. Bai Y, Huang W, Ma LT, Jiang JL, Chen ZN. Importance of N-glycosylation on CD147 for its biological functions. Int J Mol Sci. 2014 Apr 15;15(4):6356-77. PubMed PMID: 24739808. PMCID: PMC4013633. Epub 2014/04/18.
253. Pennings GJ, Yong AS, Kritharides L. Expression of EMMPRIN (CD147) on circulating platelets in vivo. J Thromb Haemost. 2010 Mar;8(3):472-81. PubMed PMID: 19995409. Epub 2009/12/10. eng.
254. Uhlén M, Fagerberg L, Hallström BM, Lindskog C, Oksvold P, Mardinoglu A, et al. Proteomics. Tissue-based map of the human proteome. Science. 2015 Jan 23;347(6220):1260419. PubMed PMID: 25613900. Epub 2015/01/24. eng.
255. The Human Protein Atlas 2020 [Available from: http://www.proteinatlas.org.
256. Radzikowska U, Ding M, Tan G, Zhakparov D, Peng Y, Wawrzyniak P, et al. Distribution of ACE2, CD147, CD26 and other SARS-CoV-2 associated molecules in tissues and immune cells in health and in asthma, COPD, obesity, hypertension, and COVID-19 risk factors. Allergy. 2020 Jun 4. PubMed PMID: 32496587. PMCID: PMC7300910. Epub 2020/06/05. eng.
257. Jouneau S, Khorasani N, P DES, Macedo P, Zhu J, Bhavsar PK, et al. EMMPRIN (CD147) regulation of MMP-9 in bronchial epithelial cells in COPD. Respirology. 2011 May;16(4):705-12. PubMed PMID: 21355964. Epub 2011/03/02. eng.

258. Berg J, Halvorsen AR, Bengtson MB, Taskén KA, Mælandsmo GM, Yndestad A, et al. Levels and prognostic impact of circulating markers of inflammation, endothelial activation and extracellular matrix remodelling in patients with lung cancer and chronic obstructive pulmonary disease. BMC Cancer. 2018 Jul 13;18(1):739. PubMed PMID: 30005623. PMCID: PMC6045874. Epub 2018/07/15. eng.

259. Lian C, Guo Y, Zhang J, Chen X, Peng C. Targeting CD147 is a Novel Strategy for Antitumor Therapy. Curr Pharm Des. 2017 Nov 16;23(29):4410-21. PubMed PMID: 28699528. Epub 2017/07/13. eng.

260. Wang P, Heitman J. The cyclophilins. Genome Biol. 2005;6(7):226. PubMed PMID: 15998457. PMCID: PMC1175980. Epub 2005/07/07. eng.

261. Gothel SF, Marahiel MA. Peptidyl-prolyl cis-trans isomerases, a superfamily of ubiquitous folding catalysts. Cell Mol Life Sci. 1999 Mar;55(3):423-36. PubMed PMID: 10228556. Epub 1999/05/06. eng.

262. Galat A. Peptidylprolyl cis/trans isomerases (immunophilins): biological diversity--targets--functions. Curr Top Med Chem. 2003;3(12):1315-47. PubMed PMID: 12871165. Epub 2003/07/23. eng.

263. Waldmeier PC, Zimmermann K, Qian T, Tintelnot-Blomley M, Lemasters JJ. Cyclophilin D as a drug target. Curr Med Chem. 2003 Aug;10(16):1485-506. PubMed PMID: 12871122. Epub 2003/07/23. eng.

264. Arevalo-Rodriguez M, Wu X, Hanes SD, Heitman J. Prolyl isomerases in yeast. Front Biosci. 2004 Sep 1;9:2420-46. PubMed PMID: 15353296. Epub 2004/09/09. eng.

265. Marks AR. Cellular functions of immunophilins. Physiol Rev. 1996 Jul;76(3):631-49. PubMed PMID: 8757784. Epub 1996/07/01. eng.

266. McDonald ML, Ardito T, Marks WH, Kashgarian M, Lorber MI. THE EFFECT OF CYCLOSPORINE ADMINISTRATION ON THE CELLULAR DISTRIBUTION AND CONTENT OF CYCLOPHILIN 1. Transplantation. 1992;53(2).

267. Göthel SF, Marahiel MA. Peptidyl-prolyl cis-trans isomerases, a superfamily of ubiquitous folding catalysts. Cellular and Molecular Life Sciences CMLS. 1999 1999/03/01;55(3):423-36.

268. Galat A. Peptidylproline cis-trans-isomerases: immunophilins. European Journal of Biochemistry. 1993 1993/09/01;216(3):689-707.

269. Kallen J, Spitzfaden C, Zurini MG, Wider G, Widmer H, Wüthrich K, et al. Structure of human cyclophilin and its binding site for cyclosporin A determined by X-ray crystallography and NMR spectroscopy. Nature. 1991 Sep 19;353(6341):276-9. PubMed PMID: 1896075. Epub 1991/09/19. eng.

270. Ke HM, Zydowsky LD, Liu J, Walsh CT. Crystal structure of recombinant human T-cell cyclophilin A at 2.5 A resolution. Proc Natl Acad Sci U S A. 1991 Nov 1;88(21):9483-7. PubMed PMID: 1946361. PMCID: PMC52742. Epub 1991/11/01. eng.
271. Mikol V, Kallen J, Pflügl G, Walkinshaw MD. X-ray Structure of a Monomeric Cyclophilin A-Cyclosporin A Crystal Complex at 2·1 Å Resolution. Journal of Molecular Biology. 1993 1993/12/20/;234(4):1119-30.
272. Handschumacher RE, Harding MW, Rice J, Drugge RJ, Speicher DW. Cyclophilin: a specific cytosolic binding protein for cyclosporin A. Science. 1984 Nov 2;226(4674):544-7. PubMed PMID: 6238408. Epub 1984/11/02. eng.
273. Liu J, Albers MW, Wandless TJ, Luan S, Alberg DG, Belshaw PJ, et al. Inhibition of T cell signaling by immunophilin-ligand complexes correlates with loss of calcineurin phosphatase activity. Biochemistry. 1992 Apr 28;31(16):3896-901. PubMed PMID: 1373650. Epub 1992/04/28. eng.
274. Colgan J, Asmal M, Neagu M, Yu B, Schneidkraut J, Lee Y, et al. Cyclophilin A regulates TCR signal strength in CD4+ T cells via a proline-directed conformational switch in Itk. Immunity. 2004 Aug;21(2):189-201. PubMed PMID: 15308100. Epub 2004/08/17. eng.
275. Franke EK, Yuan HE, Luban J. Specific incorporation of cyclophilin A into HIV-1 virions. Nature. 1994 Nov 24;372(6504):359-62. PubMed PMID: 7969494. Epub 1994/11/24. eng.
276. Bukrinsky MI. Cyclophilins: unexpected messengers in intercellular communications. Trends Immunol. 2002 Jul;23(7):323-5. PubMed PMID: 12103338. Epub 2002/07/10. eng.
277. Suzuki J, Jin Z-G, Meoli DF, Matoba T, Berk BC. Cyclophilin A Is Secreted by a Vesicular Pathway in Vascular Smooth Muscle Cells. Circulation Research. 2006;98(6):811-7.
278. Soe NN, Sowden M, Baskaran P, Kim Y, Nigro P, Smolock EM, et al. Acetylation of cyclophilin A is required for its secretion and vascular cell activation. Cardiovascular Research. 2013;101(3):444-53.
279. Sherry B, Yarlett N, Strupp A, Cerami A. Identification of cyclophilin as a proinflammatory secretory product of lipopolysaccharide-activated macrophages. Proceedings of the National Academy of Sciences. 1992;89(8):3511-5.
280. Seizer P, Ungern-Sternberg SN, Schonberger T, Borst O, Munzer P, Schmidt EM, et al. Extracellular cyclophilin A activates platelets via EMMPRIN (CD147) and PI3K/Akt signaling, which promotes platelet adhesion and thrombus formation in vitro and in vivo. Arterioscler Thromb Vasc Biol. 2015 Mar;35(3):655-63. PubMed PMID: 25550208. Epub 2015/01/01. eng.

281. Kim S-H, Lessner SM, Sakurai Y, Galis ZS. Cyclophilin A as a Novel Biphasic Mediator of Endothelial Activation and Dysfunction. The American Journal of Pathology. 2004;164(5):1567-74.

282. Jin Z-G, Melaragno Matthew G, Liao D-F, Yan C, Haendeler J, Suh Y-A, et al. Cyclophilin A Is a Secreted Growth Factor Induced by Oxidative Stress. Circulation Research. 2000 2000/10/27;87(9):789-96.

283. Flora GK, Anderton RS, Meloni BP, Guillemin GJ, Knuckey NW, MacDougall G, et al. Microglia are both a source and target of extracellular cyclophilin A. Heliyon. 2019 Sep;5(9):e02390. PubMed PMID: 31517118. PMCID: PMC6731207. Epub 2019/09/14. eng.

284. Coppinger JA, Cagney G, Toomey S, Kislinger T, Belton O, McRedmond JP, et al. Characterization of the proteins released from activated platelets leads to localization of novel platelet proteins in human atherosclerotic lesions. Blood. 2004 Mar 15;103(6):2096-104. PubMed PMID: 14630798. Epub 2003/11/25. eng.

285. Christofferson DE, Yuan J. Cyclophilin A release as a biomarker of necrotic cell death. Cell death and differentiation. 2010;17(12):1942-3. PubMed PMID: 20930851. Epub 2010/10/08. eng.

286. Suzuki J, Jin ZG, Meoli DF, Matoba T, Berk BC. Cyclophilin A is secreted by a vesicular pathway in vascular smooth muscle cells. Circ Res. 2006 Mar 31;98(6):811-7. PubMed PMID: 16527992. Epub 2006/03/11.

287. Jin ZG, Melaragno MG, Liao DF, Yan C, Haendeler J, Suh YA, et al. Cyclophilin A is a secreted growth factor induced by oxidative stress. Circ Res. 2000 Oct 27;87(9):789-96. PubMed PMID: 11055983. Epub 2000/10/31. eng.

288. Heine SJ, Olive D, Gao JL, Murphy PM, Bukrinsky MI, Constant SL. Cyclophilin A cooperates with MIP-2 to augment neutrophil migration. J Inflamm Res. 2011;4:93-104. PubMed PMID: 22096373. PMCID: PMC3218749. Epub 2011/11/19.

289. Xu Q, Leiva MC, Fischkoff SA, Handschumacher RE, Lyttle CR. Leukocyte chemotactic activity of cyclophilin. J Biol Chem. 1992 Jun 15;267(17):11968-71. PubMed PMID: 1601866. Epub 1992/06/15. eng.

290. Yurchenko V, Zybarth G, O'Connor M, Dai WW, Franchin G, Hao T, et al. Active site residues of cyclophilin A are crucial for its signaling activity via CD147. J Biol Chem. 2002 Jun 21;277(25):22959-65. PubMed PMID: 11943775. Epub 2002/04/12.

291. Arora K, Gwinn WM, Bower MA, Watson A, Okwumabua I, MacDonald HR, et al. Extracellular cyclophilins contribute to the regulation of inflammatory responses. J Immunol. 2005 Jul 1;175(1):517-22. PubMed PMID: 15972687. PMCID: PMC2862457. Epub 2005/06/24.

292. Dawar FU, Wu J, Zhao L, Khattak MN, Mei J, Lin L. Updates in understanding the role of cyclophilin A in leukocyte chemotaxis. J Leukoc Biol. 2017 Apr;101(4):823-6. PubMed PMID: 28062572. Epub 2017/01/08.

293. Jin ZG, Lungu AO, Xie L, Wang M, Wong C, Berk BC. Cyclophilin A is a proinflammatory cytokine that activates endothelial cells. Arterioscler Thromb Vasc Biol. 2004 Jul;24(7):1186-91. PubMed PMID: 15130913. Epub 2004/05/08.

294. Kim H, Kim WJ, Jeon ST, Koh EM, Cha HS, Ahn KS, et al. Cyclophilin A may contribute to the inflammatory processes in rheumatoid arthritis through induction of matrix degrading enzymes and inflammatory cytokines from macrophages. Clin Immunol. 2005 Sep;116(3):217-24. PubMed PMID: 15993649. Epub 2005/07/05.

295. Nigro P, Pompilio G, Capogrossi MC. Cyclophilin A: a key player for human disease. Cell Death Dis. 2013 Oct 31;4:e888. PubMed PMID: 24176846. PMCID: PMC3920964. Epub 2013/11/02.

296. Payeli SK, Schiene-Fischer C, Steffel J, Camici GG, Rozenberg I, Luscher TF, et al. Cyclophilin A differentially activates monocytes and endothelial cells: role of purity, activity, and endotoxin contamination in commercial preparations. Atherosclerosis. 2008 Apr;197(2):564-71. PubMed PMID: 17919644. Epub 2007/10/09. eng.

297. Soe NN, Sowden M, Baskaran P, Smolock EM, Kim Y, Nigro P, et al. Cyclophilin A is required for angiotensin II-induced p47phox translocation to caveolae in vascular smooth muscle cells. Arterioscler Thromb Vasc Biol. 2013 Sep;33(9):2147-53. PubMed PMID: 23846495. PMCID: PMC3817838. Epub 2013/07/13. eng.

298. Wang L, Soe NN, Sowden M, Xu Y, Modjeski K, Baskaran P, et al. Cyclophilin A is an important mediator of platelet function by regulating integrin alphaIIbbeta3 bidirectional signalling. Thromb Haemost. 2014 May 5;111(5):873-82. PubMed PMID: 24429998. Epub 2014/01/17. eng.

299. Wang L, Wang CH, Jia JF, Ma XK, Li Y, Zhu HB, et al. Contribution of cyclophilin A to the regulation of inflammatory processes in rheumatoid arthritis. J Clin Immunol. 2010 Jan;30(1):24-33. PubMed PMID: 19789967. Epub 2009/10/01. eng.

300. Xue Z, Yuan W, Li J, Zhou H, Xu L, Weng J, et al. Cyclophilin A mediates the ox-LDL-induced activation and apoptosis of macrophages via autophagy. Int J Cardiol. 2017 Mar 1;230:142-8. PubMed PMID: 28038796. Epub 2017/01/01. eng.

301. Yang Y, Lu N, Zhou J, Chen ZN, Zhu P. Cyclophilin A up-regulates MMP-9 expression and adhesion of monocytes/macrophages via CD147 signalling pathway in rheumatoid arthritis. Rheumatology (Oxford). 2008 Sep;47(9):1299-310. PubMed PMID: 18567920. Epub 2008/06/24.

302. Zhu C, Wang X, Deinum J, Huang Z, Gao J, Modjtahedi N, et al. Cyclophilin A participates in the nuclear translocation of apoptosis-inducing factor in neurons after cerebral hypoxia-ischemia. Journal of Experimental Medicine. 2007;204(8):1741-8.
303. Pushkarsky T, Yurchenko V, Laborico A, Bukrinsky M. CD147 stimulates HIV-1 infection in a signal-independent fashion. Biochem Biophys Res Commun. 2007 Nov 23;363(3):495-9. PubMed PMID: 17888876. PMCID: PMC2080668. Epub 2007/09/25. eng.
304. Pakula R, Melchior A, Denys A, Vanpouille C, Mazurier J, Allain F. Syndecan-1/CD147 association is essential for cyclophilin B-induced activation of p44/42 mitogen-activated protein kinases and promotion of cell adhesion and chemotaxis. Glycobiology. 2007 May;17(5):492-503. PubMed PMID: 17267519. Epub 2007/02/03. eng.
305. Khunkaewla P, Schiller HB, Paster W, Leksa V, Cermák L, Andera L, et al. LFA-1-mediated leukocyte adhesion regulated by interaction of CD43 with LFA-1 and CD147. Mol Immunol. 2008 Mar;45(6):1703-11. PubMed PMID: 17996943. Epub 2007/11/13. eng.
306. Schlegel J, Redzic JS, Porter CC, Yurchenko V, Bukrinsky M, Labeikovsky W, et al. Solution characterization of the extracellular region of CD147 and its interaction with its enzyme ligand cyclophilin A. J Mol Biol. 2009 Aug 21;391(3):518-35. PubMed PMID: 19500591. PMCID: PMC2940942. Epub 2009/06/09. eng.
307. Yang H, Li M, Chai H, Yan S, Lin P, Lumsden AB, et al. Effects of cyclophilin A on cell proliferation and gene expressions in human vascular smooth muscle cells and endothelial cells. J Surg Res. 2005 Feb;123(2):312-9. PubMed PMID: 15680395. Epub 2005/02/01. eng.
308. Xue C, Sowden MP, Berk BC. Extracellular and Intracellular Cyclophilin A, Native and Post-Translationally Modified, Show Diverse and Specific Pathological Roles in Diseases. Arterioscler Thromb Vasc Biol. 2018 May;38(5):986-93. PubMed PMID: 29599134. PMCID: PMC5920743. Epub 2018/03/31. eng.
309. Tegeder I, Schumacher A, John S, Geiger H, Geisslinger G, Bang H, et al. Elevated Serum Cyclophilin Levels in Patients with Severe Sepsis. Journal of Clinical Immunology. 1997 1997/09/01;17(5):380-6.
310. Billich A, Winkler G, Aschauer H, Rot A, Peichl P. Presence of Cyclophilin A in Synovial Fluids of Patients with Rheumatoid Arthritis. Journal of Experimental Medicine. 1997;185(5):975-80.
311. Konttinen YT, Li TF, Mandelin J, Liljestrom M, Sorsa T, Santavirta S, et al. Increased expression of extracellular matrix metalloproteinase inducer in rheumatoid synovium. Arthritis Rheum. 2000 Feb;43(2):275-80. PubMed PMID: 10693866. Epub 2000/02/29. eng.
312. Zhu P, Lu N, Shi ZG, Zhou J, Wu ZB, Yang Y, et al. CD147 overexpression on synoviocytes in rheumatoid arthritis enhances matrix metalloproteinase production and

invasiveness of synoviocytes. Arthritis Res Ther. 2006;8(2):R44. PubMed PMID: 16507143. PMCID: PMC1526600. Epub 2006/03/02. eng.

313. Tomita T, Nakase T, Kaneko M, Shi K, Takahi K, Ochi T, et al. Expression of extracellular matrix metalloproteinase inducer and enhancement of the production of matrix metalloproteinases in rheumatoid arthritis. Arthritis Rheum. 2002 Feb;46(2):373-8. PubMed PMID: 11840439. Epub 2002/02/13. eng.

314. Damsker JM, Okwumabua I, Pushkarsky T, Arora K, Bukrinsky MI, Constant SL. Targeting the chemotactic function of CD147 reduces collagen-induced arthritis. Immunology. 2009 Jan;126(1):55-62. PubMed PMID: 18557953. PMCID: PMC2632695. Epub 2008/06/19. eng.

315. Satoh K. Development of Novel Therapies for Cardiovascular Diseases by Clinical Application of Basic Research. Circulation Journal. 2017;81(11):1557-63.

316. Satoh K, Shimokawa H, Berk BC. Cyclophilin A: promising new target in cardiovascular therapy. Circ J. 2010 Nov;74(11):2249-56. PubMed PMID: 20962430. PMCID: PMC3052698. Epub 2010/10/22. eng.

317. Nigro P, Satoh K, O'Dell MR, Soe NN, Cui Z, Mohan A, et al. Cyclophilin A is an inflammatory mediator that promotes atherosclerosis in apolipoprotein E-deficient mice. J Exp Med. 2011 Jan 17;208(1):53-66. PubMed PMID: 21173104. PMCID: PMC3023134. Epub 2010/12/22. eng.

318. Damsker JM, Bukrinsky MI, Constant SL. Preferential chemotaxis of activated human CD4+ T cells by extracellular cyclophilin A. Journal of Leukocyte Biology. 2007;82(3):613-8.

319. Seizer P, Ochmann C, Schönberger T, Zach S, Rose M, Borst O, et al. Disrupting the EMMPRIN (CD147)-cyclophilin A interaction reduces infarct size and preserves systolic function after myocardial ischemia and reperfusion. Arteriosclerosis, thrombosis, and vascular biology. 2011;31(6):1377-86. PubMed PMID: 21441138. Epub 2011/03/24. eng.

320. Seizer P, Schönberger T, Schött M, R. Lang M, Langer HF, Bigalke B, et al. EMMPRIN and its ligand cyclophilin A regulate MT1-MMP, MMP-9 and M-CSF during foam cell formation. Atherosclerosis. 2010;209(1):51-7.

321. Schmidt R, Bültmann A, Fischel S, Gillitzer A, Cullen P, Walch A, et al. Extracellular Matrix Metalloproteinase Inducer (CD147) Is a Novel Receptor on Platelets, Activates Platelets, and Augments Nuclear Factor κB–Dependent Inflammation in Monocytes. Circulation Research. 2008;102(3):302-9.

322. Pahk K, Joung C, Song HY, Kim S, Kim W-K. SP-8356, a Novel Inhibitor of CD147-Cyclophilin A Interactions, Reduces Plaque Progression and Stabilizes Vulnerable Plaques in apoE-Deficient Mice. International journal of molecular sciences. 2019;21(1):95. PubMed PMID: 31877775. eng.

323. Huang C-H, Chang C-C, Kuo C-L, Huang C-S, Lin C-S, Liu C-S. Decrease in plasma cyclophilin A concentration at 1 month after myocardial infarction predicts better left ventricular performance and synchronicity at 6 months: a pilot study in patients with ST elevation myocardial infarction. Int J Biol Sci. 2015;11(1):38-47. PubMed PMID: 25552928. eng.

324. Vinitha A, Kutty VR, Vivekanand A, Reshmi G, Divya G, Sumi S, et al. PPIA rs6850: A > G single-nucleotide polymorphism is associated with raised plasma cyclophilin A levels in patients with coronary artery disease. Mol Cell Biochem. 2016 Jan;412(1-2):259-68. PubMed PMID: 26702934. Epub 2015/12/26. eng.

325. Kao H-W, Lee K-W, Chen W-L, Kuo C-L, Huang C-S, Tseng W-M, et al. Cyclophilin A in Ruptured Intracranial Aneurysm: A Prognostic Biomarker. Medicine. 2015;94(39):e1683-e. PubMed PMID: 26426668. eng.

326. Zuern CS, Müller KAL, Seizer P, Geisler T, Banya W, Klingel K, et al. Cyclophilin A predicts clinical outcome in patients with congestive heart failure undergoing endomyocardial biopsy. European Journal of Heart Failure. 2013;15(2):176-84.

327. Ohtsuki T, Satoh K, Omura J, Kikuchi N, Satoh T, Kurosawa R, et al. Prognostic Impacts of Plasma Levels of Cyclophilin A in Patients With Coronary Artery Disease. Arteriosclerosis, Thrombosis, and Vascular Biology. 2017;37(4):685-93.

328. Satoh K, Fukumoto Y, Sugimura K, Miura Y, Aoki T, Nochioka K, et al. Plasma cyclophilin A is a novel biomarker for coronary artery disease. Circ J. 2013;77(2):447-55. PubMed PMID: 23138189. Epub 2012/11/10. eng.

329. Gwinn WM, Damsker JM, Falahati R, Okwumabua I, Kelly-Welch A, Keegan AD, et al. Novel Approach to Inhibit Asthma-Mediated Lung Inflammation Using Anti-CD147 Intervention. The Journal of Immunology. 2006;177(7):4870-9.

330. Wilson MR, Patel BV, Takata M. Ventilation with "clinically relevant" high tidal volumes does not promote stretch-induced injury in the lungs of healthy mice. Crit Care Med. 2012 Oct;40(10):2850-7. PubMed PMID: 22890257. PMCID: PMC3698535. Epub 2012/08/15.

331. Ewart S, Levitt R, Mitzner W. Respiratory system mechanics in mice measured by end-inflation occlusion. J Appl Physiol (1985). 1995 Aug;79(2):560-6. PubMed PMID: 7592218. Epub 1995/08/01. eng.

332. Lang K, Schmid FX, Fischer G. Catalysis of protein folding by prolyl isomerase. Nature. 1987 1987/09/01;329(6136):268-70.

333. Sherry B, Yarlett N, Strupp A, Cerami A. Identification of cyclophilin as a proinflammatory secretory product of lipopolysaccharide-activated macrophages. Proceedings of the National Academy of Sciences of the United States of America. 1992;89(8):3511-5. PubMed PMID: 1565646. eng.

334. Nehme CL, Fayos BE, Bartles JR. Distribution of the integral plasma membrane glycoprotein CE9 (MRC OX-47) among rat tissues and its induction by diverse stimuli of metabolic activation. Biochem J. 1995;310 (Pt 2)(Pt 2):693-8. PubMed PMID: 7654213. eng.
335. Gwinn WM, Damsker JM, Falahati R, Okwumabua I, Kelly-Welch A, Keegan AD, et al. Novel approach to inhibit asthma-mediated lung inflammation using anti-CD147 intervention. J Immunol. 2006 Oct 1;177(7):4870-9. PubMed PMID: 16982929. PMCID: PMC2855298. Epub 2006/09/20.
336. Cross LJ, O'Kane CM, McDowell C, Elborn JJ, Matthay MA, McAuley DF. Keratinocyte growth factor in acute lung injury to reduce pulmonary dysfunction--a randomised placebo-controlled trial (KARE): study protocol. Trials. 2013 Feb 18;14:51. PubMed PMID: 23419093. PMCID: PMC3620926. Epub 2013/02/20. eng.
337. Craig TR, Duffy MJ, Shyamsundar M, McDowell C, O'Kane CM, Elborn JS, et al. A randomized clinical trial of hydroxymethylglutaryl- coenzyme a reductase inhibition for acute lung injury (The HARP Study). Am J Respir Crit Care Med. 2011 Mar 1;183(5):620-6. PubMed PMID: 20870757. Epub 2010/09/28. eng.
338. Patel BV, Tatham KC, Wilson MR, O'Dea KP, Takata M. In vivo compartmental analysis of leukocytes in mouse lungs. Am J Physiol Lung Cell Mol Physiol. 2015 Oct 1;309(7):L639-52. PubMed PMID: 26254421. PMCID: PMC4593833. Epub 2015/08/09.
339. McQualter JL, Yuen K, Williams B, Bertoncello I. Evidence of an epithelial stem/progenitor cell hierarchy in the adult mouse lung. Proceedings of the National Academy of Sciences. 2010;107(4):1414-9.
340. Uhal BD. Cell cycle kinetics in the alveolar epithelium. Am J Physiol. 1997 Jun;272(6 Pt 1):L1031-45. PubMed PMID: 9227501. Epub 1997/06/01. eng.
341. Hasegawa K, Sato A, Tanimura K, Uemasu K, Hamakawa Y, Fuseya Y, et al. Fraction of MHCII and EpCAM expression characterizes distal lung epithelial cells for alveolar type 2 cell isolation. Respir Res. 2017 Aug 7;18(1):150. PubMed PMID: 28784128. PMCID: PMC5545863. Epub 2017/08/09.
342. Snell N, Newbold P. The clinical utility of biomarkers in asthma and COPD. Current Opinion in Pharmacology. 2008 2008/06/01/;8(3):222-35.
343. Rennard SI, Basset G, Lecossier D, O'Donnell KM, Pinkston P, Martin PG, et al. Estimation of volume of epithelial lining fluid recovered by lavage using urea as marker of dilution. J Appl Physiol (1985). 1986 Feb;60(2):532-8. PubMed PMID: 3512509. Epub 1986/02/01. eng.
344. Haslam P, Baughman R. Report of ERS Task Force: guidelines for measurement of acellular components and standardization of BAL. European Respiratory Journal. 1999;14(2):245-8.

345. Franciosi L, Govorukhina N, ten Hacken N, Postma D, Bischoff R. Proteomics of Epithelial Lining Fluid Obtained by Bronchoscopic Microprobe Sampling. In: Toms SA, Weil RJ, editors. Nanoproteomics: Methods and Protocols. Totowa, NJ: Humana Press; 2011. p. 17-28.

346. Hanford LE, Enghild JJ, Valnickova Z, Petersen SV, Schaefer LM, Schaefer TM, et al. Purification and characterization of mouse soluble receptor for advanced glycation end products (sRAGE). J Biol Chem. 2004 Nov 26;279(48):50019-24. PubMed PMID: 15381690. PMCID: PMC1868562. Epub 2004/09/24. eng.

347. Neeper M, Schmidt AM, Brett J, Yan SD, Wang F, Pan YC, et al. Cloning and expression of a cell surface receptor for advanced glycosylation end products of proteins. J Biol Chem. 1992 Jul 25;267(21):14998-5004. PubMed PMID: 1378843. Epub 1992/07/25. eng.

348. Cheng C, Tsuneyama K, Kominami R, Shinohara H, Sakurai S, Yonekura H, et al. Expression profiling of endogenous secretory receptor for advanced glycation end products in human organs. Mod Pathol. 2005 Oct;18(10):1385-96. PubMed PMID: 15933755. Epub 2005/06/04. eng.

349. Morbini P, Villa C, Campo I, Zorzetto M, Inghilleri S, Luisetti M. The receptor for advanced glycation end products and its ligands: a new inflammatory pathway in lung disease? Mod Pathol. 2006 Nov;19(11):1437-45. PubMed PMID: 16941014. Epub 2006/08/31. eng.

350. Shirasawa M, Fujiwara N, Hirabayashi S, Ohno H, Iida J, Makita K, et al. Receptor for advanced glycation end-products is a marker of type I lung alveolar cells. Genes Cells. 2004 Feb;9(2):165-74. PubMed PMID: 15009093. Epub 2004/03/11. eng.

351. Raucci A, Cugusi S, Antonelli A, Barabino SM, Monti L, Bierhaus A, et al. A soluble form of the receptor for advanced glycation endproducts (RAGE) is produced by proteolytic cleavage of the membrane-bound form by the sheddase a disintegrin and metalloprotease 10 (ADAM10). The FASEB Journal. 2008 2008/10/01;22(10):3716-27.

352. Buckley ST, Ehrhardt C. The receptor for advanced glycation end products (RAGE) and the lung. J Biomed Biotechnol. 2010;2010:917108. PubMed PMID: 20145712. PMCID: PMC2817378. Epub 2010/02/11. eng.

353. Guo WA, Knight PR, Raghavendran K. The receptor for advanced glycation end products and acute lung injury/acute respiratory distress syndrome. Intensive Care Medicine. 2012 2012/10/01;38(10):1588-98.

354. Su X, Looney MR, Gupta N, Matthay MA. Receptor for advanced glycation end-products (RAGE) is an indicator of direct lung injury in models of experimental lung injury. Am J Physiol Lung Cell Mol Physiol. 2009 Jul;297(1):L1-5. PubMed PMID: 19411309. PMCID: PMC2711813. Epub 2009/05/05. eng.

355. Uchida T, Shirasawa M, Ware LB, Kojima K, Hata Y, Makita K, et al. Receptor for advanced glycation end-products is a marker of type I cell injury in acute lung injury. Am J Respir Crit Care Med. 2006 May 1;173(9):1008-15. PubMed PMID: 16456142. PMCID: PMC2662912. Epub 2006/02/04. eng.

356. Trachtenberg A, Pushkarsky T, Heine S, Constant S, Brichacek B, Bukrinsky M. The level of CD147 expression correlates with cyclophilin-induced signalling and chemotaxis. BMC Res Notes. 2011;4:396-. PubMed PMID: 21989251. eng.

357. Davidson B, Goldberg I, Berner A, Kristensen GB, Reich R. EMMPRIN (extracellular matrix metalloproteinase inducer) is a novel marker of poor outcome in serous ovarian carcinoma. Clin Exp Metastasis. 2003;20(2):161-9. PubMed PMID: 12705637. Epub 2003/04/23. eng.

358. Ju XZ, Yang JM, Zhou XY, Li ZT, Wu XH. EMMPRIN expression as a prognostic factor in radiotherapy of cervical cancer. Clin Cancer Res. 2008 Jan 15;14(2):494-501. PubMed PMID: 18223224. Epub 2008/01/29. eng.

359. Kanekura T, Chen X, Kanzaki T. Basigin (CD147) is expressed on melanoma cells and induces tumor cell invasion by stimulating production of matrix metalloproteinases by fibroblasts. Int J Cancer. 2002 Jun 1;99(4):520-8. PubMed PMID: 11992541. Epub 2002/05/07. eng.

360. Zhang Q, Zhou J, Ku XM, Chen XG, Zhang L, Xu J, et al. Expression of CD147 as a significantly unfavorable prognostic factor in hepatocellular carcinoma. Eur J Cancer Prev. 2007 Jun;16(3):196-202. PubMed PMID: 17415090. Epub 2007/04/07. eng.

361. Zucker S, Hymowitz M, Rollo EE, Mann R, Conner CE, Cao J, et al. Tumorigenic potential of extracellular matrix metalloproteinase inducer. Am J Pathol. 2001 Jun;158(6):1921-8. PubMed PMID: 11395366. PMCID: PMC1891983. Epub 2001/06/08. eng.

362. Gabison EE, Hoang-Xuan T, Mauviel A, Menashi S. EMMPRIN/CD147, an MMP modulator in cancer, development and tissue repair. Biochimie. 2005 Mar-Apr;87(3-4):361-8. PubMed PMID: 15781323. Epub 2005/03/23. eng.

363. Xin X, Zeng X, Gu H, Li M, Tan H, Jin Z, et al. CD147/EMMPRIN overexpression and prognosis in cancer: A systematic review and meta-analysis. Sci Rep. 2016 Sep 9;6:32804. PubMed PMID: 27608940. PMCID: PMC5016850. Epub 2016/09/10. eng.

364. Hatanaka M, Higashi Y, Fukushige T, Baba N, Kawai K, Hashiguchi T, et al. Cleaved CD147 shed from the surface of malignant melanoma cells activates MMP2 produced by fibroblasts. Anticancer Res. 2014 Dec;34(12):7091-6. PubMed PMID: 25503136. Epub 2014/12/17. eng.

365. Egawa N, Koshikawa N, Tomari T, Nabeshima K, Isobe T, Seiki M. Membrane type 1 matrix metalloproteinase (MT1-MMP/MMP-14) cleaves and releases a 22-kDa extracellular

matrix metalloproteinase inducer (EMMPRIN) fragment from tumor cells. J Biol Chem. 2006 Dec 8;281(49):37576-85. PubMed PMID: 17050542. Epub 2006/10/20. eng.

366. Dri P, Gasparini C, Menegazzi R, Cramer R, Albéri L, Presani G, et al. TNF-Induced Shedding of TNF Receptors in Human Polymorphonuclear Leukocytes: Role of the 55-kDa TNF Receptor and Involvement of a Membrane-Bound and Non-Matrix Metalloproteinase. The Journal of Immunology. 2000;165(4):2165-72.

367. Xanthoulea S, Pasparakis M, Kousteni S, Brakebusch C, Wallach D, Bauer J, et al. Tumor necrosis factor (TNF) receptor shedding controls thresholds of innate immune activation that balance opposing TNF functions in infectious and inflammatory diseases. The Journal of experimental medicine. 2004;200(3):367-76. PubMed PMID: 15289505. eng.

368. Zhang M, Tang J, Yin J, Wang X, Feng X, Yang X, et al. The clinical implication of serum cyclophilin A in patients with chronic obstructive pulmonary disease. Int J Chron Obstruct Pulmon Dis. 2018;13:357-63. PubMed PMID: 29403273. PMCID: PMC5783015. Epub 2018/02/07. eng.

369. Pastor MD, Nogal A, Molina-Pinelo S, Meléndez R, Salinas A, González De la Peña M, et al. Identification of proteomic signatures associated with lung cancer and COPD. J Proteomics. 2013 Aug 26;89:227-37. PubMed PMID: 23665002. Epub 2013/05/15. eng.

370. Chapman KE, Sinclair SE, Zhuang D, Hassid A, Desai LP, Waters CM. Cyclic mechanical strain increases reactive oxygen species production in pulmonary epithelial cells. Am J Physiol Lung Cell Mol Physiol. 2005 Nov;289(5):L834-41. PubMed PMID: 15964900. Epub 2005/06/21.

371. Davidovich N, DiPaolo BC, Lawrence GG, Chhour P, Yehya N, Margulies SS. Cyclic stretch-induced oxidative stress increases pulmonary alveolar epithelial permeability. Am J Respir Cell Mol Biol. 2013 Jul;49(1):156-64. PubMed PMID: 23526210. PMCID: PMC3727879. Epub 2013/03/26. eng.

372. Song MJ, Davidovich N, Lawrence GG, Margulies SS. Superoxide mediates tight junction complex dissociation in cyclically stretched lung slices. J Biomech. 2016 May 24;49(8):1330-5. PubMed PMID: 26592435. PMCID: PMC4864146. Epub 2015/11/26. eng.

373. Tanaka T, Saito Y, Matsuda K, Kamio K, Abe S, Kubota K, et al. Cyclic mechanical stretch-induced oxidative stress occurs via a NOX-dependent mechanism in type II alveolar epithelial cells. Respir Physiol Neurobiol. 2017 Aug;242:108-16. PubMed PMID: 28442445. Epub 2017/04/27. eng.

374. Patel BV, Wilson MR, O'Dea KP, Takata M. TNF-Induced Death Signaling Triggers Alveolar Epithelial Dysfunction in Acute Lung Injury. The Journal of Immunology. 2013;190(8):4274-82.

375. Systems RD. 7-Amino Actinomycin D (7-AAD) Cell Viability Flow Cytometry Protocol [Available from: https://www.rndsystems.com/resources/protocols/analysis-cell-viability-using-7-amino-actinomycin-d-7-aad.
376. FRANK JA, GUTIERREZ JA, JONES KD, ALLEN L, DOBBS L, MATTHAY MA. Low Tidal Volume Reduces Epithelial and Endothelial Injury in Acid-injured Rat Lungs. American Journal of Respiratory and Critical Care Medicine. 2002;165(2):242-9. PubMed PMID: 11790662.
377. Sibille Y, Reynolds HY. Macrophages and polymorphonuclear neutrophils in lung defense and injury. Am Rev Respir Dis. 1990 Feb;141(2):471-501. PubMed PMID: 2405761. Epub 1990/02/01. eng.
378. Montón C, Torres A. Lung inflammatory response in pneumonia. Monaldi Arch Chest Dis. 1998 Feb;53(1):56-63. PubMed PMID: 9632909. Epub 1998/06/20. eng.
379. Forrest JB. The effect of changes in lung volume on the size and shape of alveoli. J Physiol. 1970 Oct;210(3):533-47. PubMed PMID: 5499810. PMCID: PMC1395606. Epub 1970/10/01. eng.
380. Fredberg JJ, Kamm RD. Stress transmission in the lung: pathways from organ to molecule. Annu Rev Physiol. 2006;68:507-41. PubMed PMID: 16460282. Epub 2006/02/08. eng.
381. Oldmixon EH, Hoppin FG, Jr. Alveolar septal folding and lung inflation history. J Appl Physiol (1985). 1991 Dec;71(6):2369-79. PubMed PMID: 1778935. Epub 1991/12/11. eng.
382. Roan E, Waters CM. What do we know about mechanical strain in lung alveoli? American Journal of Physiology-Lung Cellular and Molecular Physiology. 2011;301(5):L625-L35. PubMed PMID: 21873445.
383. Chang J, Xia Y, Wasserloos K, Deng M, Blose KJ, Vorp DA, et al. Cyclic stretch induced IL-33 production through HMGB1/TLR-4 signaling pathway in murine respiratory epithelial cells. PLoS One. 2017;12(9):e0184770. PubMed PMID: 28898270. PMCID: PMC5595336. Epub 2017/09/13. eng.
384. Hu X, Zhang Y, Cheng D, Ding Y, Yang D, Jiang F, et al. Mechanical stress upregulates intercellular adhesion molecule-1 in pulmonary epithelial cells. Respiration. 2008;76(3):344-50. PubMed PMID: 18523380. Epub 2008/06/05. eng.
385. Cohen TS, Cavanaugh KJ, Margulies SS. Frequency and peak stretch magnitude affect alveolar epithelial permeability. Eur Respir J. 2008 Oct;32(4):854-61. PubMed PMID: 18614557. Epub 2008/07/11.
386. Jafari B, Ouyang B, Li LF, Hales CA, Quinn DA. Intracellular glutathione in stretch-induced cytokine release from alveolar type-2 like cells. Respirology. 2004 Mar;9(1):43-53. PubMed PMID: 14982601. Epub 2004/02/26. eng.

387. Li LF, Ouyang B, Choukroun G, Matyal R, Mascarenhas M, Jafari B, et al. Stretch-induced IL-8 depends on c-Jun NH2-terminal and nuclear factor-kappaB-inducing kinases. Am J Physiol Lung Cell Mol Physiol. 2003 Aug;285(2):L464-75. PubMed PMID: 12716652. Epub 2003/04/30. eng.

388. Ning Q-m, Wang X-r. Response of alveolar type II epithelial cells to mechanical stretch and lipopolysaccharide. Respiration; international review of thoracic diseases. 2007 2007;74(5):579-85. PubMed PMID: 17435381. eng.

389. Ning QM, Sun XN, Zhao XK. Role of mechanical stretching and lipopolysaccharide in early apoptosis and IL-8 of alveolar epithelial type II cells A549. Asian Pac J Trop Med. 2012 Aug;5(8):638-44. PubMed PMID: 22840453. Epub 2012/07/31. eng.

390. Vlahakis NE, Schroeder MA, Limper AH, Hubmayr RD. Stretch induces cytokine release by alveolar epithelial cells in vitro. Am J Physiol. 1999 Jul;277(1):L167-73. PubMed PMID: 10409244. Epub 1999/07/17. eng.

391. Yamamoto H, Teramoto H, Uetani K, Igawa K, Shimizu E. Cyclic stretch upregulates interleukin-8 and transforming growth factor-beta1 production through a protein kinase C-dependent pathway in alveolar epithelial cells. Respirology. 2002 Jun;7(2):103-9. PubMed PMID: 11985731. Epub 2002/05/03. eng.

392. Okada M, Matsumori A, Ono K, Furukawa Y, Shioi T, Iwasaki A, et al. Cyclic stretch upregulates production of interleukin-8 and monocyte chemotactic and activating factor/monocyte chemoattractant protein-1 in human endothelial cells. Arterioscler Thromb Vasc Biol. 1998 Jun;18(6):894-901. PubMed PMID: 9633928. Epub 1998/06/20. eng.

393. Iwaki M, Ito S, Morioka M, Iwata S, Numaguchi Y, Ishii M, et al. Mechanical stretch enhances IL-8 production in pulmonary microvascular endothelial cells. Biochem Biophys Res Commun. 2009 Nov 20;389(3):531-6. PubMed PMID: 19747898. Epub 2009/09/15. eng.

394. Roberts LM, Ledvina HE, Tuladhar S, Rana D, Steele SP, Sempowski GD, et al. Depletion of alveolar macrophages in CD11c diphtheria toxin receptor mice produces an inflammatory response. Immunity, Inflammation and Disease. 2015;3(2):71-81.

395. Suryadevara V, Fu P, Ebenezer DL, Berdyshev E, Bronova IA, Huang LS, et al. Sphingolipids in Ventilator Induced Lung Injury: Role of Sphingosine-1-Phosphate Lyase. Int J Mol Sci. 2018 Jan 1;19(1). PubMed PMID: 29301259. PMCID: PMC5796063. Epub 2018/01/06. eng.

396. Grazioli S, Dunn-Siegrist I, Pauchard LA, Blot M, Charles PE, Pugin J. Mitochondrial alarmins are tissue mediators of ventilator-induced lung injury and ARDS. PLoS One. 2019;14(11):e0225468. PubMed PMID: 31756204. PMCID: PMC6874419. Epub 2019/11/23. eng.

397. Mascarenhas MM, Day RM, Ochoa CD, Choi W-I, Yu L, Ouyang B, et al. Low Molecular Weight Hyaluronan from Stretched Lung Enhances Interleukin-8 Expression. American Journal of Respiratory Cell and Molecular Biology. 2004;30(1):51-60. PubMed PMID: 12738686.

398. Quinn D, Tager A, Joseph PM, Bonventre JV, Force T, Hales CA. Stretch-induced mitogen-activated protein kinase activation and interleukin-8 production in type II alveolar cells. Chest. 1999 Jul;116(1 Suppl):89s-90s. PubMed PMID: 10424608. Epub 1999/07/29. eng.

399. Schmitz C, Welck J, Tavernaro I, Grinberg M, Rahnenführer J, Kiemer AK, et al. Mechanical strain mimicking breathing amplifies alterations in gene expression induced by SiO(2) NPs in lung epithelial cells. Nanotoxicology. 2019 Nov;13(9):1227-43. PubMed PMID: 31418614. Epub 2019/08/17. eng.

400. Charles PE, Tissières P, Barbar SD, Croisier D, Dufour J, Dunn-Siegrist I, et al. Mild-stretch mechanical ventilation upregulates toll-like receptor 2 and sensitizes the lung to bacterial lipopeptide. Crit Care. 2011 Jul 27;15(4):R181. PubMed PMID: 21794115. PMCID: PMC3387624. Epub 2011/07/29. eng.

401. Yamamoto H, Teramoto H, Uetani K, Igawa K, Shimizu E. Stretch induces a growth factor in alveolar cells via protein kinase. Respiration Physiology. 2001 2001/09/01/;127(2):105-11.

402. YAMAMOTO H, TERAMOTO H, UETANI K, IGAWA K, SHIMIZU E. Cyclic stretch upregulates interleukin-8 and transforming growth factor-β1 production through a protein kinase C-dependent pathway in alveolar epithelial cells. Respirology. 2002;7(2):103-9.

403. Pugin J, Dunn I, Jolliet P, Tassaux D, Magnenat JL, Nicod LP, et al. Activation of human macrophages by mechanical ventilation in vitro. Am J Physiol. 1998 Dec;275(6):L1040-50. PubMed PMID: 9843840. Epub 1998/12/09. eng.

404. Lang CJ, Barnett EK, Doyle IR. Stretch and CO2 modulate the inflammatory response of alveolar macrophages through independent changes in metabolic activity. Cytokine. 2006 Mar 21;33(6):346-51. PubMed PMID: 16713281. Epub 2006/05/23. eng.

405. Matsuda S, Koyasu S. Mechanisms of action of cyclosporine. Immunopharmacology. 2000 May;47(2-3):119-25. PubMed PMID: 10878286. Epub 2000/07/06. eng.

406. Malesevic M, Kuhling J, Erdmann F, Balsley MA, Bukrinsky MI, Constant SL, et al. A cyclosporin derivative discriminates between extracellular and intracellular cyclophilins. Angew Chem Int Ed Engl. 2010;49(1):213-5. PubMed PMID: 19957254. PMCID: PMC2940222. Epub 2009/12/04.

407. Malesevic M, Gutknecht D, Prell E, Klein C, Schumann M, Nowak RA, et al. Anti-inflammatory effects of extracellular cyclosporins are exclusively mediated by CD147. J Med Chem. 2013 Sep 26;56(18):7302-11. PubMed PMID: 23964991. Epub 2013/08/24.

408. Bahmed K, Henry C, Holliday M, Redzic J, Ciobanu M, Zhang F, et al. Extracellular cyclophilin-A stimulates ERK1/2 phosphorylation in a cell-dependent manner but broadly stimulates nuclear factor kappa B. Cancer Cell International. 2012 2012/07/04;12(1):19.
409. Heinzmann D, Bangert A, Muller AM, von Ungern-Sternberg SN, Emschermann F, Schonberger T, et al. The Novel Extracellular Cyclophilin A (CyPA) - Inhibitor MM284 Reduces Myocardial Inflammation and Remodeling in a Mouse Model of Troponin I -Induced Myocarditis. PLoS One. 2015;10(4):e0124606. PubMed PMID: 25894208. PMCID: PMC4404136. Epub 2015/04/22.
410. Ditiatkovski M, Neelisetti VN, Cui HL, Malesevic M, Fischer G, Bukrinsky M, et al. Inhibition of extracellular cyclophilins with cyclosporine analog and development of atherosclerosis in apolipoprotein E-deficient mice. J Pharmacol Exp Ther. 2015 Jun;353(3):490-5. PubMed PMID: 25788712. Epub 2015/03/20. eng.
411. Matthew E, Kutcher L, Dedman J. Protection of lungs from hyperoxic injury: gene expression analysis of cyclosporin A therapy. Physiological Genomics. 2003;14(2):129-38. PubMed PMID: 12771387.
412. Matthew E, Pun R, Simonich M, Iwamoto H, Dedman J. Cyclosporin A protects lung function from hyperoxic damage. American Journal of Physiology-Lung Cellular and Molecular Physiology. 1999;276(5):L786-L95. PubMed PMID: 10330035.
413. Corbel M, Lagente V, Théret N, Germain N, Clément B, Boichot E. Comparative effects of betamethasone, cyclosporin and nedocromil sodium in acute pulmonary inflammation and metalloproteinase activities in bronchoalveolar lavage fluid from mice exposed to lipopolysaccharide. Pulm Pharmacol Ther. 1999;12(3):165-71. PubMed PMID: 10419836. Epub 1999/07/27. eng.
414. Pagano A, Donati Y, Métrailler I, Barazzone Argiroffo C. Mitochondrial cytochrome c release is a key event in hyperoxia-induced lung injury: protection by cyclosporin A. Am J Physiol Lung Cell Mol Physiol. 2004 Feb;286(2):L275-83. PubMed PMID: 14527930. Epub 2003/10/07. eng.
415. Kleiner DE, Stetler-Stevenson WG. Quantitative zymography: detection of picogram quantities of gelatinases. Anal Biochem. 1994 May 1;218(2):325-9. PubMed PMID: 8074288. Epub 1994/05/01. eng.
416. Blázquez-Prieto J, López-Alonso I, Amado-Rodríguez L, Huidobro C, González-López A, Kuebler WM, et al. Impaired lung repair during neutropenia can be reverted by matrix metalloproteinase-9. Thorax. 2018;73(4):321.
417. Albaiceta GM, Gutierrez-Fernández A, García-Prieto E, Puente XS, Parra D, Astudillo A, et al. Absence or Inhibition of Matrix Metalloproteinase–8 Decreases Ventilator-Induced

Lung Injury. American Journal of Respiratory Cell and Molecular Biology. 2010 2010/11/01;43(5):555-63.

418. Zhang F, Hu L, Wu Y-x, Fan L, Liu W-t, Wang J, et al. Doxycycline alleviates paraquat-induced acute lung injury by inhibiting neutrophil-derived matrix metalloproteinase 9. International Immunopharmacology. 2019 2019/07/01/;72:243-51.

419. Balsley MA, Malesevic M, Stemmy EJ, Gigley J, Jurjus RA, Herzog D, et al. A cell-impermeable cyclosporine A derivative reduces pathology in a mouse model of allergic lung inflammation. J Immunol. 2010 Dec 15;185(12):7663-70. PubMed PMID: 21057089. PMCID: PMC3603141. Epub 2010/11/09.

420. Iordanskaia T, Malesevic M, Fischer G, Pushkarsky T, Bukrinsky M, Nadler EP. Targeting Extracellular Cyclophilins Ameliorates Disease Progression in Experimental Biliary Atresia. Mol Med. 2015 Oct;21(1):657-64. PubMed PMID: 26225831. PMCID: PMC4749494. Epub 2015/08/01. eng.

421. Ramachandran S, Vinitha A, Kartha CC. Cyclophilin A enhances macrophage differentiation and lipid uptake in high glucose conditions: a cellular mechanism for accelerated macro vascular disease in diabetes mellitus. Cardiovascular Diabetology. 2016 2016/11/03;15(1):152.

422. Reutershan J, Morris MA, Burcin TL, Smith DF, Chang D, Saprito MS, et al. Critical role of endothelial CXCR2 in LPS-induced neutrophil migration into the lung. The Journal of Clinical Investigation. 2006 03/01/;116(3):695-702.

423. Barron V, Brougham C, Coghlan K, McLucas E, O'Mahoney D, Stenson-Cox C, et al. The effect of physiological cyclic stretch on the cell morphology, cell orientation and protein expression of endothelial cells. Journal of Materials Science: Materials in Medicine. 2007 2007/10/01;18(10):1973-81.

424. Imanaka H, Shimaoka M, Matsuura N, Nishimura M, Ohta N, Kiyono H. Ventilator-induced lung injury is associated with neutrophil infiltration, macrophage activation, and TGF-beta 1 mRNA upregulation in rat lungs. Anesth Analg. 2001 Feb;92(2):428-36. PubMed PMID: 11159246. Epub 2001/02/13. eng.

425. Bertok S, Wilson MR, Morley PJ, de Wildt R, Bayliffe A, Takata M. Selective inhibition of intra-alveolar p55 TNF receptor attenuates ventilator-induced lung injury. Thorax. 2012;67(3):244-51.

426. Woods SJ, Waite AAC, O'Dea KP, Halford P, Takata M, Wilson MR. Kinetic profiling of in vivo lung cellular inflammatory responses to mechanical ventilation. American journal of physiology Lung cellular and molecular physiology. 2015;308(9):L912-L21. PubMed PMID: 25770178. Epub 2015/03/13. eng.

427. Frank JA, Wray CM, McAuley DF, Schwendener R, Matthay MA. Alveolar macrophages contribute to alveolar barrier dysfunction in ventilator-induced lung injury. Am J Physiol Lung Cell Mol Physiol. 2006 Dec;291(6):L1191-8. PubMed PMID: 16877636. Epub 2006/08/01.

428. Eyal FG, Hamm CR, Parker JC. Reduction in alveolar macrophages attenuates acute ventilator induced lung injury in rats. Intensive Care Medicine. 2007 2007/07/01;33(7):1212-8.

429. Davey A, McAuley DF, O'Kane CM. Matrix metalloproteinases in acute lung injury: mediators of injury and drivers of repair. Eur Respir J. 2011 Oct;38(4):959-70. PubMed PMID: 21565917. Epub 2011/05/14.

430. Greenlee KJ, Werb Z, Kheradmand F. Matrix metalloproteinases in lung: multiple, multifarious, and multifaceted. Physiol Rev. 2007 Jan;87(1):69-98. PubMed PMID: 17237343. PMCID: PMC2656382. Epub 2007/01/24.

431. Albaiceta GM, Gutierrez-Fernandez A, Garcia-Prieto E, Puente XS, Parra D, Astudillo A, et al. Absence or inhibition of matrix metalloproteinase-8 decreases ventilator-induced lung injury. Am J Respir Cell Mol Biol. 2010 Nov;43(5):555-63. PubMed PMID: 19995943. Epub 2009/12/10.

432. Hergrueter AH, Nguyen K, Owen CA. Matrix metalloproteinases: all the RAGE in the acute respiratory distress syndrome. Am J Physiol Lung Cell Mol Physiol. 2011 Apr;300(4):L512-5. PubMed PMID: 21296893. PMCID: PMC3075103. Epub 2011/02/08.

433. Cederqvist K, Janer J, Tervahartiala T, Sorsa T, Haglund C, Salmenkivi K, et al. Up-Regulation of Trypsin and Mesenchymal MMP-8 During Development of Hyperoxic Lung Injury in the Rat. Pediatric Research. 2006 2006/10/01;60(4):395-400.

434. Eichler W, Bechtel JF, Schumacher J, Wermelt JA, Klotz KF, Bartels C. A rise of MMP-2 and MMP-9 in bronchoalveolar lavage fluid is associated with acute lung injury after cardiopulmonary bypass in a swine model. Perfusion. 2003 Apr;18(2):107-13. PubMed PMID: 12868788. Epub 2003/07/19. eng.

435. Gushima Y, Ichikado K, Suga M, Okamoto T, Iyonaga K, Sato K, et al. Expression of matrix metalloproteinases in pigs with hyperoxia-induced acute lung injury. Eur Respir J. 2001 Nov;18(5):827-37. PubMed PMID: 11757634. Epub 2002/01/05. eng.

436. Kim JY, Choeng HC, Ahn C, Cho SH. Early and late changes of MMP-2 and MMP-9 in bleomycin-induced pulmonary fibrosis. Yonsei Med J. 2009 Feb 28;50(1):68-77. PubMed PMID: 19259351. PMCID: PMC2649867. Epub 2009/03/05. eng.

437. Loffek S, Schilling O, Franzke CW. Series "matrix metalloproteinases in lung health and disease": Biological role of matrix metalloproteinases: a critical balance. Eur Respir J. 2011 Jul;38(1):191-208. PubMed PMID: 21177845. Epub 2010/12/24.

438. Okuma T, Terasaki Y, Kaikita K, Kobayashi H, Kuziel WA, Kawasuji M, et al. C-C chemokine receptor 2 (CCR2) deficiency improves bleomycin-induced pulmonary fibrosis by attenuation of both macrophage infiltration and production of macrophage-derived matrix metalloproteinases. J Pathol. 2004 Dec;204(5):594-604. PubMed PMID: 15538737. Epub 2004/11/13. eng.

439. Liang Y, Yang N, Pan G, Jin B, Wang S, Ji W. Elevated IL-33 promotes expression of MMP2 and MMP9 via activating STAT3 in alveolar macrophages during LPS-induced acute lung injury. Cell Mol Biol Lett. 2018;23:52. PubMed PMID: 30410547. PMCID: PMC6208075. Epub 2018/11/10. eng.

440. John M, Oltmanns U, Fietze I, Witt C, Jung K. Increased production of matrix metalloproteinase-2 in alveolar macrophages and regulation by interleukin-10 in patients with acute pulmonary sarcoidosis. Exp Lung Res. 2002 Jan-Feb;28(1):55-68. PubMed PMID: 11792075. Epub 2002/01/17. eng.

441. Dooley JL, Abdel-Latif D, St Laurent CD, Puttagunta L, Befus D, Lacy P. Regulation of inflammation by Rac2 in immune complex-mediated acute lung injury. Am J Physiol Lung Cell Mol Physiol. 2009 Dec;297(6):L1091-102. PubMed PMID: 19801448. PMCID: PMC2793190. Epub 2009/10/06. eng.

442. Chiu WC, Lee YC, Su YH, Chai CY, Hu SC, Yuan SF, et al. Correlation of matrix metalloproteinase-2 and -9 expression with recurrences in primary spontaneous pneumothorax patients. J Thorac Dis. 2016 Dec;8(12):3667-75. PubMed PMID: 28149562. PMCID: PMC5227284. Epub 2017/02/06. eng.

443. Bell RD, Winkler EA, Singh I, Sagare AP, Deane R, Wu Z, et al. Apolipoprotein E controls cerebrovascular integrity via cyclophilin A. Nature. 2012 2012/05/01;485(7399):512-6.

444. Main BS, Villapol S, Sloley SS, Barton DJ, Parsadanian M, Agbaegbu C, et al. Apolipoprotein E4 impairs spontaneous blood brain barrier repair following traumatic brain injury. Molecular Neurodegeneration. 2018 2018/04/04;13(1):17.

445. Kenneth J. Cavanaugh J, Oswari J, Margulies SS. Role of Stretch on Tight Junction Structure in Alveolar Epithelial Cells. American Journal of Respiratory Cell and Molecular Biology. 2001;25(5):584-91. PubMed PMID: 11713100.

446. Gu C, Liu M, Zhao T, Wang D, Wang Y. Protective role of p120-catenin in maintaining the integrity of adherens and tight junctions in ventilator-induced lung injury. Respir Res. 2015 May 20;16:58. PubMed PMID: 25986488. PMCID: PMC4489357. Epub 2015/05/20.

447. Lischper M, Beuck S, Thanabalasundaram G, Pieper C, Galla HJ. Metalloproteinase mediated occludin cleavage in the cerebral microcapillary endothelium under pathological

conditions. Brain Res. 2010 Apr 22;1326:114-27. PubMed PMID: 20197061. Epub 2010/03/04. eng.

448. Seizer P, Schonberger T, Schott M, Lang MR, Langer HF, Bigalke B, et al. EMMPRIN and its ligand cyclophilin A regulate MT1-MMP, MMP-9 and M-CSF during foam cell formation. Atherosclerosis. 2010 Mar;209(1):51-7. PubMed PMID: 19758589. Epub 2009/09/18. eng.

449. Kim SH, Lessner SM, Sakurai Y, Galis ZS. Cyclophilin A as a novel biphasic mediator of endothelial activation and dysfunction. Am J Pathol. 2004 May;164(5):1567-74. PubMed PMID: 15111303. PMCID: PMC1615642. Epub 2004/04/28. eng.

450. Soe NN, Sowden M, Baskaran P, Kim Y, Nigro P, Smolock EM, et al. Acetylation of cyclophilin A is required for its secretion and vascular cell activation. Cardiovasc Res. 2014 Mar 1;101(3):444-53. PubMed PMID: 24293519. PMCID: PMC3928000. Epub 2013/12/03.

451. Satoh K, Nigro P, Matoba T, O'Dell MR, Cui Z, Shi X, et al. Cyclophilin A enhances vascular oxidative stress and the development of angiotensin II–induced aortic aneurysms. Nature Medicine. 2009 2009/06/01;15(6):649-56.

452. Dang B, Li H, Xu X, Shen H, Wang Y, Gao A, et al. Cyclophilin A/Cluster of Differentiation 147 Interactions Participate in Early Brain Injury After Subarachnoid Hemorrhage in Rats. Critical care medicine. 2015 2015/09//;43(9):e369-81. PubMed PMID: 26132882. eng.

453. Seizer P, Ochmann C, Schönberger T, Zach S, Rose M, Borst O, et al. Disrupting the EMMPRIN (CD147)-cyclophilin A interaction reduces infarct size and preserves systolic function after myocardial ischemia and reperfusion. Arterioscler Thromb Vasc Biol. 2011 Jun;31(6):1377-86. PubMed PMID: 21441138. PMCID: PMC3113549. Epub 2011/03/29. eng.

454. Lu G, Jia Z, Zu Q, Zhang J, Zhao L, Shi H. Inhibition of the cyclophilin A-CD147 interaction attenuates right ventricular injury and dysfunction after acute pulmonary embolism in rats. J Biol Chem. 2018 Aug 3;293(31):12199-208. PubMed PMID: 29914983. PMCID: PMC6078437. Epub 2018/06/20. eng.

455. Satoh K, Satoh T, Kikuchi N, Omura J, Kurosawa R, Suzuki K, et al. Basigin Mediates Pulmonary Hypertension by Promoting Inflammation and Vascular Smooth Muscle Cell Proliferation. Circulation Research. 2014 2014/09/26;115(8):738-50.

456. Manzanero S. Generation of Mouse Bone Marrow-Derived Macrophages. In: Ashman RB, editor. Leucocytes: Methods and Protocols. Totowa, NJ: Humana Press; 2012. p. 177-81.

457. Zhang X, Goncalves R, Mosser DM. The isolation and characterization of murine macrophages. Curr Protoc Immunol. 2008;Chapter 14:Unit-14.1. PubMed PMID: 19016445. eng.

458. Holt PG. Alveolar macrophages. I. a simple technique for the preparation of high numbers of viable alveolar macrophages from small laboratory animals. Journal of Immunological Methods. 1979 1979/05/24/;27(2):189-98.
459. Gordon S, Taylor PR. Monocyte and macrophage heterogeneity. Nat Rev Immunol. 2005 Dec;5(12):953-64. PubMed PMID: 16322748. Epub 2005/12/03. eng.
460. Cohn ZA. Activation of mononuclear phagocytes: fact, fancy, and future. J Immunol. 1978 Sep;121(3):813-6. PubMed PMID: 357655. Epub 1978/09/01. eng.
461. Strauss-Ayali D, Conrad SM, Mosser DM. Monocyte subpopulations and their differentiation patterns during infection. J Leukoc Biol. 2007 Aug;82(2):244-52. PubMed PMID: 17475785. Epub 2007/05/04. eng.
462. Stanley ER. The macrophage colony-stimulating factor, CSF-1. Methods Enzymol. 1985;116:564-87. PubMed PMID: 3003518. Epub 1985/01/01. eng.
463. Mitsi E, Kamng'ona R, Rylance J, Solórzano C, Jesus Reiné J, Mwandumba HC, et al. Human alveolar macrophages predominately express combined classical M1 and M2 surface markers in steady state. Respiratory Research. 2018 2018/04/18;19(1):66.
464. Akagawa KS. Functional Heterogeneity of Colony-Stimulating Factor-Induced Human Nonocyte-Derived Macrophages. International Journal of Hematology. 2002 2002/07/01;76(1):27-34.
465. Kelly A, Grabiec AM, Travis MA. Culture of Human Monocyte-Derived Macrophages. In: Rousselet G, editor. Macrophages: Methods and Protocols. New York, NY: Springer New York; 2018. p. 1-11.
466. Genecards. PPIA Gene: Weizmaan Institue of Science; 2020 [Available from: https://www.genecards.org/cgi-bin/carddisp.pl?gene=PPIA.
467. Xue C, Sowden M, Berk Bradford C. Extracellular Cyclophilin A, Especially Acetylated, Causes Pulmonary Hypertension by Stimulating Endothelial Apoptosis, Redox Stress, and Inflammation. Arteriosclerosis, Thrombosis, and Vascular Biology. 2017 2017/06/01;37(6):1138-46.
468. Lammers M, Neumann H, Chin JW, James LC. Acetylation regulates cyclophilin A catalysis, immunosuppression and HIV isomerization. Nat Chem Biol. 2010 May;6(5):331-7. PubMed PMID: 20364129. PMCID: PMC3867001. Epub 2010/04/07. eng.
469. Matthay MA, Zimmerman GA, Esmon C, Bhattacharya J, Coller B, Doerschuk CM, et al. Future Research Directions in Acute Lung Injury. American Journal of Respiratory and Critical Care Medicine. 2003;167(7):1027-35. PubMed PMID: 12663342.
470. Wilson MR, Takata M. Inflammatory mechanisms of ventilator-induced lung injury: a time to stop and think? Anaesthesia. 2013;68(2):175-8.

471. Schouten LRA, Bos LDJ, Serpa Neto A, van Vught LA, Wiewel MA, Hoogendijk AJ, et al. Increased mortality in elderly patients with acute respiratory distress syndrome is not explained by host response. Intensive Care Medicine Experimental. 2019 2019/10/29;7(1):58.
472. Soni S, O'Dea KP, Tan YY, Cho K, Abe E, Romano R, et al. ATP redirects cytokine trafficking and promotes novel membrane TNF signaling via microvesicles. The FASEB Journal. 2019;33(5):6442-55.
473. Kalra H, Simpson RJ, Ji H, Aikawa E, Altevogt P, Askenase P, et al. Vesiclepedia: A Compendium for Extracellular Vesicles with Continuous Community Annotation. PLOS Biology. 2012;10(12):e1001450.
474. Pan H, Luo C, Li R, Qiao A, Zhang L, Mines M, et al. Cyclophilin A is required for CXCR4-mediated nuclear export of heterogeneous nuclear ribonucleoprotein A2, activation and nuclear translocation of ERK1/2, and chemotactic cell migration. J Biol Chem. 2008 Jan 4;283(1):623-37. PubMed PMID: 17991743. Epub 2007/11/10. eng.
475. Ghezzi P, Casagrande S, Massignan T, Basso M, Bellacchio E, Mollica L, et al. Redox regulation of cyclophilin A by glutathionylation. PROTEOMICS. 2006;6(3):817-25.
476. Kim SC, Sprung R, Chen Y, Xu Y, Ball H, Pei J, et al. Substrate and functional diversity of lysine acetylation revealed by a proteomics survey. Mol Cell. 2006 Aug;23(4):607-18. PubMed PMID: 16916647. Epub 2006/08/19. eng.
477. Massignan T, Casoni F, Basso M, Stefanazzi P, Biasini E, Tortarolo M, et al. Proteomic analysis of spinal cord of presymptomatic amyotrophic lateral sclerosis G93A SOD1 mouse. Biochem Biophys Res Commun. 2007 Feb 16;353(3):719-25. PubMed PMID: 17196550. Epub 2007/01/02. eng.
478. Oakley C, Koh M, Baldi R, Soni S, O'Dea K, Takata M, et al. Ventilation following established ARDS: a preclinical model framework to improve predictive power. Thorax. 2019 Dec;74(12):1120-9. PubMed PMID: 31278170. PMCID: PMC6858882. Epub 2019/07/07. eng.